The Giraffidae (Mammalia, Artiodactyla) and the Study of the Histology and Chemistry of Fossil Mammal Bone from the Late Miocene of Kerassia (Euboea Island, Greece)

By

George Iliopoulos BSc. (Athens, Greece)

Thesis submitted for the degree of
Doctor of Philosophy
at the University of Leicester

Department of Geology
University of Leicester
September 2003

ProQuest LLC
789 East Eisenhower Parkway
P.O. Box 1346
Ann Arbor, MI 48106-1346


UNIVERSITY OF LEICESTER
LIBRARY

The Giraffidae (Mammalia, Artiodactyla) and the Study of the Histology and Chemistry of Fossil Mammal Bone from the Late Miocene of Kerassia (Euboea Island, Greece)

by George Iliopoulos BSc. (Athens, Greece)

ABSTRACT

A taphonomic investigation of Late Miocene mammal bones and teeth and a taxonomic study of the abundant and diverse giraffid material from Kerassia, Greece, were undertaken. The material was collected from seven different sites near Kerassia, where at least two fossiliferous horizons occur.

Microbial action caused extensive destruction in almost all the examined specimens of bone and teeth tissues from both horizons. Despite this, and contrary to the established ideas, bioeroded tissues survived to become fossils, preserving their histological and bioerosion features. The diameters of the microtunnels (150-600 nm) in the destructive foci indicate that the invading microorganisms were bacteria. Recrystallization of the apatite crystallites in the foci of damaged tissues occurred immediately after the end of bacterial activity, restraining later diagenetic recrystallization. This process is responsible for differences in the chemistry of the three structural areas of the bioeroded tissues, the undamaged areas, the foci and the rims of the foci.

X-ray diffraction mineralogical analyses showed that fossil bone and dentine consist of carbonate fluorapatite and enamel consists of carbonate hydroxyapatite. The crystallinity of the fossil tissues is not age dependent but rather reflects the type of the hard tissue and the conditions of the local burial environment.

To date, five different species of giraffes have been determined in Kerassia. Four species were found in the lower horizon, *Palaeotragus rouenii, Palaeotragus sp., Samotherium major* and *Helladotherium duvernoyi* and four species were found in the upper horizon *Palaeotragus rouenii, Samotherium major, Helladotherium duvernoyi* and *Bohlinia attica.*

Finally, this study shows that a seasonal Mediterranean type, relatively temperate to warm and moist climate, can be inferred for the MN12 (Middle Turolian) of the Kerassia region.

Table of contents

List of figures

Chapter 2

X-ray emission microanalysis of bacterially damaged bones and teeth from the Late Miocene of Kerassia, Greece

Chapter 3

X-Ray Diffraction studies of Late Miocene mammal bones and teeth

Chapter 4

Giraffidae (Artiodactyla, Mammalia) from the Late Miocene of Kerassia, Northern Euboea Island, Greece

List of tables

Chapter 3

X-Ray Diffraction studies of Late Miocene mammal bones and teeth

Chapter 4

Giraffidae (Artiodactyla, Mammalia) from the Late Miocene of Kerassia, Northern Euboea Island, Greece

List of abbreviations

Agr	Agridi, modern weathered bone
BEI	SEM backscattered electron imaging
Bos	Modern bone belonging to *Bos taurus*
C	Canine
CFA	Carbonated fluorapatite
CHA	Carbonated hydroxyapatite
Chal	Chalkoutsi (Greece, Late Miocene)
CHFA	Carbonated hydroxyl-fluorapatite
CI	Crystallinity index
CI_A	CI calculated with the method of Person *et al.* (1995)
CI_B	CI calculated with the method of Bartsiokas and Middleton (1992)
DAP	Anteroposterior diameter
dM	Deciduous molar
DT	Transverse diameter
DTK1	Ditiko 1 (Greece, Late Miocene)
DTK2	Ditiko 2 (Greece, Late Miocene)
I	Incisor
K1-7	The seven excavated sites in the locality of Kerassia
Kas	Kassandria (Greece, Late Miocene)
Ke	The amterial from 1982 excavation
M	Molar
MFD	Microscopical Focal Destruction
MN	Mammal Neogene
MN1-17	The European Land Mammal Zones for the Neogene (Mein, 1975)
NP	New Pikermi (Chomateri; Greece, Late Miocene)
OP	Old Pikermi (Megalo Rema; Greece, Late Miocene)
P	Premolar
Qu	Quorn (Loughborough, England, Late Pleistocene)
RP 2	Ravin de la Pluie 2 (Greece, Late Miocene)
SEM	Scanning Electron Microscope
VTK1	Vathilakos (Greece, Late Miocene)
XRD	X-Ray Diffraction

XREMA	X-Ray Emission MicroAnalysis

Museum abbreviations

AMPG	Athens Museum of Palaeontology and Geology (Museum of Historical Geology and Palaeontology), University of Athens, Athens
FMNH	Field Museum of Natural History, Chicago
MNHNP	Museum National d'Historie Naturelle, Paris (National Museum of Natural History, Paris).
NHML	Natural History Museum, London
SAM	South African Museum, Cape Town
Sedgwick	Sedgwick Museum of Earth Sciences, Cambridge

Acknowledgements

"I am indebted to my father for living, but to my teacher for living well"

Alexander the Great

Although it is not conventional to acknowledge your loved ones first, I feel that I should start with them. First of all I would like to thank my dear Natasha for being there and supporting me all these years, sharing with me all the good and bad moments of our life. And I should not forget to acknowledge her for looking me after during the last, miserable, writing-up year, but I hope I will be able to repay her and support her this year during her writing-up effort. Lots of thanks and gratitude to my parents, my late grandmother and my sister, without their support (ethical and financial) I could not have done it.

I am really grateful to my supervisors Dick Aldridge, Sarah Gabbott, Arthur Cruickshank and my supervisor in Greece George Theodorou, for their support and guidance all these years. In particular George is thanked for authorising me to use material from Kerassia for this study and for putting me in all these "trouble" in the first place. I was still an undergrad participating in my first excavation at the locality of Kerassia when George told me one day that the material from the excavation could be used for my future PhD project. Back then I thought that he was joking, but George was apparently serious, because he did believe in me and since then he kept urging me and encouraging me to go for it. Dick is thanked for bringing me to Leicester, for his guidance and for being always there for me to solve my insignificant problems. If it wasn't for Dick I wouldn't be here today. Sarah is thanked for bearing the burden of my supervision, for being patient with me, encouraging me and reading of poor drafts (that daunting second chapter...). Arthur is thanked for his constant encouragement and his regular phone calls and visits, as well as for his invaluable advice and discussions and the quick return of corrected drafts. Honestly, I owe you a lot guys.

I am also really obliged to my two unofficial supervisors Socrates Roussiakis and Clive Trueman. My good friend Socrates not only spend two summers with me in Kerassia digging and collecting material under the hot Greek sun but was helpful in countless ways. He allowed me to use his reprint collection and his advice and discussions on the giraffids were more than useful. Clive's help and advice, particularly at the very early stages of my project,

was not only important but also crucial for planning the final project. And wherever he was Clive always kept an eye on me making sure that everything was getting on well.

I would like to thank Constantin Doukas for his support and for authorising me to use in this project the material from the 1982 excavation. For the latter I also need to thank Hans de Bruijn and Albert van der Meulen. George Koufos is thanked for providing me with bone material from the localities of the Axios Valley. George Lyras is thanked for providing me with bone material from the locality of Kassandria. Mark Evans and the New Walk Museum in Leicester are thanked for providing me with bone material from the Pleistocene localities of Cotes and Quorn. Tony Gouldwell is thanked for providing me with recent bone material from the collections of the Archaeology Department.

David Siveter, Mark Purnell and Mike Norry are also thanked for their advice and useful discussions. I really appreciated Gary Mullins' help with the incomprehensible statistics and his digital camera, Richy Brown's tutorials on "hand-made" sediment logs and lifelong friend Nikos Karamitsos for his veterinary experties. I am also grateful to Denis Geraads, Nikos Solounias, Dimitris Kostopoulos, Athanassios Athanassiou, Dave Martill and Cristine Janis for providing me with key papers and useful discussions. I would like also to thank Jerry Hooker and Andy Currant from the Natural History Museum in London, Roger Smith from the South-African Museum in Capetown, William Simpson and Minh-Tho Schulenberg from the Field Museum in Chicago and Mike Dorling from Sedgwick Museum in Cambridge for their help and for providing access to the respective museum collections.

I sincerely thank all the members of the technical staff at the Department of Geology for their advice and help with the preparation and analyses of my bone samples and in particular: Rod Branson for helping me in my long SEM sessions and the dozens of quality photographs that he printed for me, Emma Mansley for helping me to put together the preparation protocol for bone apatite digestion and running the numerous samples on the ICP, Kevin Sharkey for helping me interpret the XRD results and running my samples twice, Colin Cunningham for preparing my polished thin sections (sorry Colin for my stinging bones...), Rob Wilson for his patience and his help with the temperamental electron microprobe, as well as Roy Clements, Steve Powell, Lin Marvin, Rob Kelly, Nick Marsh and Dave York who helped me all these years.

I would like to thank all the people from the village of Kerassia for their hospitality and their help and particularly the family of Kostas Georgakas. Also, I would be ungrateful not to thank all the people that have worked all these years in the excavations in Kerassia and in the preparation of the material and particularly Konstantina Agiadi.

Lots of thanks to my good friends in Greece Christos, Nikos, Sotiris, Alexandros, Vassilis and Yiannis that have supported me all these years through telephone calls and email messages and who would be very happy and proud for me right now. Lots of thanks to my good friends in Leicester and the Department of Geology for their support and friendship, including Wesley, Paul, Petar and his family, my ex-housemates Rachel and Dave, Patricio, Craig S., Craig B., Marky, Adel, Ann-Marie, Natalie, Heike, Gavin, Dave B., Andrew and my team-mates in the glorious 5-aside Geology team, Andy, Matt, Alex, Graham A., Tim, James T., James H. and James B. If I did forget to mention somebody that I ought to thank, it was not intentional and I do apologise. So lots of thanks to those I might have missed.

Finally I would like to thank my good friend and teacher, the late Costas Theocharopoulos who unfortunately left us so early and to whom I dedicate this work.

Introduction

GEOGRAPHY

Kerassia is a new Late Miocene mammal locality, located on the northern part of Euboea Island in Greece (Fig. 1). Euboea Island, the second largest Greek island after Crete, found to the northeast of the city of Athens, is separated from the mainland through a narrow sea channel. Kerassia is situated in the Limni-Istiea basin, the largest Neogene basin on Euboea Island which occupies the Northern part of the island. The actual fossiliferous locality (38° 55'N, 23° 19'E) is found 2 km north of the village of Kerassia, located on the south side of a gully (Fig. 2), at an altitude of about 450 meters.

GEOLOGY AND STRATIGRAPHY

The geology of Euboea Island has been well studied since the second half of the 19th century (Spratt 1847, 1856; Cordela 1878; Gorceix 1878; Teller 1880; Deprat 1904; Guernet 1971; Katsikatsos *et al.* 1986; De Bono, 1998). The southern part of the island is covered by HP/LT metamorphic rocks (Makrotandalou-Ochi unit, North Cyclades unit) and LP Mesozoic marbles (Almyropotamos unit) (De Bono, 1998). The central and northern parts of the island are dominated by the formations of the Pelagonian zone; a succession of metaplutonic rocks, Late Permian - Middle Triassic limestones, Middle - Late Triassic volcanoclastic sediments, Late Triassic – Late Jurassic limestones, Late Jurassic radiolarites (De Bono, 1998). During the Early Cretaceous the tectonic nappe of the Axios-originated ophiolites (Middle-Late Jurassic age) was obducted upon the carbonate platform and was followed by a transgression event and the deposition of Late Cretaceous limestones (De Bono, 1998). Nevertheless, there are also extensive Neogene deposits found on the island, the majority of which are of continental origin. These successions mainly occur in the three major sedimentary basins of the island (Fig. 1); the Aliveri-Kymi basin, the Palioura-Gides basin, and the Limni-Istiea basin (Katsikatsos *et al.*, 1981). A number of smaller size occurrences are of minor geographical and stratigraphical importance. However, an exception is the occurrence near Almyropotamos, because of the significant outcrops of fossil mammal remains. In general, the deposits in the three basins consist of a lower, low energy sequence with fine-grained

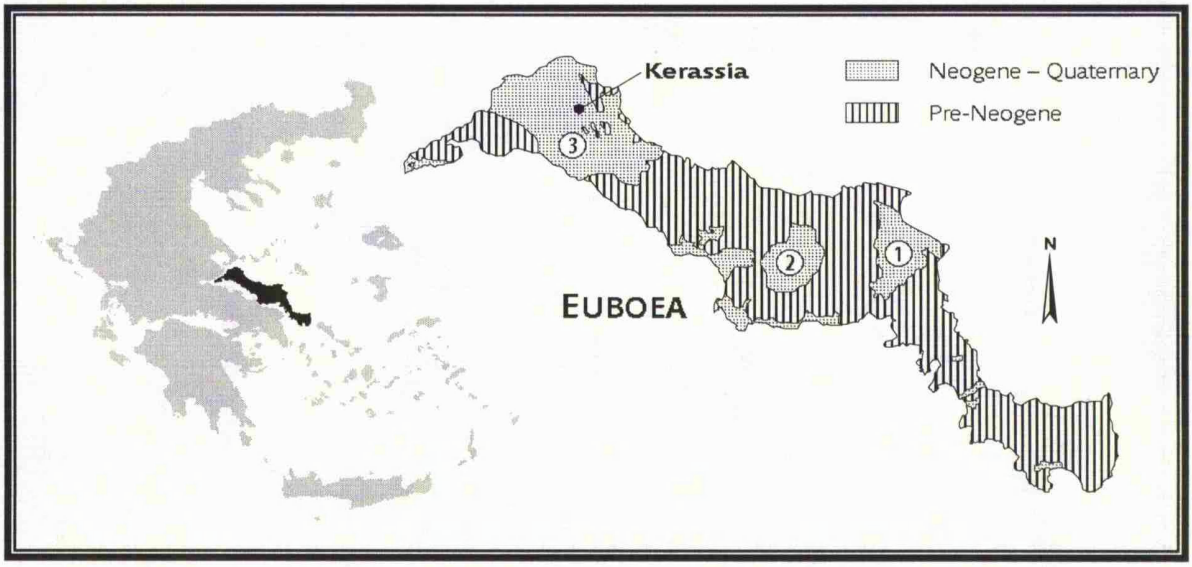

Figure 1: Location map showing Euboea Island and the locality of Kerassia. The distribution of Neogene-Quaternary and Preneogene rocks on Euboea Island, and the position of the three major Neogene basins on the island are also displayed: 1. Aliveri-Kymi basin, 2. Palioura-Gides basin, and 3. Limni-Istiea basin; adapted from Katsikatsos *et al.* (1981).

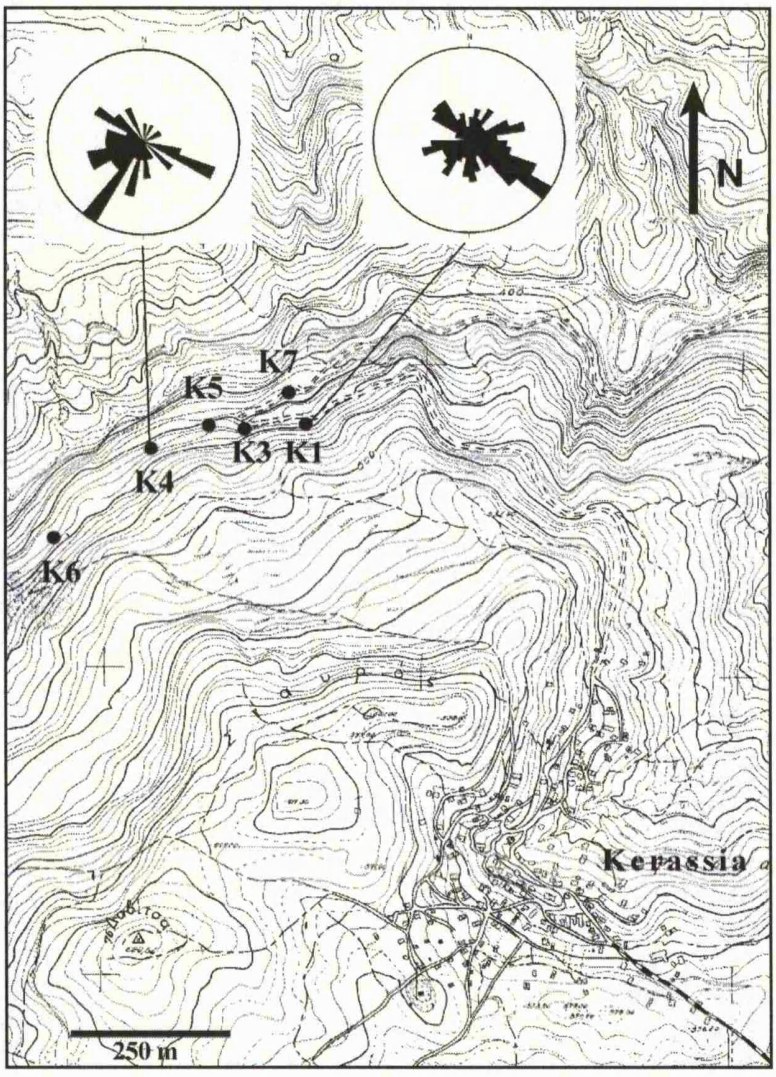

Figure 2: Location map with the exact position of the seven sites (K1 to K7) in the locality of Kerassia (38° 55'N, 23° 19'E), North of the village of Kerassia. The rose diagrams with the prevailing orientations of the long bones are also provided for the two main dig sites in the locality, sites K1 and K4, which depict the direction of the main palaeocurrents.

lacustrine sediments which locally contain lignite layers, and an upper high-energy sequence of coarse-grained fluvial sediments.

The Limni-Istiea basin occupies the largest part of Northern Euboea (Fig. 1). The Late Miocene - Late Pliocene sediments (sediments of the upper sequence), which have been deposited unconformably on the Early Miocene sediments of the lower sequence, cover most of the basin (Mettos *et al*, 1991). The occurrences of the sediments of the lower sequence are confined to the area between the villages of Agia Anna and Kerassia (Mettos *et al.*, 1991). According to Mettos *et al.* (1991) the sediments of the lower sequence consist of Early Miocene marls, silts, clays, and conglomerates, whereas the sediments of the Late Miocene sequence comprise four distinct sequences: a. the red-brown fluvial deposits, a succession of conglomerates, sands and clays of the Late Miocene which contain the mammal remains, b. the Agia Anna - Kerassia, marls, clays, travertines, marlstones of the Late Miocene, that contain fossil tree remains at the lower part of the travertine deposits, c. the Limni marls, conglomerates and marlstones of the Early Pliocene, and d. the Early Pliocene conglomerates of mount of Xiro that laterally transit to the marls and conglomerates of Istiea. Mettos *et al.* (1991) also reported that three tectonic phases can be observed in northern Euboea; one tensional phase of Miocene-Pliocene age with NE-SW trend; a second compressional phase during the Quaternary with NNW-SSE trend; and a third one with tear faults and horizontal, counter clock-wise movement, with N 100^{o}-120^{o} trend, probably of Late Pliocene or Early Pleistocene age. Due to the significant Neogene and Quaternary tectonism, a large number of faults run through the basin, and thus block displacements should be expected.

PREVIOUS WORK AND HISTORY OF RESEARCH

In 1835 Finlay and Lindermayer carried out the first excavation in Pikermi (Attica, Greece) bringing to light some of the richest outcrops of the Upper Miocene fauna (Turolian). For more than a century the richness and diversity of the fauna of the locality attracted the interest of many renowned workers (Wagner, 1840, 1848; Gaudry, 1862-67; Woodward, 1901; Abel, 1912; Symeonidis *et al.*, 1973) and the importance was such that Crusafont – Pairo (1951) coined the term 'Pikermian fauna' to describe the Eurasian Late Miocene faunas. Since then, numerous other large mammal localities of Late Miocene age have been added in the Greek fossil record (de Bonis and Koufos, 1999), with the localities of the Axios Valley and Samos as the most prominent.

A significant number of these Late Miocene localities are located on Euboea Island: the localities of Aliveri (De Bruijn *et al.*, 1979), Kazarma (De Bruijn *et al*, 1979), Panagia Heria (Deprat, 1904; Mitzopoulos, 1947) and Almyropotamos (Melentis, 1967, 1969) are found in the central part of the island, whereas, the localities of Limni (Cordella, 1878), Ahmet Aga (Prokopi) (Woodward, 1901), Achladi (Mitzopoulos, 1947) and Palaeovrisi (Jacobi, 1982) are situated on the northern part of the island.

The locality of Kerassia (Fig. 2) was made known to the local people in 1966 during the cutting of a new road north of the village. In 1981, R.W. Kohler, a German student, tracked down the locality during his dissertation fieldwork. A year later Hans de Bruijn and Albert van de Meulen (University of Utrecht) and Constantin Doukas (University of Athens) carried out the first excavation. The exact locality of this first collection is not known, as there are no available data about the excavation. The material from this excavation is still unpublished and was kindly offered to me for study. Made and Moya-Sola (1989) in their paper on the European Suinae provided a brief description on the suids and the first biostratigraphic data for the locality of Kerassia (probably using material from the 1982 excavation), though the exact locality and the date of collection are not stated clearly. They considered that the suid material belongs to *Microstonyx major erymanthius* and determined the age of the locality as Middle Turolian (MN 12). In their study, Kostopoulos *et al.* (2001) after comparing the suid material from the 1982 excavation, argued that this belongs to a small sized form, related with the Maragha suid, which probably can be ascribed to a new subspecies different from the typical and larger *M. major erymanthius*. According to their data, they also considered that the age of the locality is Middle Turolian (MN 12).

Since 1992 Associate Professor Theodorou from the University of Athens has conducted systematic excavations in the locality. The excavations have been financed by the University of Athens, the local Municipality and the Council of Research and Technology. To date, more than 2000 specimens of large mammals have been recovered from the seven fossiliferous sites in the locality and have been prepared, although, a significant portion of the material is still under preparation. Currently, all the excavated material from Kerassia, including the material from the 1982 excavation, is temporarily stored in the collections of the Museum of Palaeontology and Geology of the National and Kapodistrian University of Athens, Greece. The excavated material has revealed the presence of a rich Late Miocene "Pikermian" fauna. Theodorou *et al.* (2003) provided the first preliminary data on the sedimentological setting and the faunal content of the locality. Roussiakis and Theodorou (2003) described the

carnivore material from the locality. According to their data the age of the locality is Turolian and probably belongs to MN 11-12.

During the last ten years, ten field periods have been conducted in the locality of Kerassia. Since 1994, I was fortunate to be present in eight out of the ten field periods when the majority of the material was collected. During these ten years I have helped not only in the excavation of the material but also in the preparation and the conservation of hundreds of specimens and their preliminary identification, and the collection of taphonomic data. Cataloguing the specimens has also been one of my tasks. In the three years of my PhD, my research project involved two field periods in Kerassia for collection of sedimentological data from the seven localities of Kerassia and collection of fossil specimens and taphonomic data primarily from site K1. Several hundreds of specimens were collected during these two field periods. In addition to my other research tasks, the preparation and conservation of the majority of these specimens was also undertaken. The preparation and conservation of this material took place in the Department of Geology at the University of Athens and in the Department of Geology at the University of Leicester.

THE STRATIGRAPHY AND SEDIMENTOLOGY OF KERASSIA

In Kerassia the bone bearing layers are part of the so called red-brown fluvial deposits which comprise the lower layers of the upper sequence (Mettos *et al.* 1991). According to Mettos *et al.* (1991) in the Limni-Istiea basin the lower sequence occurs between the villages of Agia Anna and Kerassia. The sediments of the lower sequence and also their contact with the basement of the basin were located to the northeast of the village of Kerassia. Successions of marls, clays, siltstones and conglomerates were observed, indicating a low energy environment of deposition, probably lacustrine. In this part of the basin the basement rocks are the Axios ophiolites, part of the Early Cretaceous tectonic nappe of the Pelagonian zone (see above). In succession above the sediments of the lower sequence, the red-brown fluvial deposits occur; red-brown clays, conglomerates, sands, and siltstones. The thickness of these sediments ranges between 250-300 meters (Mettos *et al.,* 1991). Nevertheless, the exact location of the unconformity between the two sequences was not traced because of the presence of debris, overgrowth and faulting. The Agia Anna-Kerassia marls, clays, travertines and marlstones are situated to the northwest, west and south of the village of Kerassia, at the lower parts of which fossil trees are found. The surrounding rocks to the North and East of the

locality also consist of ophiolites. Apart from the ophiolites, a few exposures of Jurassic limestones of the Pelagonian unit (*sensu stricto*) also occur south of the village of Kerassia.

The collected fossil mammal material comes from seven different sites (Fig. 2) in the locality, namely K1 to K7, where separate lenses of bone beds are found, deposited in different fluvial channels. The sections of the seven sites and the respective bone outcrops are found across roadside cuttings. Sites K1 and K2 are located in the same undisturbed section which apparently comprises the longest exposed section. From this section it is obvious that there are two fossiliferous layers. The upper fossiliferous layer (K1) lies 6.7 meters above the lower fossiliferous layer (K2), which is found at the level of the road (Fig. 3). K1 was excavated for the first time in the summer of 2000 and most likely comprises the site of the very first collection in 1982. Personal communication with Doukas (2000), a map by Kohler (1983), the state of fossilization of the material, and in addition geochemical data suggest that the collected material of the 1982 excavation came from site K1. At this site a dense concentration of bones occurs in the lower part of the layer. The fossil bones become more scarce and scattered in the middle and disappear towards the top of the layer. Ten centimetres above the contact of the fossiliferous layer, a distinct continuous grey white, thin (2cm thick) bed of brown clays and white marl nodules occurs (Fig. 3). The same thin bed is also traced in site K6 above the fossiliferous layer (Fig. 3), where the recovered material only consists of a big mastodon tusk (*Choerolophodon sp.*). The normalised REE concentration patterns for the sediments of the two beds are practically identical. Therefore, K1 and K6 probably belong to the same fossiliferous layer, the upper one, and the position of the tusk can be attributed to the middle of the layer with the scattered bones.

At site K3 the different beds in the section are clear and well defined due to a relatively fresh road cut. In this section only one fossiliferous layer can be observed, the lower one. Right above the fossiliferous layer there is a distinct, 50 cm thick, red-brown mud bed with distinct perpendicular cracks (Fig. 3). This characteristic bed can be observed in the K1- K2 section right above the lower fossiliferous layer (K2). Also, the sedimentological characters of the lower fossiliferous layer in K2 are exactly the same as in K3. Brown silted mud with few scattered rounded to sub-rounded, polymict grains in a homogenous matrix, and a deep calcitic horizon that occurs at the same level as the bonebeds with significant encrustations around the bones. Sites K2 and K3 are located relatively close to each other (35 meters) in the same undisturbed section and there is no doubt that they belong to the same stratigraphic level. Site K4 shares similar lithologies with sites K2 and K3: the distinct red-brown bed

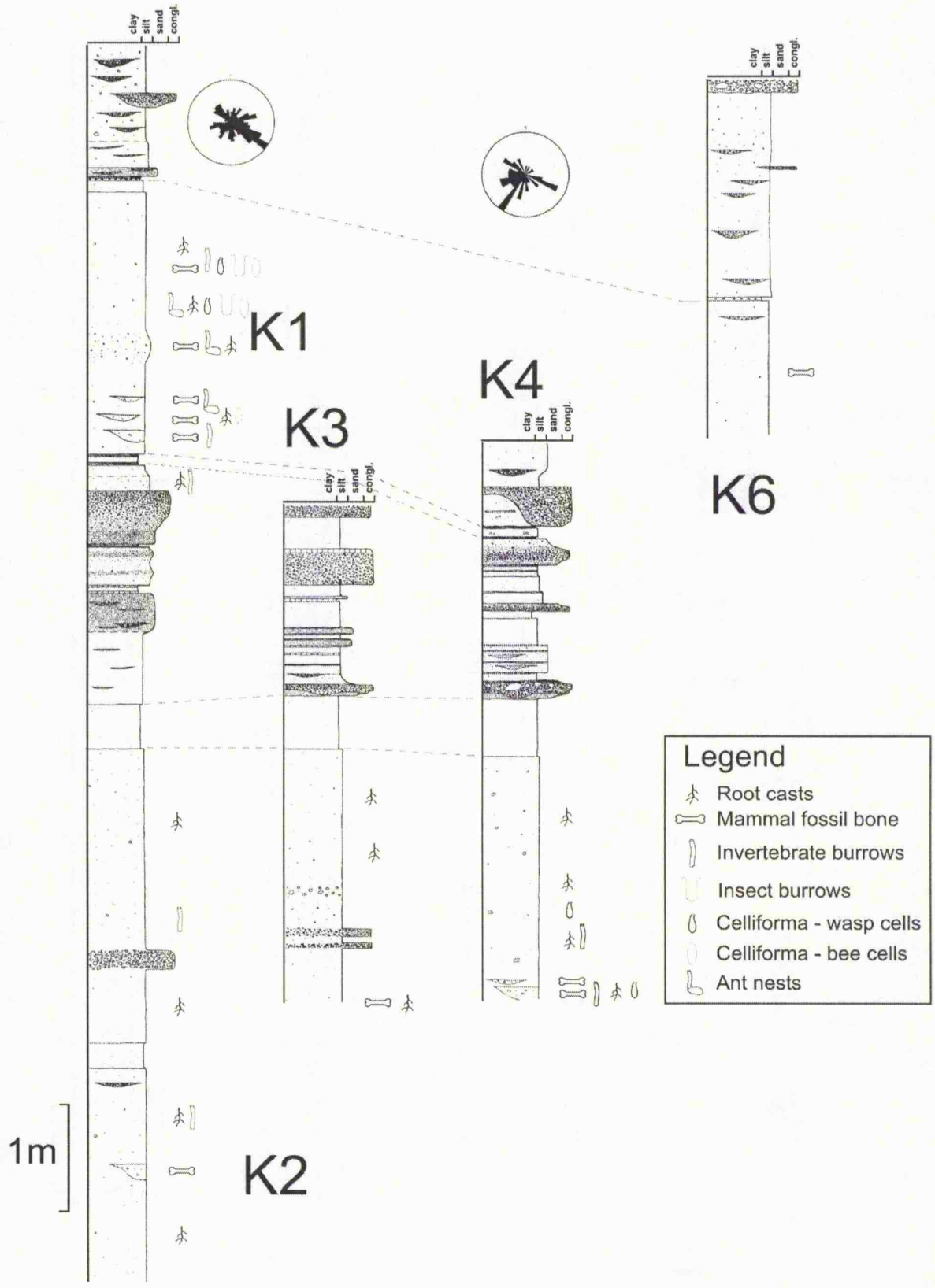

Figure 3: Stratigraphical logs of sections from sites K1-K2, K3, K4 and K6. Rose diagrams with the prevailing orientations of long bones from the two main dig sites in the locality, sites K1 and K4, are also provided.

above the fossiliferous layer, the sedimentological characters of the bone bearing layer and a similar degree of calcification and encrustations around the bones (Fig. 3). In the upper fossiliferous layer the calcitic horizon is also deep, but the calcification is less and the encrustations around the bone are imperceptible. In addition, the similar state of preservation of the bone material from sites K2, K3 and K4 which is clearly different from that of the upper horizon and geochemical data indicate that K2, K3 and K4 represent the same fossiliferous level, the lower one.

Sites K5 and K7 are not correlated to date with either the upper or the lower fossiliferous level. Both bone-bearing layers (K5 and K7) seem to have high-energy deposits with increased percentage and size of pebbles in the sediments compared with the other sites. At site K5 in particular, the presence of high-energy channel deposits is evident. There are clear indications for bone sorting as the majority of the collected material consists of skulls, mandibles and large bones. Also, some of the extracted bone material shows significant abrasion marks. The 2 meters exposure at site K5 cannot provide very accurate correlations. However, the position of the site, the similarities in the state of preservation of the bone material with the bones from the lower horizon, and despite some differences in the geochemical data (chapter 3) which can be attributed to the different hydrological regimes, it can be assumed that site K5 belongs to the same stratigraphic level as sites K2, K3 and K4. As for site K7, the collected material is still under preparation; therefore, data that could provide further correlations is not complete. Site K7 is found about 15 meters below the level of sites K2 and K3. A large number of faults run through the basin and block displacements are expected. Therefore, if a displacement occurred, K7 could possibly be correlated with the lower or the upper fossiliferous levels, or if no displacement occurred K7 constitutes a third fossiliferous level, older than the other two.

In sites K1-K2, K3, K4 and K6 it is clear that typical pedogenic features are present and thus some of the beds represent well developed paleosols (Fig. 3). In the longest studied section from sites K1-K2 at least three different paleosols sequences can be identified: one at the top, one in the middle and one at the bottom. The one at the top and the one at the bottom are related to the two fossiliferous horizons. These sequences are interrupted by fluvial channels and the deposition of coarser grained deposits (Fig. 3). The bone bearing fluvial channels belong to this category and their relative position is at the bottom of the respective paleosol sequences. These sequences mainly consist of B horizons. The beds that form these sequences are red-brown, carbonate rich silty muds with deep calcic horizons which consist of nodular

carbonates and calcitic encrustations around bones. These calcareous horizons are interpreted as the Bk horizons. Non calcareous clay-rich zones are also found and probably comprise the Bt horizons. The thin red mud beds at the top of each sequence probably represent the organic rich humic horizons. These horizons are not present in every sequence, possibly indicating small scale erosion events. Thin laminar calcrete bands are found in the middle paleosol sequence indicating possibly drier periods. According to Retallack (1990, 1997) the preceding features of these paleosols are characteristic of alfisols.

The majority of the major beds in the seven sites, including the bone bearing ones, consist of red-brown silty muds with scattered rounded to sub-rounded, polymict grains, mainly of ophiolitic origin in a homogenous matrix. This observation suggests that the rock source which provided the deposited sediments was an ophiolite.

Apart from the mammal fossil remains, a significant number of trace fossils in the form of root casts and insect or other invertebrate burrows were also identified in the B horizons. Such trace fossils are good indicators of paleosols. Oxidising and alkaline soils like the paleosols of Kerassia (chapter 3) may contain abundant evidence of life in the form of burrows and roots. These features indicate stable ground surface conditions for a rather long period to allow the growth of plants, and the exploitation of the soil by insects and other invertebrates. Thus, this constitutes evidence for the maturity of the soils. The majority of the observed and the collected burrows belong to three groups of the Hymenoptera; ant nests (Formicidae), solitary bee larval chambers (Apoidae) and solitary wasp larval chambers (Fig. 4). The bee and wasp larval chambers are attributed to the ichnogenus *Celliforma* (Brown, 1934). The bee chambers are ellipsoid, whereas the wasp chambers are tear-shaped with a wide rounded base and a thin neck (Fig. 4). The ant nests consist mostly of long vertical burrows and irregular shaped chambers found at the bottom of the burrows or at variable heights. According to Michener (1974) the chambers of solitary digging bees (Halictinae) have to occur in sediments moist enough in order to be easily worked and humid enough for the survival of the larvae. Possibly the same conditions are also required for the construction of chambers by solitary wasps. Ants also require relatively moist soil conditions for their survival (Dumpert, 1978)

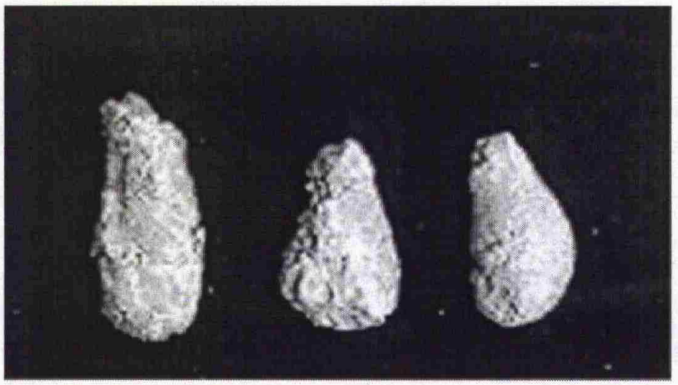

Figure 4: Three internal moulds of wasp larval chambers (*Celliforma sp.*).Scale: ×2.

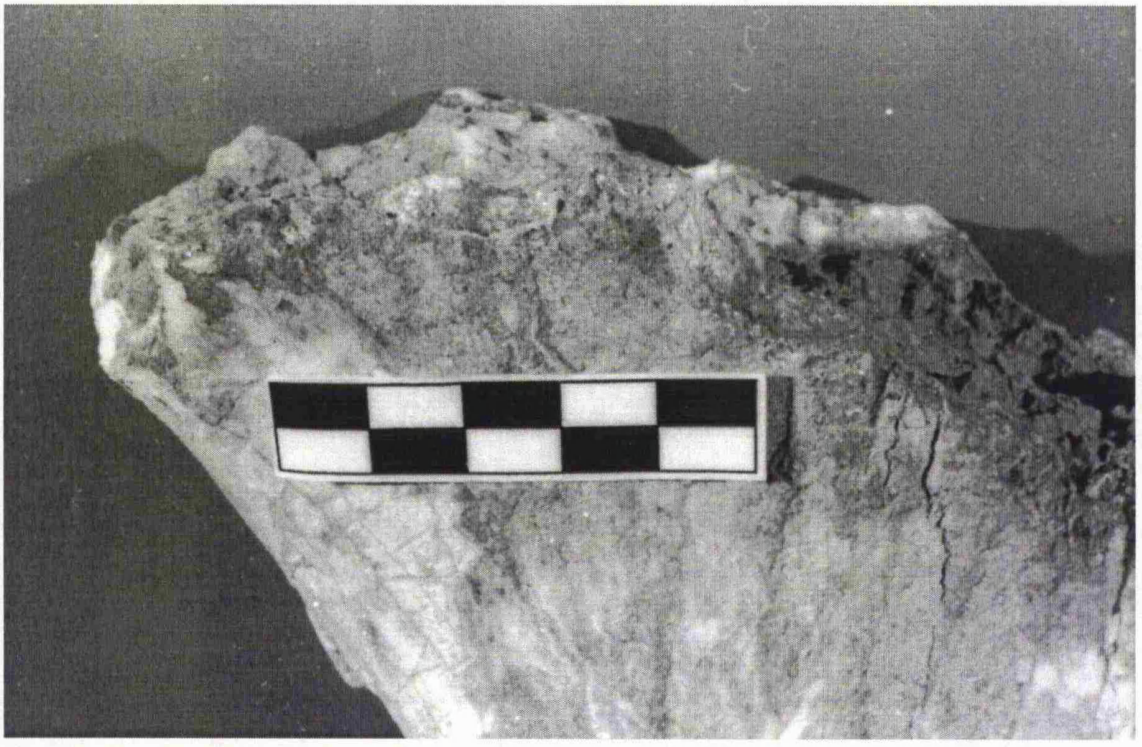

Figure 5: The upper portion of a Rhinoceros humerus shaft with crenulated edges, probably produced by the gnawing action of hyaenas. Scale = 5cm.

THE KERASSIA FAUNA

The Kerassia fauna mainly consists of Perissodactyla (Equidae, Rhinocerotidae) and Artiodactyla (Bovidae, Giraffidae), with *Hipparion* being the most abundant genus. Despite the dominance of the *Hipparion* and secondarily of the bovids, the number of collected specimens from the two taxa is proportionally less compared with the other Late Miocene Greek localities (Theodorou *et al.*, 2003). Carnivores and Proboscidea are also present, and a few more taxa are represented only by rare occurences number of specimens (Roussiakis and Theodorou, 2003; Theodorou *et al.*, 2003). The faunal content of the two fossiliferous layers is given in Table 1. For the moment, the collected material from site K5 can be attributed only to two taxa *Hipparion sp.* and Rhinocerotidae (Rhinocerotidae sp. indet). The material from site K7 is still under preparation and has not been studied yet.

TAPHONOMY

The taphonomic study of the exposed and collected material showed that a variety of pre-burial and post-burial processes affected the bones and teeth of Kerassia. Significant modifications were observed in the vast majority of the examined specimens. Extensive weathering cracks indicate that the bones were exposed on the surface of the ground for a significant period of time. Gnawing marks including spiral fractures, tooth marks, perforations, crenulated shafts (Fig. 5), gnawed epiphycal ends and channelled long bones suggest extensive exploitation of the bones and scavenging by carnivores (mainly by hyaenas). Partly articulated, partly associated and mostly dispersed skeletal parts indicate that transportation and dispersal of the skeletal elements occurred. Abraded specimens and sorting in site K5 evince higher energy currents and longer transportation. The bones were accumulated within fluvial channels and possibly represent channel fill deposits (Behrensmeyer, 1988) of short duration. The orientations of the long bones from all sites show some preferred orientations that can possibly be related to the directions of the paleocurrents. In site K1, the easternmost site in the locality, the main orientation of the bones is northwest – southeast, whilst, the main orientation of the bones in site K4, located at the west part of the locality, is northeast – southwest (Figs. 2, 3). Generally, the prevailing orientation of the long bones is north-south indicating a water flow from north to south. This observation agrees with the ophiolitic origin of the clasts in the sediments and the position of the surrounding ophiolitic rocks north of the locality. A number of post-burial processes also

Upper fossiliferous layer	Lower fossiliferous layer
Artiodactyla	Artiodactyla
Giraffidae	Giraffidae
Helladotherium duvernoyi	*Helladotherium duvernoyi.*
Palaeotragus rouenii	*Palaeotragus rouenii*
Bohlinia attica	*Samotherium major*
Samotherium major	Bovidae
Bovidae	*Gazella capricornis*
Gazella capricornis	4-5 other bovid species
Tragoportax cf. amalthea	
2-3 other bovid species	Perissodactyla
Tragulidae	Equidae
Dorcatherium sp.	*Hipparion sp.* (2 species)
Suidae	Rhinocerotidae
Microstonyx major erymanthius	*Ceratotherium neumayri*
	Dicerorhinus cf. pikermiensis
Perissodactyla	Rhinocerotidae sp. nova
Equidae	Chalirotheriidae
Hipparion sp. (2 species)	*Ancylotherium sp.*
Rhinocerotidae	
Rhinocerotidae sp. indet.	Proboscidea
Chalicotheriidae	Deinotheriidae
Ancylotherium sp.	*Deinotherium sp.?*
	Mastodontidae
Proboscidea	*Mastodon sp.*
Deinotheriidae	*Tetralophodon cf. longirostris*
Deinotherium sp.	
Mastodontidae	Carnivores
Mastodon sp.	Felidae
Choerolophodon sp.	*Machairodus giganteus*
	Hyenidae
Carnivores	*Adcrocuta eximia*
Felidae	*Hyenotherium wongii?*
Metailurus parvulus	*Or H. cf pannonicum*
Hyenidae	Small carnivore
Adcrocuta eximia?	Viverridae
Hyenotherium wongii	*Plioviverrops sp.*
Small carnivore	
	Aves
Tubulidentata	Genus and species indet.
Orycteropus gaudryi	
Micromammal	
Genus and species indet.	

Table 1: The faunal content in the two fossiliferous levels; sites K1 and K6 belong to the upper fossiliferous level, sites K2, K3, K4 and possibly K5 belong to the lower level.

affected the bones and teeth. Extensive microbial damage was observed in the majority of the examined specimens (chapter 1). Seismoturbation and faulting caused the post burial fracturing of some bones. Finally, a number of diagenetic changes occurred, altering the overall chemistry of the original bone and tooth tissues mineral phase (chapters 2 and 3).

OBJECTIVES OF PRESENT STUDY

My PhD project is multidisciplinary in nature. The main aim of this study has been to provide the first complete documentation of the mammal bonebeds found in the locality of Kerassia by tackling aspects of stratigraphy, palaeontology and taphonomy (Fig.1). An ecologically important family, the Giraffidae, was selected for study as the collected giraffid material presented notable diversity and thus could provide significant ecological, palaeoenvironmental and biostratigraphic information. The taphonomic study of Kerassia has been focused firstly in the study of the remarkable and extensive microbial damage observed in the bones and teeth. In addition, the early diagenetic conditions that influenced the preservation of these bones and teeth and the geochemical changes that occurred in these tissues was investigated. Finally, the results from the three distinct disciplines will be compiled to provide information about the palaeoenvironmental conditions that prevailed during the Late Miocene in Kerassia.

THESIS LAYOUT

This thesis consists of four distinct, separate and autonomous thematic units structured in a format that will be suitable for publication. Consequently, repetition of descriptive introductory information about the locality, the geology and the stratigraphy of the locality, does occur. The first chapter entitled "Extensive microbial destruction in Late Miocene mammal bone" has been accepted for publication in the *Journal of the Geological Society*. It provides information about the structure and mechanisms behind the formation of bacterial bioerosion structures and interpretations about the palaeoclimate and the palaeoenvironment. The second chapter with the title "X-ray emission microanalysis of bacterially damaged bones and teeth from the Late Miocene of Kerassia, Greece" will be submitted for publication to an international palaeontology or interdisciplinary geology journal. This chapter elaborates geochemical data from bacterially damaged bones and teeth collected using an electron

microprobe, and identifies the changes in the distribution of elements that occur in the bioeroded hard tissues. The third chapter is entitled "X-Ray Diffraction studies of Late Miocene mammal bones and teeth" and will be submitted for publication to an international palaeontology or interdisciplinary geology journal. In this chapter the mineralogy and crystallinity of fossil bone, dentine and enamel is discussed. Finally, the fourth chapter is entitled "The Giraffidae (Artiodactyla, Mammalia) from the Late Miocene of Kerassia, Northern Euboea Island, Greece" and has been prepared for publication in the *Special Papers in Palaeontology*. This chapter presents the taxonomical and morphological features of five species of giraffes and their palaeoecological and palaeoenvironmental requirements.
One additional paper which comprised part of my PhD studies has been already published:

"Theodorou, G., Athanassiou, A., Roussiakis, S. & Iliopoulos, G., (2003), Preliminary remarks on the Late Miocene herbivores of Kerassiá (Northern Euboea, Greece), *Deinsea*, v. 10, p. 519-530."

My contribution to this paper has been the sedimentological study of the seven sites in the locality of Kerassia, and the stratigraphic correlations between these sites and also, the description of two groups of the fauna, the Giraffidae and the Bovidae.

Extensive microbial destruction in Late Miocene mammal bone

INTRODUCTION

A number of physical, chemical and biological processes determine an organism's fossilization potential and preservation. Bio-mineralized tissues of organisms are generally more resistant than the non-mineralized tissues but they are still subject to deterioration and to destructive processes. Bones and teeth, the hard tissues of vertebrates, are not excluded. According to the established ideas of bone preservation, bones that exhibit considerable microbial damage would have no chance (Grupe, 2001) or little chance (Trueman and Martill, 2002; Hedges, 2002) of turning into fossils. However, the histological study of Late Miocene mammal bones herein has revealed for the first time that well-preserved fossil bone can be extensively bioeroded.

Vertebrate hard tissues are complex materials consisting of interdependent organic and mineral inorganic components. Four mineralised hard tissues are generally recognised in advanced vertebrates (including mammals) namely bone, dentine, cement and enamel; the last three of which represent dental tissues. Approximately, the mineral component in the bone constitutes 72% of its weight, while the organic component is 20% and the remaining 8% is water (Elliott, 2002; Price, 1989). 90% of the organic component is collagen and 10% is non-collagenous proteins, lipids and carbohydrates (Price, 1989; Cormack, 1987). Despite minor variations it could be assumed that dentine and cement have a similar composition to bone (Carlson, 1990; Elliott, 2002). In enamel, on the other hand, the apatite component is about 97%, the organic component is less than 1%, and the remaining percentage is water (Carlson, 1990; Elliott, 2002). Microbes are the primary decomposers of organic matter and will readily attack bones and teeth to feed on their organic components. Hackett (1981) coined the term microscopical focal destruction (MFD) to describe the histomorphological alterations in bone or other vertebrate hard tissues that are produced by microbial action. This damage can be attributed either to bacteria (Hackett, 1981), fungi (Wedl, 1864), algae (Davis, 1997) or protozoa (Ascenzi and Silvestrini, 1984). These organisms invade the bone producing recognisable destructive features in the form of tunnels or borings. These features have been known since the second half of the 19th century and were originally recognised in fossil specimens (Wedl, 1864; Roux, 1887; Schaffer, 1889; Thomasset, 1931), but later the majority of descriptions were of modern and archaeological material (Morgenthaler and Baud, 1956;

Werelds, 1962; Marchiafava *et al.*, 1974; Herrmann, 1977; Baud and Lacotte, 1984; Piepenbrink, 1986; Hanson and Buikstra, 1987; Bell, 1990;Yoshino *et al.*, 1991; Bell *et al.*, 1991; Child *et al.*, 1993; Bell *et al.*, 1996; Davis, 1997; Jackes *et al.*, 2001; Turner-Walker and Syversen, 2002; Turner-Walker *et al.*, 2002).

According to Nielsen-Marsh *et al.* (2000) groundwater is the most influential agent of bone diagenesis. Groundwater is the required medium for most post-burial processes and the catalyst for chemical reactions (Hedges and Millard, 1995; Nielsen-March *et al.*, 2000). The porosity of the different tissues will influence the action of groundwater (Hedges *et al.*, 1995). In bone, dentine and cement the intimate association between the mineral phase and collagen provides the means to protect the whole tissue (Lucas and Prevot, 1991): collagen protects apatite crystallites from the dissolving action of water (Trueman and Martill, 2002) and concomitantly the crystallites protect collagen from the hydrolytic action of microbial enzymes (Nielsen-Marsh *et al.*, 2000). However, once this bond is broken alteration or deterioration of the tissues will occur and their porosity will increase. Increased porosity allows more water to flow through the tissues, so that more apatite crystallite surfaces are exposed, and consequently the overall reactivity of the system increases (Nielsen-March *et al.,* 2000). The tunnelling action of microorganisms will greatly promote the porosity of the tissues (Nielsen-March and Hedges, 1999) and will accelerate their diagenetic alteration. The increase in the porosity will ease water flow which subsequently will facilitate microbial development and will aid the proliferation of the microorganisms' tunnels by bringing in more oxygen and removing toxic metabolic by-products. Thus, once microbial activity commences, and under favourable conditions, it will proceed rapidly to the total destruction of the affected tissues (Trueman and Martill, 2002). Extensive tunnelling and consequently high porosities will promote the dissolution of the tissues' apatite mineral. Furthermore, extensive tunnelling and significant increase in the pore volume of the tissues will reduce the tensile strength of the tissues (Turner-Walker and Parry, 1995); this reduction will facilitate further deterioration. To date, evidence from the archaeological (Grupe, 2001; Hedges, 2002) and the palaeontological (Trueman and Martill, 2002) "fossil" record shows that extensively bioeroded vertebrate tissues will readily deteriorate, and most likely will be removed from the fossil record.

In this study, the histological investigation of Late Miocene mammal bones and teeth has shown that, contrary to previous opinions (Grupe, 2001; Hedges, 2002; Trueman and Martill, 2002), extensively bioeroded bones and teeth have been preserved. The aim of this paper is

firstly to provide evidence that extensively bioeroded bones and teeth under favourable burial conditions can actually survive in the fossil record. Secondly, an attempt is made to determine the microorganism responsible for this destruction. Finally, the mechanisms and the burial and climatic conditions that favoured microbial activity and the preservation of histological and bioerosion features in the examined bone and tooth tissues are investigated.

MATERIAL AND METHODS

The studied material comes from a new Late Miocene (Early Turolian) mammal locality, Kerassia, in Greece. Kerassia is located in the northern part of Euboea Island. Seven different fossiliferous sites are known, and two fossiliferous horizons have been recognised (Theodorou *et al.*, 2003). The bone-bearing layers consist of red-brown silts and clays and the bones were accumulated within fluvial channels. Polished thin sections of fossil bone and teeth specimens, as well as fragments of bone and teeth from both horizons of Kerassia were prepared. Bones from eight other localities around the Aegean Sea were studied in the same way for comparison with the Kerassia specimens. Ravin de la Plui 2, Vathylakkos 1, Ditiko 1 and Ditiko 2 are situated to the north in Macedonia, Samos to the East on Samos Island, whereas Old Pikermi, New Pikermi and Chalkoutsi are from the south close to Athens. Stratigraphically, they range from the Late Vallesian (Ravin de la Plui) to the late Turolian (Ditiko). The specimens from Kerassia were collected from five localities representing both fossiliferous horizons, and from different areas in the bone accumulations, those from the Late Miocene localities were randomly selected. Two specimens represent bones found scattered above the main bone accumulations of the upper horizon at Kerassia. Specimens were examined using an Hitachi S 520 scanning-electron microscope (SEM) and probed under a JEOL JXA 8600-S electron-microprobe where a focused beam at 15kV was used for analyses. Electron microprobe analysis was employed to determine the elemental composition of bone, dentine, cement and enamel apatite in the unaltered parts of the tissues, as well as in the rims and the interior of the destructive foci (microscopic areas of damaged bone).

RESULTS

Extensive MFD was identified in every examined bone and tooth specimen from the main bone assemblages of both horizons at Kerassia (Fig. 1a, 1b). However, microbial action was not observed in the scattered bones examined from above the upper horizon.

Despite extensive MFD, Haversian systems are still clear and the foci can be easily identified around them. Zones of damaged bone occur around the bone perimeter, around the marrow cavity and as randomly scattered foci. Evidence indicates that the microorganisms attacked the bone from the external surfaces as well as from the marrow cavity, and through bone cavities such as the osteon canals. It has been observed that the majority of the foci follow the development of the bone lamellae and in longitudinal section they are parallel to the structures of the bone. In transverse section, the foci are clearly seen to follow the development of the lamellae around the Haversian canal (Fig. 2a). Most foci are rounded in transverse section although irregular shapes are common (Fig. 2a). Crescentic forms can be also found around Haversian systems (Fig. 2a). The pattern of damaged bone seen in the Kerassia specimens is similar to that described by Hackett (1981) as lamellate foci. The size of the foci ranges between 10 μm and 200 μm and may be as much as 300 μm, although the majority of the foci are shorter than 100 μm. The borders of most, but not all, foci are confined by relatively thick rims (Fig. 2a, 2b), distinguishable as bright areas in SEM backscattered images owing to a relatively higher mineral density caused by a hypermineralization process. The width of these bright rims is between 2-10μm. The internal structure of the foci, seen at high magnification (>2000 times), consists of a number of randomly distributed tiny holes and elongated tubules – essentially representing a network of microtunnels (Fig. 2b, 5a). Conversely, in longitudinal section the majority of the elliptically shaped foci are elongated and usually shorter than 300 μm, with rare examples reaching 500 μm (Fig. 3a). Microtunnels, 150-600 nm in diameter, are also visible, streaming across the foci, parallel to each other and parallel to the elongated foci (Fig. 5b). A few larger tunnel may get up to 900 nm, but the majority range between 300-600 nm. In some specimens it is possible to divide the foci into two size groups that are distinct within any given specimen: foci with microtunnel diameters between 300-600 nm, and foci with microtunnel diameters between 150-400 nm (Fig. 3b). As well as Haversian systems, other histological features of the bones such as lacunae (Fig. 2a, 2b) and even finer structures like canaliculi have been preserved. The striking feature is that in the damaged bone, lacunae are not found only around the foci but also in the foci. In some of the examined specimens, especially around the perimeter of the bone, some foci appear dark and "empty"

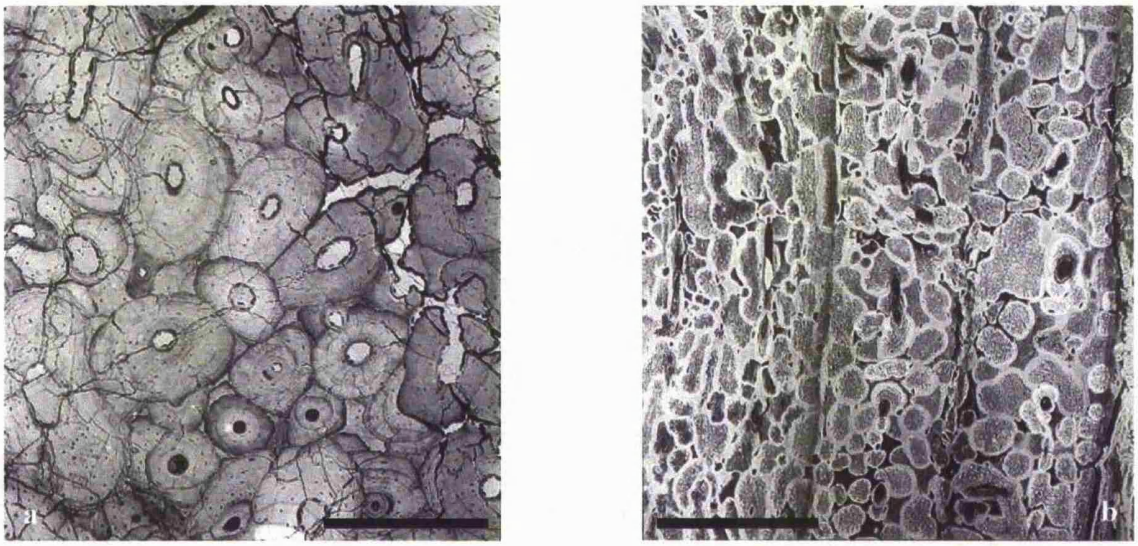

Figure 1. a. Backscattered electron image (BEI) of unaltered (undamaged) cortical bone (undetermined long bone fragment from site K1, thin section GI15A), displaying well preserved Haversian systems with lacunae around them, (scale bar 500 μm). **b.** The displayed portion of compact bone (undetermined long bone fragment from site K5, thin section GI18A) is extensively damaged, illustrating the extent of bacterial destruction of the bone tissue. However, Haversian systems are still clear and the foci of bacterially eroded bone can be easily identified around the Haversian canals, BEI (scale bar 231 μm).

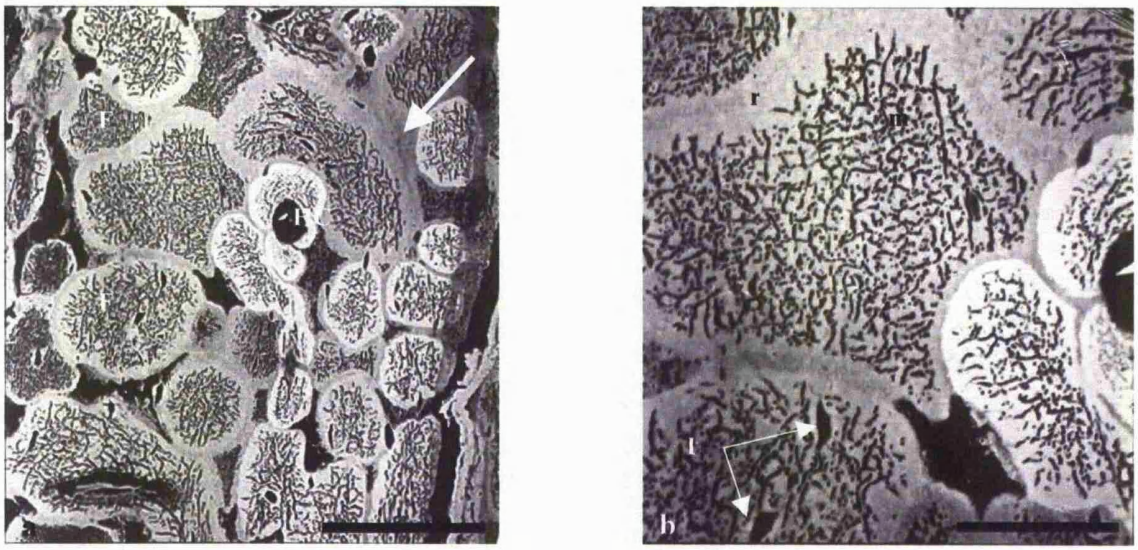

Figure 2. a. Lamellar bone around a Haversian system (seen in the lower left corner of Figure 1.b) completely damaged by bacterial activity. Foci of bacterially eroded bone are evident around the Haversian canal. The arrow points to the only portion of bone that remained undamaged. F=focus, HC=Haversian canal, BEI (scale bar= 75 μm). **b**. The area on the left of the Haversian canal in Figure 2.a. The structure of the foci is revealed at higher magnifications, the distinctive rims (r) of the foci and the microtunnel (m) network of the invading bacteria. Interestingly, some lacunae (L) are situated in the foci, BEI (scale bar= 30μm).

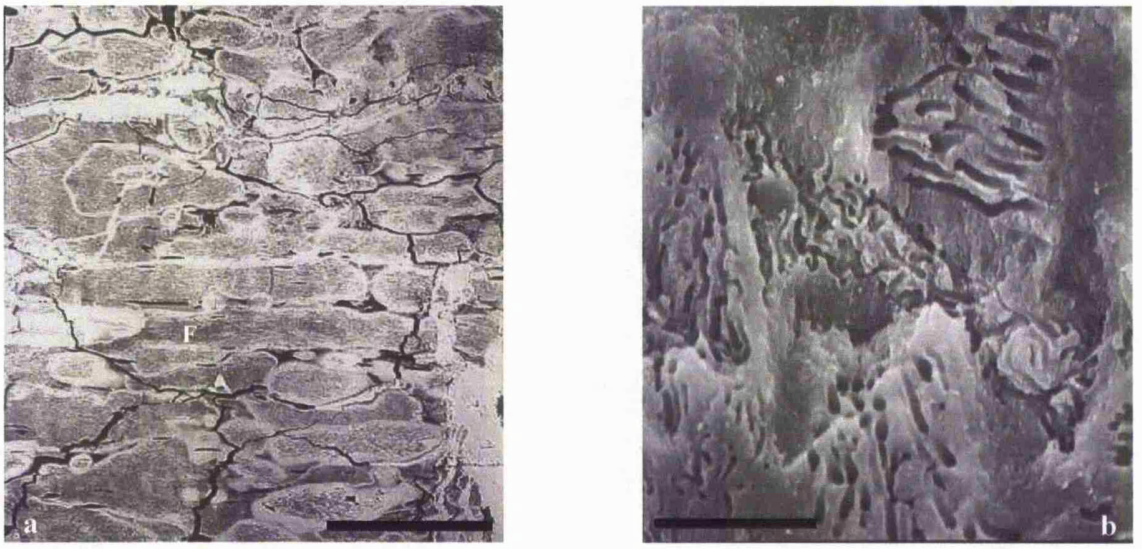

Figure 3. a. Longitudinal section of bone cortex (undetermined long bone fragment from site K5, thin section GI18B), showing elongated and elliptically shaped foci. The bright hypermineralized rims are visible around the foci. F=focus, BEI (scale bar= 150 μm). **b.** Fragment of bone (undetermined long bone fragment from site K1, specimen K1/Δ68, stub 24) on stub, showing neighbouring foci with ostensible differences in the diameter of their microtunnels which can be attributed to a small-size and a large-size microtunnel groups and which possibly correspond to two different species of bacteria, SEM (scale bar= 10 μm).

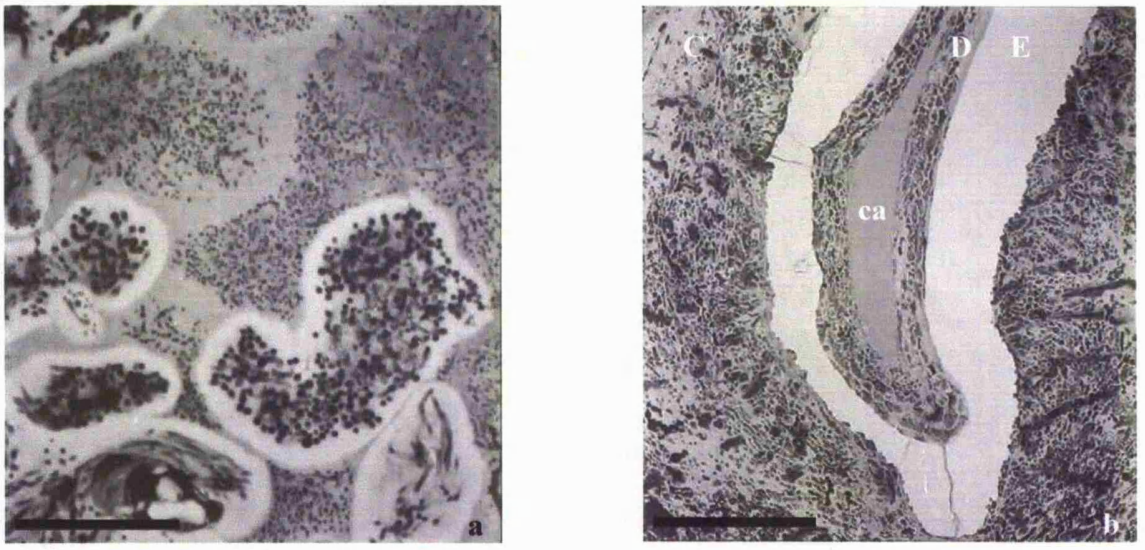

Figure 4. a. Portion of bacterially damaged bone (undetermined long bone fragment from site K1, specimen K1/Δ68, thin section GI24A), showing the overlapping "dark" and "bright" foci. BEI (scale bar= 20 μm). **b.** Transverse section of a *Hipparion* tooth (specimen K4/Δ66/3 from site K4, thin section GI23A), where extensive bacterial damage can be identified in the dentine (D) and in the cement (C). E=enamel, ca=calcite in the pulp cavity, BEI (scale bar= 500 μm).

without any obvious microtunnel structure. These "empty" foci may correspond to the "holes" of Hedges *et al.* (1995). In a large number of thin sections and stubs it was possible to identify overlapping foci that are usually smaller and brighter under backscattered electron imaging (BEI) than the discrete foci (Fig. 4a). Lamellate foci damage was also observed in fossil tooth dentine and cement, but not in the enamel. Zones of extremely damaged dentine and cement respectively occur around the pulp cavities (fig 4b) and the outer perimeter of the cement (fig 4b). As observed in bone, fine histological features like the dentinal tubules and the cement voids are also preserved in teeth despite the extensive damage, encircled by the microtunnels of the destructive foci. It is apparent that the microorganisms attacked the teeth through both the external surfaces and the pulp cavities. The bone material from the eight other Late Miocene Greek localities revealed similar extensive bacterial damage.

DISCUSSION

Foci produced by MFD have been variously described as "lamellate foci" (Hackett, 1981), "hypermineralised destructive foci" (Bell, 1990) and "nodules" (Hedges *et al.*, 1995). This study has shown that all these structures may well be represented in three dimensions by an ellipsoid, where the hypermineralised rim wall surrounds and confines the ellipsoid focus (Fig. 5a, 5b, 6). The long axis of the ellipsoid usually lies parallel to the long axis of the bone. In longitudinal section, the ellipsoid focus is manifest as a series of parallel microtunnels, also parallel to the long axis of the focus (Fig. 5b, 6). These microtunnels occupy the whole focus and stream from one edge of the focus to the other. Bifurcating tunnels are observed quite frequently, as well as microtunnels with random orientations. In transverse section, a number of random circular perforations represent the cross-sections of the microtunnels (Fig. 5a, 6).

This form of microbial damage has been attributed to either bacteria or fungi (Hackett, 1981; Piepenbrink, 1986). Previous interpretations may have been limited through study of thin sections at relatively low magnifications. The isolation of fungi from archaeological bone and from experimental cultures in modern bone (Marchiafava *et al.*, 1974; Piepenbrink, 1986; Grupe and Piepenbrink, 1988) supported the idea that the invading organisms in MFD were fungi. The ostensible similarity of the hypermineralised rims of the foci to the hypermineralised walls of fungal hyphae tunnels and the size of the foci also supported this interpretation. According to Marchiafava *et al.* (1974) the diameters of the fungal tunnels that they observed in modern bone ranged from 2-4 μm, whereas the diameters of the hyphae of

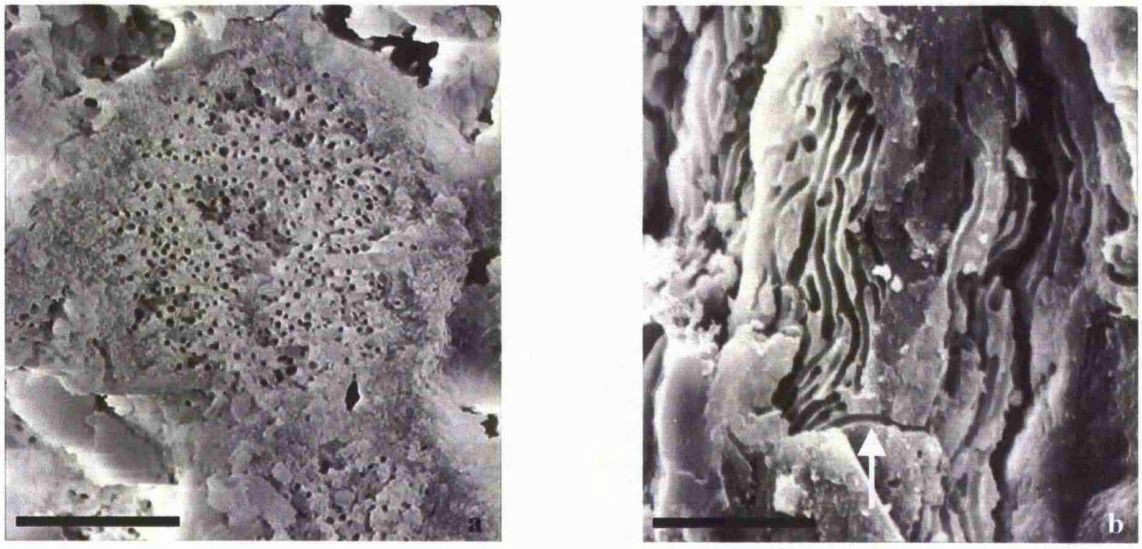

Figure 5. Fragments of bone on stubs. **a.** Transverse section of a focus of bacterially damaged bone from a *Hipparion* metapodial (specimen K4/Δ119/23 from site K4, stub 5), showing its microstructure with the thick rim and the microtunnels in the focus. The sectioned microtunnels in the focus can be well described as randomly distributed perforations. SEM (scale bar= 10 μm). **b.** Longitudinal section of a focus of bacterially damaged bone (undetermined long bone fragment from site K1, specimen K1/Δ68, stub 24), where transected parallel microtunnels in the focus stream across its long axis. The arrow at the bottom of the image points to a microtunnel that connects two different foci and provides evidence for bacterial migration in the bone and the formation of a new colony and thus a new focus. SEM (scale bar= 10 μm).

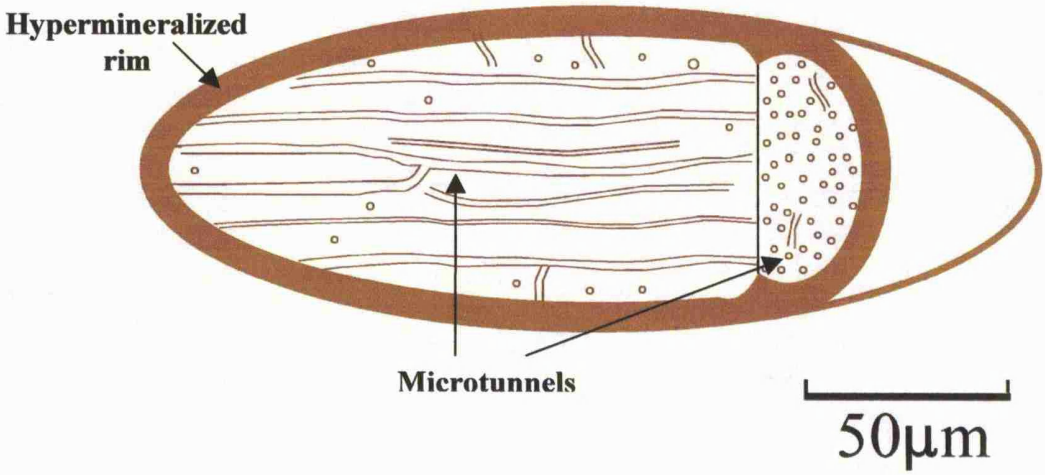

Figure 6. A reconstruction of the ellipsoid focus, based on figures 5a and 5b, showing the microstructure of the focus with the external hypermineralized rim and the microtunnel network which streams across the long axis of the focus.

the isolated genus *Mucor* ranged from 2-6 μm. Hackett (1981) named as Wedl tunnels, tunnels with uniform diameters ranging from 5-10 μm and ascribed them to fungi. Trueman and Martill (2002) noted that their type I Wedl tunnels and type II Wedl tunnels had diameters of 10-15 μm and 5 μm respectively. Tunnels larger than 1 μm were not observed in the studied material from Kerassia. Therefore, the size of these tunnels indicates that if fungi had attacked the hard tissues the fine histological features in the foci would have been destroyed.

In the Kerassia material the small diameter of the studied microtunnels (150-600nm) and the preservation of fine histological features in the foci, such as the lacunae and the dentinal tubules, indicate that the invading organisms were bacteria. The microtunnels in the Kerassia specimens are an order of magnitude smaller than previously reported tunnels attributed to fungi. Other authors studying archaeological and recent bone have also attributed similar patterns of bioerosion to bacteria (Hackett, 1981; Baud and Lacotte, 1984; Bell, 1990; Bell *et al.*, 1991; Yoshino *et al.*, 1991; Jackes *et al.*, 2001; Turner-Walker and Syversen, 2002). Some of them were even able to identify bacterial cells (Baud and Lacotte, 1984; Yoshino *et al.*, 1991; Jackes *et al.*, 2001). Jackes *et al.* (2001) and Turner-Walker and Syversen (2002) provided some high magnification images in which the microtunnel structure in the foci is clearly visible. The identification of two foci groups in some specimens of the Kerassia bone may well be attributable to the action of two different bacteria species.

Bell (1996) after studying bone material from human burials postulated that the source of the bone-degrading microbes was the gut microflora. Trueman and Martill (2002) argued that in fossil bones the source of the microorganisms could not be from the gut because the carcasses would not have been buried intact in the ground as in human burials. In animals now preserved as fossils, predation and scavenging would have rapidly removed the soft tissues, leaving bare bones on the surface exposed to environmental conditions. It is relevant that Yoshino *et al.* (1991), in their experimental study, did not observe any histomorphological alterations in the vast majority of bones left in open air, except for one sample left for 15 years. However, they did observe alterations of the lamellate type in buried bones after about 5 years. Therefore, burial seems to be a requirement for the exploitation of bones by soil microorganisms. The majority of the Kerassia material displays weathering cracks indicating that the bones were exposed on the surface of the ground for a considerable period of time before their final burial (see Behrensmeyer, 1978) but, as the presence of MFD foci denotes, not long enough so as to loose their organic components.

Each ellipsoid focus comprises a trace microfossil of a separate bacterial colony that started, developed and finally died. Bacteria invade bones to feed on the collagen. The collagen fibrils accommodate apatite crystallites intrafibrillarly (between the fibrils' molecules) as well as interfibrillarly (Eppel *et al.*, 2001). The microtunnels seem to follow the collagen fibrils. To access collagen, bacteria must be able to produce acids to dissolve the apatite, and collagenases (enzyme complexes) to hydrolize the collagen (Child, 1995). A large number of bacteria can produce organic acids or chelators as metabolic waste products capable of disolving the apatite (Ehrlich, 1990). However, only a very small number of soil bacteria can produce such collagenolytic enzymes (Vrany *et al.*, 1988). Such properties are well demonstrated by *Clostridium histolyticum* (Harper, 1980; Child, 1995).

Bacteria must live in a solution so that they may achieve apatite dissolution and depolymerisation of the large collagen protein molecules using their extracellular collagenases, and also to assimilate this hydrolised collagen (Child, 1995). Drying conditions will inhibit or even stop their access to collagen, and thus relatively wet conditions are needed for their survival (Paul and Clark, 1989; Micozzi, 1991). Bacteria dissolve mineral apatite, which thereafter exists as ions in solution, so that after extended bacterial action solutions become saturated in apatite. Apatite then precipitates through the walls of the foci and concentrates around their borders to form the recrystallised, hypermineralized rims (Hackett, 1981; Bell, 1990; Jackes *et al.*, 2001). The formation mechanism of hypermineralized rims has not been well defined. From the values of Ca and P in Table 1 it is clear that the rims are generally more enriched in calcium phosphate, relative to the whole bone, while calcium phosphate is depleted in the foci. Interestingly, the Ca/P ratio for foci, rims and undamaged bone is very similar, indicating that the source of apatite for the rims and the foci is probably the same as that for the undamaged bone. As expected, the values of the Ca/P ratio are higher for the fossil bone than for modern bone suggesting that during diagenesis the fossil bone apatite was enriched in Ca and/or was depleted in phosphate. Hubert *et al.* (1996) demonstrated that fossil bone is composed of francolite, a carbonated fluorapatite which is more stable than the carbonated hydroxyapatite (dahlite) of the original bone; during diagenesis dahlite is enriched in Ca (and other cations) and fluorine. Carbonated fluorapatites that contain over 1 wt% F are considered as francolite, whereas if the F content is less than 1 wt% they are considered as dahlite (Wilson *et al.*, 1999). In the francolite lattice, carbonates are added in the PO_4^{3-} position to provide stoichiometric balance. These changes are also recognised in the studied bioeroded specimens, both in the unaltered bone but also in the hypermineralised rims and the foci. The fossil specimens are highly enriched in F compared

with recent bone and the Ca/F ratio (table 1) is consistently higher in the foci, lower in the undamaged bone and intermediate in the rims in all the examined specimens. This indicates that the F content is consistently higher in the undamaged bone and lower in the foci. The same pattern is also evident in the cement and dentine. A possible explanation for this would be that recrystallisation in the ellipsoid foci affected not only the rims but also the interior of the foci. In biological experiments with mineral apatite, Welch *et al.* (2002) observed that when bacteria dominated microbial assemblages the dissolution of apatite (fluoroapatite) was accelerated. Nevertheless, the pH in the solutions remained near neutral, indicating a buffering effect by the apatite or the metabolic products of the microbes (Welch *et al.*, 2002). In the MFD foci such a reaction would cause saturation of the solution and would probably trigger the precipitation and possibly the crystallization of the dissolved apatite. The crystallites at the walls of the microtunnels would have suffered more intensive dissolution than the crystallites at the rims, and would be more demineralised with etched surfaces, but they would provide good nuclei for recrystallisation. Despite extensive demineralisation by bacterial acids the walls of the microtunnel network in the foci were recrystallised, and the degree of recrystallisation was probably higher than that in the rims. If this is the case then the foci would be more enriched in OH^-. Inter-crystallite spaces would be filled and this would therefore limit the effect of diagenetic recrystallisation. The lower content of F in the foci may be explained by the lower degree of recrystallisation and associated F influx in the foci than in the undamaged bone and the rims. This interpretation is supported by observations on the tooth enamel, where the highly crystallised carbonated hydroxyapatite is only slightly affected by diagenetic recrystallisation and thus the content of F is relatively low (table 1).

Carbonated hydroxyapatite, however, is less stable than francolite and low fluorine apatites would also be less stable and more easily dissolved than more fluorinated ones. This may provide an explanation for the existence of "empty" foci. The interior of the foci is more vulnerable to dissolution owing to the lower fluorine content of the apatite and the increased porosity of the microtunnel network (Turner-Walker *et al.*, 2002), creating more reactive surfaces than the recrystallized rims and undamaged bone. Slightly acidic porewaters may be able to dissolve the interior of the foci but not the more resistant hypermineralised and more fluorinated rims. Pore waters are more reactive at the exterior zone of the bone and this may explain why "empty" foci are found at the exterior perimeter of the bone.

	GI 8 (lower horizon)			GI 15a (upper horizon)			GI 23b (lower horizon)							GI 12 (upper horizon)							GI 21b
	Un. bone	**Rims**	**Foci**	**Un. bone**	**Rims**	**Foci**	**Un. cement**	**Rims**	**Foci**	**Enamel**	**Un. dentine**	**Rims**	**Foci**	**Un. cement**	**Rims**	**Foci**	**Enamel**	**Un. dentine**	**Rims**	**Foci**	**modern bone**
Ca	34.3	35.4	32.0	29.1	30.1	28.8	33.7	33.2	32.1	37.9	33.9	34.5	29.5	33.8	30.7	32.3	41.6	34.3	32.6	29.9	28.9
P	14.0	14.7	13.2	12.0	12.6	11.9	13.9	13.8	13.4	16.5	14.2	14.6	12.3	13.3	12.0	12.7	14.9	13.7	13.0	12.1	13.5
F	2.6	2.5	2.1	2.2	2.0	1.8	2.4	1.9	1.6	0.9	2.2	1.8	1.5	1.9	1.6	1.6	0.7	1.9	1.5	1.2	0.2
Ca/P	2.4	2.4	2.4	2.4	2.4	2.4	2.4	2.4	2.4	2.3	2.4	2.4	2.4	2.5	2.6	2.5	2.8	2.5	2.5	2.5	2.1
Ca/F	13.5	14.7	15.3	13.6	15.1	15.9	14.3	18.9	20.4	48.0	16.2	20.2	20.8	17.9	19.8	20.6	57.6	18.4	24.8	26.3	224.9

Table 1: Electron microprobe analysis (EPMA) data. The average stoichiometric values of Ca, P and F for the unaltered parts, the rims and the interior of the foci are provided for bone and teeth specimens from both fossiliferous horizons of Kerassia and also for comparison for modern bone.

As mentioned above microbial action was not identified in the two scattered specimens found above the main bone accumulations of the upper horizon. It is possible that solitary bones or fragments of bone would not attract microbial activity. Bacteria or other microorganisms probably prefer to attack, and develop colonies in accumulations of bones, where there is a rich source of nutrients. Large or significant bone accumulations could therefore be a requirement for extensive microbial damage and also a condition for the preservation of bones with features of such extensive bioerosion. However, further research is needed to provide evidence for this hypothesis.

Although bacteria can survive in a wide range of environmental conditions, most soil bacteria are mesophylous, needing moderate moisture, and grow better in neutral pH (Doetsch and Cook, 1973, Paul and Clark, 1989). Accordingly, maximum development of soil bacteria needs favourable conditions. Significant changes in the environment restrain their development as well as their ability to produce enzymes (Child *et al.*, 1993; Child, 1995). The extreme and extensive MFD in Kerassia bone material suggests such favourable conditions.

That bones from the other Late Miocene Greek localities show the same or similar bacterial damage as those from Kerassia is probably related to the Late Miocene climate in the North-Eastern Mediterranean, which was probably temperate to warm and relatively moist. A seasonal climate similar to today's Mediterranean climate, but warmer and much wetter, would favour the development of the bacteria. There is evidence for a general alternation of a dry and hot season with a humid and cool season from the recent results of Ivanov *et al.* (2002), who provided a palynological analysis for the climate of the Late Miocene of Bulgaria, and by extension of the North-Eastern Mediterranean. According to Schaefer (1973), bacteria and other soil microorganisms in Mediterranean type climates show two annual growth cycles; one at the onset of the dry period and a second at the start of the humid period. Dryness and dessication, as well as cold, inhibit the development of microorganisms. The observed overlapping foci may therefore belong to at least two different generations of foci, and perhaps characterise the adaptation of the bacteria to this seasonality. Clearly, microorganisms re-exploited areas of bone that had already been tunnelled previously. The overlapping foci would correspond either to different bacterial invasions in the bone or to the reactivation of the bacterial colonies that survived during the stress periods. Thus a new microbial attack indicates that the bone still contained unexploited nutrients. In addition, the presence of foci without bright rims in other specimens provides further evidence for this seasonality. The bright and dark foci are probably similar to what Bell *et al.* (1996) described

as remineralised and demineralised foci and Turner-Walker and Syversen (2002) hypermineralised and demineralised zones respectively. During the first period of growth (spring-summer), temperatures would gradually rise to levels that would favour the optimum growth of bacteria, while at the same time precipitation and thus soil moisture would gradually drop to dryness levels producing an inhibiting effect on bacterial growth. Dryness would also affect significantly the solutions in the bone. Therefore, the gradual evaporation of the solution medium would cause saturation of calcium phosphate ions in the solution so that relatively fast precipitation of dissolved apatite would occur around the walls of the foci resulting in the mineralised rims, causing them to be bright under backscatter. Conversely, dropping temperature during the second period of growth (autumn-winter) would be an inhibiting factor for bacterial growth. The gradual increase of precipitation would increase soil moisture and pore waters. The pore waters would remove the dissolved apatite and would keep solutions in the foci undersaturated, inhibiting precipitation of the apatite in the foci and thus resulting to "dark" rims. The dissolved apatite would then either leach out in the soil, or become redistributed in the bone rather than concentrating in the rims of the foci. Further study is required to test these hypotheses for the mechanisms behind the formation and the preservation of the foci.

X-ray emission microanalysis of bacterially damaged bones and teeth from the Late Miocene of Kerassia, Greece

INTRODUCTION

Bone is a composite material consisting of carbonated calcium phosphate mineral crystals (dahlite) and an organic framework of protein fibres. The mineral and organic components constitute about 72% and 20% of the weight respectively and the remaining 8% is water (Elliott, 2002); 90% of the organic component is collagen, 10% is non-collagenous proteins, lipids and carbohydrates (Price, 1989; Cormack, 1987). Of the tooth tissues, dentine and cement have a similar composition to bone, whereas in enamel apatite accounts for up to 97% of the weight, the organic component is less than 1%, and 2% is water (Carlson, 1990). The main mineral phase in these mineralised tissues is a nonstoichiometric carbonated hydroxylapatite, an imperfect analogue of dahlite (Lowenstam and Weiner, 1989).

The taphonomic aspects investigated in this paper highlight some of the geochemical properties of fossil mammal bones and teeth from a new Late Miocene locality: Kerassia, in Greece. As reported in chapter one, the histological study of fossil bones and teeth from Kerassia showed that bone, dentine and cement presented extensive microscopical focal destruction (MFD, Hackett, 1981). The term MFD characterises changes in the histomorphology of vertebrate hard tissues produced by microbial (bacterial, fungal, protozoan, algal) activity. The microbes involved in the bioerosion of the fossil tissues from Kerassia were determined to be bacteria on the basis of the small diameters (150-600 nm) of the microtunnels in the foci of the damaged tissues, (Chapter one, Iliopoulos, 2003). Previous work has shown that the rims of the foci of bacterially damaged bone, dentine and cement are more mineralised than the respective interior of the foci and the undamaged areas of the tissues (Hackett, 1981; Bell, 1990; Bell *et al.*, 1991; Jackes *et al.*, 2001; Turner-Walker and Syverson, 2002). These findings were based on scanning electron microscope and microradiograph observations (Hackett, 1981), on backscattered electron microscope observations (Bell, 1990; Bell *et al.*, 1991) and on analyses of the Ca and P contents in the different microstructural areas of damaged tissues (Jackes *et al.*, 2001; Turner-Walker and Syverson, 2002).

This investigation demonstrates for the first time that MFD is responsible for changes in the distribution of an array of elements within bioeroded vertebrate hard tissues. It also attempts to determine the effect that early recrystallization in the foci of the damaged tissues has on the uptake mechanism of these elements during diagenesis. This investigation shows that during diagenesis, the uptake of elements in these tissues is not only controlled by the prevailing burial conditions but also by the structural and mineralogical properties of the structurally differentiated areas of the damaged hard tissues. As fossil and recent hard tissues are often used in biogeochemical analyses (e.g. palaeodietary research) and in DNA analysis, it is important to identify MFD in advance to avoid erroneous and biased determinations.

GEOLOGICAL AND SEDIMENTOLOGICAL SETTING

The studied material comes from a new Late Miocene mammal locality, Kerassia in Greece (Fig. 1). Kerassia is located approximately in the middle of the Limni-Istiea basin, the largest of the three major Neogene basins occuring on Euboea Island (Katsikatsos *et al.*, 1981). This basin occupies the Northern part of the island, and contains sediments of continental origin, comprising a lower sequence of lacustrine sediments and an upper sequence of fluviatile sediments (Katsikatsos *et al.*, 1981; Mettos *et al.*, 1991). The actual fossiliferous locality is situated north of the village of Kerassia. The bone-bearing layers belong to the upper sequence and they mainly consist of red-brown silts and clays. To date, seven different fossiliferous sites have been discovered (namely K1 to K7) and two fossiliferous horizons have been recognised. Sites K1 and K6 belong to the upper horizon, sites K2, K3, K4 and probably K5 belong to the lower horizon; the exact position of site K7 is still undetermined. The bulk of the collected fossil material had accumulated within fluvial channels. In this part of the basin, the basement rocks, as well as the surrounding rocks to the north and to the east of the locality, are ophiolites that belong to the Lower Cretaceous tectonic nappe of the so-called Pelagonian (sensu stricto) unit. Apart from the ophiolites, a few Jurassic limestones (of the Pelagonian unit) occur to the south of the village of Kerassia. The majority of the clasts in the bone bearing sediments are of ophiolitic origin. Observations on the prevailing orientation of long bones in these sediments suggest a flow of water and sediments from a northern source, and this fits in with the position of the ophiolites in the area. During the last decade, systematic excavations conducted by Theodorou and others from the University of Athens have brought to light a plethora of specimens representing a diverse mammal fauna of Turolian age (Theodorou *et al.*, 2003). In 1982 Hans de Bruijn, Albert van der Meulen and

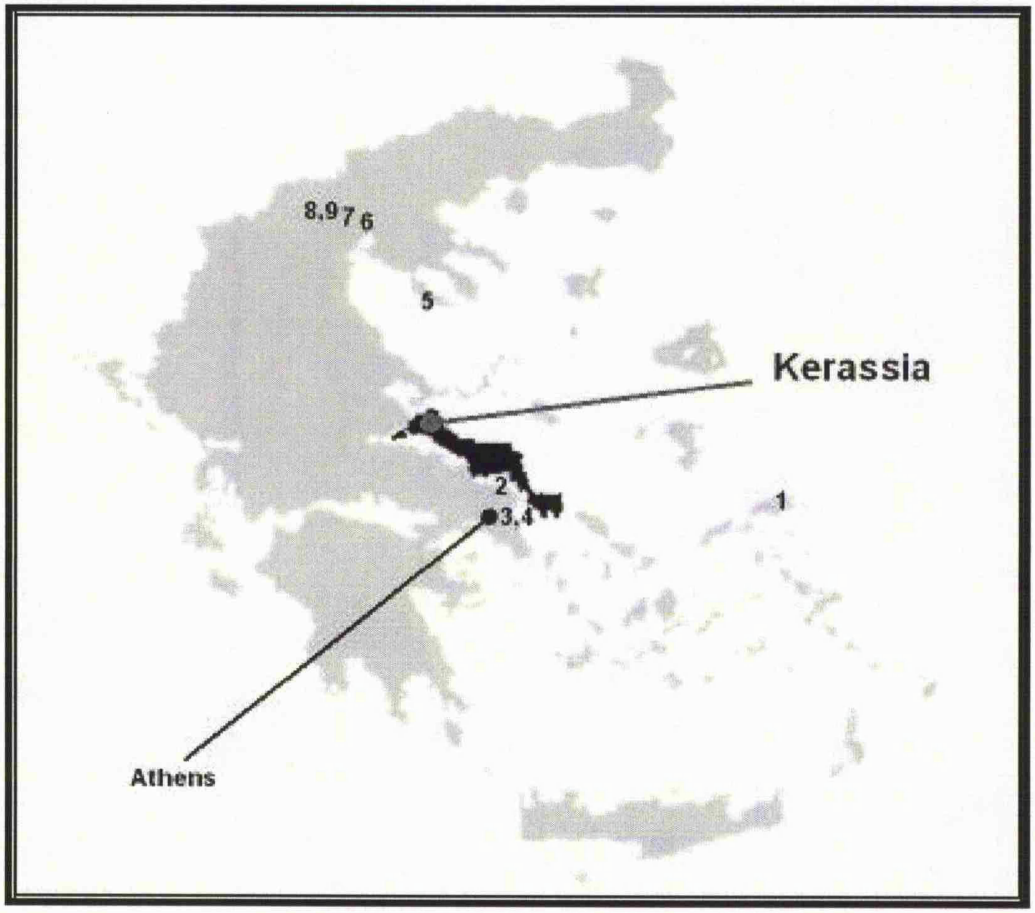

Figure 1: Sketch map of Greece showing the location of Euboea Island and Kerassia and of the other Greek Late Miocene localities mentioned in the text. 1. Samos, 2. Chalkoutsi (Chal), 3. Old Pikermi (OP), 4. New Pikermi (NP), 5. Kassandria (Kas), 6. Ravin de la Pluie 2 (RP2), 7. Vathylakkos 1 (VTK1), 8. Ditiko 1 (DTK1), 9. Ditiko 2 (DTK2).

Constantine Doukas carried out a small scale excavation in the locality. The exact site of collection is not known, as there are no data available about this excavation. However, information provided by Doukas (pers. com.) and the overall state of the material indicate that the collection site was K1.

MATERIAL AND METHODS

Polished thin sections of fossil bone and teeth specimens from both horizons at Kerassia (sites K1, K3, K4 and K5), including specimens from the 1982 excavation (Ke), were prepared. The majority of the specimens used in this study come from sites K1 and K4, as the excavations to date have been focused at these two sites. The scarcity of the collected material from the other five sites restricted the number of sectioned specimens from these sites; no specimens were available for sectioning from sites K2, K6 and K7 and sites K3 and K5 are represented by one bone specimen each. In addition, thin sections of bones from nine other Late Miocene Greek localities (Fig. 1), from the Late Pleistocene localities of Cotes and Quorn (Loughborough, England), and from recent weathered and fresh defatted bones were also prepared for comparison with the Kerassia specimens. Unfortunately, the exact period of surface exposure for the weathered recent sample is not known. The nine Late Miocene localities are: the localities of Ravin de la Plui 2, Vathylakkos 1, Ditiko 1 and Ditiko 2 in the Axios River valley in Macedonia, Kassandria on Chalkidiki peninsula, Samos on Samos Island, and Old Pikermi, New Pikermi and Chalkoutsi which are situated close to Athens in Attica (Fig. 1).

The analytical study of bacterially damaged tissues required a method that could analyse the different microstructural areas of the damaged tissues, thus X-ray emission micro analysis (XREMA) was selected. Spot analyses were collected on carbon-coated, polished thin sections, using a JEOL JXA 8600-S electron-microprobe. The wavelength dispersive system of the microprobe used three spectrometers with gas proportional detectors equipped with fully focussing curved crystals. Two of the detectors were flow proportional with Argon (P-10) and the third was a sealed one with xenon. A focused beam was used at an accelerating voltage of 15keV and a beam current of 30 nA, while the following elements were measured: Ca, P, Si, Fe, Mn, Mg, Na, Sr, Ba, La, Ce, Y, F and Cl. Standards used included well-characterized natural and synthetic minerals. Corrections for differences in atomic number (Z), absorption (A) and fluorescence (F) between standards and specimens were applied using version 1·08 of JEOL's ZAF quantitative analysis program. Several spot analyses were

performed in the undamaged areas and in addition in the foci and the foci rims of bacterially damaged bone, dentine and cement (see chapter 1). For example, in thin section gi5a a bone specimen from site K4, 33 spot analyses were performed in the rims, 31 in the foci and 23 in the undamaged areas of the bone (Table 1). In the specimen from Kassandria which exhibits fungal damage spot analyses were made in the undamaged bone and around the rims of the Wedl tunnels. In the weathered recent bone spot analyses were collected from both the unweathered part of the bone and the external weathered portion of the bone cortex.

RESULTS

Microscopical focal destruction (MFD; Hackett, 1981) was identified in all the examined thin sections from Kerassia and the other Late Miocene Greek localities. It has been shown that extensive damage was caused by bacteria in all cases (see Chapter 1; Iliopoulos, 2002, 2003), except from the section from Kassandria. In Kassandria the bioeroding microorganisms were most probably fungi, and the pattern of destruction has been determined to be the Trueman and Martill (2002) type 1 Wedl tunnels.

Total values

The total value is the total sum of the wt % values of the measured elements used in this study. Table 1 presents the data from fossil and recent weathered and unweathered bones and fossil teeth. It shows the average concentrations for both major and minor elements in the undamaged bone, dentine and cement, the foci and the rims of the foci. The total wt % values of analyses were always below 90 % for bone, dentine and cement; some were as low as 70 %. Enamel gave better totals where values were mostly above 90 %. The vast majority of the fossil samples and the weathered recent bone have higher total values than the unweathered recent bone samples (Table 1). Interestingly, in the recent weathered sample the total values of the weathered part are higher than the unweathered part of the bone. In the majority of the bone, dentine, and cement specimens from both the upper and the lower horizons of Kerassia the rims have the highest total wt % values, and the foci consistently present the lowest total wt % values in every tissue (Table 1, Fig. 2). This trend was also identified in specimens from other Miocene Greek localities and in the Pleistocene specimen from Cotes. However, in the specimen from Ditiko 2 the foci have the highest values and the rims the lowest total values; while in the specimen from Ditiko 1 the rims, as expected, have the highest values; however,

Table 1

section	structure type	No of analyses	MgO	sd	CaO	sd	Na_2O	sd	SrO	sd	P_2O_5	sd	F	sd	Cl	sd	Total	sd
det. limits			0.02		0.03		0.02		0.07		0.05		0.10		0.03			
	rims	46	0.18	0.03	45.87	4.29	0.28	0.07	bd		30.04	3.13	1.94	0.30	0.04	0.02	77.75	7.56
gi13/Ke	foci	53	0.17	0.04	43.81	5.92	0.25	0.07	bd		28.60	4.07	1.82	0.42	0.05	0.02	74.15	10.24
	bone	16	0.16	0.03	45.72	4.98	0.27	0.06	bd		30.35	3.33	1.89	0.26	0.04	0.01	77.87	8.41
	rims	51	0.23	0.05	47.25	4.43	0.31	0.09	bd		31.08	2.94	2.03	0.42	0.06	0.05	80.35	7.61
Ke49b	foci	47	0.23	0.05	44.34	3.30	0.28	0.07	0.07	0.03	28.82	2.42	1.79	0.37	0.06	0.03	74.99	5.81
	bone	27	0.17	0.05	46.49	4.69	0.25	0.10	bd		30.29	2.96	2.24	0.46	0.07	0.05	78.87	7.73
	rims	53	0.17	0.02	42.29	2.59	0.24	0.04	bd		28.84	1.84	2.02	0.25	0.07	0.03	72.98	4.42
gi15a/K1	foci	55	0.17	0.02	40.37	2.64	0.24	0.05	bd		27.26	1.93	1.84	0.26	0.08	0.04	69.36	4.69
	bone	40	0.17	0.10	40.68	2.72	0.22	0.03	bd		27.58	2.00	2.15	0.20	0.06	0.02	70.25	4.62
	rims	33	0.27	0.13	42.37	5.41	0.28	0.08	bd		28.71	3.92	1.99	0.40	0.05	0.02	73.46	9.18
gi16/K1	foci	24	0.30	0.27	40.39	5.63	0.29	0.06	bd		27.08	3.96	1.88	0.38	0.06	0.02	69.68	9.56
	bone	20	0.33	0.36	40.98	4.80	0.28	0.07	bd		27.41	3.22	2.12	0.30	0.05	0.01	71.65	5.86
	rims	50	0.23	0.05	43.14	4.62	0.21	0.06	bd		28.90	3.18	2.09	0.42	0.06	0.01	73.99	7.97
gi24/K1	foci	50	0.21	0.04	39.67	5.11	0.20	0.05	bd		26.61	3.51	1.97	0.44	0.07	0.02	68.11	8.86
	bone	28	0.22	0.05	44.35	3.94	0.22	0.06	bd		30.00	2.67	2.34	0.40	0.05	0.01	76.42	6.74
	rims	52	0.26	0.04	46.98	3.45	0.35	0.08	bd		32.22	2.26	1.85	0.37	0.07	0.03	81.14	5.73
K1/A3	foci	49	0.24	0.04	43.42	4.22	0.33	0.09	bd		29.69	2.98	1.67	0.36	0.08	0.03	74.92	7.35
	bone	34	0.19	0.04	43.74	2.36	0.30	0.08	bd		29.53	1.73	2.01	0.39	0.07	0.02	75.17	3.90
	rims	30	0.18	0.04	45.08	4.52	0.36	0.07	bd		29.81	2.88	1.63	0.40	0.10	0.03	76.97	7.53
gi14a/K3	foci	30	0.19	0.03	44.65	3.84	0.36	0.08	0.07	0.03	29.44	2.72	1.58	0.30	0.11	0.03	76.69	7.16
	bone	14	0.17	0.03	47.63	2.35	0.34	0.06	bd		31.42	1.42	1.89	0.25	0.08	0.03	81.23	3.72
	rims	17	0.26	0.04	47.15	3.24	0.36	0.06	0.08	0.03	31.01	2.22	2.27	0.34	0.10	0.04	80.48	5.40
gi2/K4	foci	16	0.24	0.05	43.98	4.99	0.34	0.06	bd		28.96	3.16	2.11	0.41	0.11	0.07	75.17	8.20
	bone	21	0.18	0.03	47.78	4.78	0.31	0.07	bd		31.80	2.60	2.51	0.44	0.12	0.06	81.85	7.41
	rims	31	0.24	0.04	46.97	2.34	0.38	0.06	bd		33.24	1.63	1.83	0.28	0.09	0.03	82.13	3.99
gi3/K4	foci	35	0.24	0.04	44.01	3.48	0.38	0.07	bd		30.62	2.79	1.74	0.42	0.10	0.03	76.56	6.28
	bone	57	0.17	0.04	46.27	4.52	0.29	0.08	bd		31.50	3.28	2.39	0.60	0.09	0.04	79.90	7.84
	rims	38	0.24	0.05	46.86	2.96	0.36	0.07	bd		33.11	2.19	1.88	0.31	0.09	0.05	81.93	5.16
gi4a/K4	foci	39	0.22	0.03	43.33	3.17	0.32	0.06	bd		30.34	2.45	1.67	0.32	0.11	0.05	75.44	5.64
	bone	45	0.17	0.03	46.05	3.06	0.28	0.06	bd		31.58	2.16	2.23	0.37	0.07	0.03	79.61	5.15
	rims	33	0.22	0.04	43.89	2.69	0.35	0.05	bd		31.15	1.92	1.95	0.37	0.09	0.05	76.99	4.67
gi5a/K4	foci	31	0.24	0.03	41.82	2.89	0.34	0.06	bd		30.03	2.46	1.61	0.29	0.11	0.07	73.66	5.34
	bone	23	0.19	0.03	44.58	2.26	0.32	0.06	bd		31.87	2.11	1.97	0.40	0.10	0.07	78.36	4.31
	rims	14	0.25	0.03	47.75	4.05	0.37	0.06	0.07	0.03	31.69	2.55	2.19	0.40	0.12	0.04	81.63	6.73
gi6/K4	foci	13	0.25	0.03	45.79	1.98	0.37	0.06	0.07	0.03	30.48	1.45	2.16	0.25	0.12	0.05	78.46	3.52

Table 1

section	structure type	No of analyses	MgO	sd	CaO	sd	Na_2O	sd	SrO	sd	P_2O_5	sd	F	sd	Cl	sd	Total	sd
	bone	11	0.21	0.05	48.44	2.11	0.33	0.08	0.09	0.03	31.91	1.37	2.60	0.31	0.08	0.04	82.69	3.61
	rims	23	0.21	0.04	47.83	3.19	0.30	0.07	0.07	0.03	32.30	2.09	2.48	0.28	0.09	0.02	82.53	5.36
gi7b/K4	foci	25	0.22	0.04	44.10	3.65	0.32	0.05	0.08	0.04	29.71	2.59	2.29	0.36	0.09	0.02	76.12	6.33
	bone	15	0.16	0.03	45.21	3.36	0.22	0.05	0.07	0.04	30.15	2.53	2.66	0.38	0.07	0.03	77.62	6.08
	rims	31	0.29	0.05	49.58	3.04	0.39	0.05	0.07	0.03	33.71	2.11	2.47	0.40	0.09	0.04	85.72	5.14
gi8/K4	foci	26	0.25	0.04	44.76	2.77	0.33	0.06	0.07	0.02	30.35	2.33	2.15	0.38	0.11	0.05	77.26	5.21
	bone	17	0.19	0.04	48.05	3.41	0.27	0.07	0.07	0.03	32.16	2.03	2.60	0.41	0.07	0.04	82.44	5.62
	rims	58	0.18	0.03	46.61	1.97	0.30	0.05	bd		32.01	1.31	2.04	0.24	0.09	0.02	80.51	3.32
gi18/K5	foci	57	0.17	0.03	43.15	2.77	0.28	0.05	bd		29.61	1.96	1.84	0.23	0.10	0.02	74.50	4.78
	bone	35	0.14	0.02	45.05	2.72	0.25	0.06	bd		30.86	1.78	2.11	0.25	0.09	0.03	77.71	4.49
	cement	7	0.23	0.05	47.24	5.11	0.38	0.06	bd		30.42	3.35	1.90	0.27	0.06	0.03	79.78	8.64
	cement rims	15	0.19	0.03	42.99	5.32	0.33	0.07	bd		27.47	3.58	1.60	0.32	0.08	0.02	72.32	9.11
	cement foci	20	0.21	0.05	45.15	3.82	0.36	0.09	bd		29.07	2.82	1.64	0.38	0.08	0.02	76.13	6.70
gi12/Ke	enamel	6	0.26	0.05	58.14	2.72	0.70	0.17	0.08	0.03	34.13	3.38	0.73	0.09	0.25	0.11	94.12	1.24
	dentine	10	0.17	0.02	47.94	3.18	0.28	0.06	bd		31.38	1.81	1.88	0.27	0.07	0.02	81.10	5.09
	dentine rims	10	0.18	0.02	45.66	4.39	0.24	0.06	bd		29.75	3.27	1.52	0.57	0.10	0.02	76.97	7.82
	dentine foci	17	0.16	0.02	41.90	4.81	0.26	0.05	bd		27.84	2.96	1.22	0.41	0.12	0.03	71.15	7.92
	cement	12	0.21	0.03	47.16	3.21	0.29	0.08	bd		31.96	2.10	2.38	0.27	0.04	0.03	81.15	5.23
	cement rims	10	0.30	0.07	46.34	3.90	0.35	0.07	bd		31.58	2.53	1.85	0.52	0.07	0.04	79.80	6.55
	cement foci	10	0.34	0.08	44.98	3.34	0.36	0.05	bd		30.71	1.94	1.63	0.36	0.08	0.04	77.52	5.43
gi23b/K4	enamel	16	0.28	0.05	52.97	2.10	0.57	0.17	bd		37.75	1.66	0.88	0.37	0.26	0.09	92.45	3.50
	dentine	20	0.18	0.04	47.48	2.19	0.29	0.11	bd		32.46	1.38	2.15	0.34	0.07	0.03	81.86	3.54
	dentine rims	25	0.24	0.03	48.29	1.57	0.33	0.09	bd		33.38	1.12	1.76	0.33	0.07	0.02	83.46	2.78
	dentine foci	26	0.23	0.04	41.24	3.29	0.31	0.10	bd		28.27	2.47	1.45	0.24	0.09	0.03	71.14	5.65
	rims	22	0.12	0.03	45.23	6.26	0.16	0.05	bd		30.54	4.15	1.36	0.48	0.10	0.04	77.16	10.60
gi1/O.P.	foci	30	0.12	0.03	41.51	5.02	0.18	0.18	bd		28.62	3.57	1.28	0.34	0.13	0.09	71.72	8.40
	bone	40	0.13	0.08	45.08	5.43	0.30	0.73	bd		30.65	3.62	1.97	0.53	0.17	0.50	77.66	9.10
	rims	33	0.19	0.04	47.73	4.74	0.20	0.07	bd		31.91	2.88	2.05	0.51	0.12	0.03	81.52	7.76
gi17a/N.P.	foci	30	0.17	0.04	43.81	5.52	0.16	0.06	bd		29.41	3.59	1.75	0.35	0.14	0.03	74.87	9.23
	bone	26	0.21	0.03	47.31	3.58	0.21	0.05	bd		31.60	2.13	2.27	0.41	0.12	0.04	80.95	5.78
	rims	30	0.24	0.06	41.24	6.40	0.35	0.09	bd		29.18	4.93	1.76	0.40	0.08	0.04	72.30	11.47
gi9/ΣA	foci	25	0.26	0.05	42.74	3.25	0.39	0.07	bd		30.53	2.51	1.84	0.19	0.08	0.03	75.23	5.89
	bone	20	0.21	0.06	44.98	2.18	0.34	0.07	bd		32.77	1.82	1.95	0.25	0.11	0.08	79.68	4.05
	rims	16	0.47	0.06	49.67	3.49	0.61	0.13	0.17	0.03	33.32	1.57	2.41	0.51	0.58	0.17	86.21	5.01
Ch1	foci	16	0.44	0.05	45.70	3.16	0.63	0.12	0.11	0.04	31.07	2.09	2.06	0.38	0.77	0.19	79.91	5.15
	bone	14	0.55	0.05	47.66	3.27	0.73	0.15	0.13	0.03	32.08	2.05	2.44	0.33	0.78	0.18	83.31	5.01

Table 1

section	structure type	No of analyses	MgO	sd	CaO	sd	Na_2O	sd	SrO	sd	P_2O_5	sd	F	sd	Cl	sd	Total	sd
	rims	5	0.51	0.07	45.05	3.82	0.60	0.14	0.12	0.03	30.04	3.10	1.44	0.43	0.48	0.09	77.78	7.03
Ch2	foci	8	0.41	0.17	44.77	6.60	0.45	0.25	0.12	0.03	29.80	4.36	1.04	0.73	0.52	0.20	76.91	10.92
	bone	20	0.50	0.12	47.26	5.38	0.48	0.09	0.12	0.05	31.03	3.27	1.41	0.44	0.40	0.12	80.80	8.66
	rims	24	0.17	0.03	43.28	4.86	0.30	0.07	0.07	0.03	29.29	3.29	1.61	0.38	0.04	0.01	74.22	8.14
DTK1	foci	22	0.19	0.13	40.98	4.68	0.27	0.07	bd		27.84	3.52	1.65	0.37	0.05	0.02	71.27	6.88
	bone	14	0.16	0.03	39.21	5.77	0.30	0.09	bd		27.06	3.21	1.42	0.32	0.05	0.02	67.83	9.09
	rims	27	0.22	0.16	40.70	6.81	0.25	0.07	bd		27.79	4.34	1.32	0.44	0.05	0.03	71.95	9.19
DTK2	foci	23	0.16	0.03	43.70	4.70	0.25	0.06	bd		29.83	3.15	1.38	0.44	0.04	0.02	75.15	7.76
	bone	16	0.14	0.03	42.05	5.46	0.22	0.06	bd		28.59	3.52	1.42	0.45	0.05	0.03	72.06	8.91
	rims	37	0.32	0.05	50.79	3.42	0.17	0.07	0.13	0.03	33.90	1.82	2.12	0.35	0.09	0.02	86.80	5.26
RP2	foci	33	0.29	0.05	48.71	4.14	0.14	0.06	0.12	0.03	32.56	2.81	2.05	0.33	0.10	0.02	83.27	7.00
	bone	23	0.28	0.03	48.77	2.32	0.15	0.05	0.11	0.04	32.88	1.50	2.19	0.20	0.09	0.02	83.70	3.67
	rims	49	0.39	0.05	48.29	3.59	0.22	0.06	0.14	0.03	33.03	2.21	1.73	0.36	0.07	0.02	83.45	5.84
VTK1a	foci	44	0.34	0.05	44.71	3.39	0.19	0.05	0.14	0.03	30.62	2.38	1.41	0.39	0.07	0.02	77.18	5.87
	bone	25	0.44	0.04	47.90	3.10	0.26	0.08	0.13	0.03	32.43	1.89	2.07	0.34	0.09	0.03	83.07	4.35
gi19a/KAS	bone	33	0.14	0.02	46.92	4.65	0.21	0.09	bd		31.84	2.60	2.74	0.51	bd	0.01	81.89	6.93
	tunnels	17	0.16	0.06	40.93	3.16	0.32	0.04	bd		28.28	2.38	2.23	0.19	0.04	0.02	73.22	4.95
Co1a	bone	48	0.20	0.06	42.79	4.04	0.09	0.08	0.11	0.06	28.34	2.49	0.66	0.71	bd	0.01	72.35	6.38
	rims	19	0.15	0.02	46.37	4.40	0.10	0.08	0.11	0.03	30.47	2.77	1.96	1.48	bd	0.01	78.81	7.42
Co2b	foci	14	0.15	0.03	45.40	5.38	0.07	0.09	0.14	0.04	29.80	3.43	1.88	1.04	bd	0.01	77.19	8.80
	bone	45	0.16	0.04	42.71	3.10	0.12	0.10	0.11	0.04	27.40	1.87	1.27	1.76	bd	0.01	71.62	5.44
Qu	bone	17	0.22	0.08	41.63	2.87	0.24	0.13	bd		31.74	2.27	0.32	0.27	0.03	0.02	76.80	4.55
gi22c/Agr	recent bone	76	0.30	0.11	42.41	3.00	0.14	0.13	bd		29.15	1.87	0.10	0.08	bd	0.01	72.20	4.73
	weathered	35	0.32	0.09	43.20	3.39	0.29	0.18	bd		29.99	2.25	0.39	0.35	0.09	0.06	74.26	5.55
gi20b/BT	recent bone	51	0.61	0.20	40.41	2.12	0.30	0.17	bd		30.99	1.54	0.22	0.15	0.05	0.01	72.56	3.55
gi21/BS	recent bone	45	0.68	0.21	40.94	3.16	0.19	0.18	bd		30.18	2.20	0.14	0.14	0.04	0.01	72.27	5.35

Table 1: Average values and their standard deviations of XREMA analyses from fossil bone, dentine, cement and enamel samples from Kerassia and the other studied localities and recent weathered and unweathered bone. In the bacterially damaged tissues spot analyses were collected from the foci, the rims and the undamaged areas of the tissues. Ke= the material collected from the 1982 excavations, OP= Old Pikermi, NP= New Pikermi, ΣA= Samos, Ch= Chalkoutsi, DTK1= Ditiko 1, DTK2= Ditiko 2, RP2= Ravin de la Pluie 2, VTK1= Vathylakkos 1, KAS= Kassandria, Co= Cotes, Qu= Quorn, Agr= recent weathered bone, BT-BS= recent defatted bone. Det. limits: The detection limits estimated from count rate greater than three standard deviations above background. bd= below detection limit.

Table 1

section	structure type	No of analyses	Ca	sd	P	sd	Ca/P	sd	Ca/F	sd	Ca/Cl	sd	Ca/P molar	sd
det. limits														
	rims	46	32.78	3.06	13.11	1.37	2.50	0.06	17.24	2.70	962.98	564.15	1.94	0.04
gi13/Ke	foci	53	31.31	4.23	12.48	1.78	2.51	0.06	17.83	3.47	854.54	460.11	1.94	0.05
	bone	16	32.68	3.56	13.25	1.45	2.47	0.06	17.46	2.46	885.34	370.19	1.91	0.04
	rims	51	33.77	3.17	13.56	1.28	2.49	0.05	17.45	4.93	876.04	494.79	1.92	0.04
Ke49b	foci	47	31.69	2.36	12.58	1.06	2.52	0.06	18.39	3.68	604.20	248.58	1.95	0.05
	bone	27	33.22	3.35	13.22	1.29	2.51	0.05	15.80	5.41	913.75	699.29	1.94	0.04
	rims	53	30.23	1.85	12.59	0.80	2.40	0.06	15.16	1.98	499.16	148.94	1.86	0.05
gi15a/K1	foci	55	28.85	1.89	11.90	0.84	2.43	0.04	15.92	2.13	408.74	115.50	1.87	0.03
	bone	40	29.08	1.94	12.04	0.87	2.42	0.06	13.60	1.45	537.76	158.32	1.87	0.04
	rims	33	30.28	3.87	12.53	1.71	2.42	0.08	15.61	2.90	681.29	323.05	1.87	0.06
gi16/K1	foci	24	28.86	4.02	11.82	1.73	2.45	0.07	15.77	3.00	634.41	497.75	1.89	0.06
	bone	20	29.29	3.43	11.96	1.41	2.45	0.03	13.94	1.46	612.60	170.04	1.89	0.03
	rims	50	30.83	3.30	12.61	1.39	2.45	0.06	15.18	2.52	601.74	205.43	1.89	0.04
gi24/K1	foci	50	28.35	3.65	11.61	1.53	2.44	0.06	14.83	2.29	474.93	178.15	1.89	0.05
	bone	28	31.69	2.81	13.09	1.16	2.42	0.09	13.96	2.55	650.07	162.48	1.87	0.07
	rims	52	33.58	2.47	14.06	0.98	2.39	0.05	18.90	4.03	588.94	261.28	1.85	0.04
K1/A3	foci	49	31.03	3.02	12.96	1.30	2.40	0.05	19.34	4.15	423.99	168.23	1.85	0.04
	bone	34	31.26	1.69	12.89	0.76	2.43	0.07	16.36	4.40	459.91	135.04	1.88	0.05
	rims	30	32.22	3.23	13.01	1.26	2.48	0.05	21.34	8.60	367.18	155.59	1.91	0.04
gi14a/K3	foci	30	31.91	2.75	12.85	1.19	2.49	0.03	20.65	3.08	323.15	100.18	1.92	0.03
	bone	14	34.04	1.68	13.71	0.62	2.48	0.05	18.28	2.30	507.84	192.16	1.92	0.04
	rims	17	33.69	2.32	13.53	0.97	2.49	0.03	15.13	2.23	414.57	213.37	1.93	0.02
gi2/K4	foci	16	31.43	3.57	12.64	1.38	2.49	0.04	15.35	2.86	415.83	289.20	1.92	0.03
	bone	21	34.15	3.41	13.88	1.13	2.46	0.07	13.90	2.37	409.28	300.59	1.90	0.05
	rims	31	33.57	1.67	14.50	0.71	2.31	0.06	18.74	2.48	436.25	144.54	1.79	0.04
gi3/K4	foci	35	31.45	2.49	13.36	1.22	2.36	0.09	18.91	3.67	353.50	104.54	1.82	0.07
	bone	57	33.07	3.23	13.75	1.43	2.41	0.08	15.69	11.13	452.65	185.04	1.86	0.06
	rims	38	33.49	2.11	14.45	0.96	2.32	0.04	18.38	3.66	432.04	166.59	1.79	0.03
gi4a/K4	foci	39	30.97	2.27	13.24	1.07	2.34	0.07	19.20	3.64	321.54	129.93	1.81	0.05
	bone	45	32.91	2.19	13.78	0.94	2.39	0.09	15.11	2.37	517.62	190.32	1.85	0.07
	rims	33	31.37	1.92	13.59	0.84	2.31	0.05	16.58	3.08	423.49	177.81	1.78	0.04
gi5a/K4	foci	31	29.89	2.07	13.10	1.07	2.28	0.07	19.31	4.36	325.03	137.78	1.77	0.05
	bone	23	31.86	1.62	13.91	0.92	2.29	0.07	16.92	4.03	479.84	233.39	1.77	0.05
	rims	14	34.12	2.90	13.83	1.11	2.47	0.04	15.96	2.09	337.90	141.60	1.91	0.03
gi6/K4	foci	13	32.72	1.41	13.30	0.63	2.46	0.03	15.31	1.75	313.40	131.80	1.90	0.02

Table 1

section	structure type	No of analyses	Ca	sd	P	sd	Ca/P	sd	Ca/F	sd	Ca/Cl	sd	Ca/P molar	sd
	bone	11	34.62	1.51	13.93	0.60	2.49	0.02	13.47	1.53	537.83	222.72	1.92	0.02
	rims	23	34.19	2.28	14.10	0.91	2.43	0.06	13.90	1.32	404.74	98.63	1.87	0.05
gi7b/K4	foci	25	31.52	2.61	12.97	1.13	2.43	0.03	14.04	1.98	355.84	123.61	1.88	0.03
	bone	15	32.31	2.40	13.16	1.10	2.46	0.05	12.30	1.31	488.79	152.25	1.90	0.04
	rims	31	35.44	2.17	14.71	0.92	2.41	0.04	14.67	2.24	488.49	220.31	1.86	0.04
gi8/K4	foci	26	31.99	1.98	13.24	1.02	2.42	0.06	15.31	2.58	333.22	111.98	1.87	0.05
	bone	17	34.34	2.44	14.03	0.89	2.45	0.04	13.47	1.84	686.04	540.92	1.89	0.04
	rims	58	33.31	1.41	13.97	0.57	2.38	0.03	16.56	2.01	403.87	89.13	1.84	0.03
gi18/K5	foci	57	30.84	1.98	12.92	0.85	2.39	0.04	17.02	2.10	327.28	65.21	1.84	0.03
	bone	35	32.20	1.95	13.47	0.78	2.39	0.05	15.51	2.10	415.90	150.06	1.85	0.04
	cement	7	33.76	3.65	13.27	1.46	2.54	0.04	17.87	1.36	703.46	535.35	1.97	0.03
	cement rims	15	30.72	3.80	11.99	1.56	2.56	0.03	19.76	3.49	448.77	201.42	1.98	0.03
	cement foci	20	32.27	2.73	12.69	1.23	2.55	0.06	20.64	4.84	445.13	153.88	1.97	0.05
gi12/Ke	enamel	6	41.55	1.94	14.90	1.47	2.82	0.38	57.63	7.09	198.24	85.54	2.18	0.29
	dentine	10	34.26	2.27	13.69	0.79	2.50	0.06	18.44	2.09	525.68	216.08	1.93	0.04
	dentine rims	10	32.63	3.14	12.98	1.43	2.52	0.13	24.82	10.52	362.21	115.74	1.95	0.10
	dentine foci	17	29.95	3.44	12.15	1.29	2.46	0.05	26.32	6.62	262.34	110.06	1.90	0.04
	cement	12	33.71	2.29	13.95	0.92	2.42	0.08	14.31	1.63	973.89	351.12	1.87	0.06
	cement rims	10	33.12	2.79	13.78	1.11	2.40	0.05	19.12	5.28	696.49	445.61	1.86	0.04
	cement foci	10	32.15	2.39	13.40	0.85	2.40	0.04	20.40	3.44	505.68	239.65	1.85	0.03
gi23b/K4	enamel	16	37.86	1.50	16.47	0.72	2.30	0.05	47.98	14.60	158.35	52.13	1.78	0.04
	dentine	20	33.93	1.57	14.17	0.60	2.40	0.05	16.20	3.10	575.52	211.97	1.85	0.04
	dentine rims	25	34.51	1.12	14.57	0.49	2.37	0.03	20.22	3.47	506.60	122.99	1.83	0.03
	dentine foci	26	29.47	2.35	12.34	1.08	2.39	0.07	20.83	3.86	342.96	112.22	1.85	0.05
	rims	22	32.33	4.48	13.33	1.81	2.43	0.05	26.08	7.59	407.47	213.96	1.87	0.04
gi1/O.P.	foci	30	29.67	3.58	12.49	1.56	2.38	0.05	24.29	5.38	273.59	112.65	1.84	0.04
	bone	40	32.22	3.88	13.37	1.58	2.41	0.07	17.66	5.99	402.72	213.23	1.86	0.05
	rims	33	34.11	3.38	13.93	1.26	2.45	0.06	17.58	4.11	303.68	112.74	1.89	0.05
gi17a/N.P.	foci	30	31.31	3.94	12.84	1.56	2.44	0.07	18.30	2.79	251.24	98.15	1.88	0.06
	bone	26	33.81	2.56	13.79	0.93	2.45	0.05	15.33	2.90	306.37	93.09	1.89	0.04
	rims	30	29.48	4.58	12.73	2.15	2.33	0.10	17.14	2.40	472.20	210.96	1.80	0.08
gi9/ΣA	foci	25	30.54	2.33	13.33	1.10	2.29	0.04	16.73	1.71	452.15	138.17	1.77	0.03
	bone	20	32.15	1.56	14.30	0.79	2.25	0.04	16.70	2.05	436.22	240.25	1.74	0.03
	rims	16	35.50	2.49	14.54	0.69	2.44	0.08	15.39	3.42	65.00	15.72	1.89	0.06
Ch1	foci	16	32.66	2.26	13.56	0.91	2.41	0.05	16.37	3.18	45.71	15.19	1.86	0.04
	bone	14	34.06	2.33	14.00	0.90	2.43	0.06	14.20	2.41	46.23	12.55	1.88	0.05

Table 1

section	structure type	No of analyses	Ca	sd	P	sd	Ca/P	sd	Ca/F	sd	Ca/Cl	sd	Ca/P molar	sd
	rims	5	32.19	2.73	13.11	1.35	2.46	0.09	23.68	6.11	69.39	17.91	1.90	0.07
Ch2	foci	8	31.99	4.72	13.00	1.90	2.46	0.05	101.86	156.54	69.27	24.18	1.90	0.04
	bone	20	33.78	3.85	13.54	1.43	2.49	0.11	25.99	7.33	92.40	31.76	1.93	0.08
	rims	24	30.93	3.48	12.78	1.43	2.42	0.11	19.93	3.63	847.79	294.45	1.87	0.09
DTK1	foci	22	29.29	3.34	12.15	1.54	2.42	0.08	18.78	5.29	707.42	210.09	1.87	0.06
	bone	14	28.02	4.13	11.81	1.40	2.37	0.10	20.40	4.04	614.01	317.00	1.83	0.08
	rims	27	29.08	4.87	12.13	1.89	2.40	0.13	23.60	6.26	843.92	849.63	1.85	0.10
DTK2	foci	23	31.23	3.36	13.02	1.38	2.40	0.12	24.38	6.13	989.89	667.41	1.86	0.09
	bone	16	30.05	3.91	12.48	1.54	2.41	0.16	22.46	4.77	781.54	417.92	1.86	0.12
	rims	37	36.30	2.45	14.79	0.79	2.45	0.07	17.51	2.91	407.81	112.66	1.90	0.06
RP2	foci	33	34.81	2.96	14.21	1.23	2.45	0.07	17.35	2.75	373.65	108.09	1.89	0.06
	bone	23	34.86	1.66	14.35	0.65	2.43	0.07	16.06	1.56	386.10	103.88	1.88	0.05
	rims	49	34.51	2.56	14.42	0.96	2.39	0.05	20.76	4.55	565.62	215.61	1.85	0.04
VTK1a	foci	44	31.96	2.42	13.36	1.04	2.39	0.04	23.95	5.02	479.46	153.34	1.85	0.03
	bone	25	34.23	2.21	14.15	0.82	2.42	0.04	16.92	2.87	410.58	137.54	1.87	0.03
gi19a/KAS	bone	33	33.53	3.32	13.90	1.13	2.41	0.05	12.48	1.43	1856.88	1130.78	1.86	0.04
	tunnels	17	29.25	2.26	12.34	1.04	2.37	0.05	13.18	1.23	735.66	242.09	1.83	0.04
Co1a	bone	48	30.58	2.88	12.37	1.09	2.47	0.09	340.01	860.01	1903.26	1816.08	1.91	0.07
	rims	19	33.14	3.15	13.30	1.21	2.49	0.09	23.35	10.45	1969.23	1253.95	1.93	0.07
Co2b	foci	14	32.45	3.85	13.00	1.50	2.50	0.08	20.96	8.36	4485.69	9837.68	1.93	0.06
	bone	45	30.52	2.22	11.96	0.82	2.55	0.09	51.67	38.92	2563.75	1985.20	1.97	0.07
Qu	bone	17	29.76	2.05	13.85	0.99	2.15	0.13	488.08	1102.19	2959.42	7728.01	1.66	0.10
gi22c/Agr	recent bone	76	30.31	2.15	12.72	0.81	2.38	0.10	615.79	908.09	1932.42	1412.10	1.84	0.07
	weathered	35	30.88	2.43	13.09	0.98	2.36	0.09	158.72	135.11	458.81	234.05	1.82	0.07
gi20b/BT	recent bone	51	28.88	1.51	13.52	0.67	2.14	0.07	224.91	242.89	667.54	231.66	1.65	0.06
gi21/BS	recent bone	45	29.26	2.26	13.17	0.96	2.22	0.10	331.27	281.96	758.44	251.52	1.72	0.08

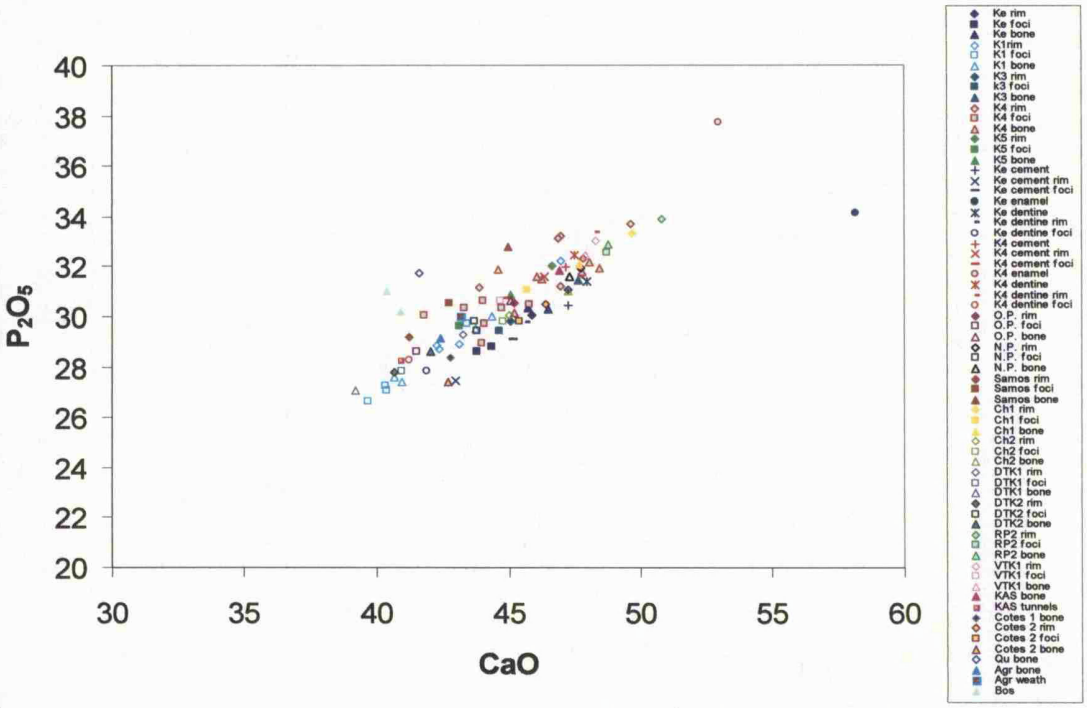

Figure 2: Plot of average values of CaO vs P_2O_5 for fossil bone and teeth and recent bone. The points in this plot for the fossil specimens represent the three structural areas of the bioeroded tissues (undamaged areas, foci and rims of the foci) from Kerassia and the other studied Miocene and Pleistocene localities. Diamonds: rims of foci in bone, squares: foci in bone, triangles: undamaged bone.

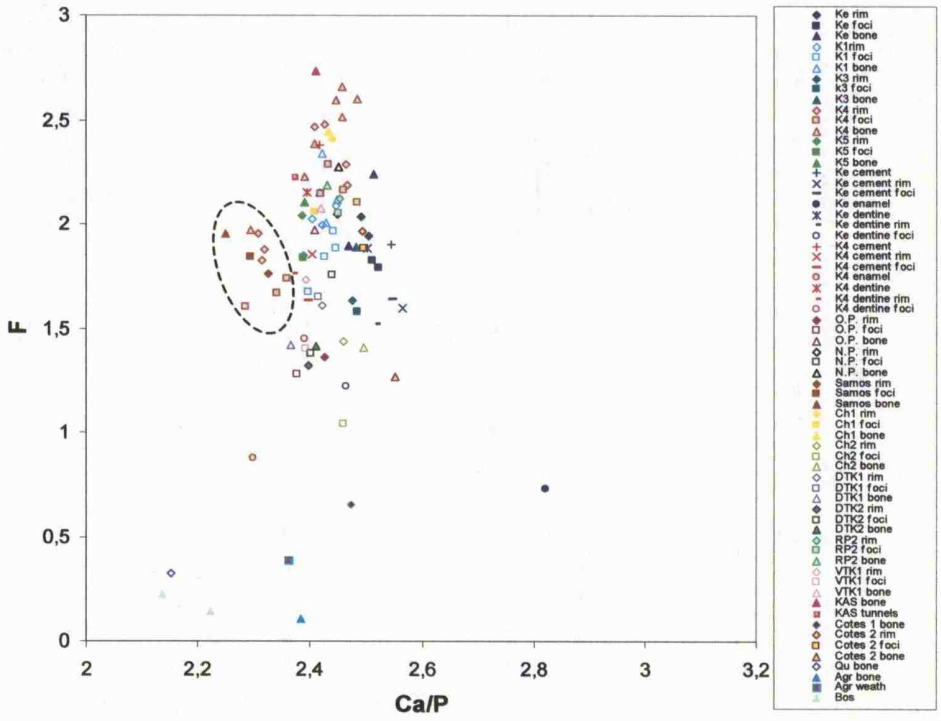

Figure 3: Plot of average values of Ca/P vs F for fossil bone and teeth and recent bone. The points in this plot for the fossil specimens represent the three structural areas of the bioeroded tissues (undamaged areas, foci and rims of the foci) from Kerassia and the other studied Miocene and Pleistocene localities. The dashed ellipse surrounds the low Ca/P ratio group from Kerassia. Qu: Quorn, Agr: recent weathered bone, Bos: recent unweathered bone.

it is the undamaged bone that has the lowest total values. In the specimen from Samos the rims present the lowest total and the undamaged bone the highest total values.

Ca and P

An enrichment in Ca is evident in most fossil samples and even in the weathered recent sample. P content values are less consistent, enriched in some samples but depleted in others. In the specimens from Kerassia it is evident that those from the lower horizon are relatively enriched in P, compared with those from the upper horizon. In the bone, dentine and cement the Ca and P concentrations are higher in the rims and lower in the foci (Table 1, Fig. 2).

F, Cl, Mg and Na

The fluorine concentrations in the fossil tissues are significantly higher than their recent counterparts (Table 1). The F content in living bone and teeth tissues is normally less than 0.1 % (Carlson, 1990; Driessens and Verbeeck, 1990). The incorporation of F into hard tissues during diagenesis and the increase of its concentration over time were first observed by Middleton in 1844. In the studied fossil bone, dentine and cement samples F always exceeds 1 wt % and may exceed 3 wt%. The maximum F concentration for stoichiometric fluorapatite is 3.77 wt % (Johnsson, 1997). According to Hubert *et al.* (1996) and Wilson (1999) and based on XRD analyses these tissues consist of carbonate fluorapatite. In enamel the F wt% concentrations are always below 1%, and thus indicate the presence of carbonated hydroxyapatite (Hubert *et al.*, 1996;Wilson, 1999). The fluorine content in all the examined Miocene bone specimens is above 1% wt. The F concentrations are higher in the undamaged areas than in the foci and the rims of the foci, and the lowest F concentrations are found in the foci (Table 1).

As for the other two major constituents of the tissues, Mg is significantly depleted relative to recent bone in most fossil samples except from the enamel samples and those from Chalkoutsi which present only a slight depletion. Na appears to be relatively enriched in fossil samples and especially those from Kerassia relative to the examined recent samples, (Table 1). However, Carlson (1990) and Gross and Berndt (2002) reported values of Na in recent bone significantly higher than those of the recent samples analysed here, with values as high as 0.7 wt %. Compared with these values the studied fossil specimens are clearly depleted in Na. It worth noting that the concentrations of Mg and Na, particularly in the samples from Kerassia, have the lowest values in the undamaged areas and the highest values most often in the rims, although occasionally foci may present the highest values.

Although, the Cl content is relatively low in most of the examined specimens, it was still high enough to be above the detection limit (Table 1). The Cl content in all the Miocene samples is elevated relative to recent bone, and in particular in the samples from Chalkoutsi this increase is very significant (up to 0.78 wt %). Recent enamel presents the highest values of Cl among recent tissues with values of 0.3 wt % (Carlson, 1990; Gross and Berndt, 2002); however, Cl in fossil enamel analysed here appears slightly depleted. The Cl content in the recent weathered bone sample is higher than in recent bone, but it is lower in the Pleistocene bone samples. Although the differences are not significant, it is evident that Cl concentrations are higher in the foci than in the rims of the foci and the undamaged areas, whereas the lowest Cl concentrations are found in the undamaged areas of bone, dentine and cement.

Other elements

Relative to the recent bone samples, the rest of the elements examined in the analysed specimens generally show an enrichment (Table 1). Of particular interest is the enrichment in Fe in the Pleistocene samples; in the samples from Cotes the Fe content ranges 0-1.79 %, whereas in the sample from Quorn it ranges between 1.28-7.98 %. This surplus in Fe is in agreement with the permineralised (permineralization is the deposition of minerals from solution in the interstices of hard tissue during diagenesis) pyrite phase found in the voids of these bones. Compared to the recent bone specimens, the studied fossil specimens have higher Sr concentrations. However, in the majority of the analysed specimens the Sr and Ba concentrations were below the detection limit. No pattern to the distribution of Sr or Ba was observed between the foci, the rims and the undamaged areas of the tissues.

The concentrations of La, Ce and Y in the majority of the samples were below 0.1 % and therefore lower than the detection limit. However, in a small number of specimens their concentrations were high enough to be considered detectable. In specimens gi 14a and gi16 from Kerassia the concentrations for Ce and Y are above their detection limits (Table 1), while the lower values are found in the foci. In Kassandria the concentrations of La, Ce and Y are significantly higher, particularly around the fungal tunnels at the exterior of the bone. Interestingly, the values for Y are 0.71 % in the undamaged bone and 1.06 % around the fungal tunnels.

X-RAY EMISSION MICROANALYSIS AND THE CHEMISTRY OF BONES AND TEETH

Total values

XREMA spot analysis is a useful tool for the geochemical study of the microbially eroded tissues, because it enables the chemical investigation of areas on a microscopic scale. The foci, rims and undamaged areas of bone, dentine and cement show chemical (Table 1) as well as structural differences (chapter 1). The total chemical values were low in samples used because the available settings of the microprobe did not allow the measurement of the structurally bound CO_2 (as CO_3^{-2}), H_2O (as OH^-), and quantities of surficially located CO_2 and H_2O. The ideal formula of a carbonated fluorapatite would be $Ca_{10}(PO_4,CO_3)_6F_2$. As the F contents in the analysed specimens are always below the maximum theoretical concentration value of 3.77% (Johnsson, 1997) and the Cl content is low (Table 1), OH^- would be an integral part in the fossil bone, dentine, cement and enamel apatite lattice. In fossil bone structural CO_2 (as CO_3^{-2}) has been found to exceed 5 % (Hubert *et al.*, 1996; Elorza *et al.*, 1999) and, similarly, concentrations of structural H_2O (as OH^-) may exceed 4 % (Hubert *et al.*, 1996). A second reason for the low totals is that the surfaces of the tissues scanned by the electron beam contain micro-pores due to the structural and intercrystalline microporosity of the tissues that have not been filled during the diagenetic recrystallization of the apatite, and thus, it was not possible to avoid them. In the foci, in particular, this would be enhanced by the presence of the microtunnel network. Even if the substrate of a selected spot struck by the beam appeared to be solid, there is a good probability of micro-pores or microtunnels (in the foci) being present underneath. Due to the fact that the emitted X-rays are not only released from the surface of the analysed specimen but also from a depth beneath the surface, the presence of pores or other micocavities will decrease the total number of counts for the measurements in such areas, hence, such total values are expected to be low and possibly biased. Finally, a third possible reason for some of the low total values is the topographic variation of the surfaces of the thin sections. During thin section polishing, certain parts that exhibit a higher rate of abrasion, possibly like the porous foci, might have worn out more easily than for example their surrounding rims. High points and ridges will allow then the emission of more X-rays, whereas, depressions will allow the emission of less X-rays. Consequently, the concentrations of the element/elements determined by the counts of the detectors could be biased. Moreover, the orientation of some high points might block X-rays emitted from a spot in a depression from reaching a certain detector and thus, reducing the total number of counts for the measurements collected by this particular detector. In this case,

the concentrations of the elements analysed by the other two detectors will be accurate but the concentrations of the elements analysed by the shaded detector will be lower than their actual values.

Despite this, the variation in the total values can be explained to a certain degree by the variation in the wt % content of CO_2 and H_2O as well as by the microporosity of the different samples. Differences in the total values can be also accounted for by the significant enrichment in F, which replaces OH and indicates a decrease in the structural H_2O content. This variation depends on the type of tissue, on the relative position of the selected spot analyses and on whether the selected spots were in rims, foci or undamaged areas. For instance enamel, the tissue with the lowest CO_2 concentration and the minimum microporosity, presents the highest total values. Similarly, rims of foci which appear bright under backscatter electron imaging (BEI) because they are probably more mineralised (chapter 1) and have higher total values than the foci and the undamaged areas. This indicates that rims may have less or very little microporosity. Conversely, foci and especially those that appear dark under BEI, present the lowest total values due to the increased microporosity (microtunnel network and perhaps diagenetic demineralization) (chapter 1). However, there are a few foci that are bright under BEI which also have relatively high total values, similar to those of the bright rims. Although, the presence of bright and dark areas in tissues, studied using the BEI mode, is mainly related to density differences and more specifically to differences in the mean atomic number probed by the beam, it can be also attributed, as mentioned above for the XREMA, to differences in the topography between the two areas (Bell *et al.*, 1991). High points and ridges will allow more back scattered electrons to escape, whereas, depressions will allow fewer back scattered electrons to escape. Therefore, under BEI the former will appear brighter and the latter darker. Consequently, some of the contrast differences between bright rims and dark foci might not be due to mineral density but due to differences in the topography. Some of the bright rims might form high ridges and conversely the respective foci might form depressions. During thin section polishing, the porous foci might have worn out more easily than their surrounding rims, exhibiting a higher rate of abrasion. Despite the possible effect that topography might have to the brightness of the structural areas of the damaged tissues, the overall features indicate varying density among the rims, the foci and the undamaged areas of the tissues and which has been also identified previously by other workers (Hackett, 1981; Bell, 1990; Bell *et al.*, 1991; Jackes *et al.*, 2001; Turner-Walker and Syverson, 2002). Therefore, there is a good reason to investigate the

varying density of the different structural areas of the damaged tissues, and the possible (quantitative) chemical differences among them.

Low total values in foci are particularly evident in some samples from the upper horizon of Kerassia (Table 1), where the average total values for the foci are below 70 wt %, lower than values from the lower horizon and lower even than the total values of recent bone. The total values of Ca, P, F, Na and Cl in the bone and tooth specimens from the lower horizon at Kerassia are markedly higher than those from the upper horizon (Table 1), suggesting that the specimens from the lower horizon are more mineralised. The different degree of mineralization that the collected specimens from the two horizons exhibit is probably responsible for the distinct differences in the overall preservation and colouration of the fossils (white in the upper horizon, grey in the lower horizon). These differences can possibly be attributed to the fact that the bone bearing sediments from the lower horizon are more carbonate rich that those from the upper horizon and thus more alkaline. This is also supported by the extensive calcitic encrustations that surround the specimens in the lower horizon. Higher alkalinities probably facilitate the recrystallization of apatite and the precipitation of calcite in the voids of the tissues.

Differences in element concentrations in some of the samples from the other Late Miocene localities may be attributed to different sedimentological settings and different hydrological regimes as well as to seasonal differences. This requires further investigation.

Ca/P ratio

The two unweathered recent bone samples gave Ca/P ratio values of 2.14 and 2.22 respectively. These values coincide with the value of 2.14 that Quattropani *et al.* (1999) and the value range of 2.09 – 2.26 that Pate *et al.* (1989) reported for recent bone. In all the examined fossil samples and even in the recent weathered bone sample the Ca/P ratio is considerably higher than in the unweathered recent bone. The only exception is the Pleistocene sample from Quorn with a value (2.15) that coincides with values for recent bone. There are also ostensible differences in the Ca/P ratio between specimens from the upper and the lower horizons at Kerassia. The average Ca/P ratio values for the analysed specimens from the upper horizon range between 2.38-2.52. The average Ca/P ratios for the bone specimens from the lower horizon, as seen in figure 3, are separated into two groups; a group with relatively high Ca/P values (2.38-2.49), within the range values of the specimens from the upper horizon, and a second group with relatively low values (2.28-2.36). In the enamel,

the difference of the average Ca/P ratio between the specimens from the two horizons is also notable; 2.3 for the lower horizon and 2.82 for the upper horizon. The average Ca/P ratios of almost all the other examined Miocene fossil bone specimens range between 2.37-2.5, the values of which coincide with those from Kerassia. Interestingly, the Ca/P ratios of the specimens from the Pleistocene locality of Cotes are among the highest ones (2.47-2.55). Conversely, in the specimen from Samos the Ca/P values are relatively low (2.25-2.33) and similar to the low values group from the lower horizon of Kerassia. The recent weathered bone also presents relatively high values (2.36 for the weathered external zone and 2.38 for the internal unweathered zone). The high Ca/P ratios in the fossil tissues, and even in the weathered bone specimen, provide evidence that the Ca/P ratios of diagenetically altered tissues cannot be used as a measure of stratigraphic age or crystallinity.

Sillen (1986, 1989) suggested that an increase in Ca content in diagenetically altered bones could be caused by the presence of calcite as a permineralizing phase in the micro voids. I believe that there is an alternative explanation. An increase in CO_3 in the recrystallized apatite lattice may also account for the increase in Ca relative to P in fossil tissues. During the recrystallization process CO_3 may either substitute for PO_4 in the apatite lattice, or, where pore waters contain a high concentration of Ca and CO_3, this CO_3 may be available for carbonated hydroxyl- or fluorapatite precipitation and is thus incorporated into the apatite lattice. That all analysed samples contained permineralized calcite in the structural and diagenetic voids of the tissues suggests that pore waters were enriched in Ca and CO_3, and therefore Ca and CO_3 were available for apatite recrystallization. Specimens with high Ca/P ratio values probably contain more CO_3 at the expense of PO_4 than the specimens with low ratio values. This is because the PO_4 content in pore waters is not proportional to the available Ca and thus pore waters that are enriched in Ca and CO_3 will facilitate the incorporation of CO_3 in the recrystallizing apatite. The variability in the Ca/P ratios, even in specimens from the same site, indicate that during diagenesis the concentrations of Ca and CO_3 in pore waters were variable on a small scale, and reflect differences in the conditions of the local burial environment, the chemistry of the local pore waters and the local hydrological regimes.

THE EFFECT OF BACTERIAL DAMAGE ON THE CHEMISTRY OF THE TISSUES

The XREMA results indicate that the rims, the foci and the undamaged areas have different chemistries as well as different structural properties (chapter one). In SEM BEI images (Fig.

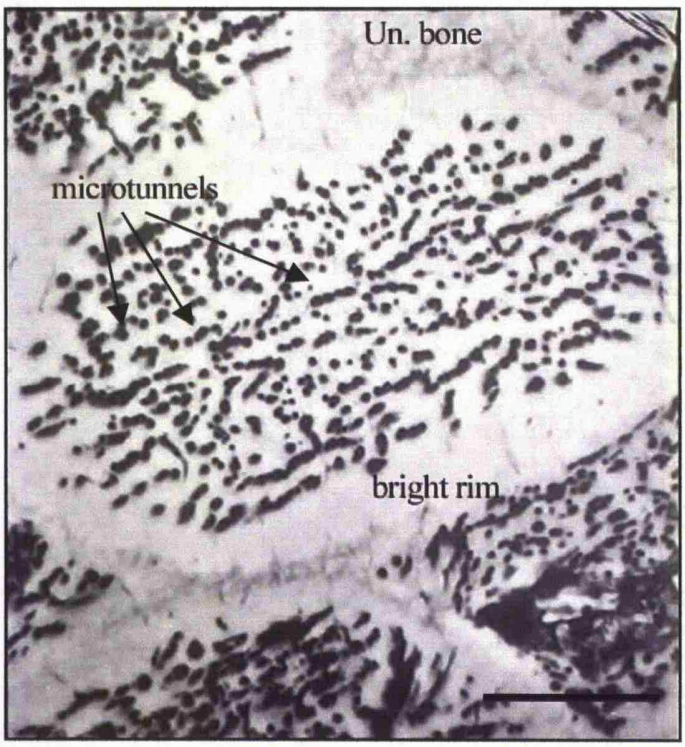

Figure 4: Portion of bacterially damaged bone (undetermined long bone fragment from site K4, specimen K4/Δ118/4, thin section GI8). An ellipsoid focus occupies the centre of the photograph; the microtunnel network can be easily identified in the focus and the bright rims at the perimeter of the focus. Portions of undamaged bone can also be seen in between the neighbouring foci (scale bar: 11μm).

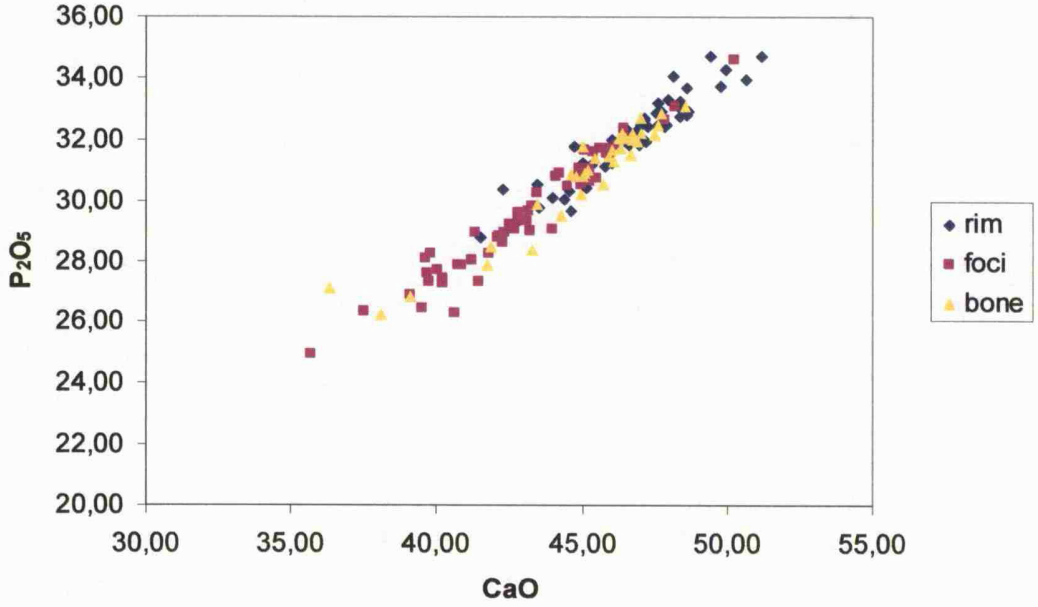

Figure 5: Plot of CaO vs P_2O_5 for a bone specimen from site K5 (thin section GI18a). The rims of the foci dominate the upper and the foci the lower part of the cluster. The plot of the selected bone specimen shows the general linear trend observed in all studied bone specimens.

4) the rims appear brighter, and thus more mineralised with higher mineral densities. Despite the limitations and problems mentioned above, the microprobe data from spot analyses in the rims, the foci and the undamaged areas of the bone, dentine and cement support this (Table 1), because the rims appear to have the highest total values and the highest Ca and P contents, whereas the foci appear to have the lowest total values and Ca and P contents (Fig. 2). Therefore, the rims appear hypermineralised (Hackett, 1981) and the foci demineralised. In figures 5 and 6 where CaO is plotted against P_2O_5 it is clear that the points of the rims occupy the upper part of the cluster, the points of the foci occupy the lower part of the cluster and the points of the undamaged bone dentine and cement are found in between the other two groups. A two-tailed t-test was employed to test the likelihood whether the Ca and P mean values for the rims, the foci and the undamaged areas of the bone specimens from Kerassia were equivalent or significantly different. The Ca and P mean values for the three structural areas of the damaged bone from Kerassia were tested in pairs. The null hypothesis was whether the mean Ca and P values in one of the structural areas were equivalent to the mean Ca and P values in the other two. The test showed that both the mean Ca and P values in the foci are significantly different from the mean Ca and P values in the rims ($t=-3.85$, $p=0.0006$ for Ca and $t=-3.77$, $p=0.0008$ for P) and the undamaged bone ($t=2.93$, $p=0.0066$ for Ca and $t=2.74$, p 0.011 for P) at the $p=0.05$ level (Table 2). For the third pairs (mean Ca and P values in the rims – mean Ca and P values in the undamaged bone) the probability was above the 0.05 level, therefore, the null hypothesis is not rejected. Hence, the Ca and P content in the foci of the tissues is significantly lower than the Ca and P content in the rims and the undamaged areas of the bacterially damaged tissues. Conversely, the difference in the Ca and P content between the rims and the undamaged areas is not significant.

However, the interpretation for the latter could be slightly different. As reported in chapter one, two different forms of foci were identified in the studied material, bright and dark foci. These foci often overlap each other and thus correspond to at least two different generations of foci and consequently to two different invasions or periods of bacterial activity. Their formation has been attributed to seasonality, and to the Mediterranean type climate that prevailed in the North-eastern Mediterranean during the Late Miocene (chapter one). According to Schaeffer (1973) microorganisms in Mediterranean type climates show two periods or seasons of growth; one at the onset of the dry season and a second at the beginning of the wet season. The more mineralised and thus bright foci were formed during the spring-summer period of growth (chapter one). Conversely, the specimens where both the rims and the foci are demineralised and thus appear dark in BEI images were formed during the

Table 2

Ho	t	p	reject Ho at P=0.05		mean values
Frim=Ffoci	-1.94	0.062		Fbone	2.25
Frim=Fbone	-2.21	0.035	√	Ffoci	1.87
Fbone=Ffoci	4.24	0.0002	√	Frims	2.04
Mgrim=Mgfoci	-0.31	0.76		Mgbone	0.19
Mgrim=Mgbone	2.55	0.016	√	Mgfoci	0.22
Mgbone=Mgfoci	-2.24	0.033	√	Mgrims	0.23
Narim=Nafoci	-0.83	0.41		Nabone	0.28
Narim=Nabone	2.71	0.011	√	Nafoci	0.31
Nabone=Nafoci	-1.81	0.082		Narims	0.32
Carim=Cafoci	-3.85	0.0006	√	Cabone	45.40
Carim=Cabone	0.68	0.5		Cafoci	43.17
Cabone=Cafoci	2.93	0.0066	√	Carims	45.96
Prim=Pfoci	-3.77	0.0008	√	Pbone	30.56
Prim=Pbone	1.12	0.27		Pfoci	29.17
Pbone=Pfoci	2.74	0.011	√	Prims	31.20
Clrim=Clfoci	1.43	0.16		Clbone	0.07
Clrim=Clbone	0.73	0.47		Clfoci	0.09
Clbone=Clfoci	-2.16	0.04	√	Clrims	0.08
Ca/Prim=Ca/Pfoci	0.44	0.66		Ca/Pbone	2.43
Ca/Prim=Ca/Pbone	-0.82	0.41		Ca/Pfoci	2.43
Ca/Pbone=Ca/Pfoc	0.33	0.74		Ca/Prims	2.42

Table 2: Two-tailed t-Test, for the Ca, P, F, Cl, Mg and Na contents and the Ca/P ratio in foci, rims and undamaged areas of the fifteen bacterially eroded fossil bone specimens from Kerassia. The mean values of each of the above elements and the Ca/P ratio for the three structural areas of the damaged bone from Kerassia were tested in pairs. The null hypothesis (Ho) was whether the content values of the two members of each pair were equivalent. The number of tested specimens (n) is 15, therefore the degrees of freedom are 14. The t and p values for each tested pair are given in the table. The selected level of significance is p=0.05. The mean values of the Ca/P ratio and the mean values of the content of each element for each structural area of the bacterially damaged bones is also provided.

autumn-winter period of growth where apatite was depleted from the foci (chapter one). The Ca and P contents of these bright rims would be significantly higher than the respective undamaged tissue Ca and P contents, whereas, the Ca and P contents of the dark demineralised rims would be similar or even lower than the respective Ca and P contents of the undamaged tissues. As the mean values of the specimens, tested in the t-test, include the Ca and P content of both the bright and dark rims, the significance of the higher Ca and P contents in the bright rims was not tested. In figures 5 and 6 it is clear that, as mentioned above, the points of the rims occupy the upper part of the clusters, and also the mean values of Ca and P of all the analysed specimens from Kerassia (Table 2) indicating that generally the rims are more mineralised than the undamaged bone. Also, the total values of the rims in the majority of the examined specimens are higher than the respective values of the foci and the undamaged areas, hence it can be concluded that most of the bacterial activity and destruction in the tissues occurred during the spring-summer period.

Ca/P ratios in the rims, the foci and the undamaged areas

Despite the differences in the degree of mineralisation between the three structural areas of the bioeroded tissues, the Ca/P ratio for neighbouring rims, foci and undamaged areas of a studied specimen remains practically the same. In each thin section, the average values of the Ca/P ratio for the rims, the foci and the undamaged areas of (Table 1) are also similar indicating that this similarity is consistent. Again, a two-tailed t-test was employed to test the likelihood whether the mean values of the Ca/P ratios for the rims, the foci and the undamaged areas of the bone specimens from Kerassia were equivalent or different. The null hypothesis was not rejected at the p=0.05 level (Table 2), and thus it is supported statistically that the Ca/P ratios in the three structural areas are relatively equivalent. Consequently, the Ca contents in the foci, the rims and the undamaged areas can be considered proportional to the respective P contents. This suggests that during the diagenetic recrystallisation of the apatite crystallites in each bone or tooth sample, the overall chemistry of the pore waters in the foci, the rims and the undamaged areas were probably similar. The recrystallised apatite appears to have come from the same source, apparently the respective hard tissue. In the CaO vs P_2O_5 scatter diagrams (Fig. 5, 6) the linear relationship among the points of the spot analyses for the rims, foci and undamaged areas is evident for each individual group as well as for all three groups together. High R^2 values ($R^2 > 0.9$) for the rims, the foci and the undamaged areas of the tissues suggest that the points in each group, as well as in the three groups as a whole show a significant linear regression with no lack of fit. A positive correlation is also evident between the two variables, CaO and P_2O_5 . Hence, the similarity in the Ca/P ratios in the rims,

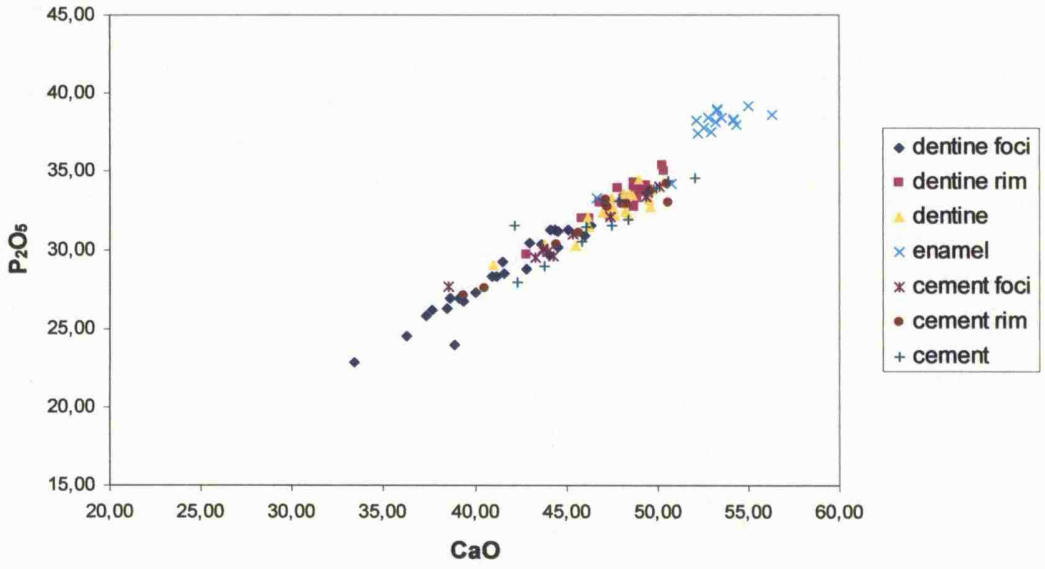

Figure 6: Plot of CaO vs P_2O_5 for tooth specimen K4/Δ66/3 from site K4 (thin section GI23b). The plot of the selected tooth specimen shows the general linear trend observed in all studied tooth specimens.

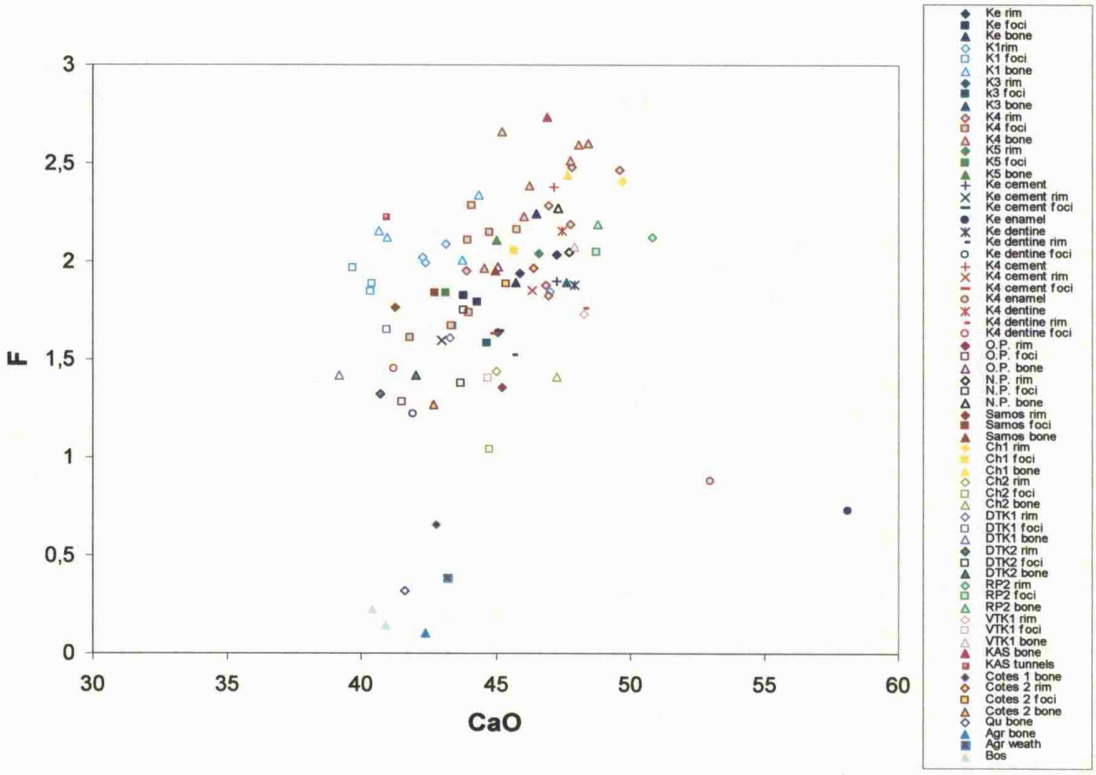

Figure 7: Plot of average values of CaO vs F for fossil bone and teeth and recent bone. The points in this plot for the fossil specimens represent the three structural areas of the bioeroded tissues (undamaged areas, foci and rims of the foci) from Kerassia and the other studied Miocene and Pleistocene localities. Diamonds: rims of foci in bone, squares: foci in bone, triangles: undamaged bone.

foci and undamaged areas indicates that the CO_3 content in the three structural areas of the tissues would be proportional to the concentrations of Ca and P. It has been suggested that the increase and variation of the Ca/P ratios in apatite can be used as an indicator of the relative diagenetic alteration (Sillen, 1986; Turner-Walker and Syverson, 2002). Evidence shows that the Ca/P ratio also accounts for the content of incorporated CO_3 in the apatite lattice. Increase and variation of the Ca/P ratios possibly indicates a similar increase and variation in the concentration of structural CO_3. Thus, Ca/P ratios could provide an indirect and relative measure of the CO_3 content in diagenetically altered tissues. That the porous tunnelled interior of the foci, the unquestionably less porous rims and the undamaged areas have similar Ca/P ratios provides further evidence that diagenetic CO_3 in the apatite is primarily structural. This is contrary to the explanation previously reported by Sillen (1986, 1989) who suggested that the increase in the Ca/P ratios was caused by a permineralized calcite phase in the microvoids. Interestingly, the low Ca/P ratio group from the lower horizon (Fig. 3) includes the rims and foci of three bone specimens (sections gi3, gi4a and gi5a) and the undamaged bone of only one specimen (gi5a). Compared to the other specimens from site K4 the members of this low Ca/P ratio group and consequently of low CO_3 contents, also have relatively low F concentration values (Table 1). This can possibly be related to the presence of pore waters with a low CO_3 content or, most likely, to pore water flows that were locally limited or reduced, even within the same sample due to early recrystallization in the foci. Thus, these bones were recrystallized under different chemical conditions.

Fluorine

In the majority of the examined specimens, including all the specimens from Kerassia, a consistent pattern in the F content between rims, foci and undamaged tissue occurs. The F content is consistently higher in the undamaged areas and lower in the foci, and this has been identified not only in bone, but in dentine and cement as well (Table 1,2; Figs. 7, 8 and 9). The only exceptions to this trend are the Pleistocene specimens from Cotes where the F content is lower in the undamaged bone and higher in the rims, and the specimen from Ditiko 1 (DTK 1) where the F content is higher in the foci and lower in the undamaged bone. The pattern cannot be explained by the higher total values of the rims and the undamaged areas, as the Ca/F ratios demonstrate. The Ca/F ratios are consistently higher in the foci and lower in the undamaged areas verifying that the highest F concentrations occur in the undamaged areas and the lowest F concentrations occur in the foci (Table 1). In figures 8 and 9 where Ca is plotted against F, the segregation between the rims, the foci and the undamaged areas is obvious in the presented bone and tooth samples. To test whether the fluorine mean values for

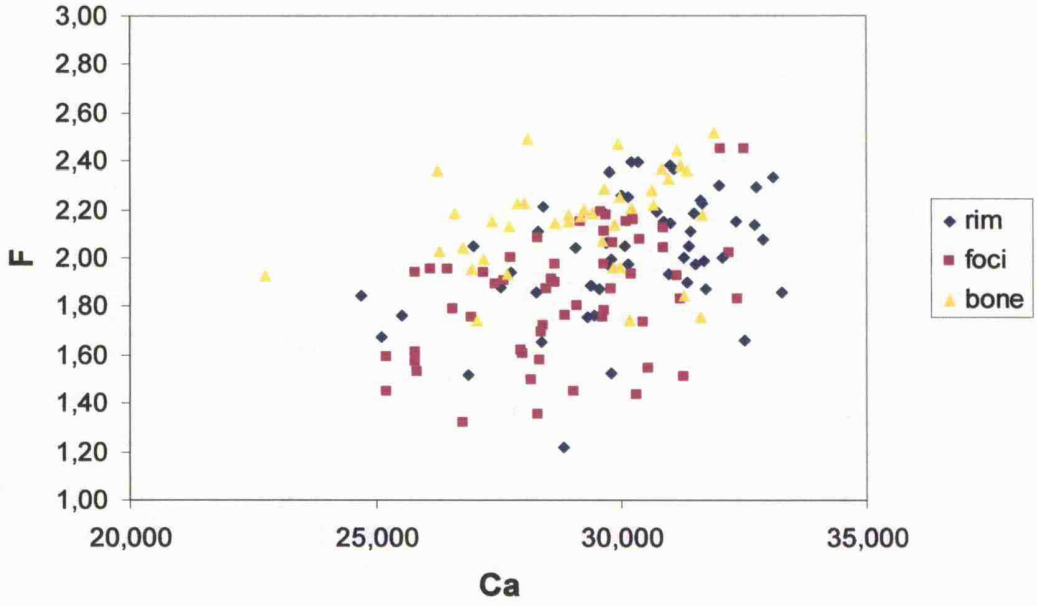

Figure 8: Plot of Ca vs F for a bone specimen from site K1 (thin section GI15a). The undamaged bone points dominate the upper part of the cluster, while the points of the foci dominate the lower part of the cluster. The selected bone specimen is representative of the general trend observed in all studied bone specimens.

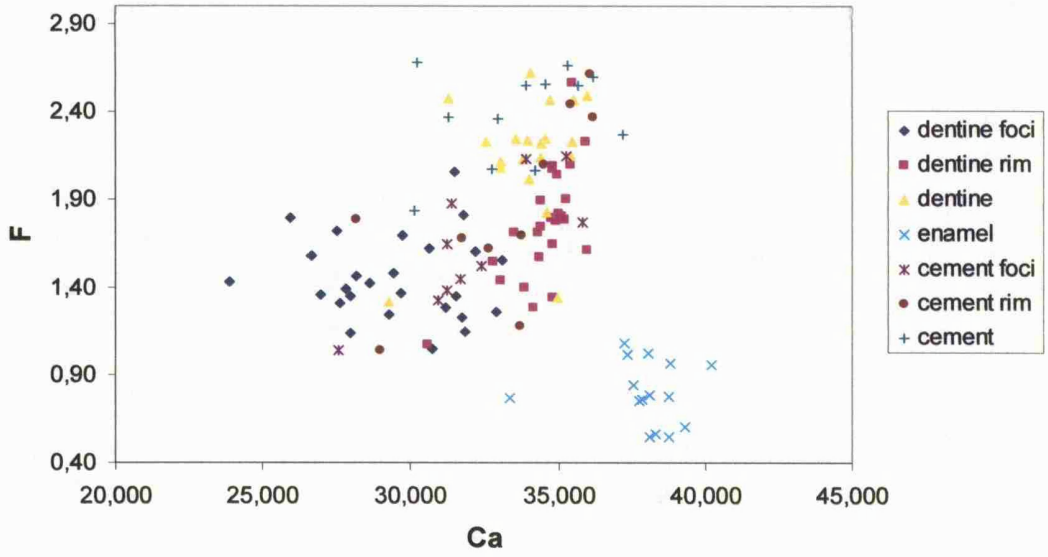

Figure 9: Plot of Ca vs F for tooth specimen K4/Δ66/3 from site K4 (thin section GI23b). The undamaged dentine and cement points dominate the upper part of the cluster, while the points of the foci dominate the lower part of the cluster. The enamel points which present the lowest F and highest Ca concentration values are clearly separated from the dentine and the cement points. The selected tooth specimen is representative of the general trend observed in all studied tooth specimens.

the rims, the foci and the undamaged areas of the bone specimens from Kerassia were equivalent or significantly different, a two-tailed t-test was employed. The null hypothesis was whether the mean F values in one of the structural areas were equivalent to the mean F values of the other two. The test showed that the mean F values in the bone are significantly different from both the mean F values in the rims ($t=-2.21$, $p=0.035$) and the foci ($t=4.24$, $p=0.0002$) (Table 2) at the $p=0.05$ level. For the third pair (mean F values in the rims – mean F values in the foci) the probability was close but still above the 0.05 level, therefore, the null hypothesis is not rejected. However, as the probability is close to the 0.05 level (Table 2) it shows that the significance for this pair is definitely less but still evident. Hence, the F content in the undamaged areas of the tissues is significantly higher than the F content in the rims and the foci of the bacterially damaged tissues.

A model has been proposed in chapter one to explain these differences in the F content and to provide a possible mechanism for the formation and preservation of the so called lamellate foci (Hackett, 1981). According to this model, the dissolution of the apatite and exploitation of the attacked hard tissues by bacterial activity was followed by the saturation of the solutions in the foci with Ca and PO_4. The dissolution of the apatite and/or the presence of bacterial metabolic products had a buffering effect and the pH was maintained to near neutral levels (Welsch *et al.*, 2002). Saturation and neutral pH values caused and promoted the precipitation and crystallisation of the dissolved apatite. According to Pate and Brown (1985) crystallization of hydroxyapatite commences when pH exceeds 6.9. This process was relatively faster around the rims of the foci and slower towards the centre of the foci and permitted the recrystallization of the crystallites around the microtunnels. The inter-crystallite spaces in the foci became filled and, therefore, the effect of diagenetic recrystallization in the foci would have been limited. Despite the ostensible porosity of the microtunnel network in the foci the reduced intercrystallite spaces would have restrained the influx of F, and this is why the interiors of the foci present lower F concentrations. Once the collagen fibrils were removed from the undamaged areas, the intercrystallite network would have provided the required porosity for the diffusion of F. The low F content in enamel can be explained by the same mechanism; indeed in enamel this process is more pronounced. Enamel has large and well crystallised crystallites with an insignificant organic content and therefore a low porosity. These factors would not only restrain the F influx but in general they would have limited any diagenetic alteration. It is worth noting that fungal tunnels also have lower F contents around them compared to the undamaged bone, as was seen in the specimen from Kassandria. In addition, in the examined recent weathered bone the weathered part of the

tissue had greater F contents than the unweathered part, indicating that the incorporation of F in the apatite commences at the very early stages of diagenesis.

Chlorine

Except from the relative high Cl concentrations in the enamel and the two samples from Chalkoutsi, the Cl concentrations in the specimens from Kerassia and the other Miocene localities are low, just above the detection limit. Therefore, there is a possibility that the measurements of these low Cl contents were influenced from Cl that could have been incorporated from the water that was used during the polishing of the thin sections and/or from Cl possibly found in the resins that were used for the preparation of the thin sections. Despite this, the distribution of Cl in the damaged tissues presents a rather consistent pattern. In 72.4% of all examined specimens, including 89.5% of the specimens from Kerassia, the Cl content is found to be higher in the foci and lower in the undamaged areas (Table 1). Conversely, the Ca/Cl ratios are lower in the foci and higher in the undamaged areas. Also, in the Pleistocene sample from Cotes the Cl content is similarly lower in the undamaged bone but higher in the rims. Two of the specimens from Kerassia as well as specimens from Old Pikermi, Samos, Ditiko 1, Ditiko 2, Vathilakkos1 and one specimen from Chalkoutsi present higher Cl values in the undamaged areas (Table 1). In figure 10 Ca vs Cl is shown for a bone sample from the upper horizon of Kerassia and it is evident that the undamaged bone points occupy the lower part of the cluster. In figure 11 a similar picture is evident for the undamaged cement and dentine, which occupy the lower part of the cluster, whereas the Cl-rich enamel is clearly segregated from the cement and the dentine. Similarly, in figure 14 the average Cl content values for all the examined specimens are displayed and the dominant trend of the higher Cl contents in the foci relative to the rims and the undamaged areas is evident. From this diagram is also clear that the specimens from the upper horizon are less chlorinated than their counterparts from the lower horizon. To test statistically the significance of this observation, that the Cl content is higher in the foci than in the undamaged areas, a two tailed t-test was employed. The null hypothesis was whether the mean Cl values in one of the structural areas of the damaged bones from Kerassia were equivalent to the mean Cl values in the other two. The null hypothesis was rejected after the mean Cl values in the bone were found to be significantly different from the mean Cl values in the foci ($t=-2.16$, $p=0.04$) at the 0.05 level (Table 2). Thus, the Cl content is significantly different, and more specifically it is higher in the foci than in the undamaged bone. Conversely, the null hypothesis was not rejected for the other two pairs (rims-foci and rims-bone) (Table 2) and

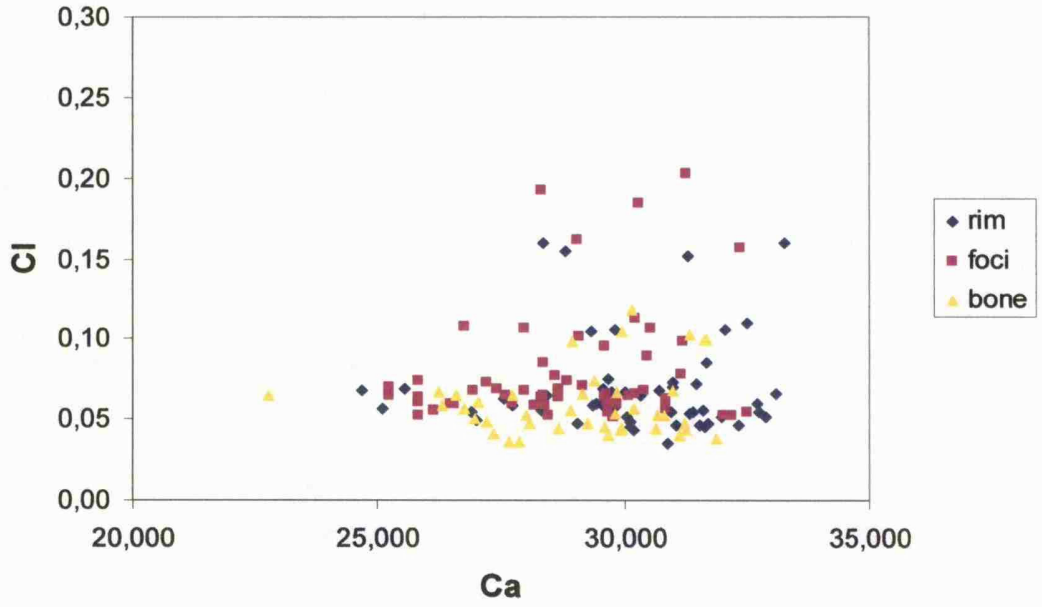

Figure 10: Plot of Ca vs Cl for a bone specimen from site K1 (thin section GI15a). The undamaged bone points dominate the lower part of the cluster, while the points of the foci dominate the upper part of the cluster. The selected bone specimen is representative of the general trend observed in all studied bone specimens.

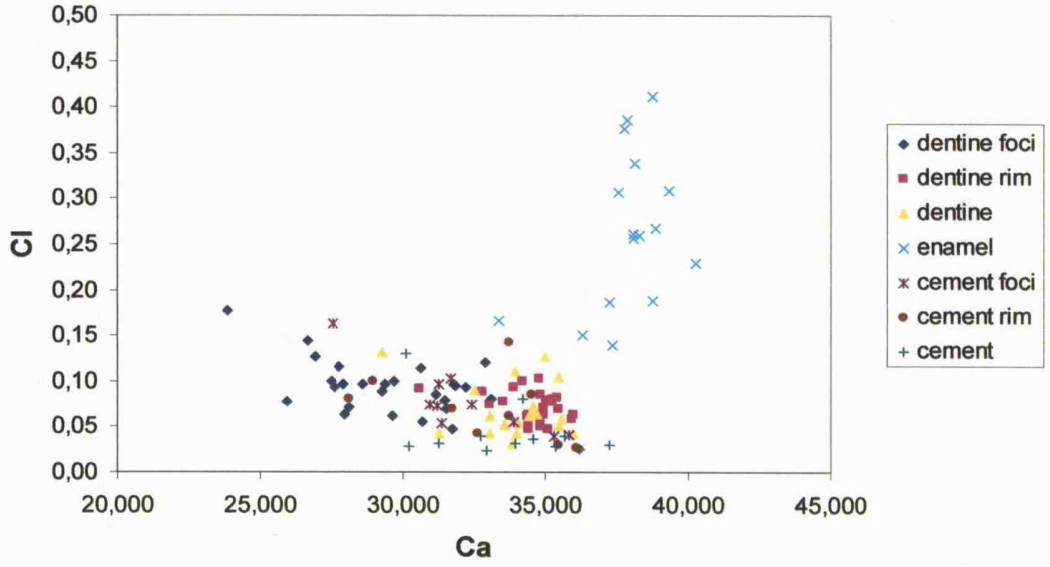

Figure 11: Plot of Ca vs Cl for tooth specimen K4/Δ66/3 from site K4 (thin section GI23b). The undamaged dentine and cement points dominate the lower, right part of the cluster, while the points of the foci dominate the upper, left part of the cluster. The enamel points which present the highest Ca and highest Cl concentration values are clearly separated from the dentine and the cement points. The selected tooth specimen is representative of the general trend observed in all studied tooth specimens.

consequently, the difference in the Cl content between the rims and the foci and between the rims and the undamaged bone was not significant.

If most of the measured Cl in the damaged tissues did not originate from water during polishing and the resins used in the preparation of the thin sections, then the mechanism, as described above and in detail in chapter one, of early recrystallization in the foci and the effect on the distribution of F in bioeroded hard tissues is probably also responsible for this consistent variation in the Cl content. In the weathered portion of the recent bone, Cl content is four times higher than in the unweathered portion. This provides evidence that the incorporation of Cl in the apatite lattice probably occurs early in the diagenetic process. Eventually, Cl will be gradually replaced by the smaller F atoms which will stabilize the apatite crystals (Posner, 1987; Hughes and Rakovan, 2002). However, early recrystallization in the foci, as described above, may restrain the influx of F and thus would limit replacement of Cl and maintain higher concentrations of it in the foci compared to the undamaged areas (Fig. 12, 13). Due to the high Cl content in the specimens from Chalkoutsi the apatite can be characterised as carbonated chloro-fluorapatite and it may be concluded that as the locality is found next to the sea it is possible that the concentration of Cl in pore waters and surrounding sediments was high enough to overcome the structural preference of the apatite for the smaller and more stable F atom (Posner, 1987; Hughes and Rakovan, 2002).

In figure 15, in the Ca/Cl vs Ca/F diagram it is clear that the Late Miocene specimens, with the exception of the enamel samples and the specimens from Chalkoutsi with the anomalous concentration in Cl, are well correlated and that their distribution ranges between 12-26 Ca/F values and 250-1000 Ca/Cl values. Recent samples present very high Ca/F values and relatively low Ca/Cl values, while specimens that have been affected by river waters and possible waterlogging such as Cotes (Loughborough, England) and Kassandria (Greece) have high Ca/Cl values. This diagram and the Ca/F and Ca/Cl ratios can potentially provide the means for comparisons of fossil bones and teeth from different burial and diagenetic environments. Further research and the study of an array of samples from different environments will provide evidence for their utility and the necessary data to make such comparisons accurate.

Magnesium and Sodium

The concentrations of Mg and Na in the majority of the samples appear to be proportional to each other (Fig. 18). Although, in the MgO vs Na_2O diagram for a bone sample from site K5

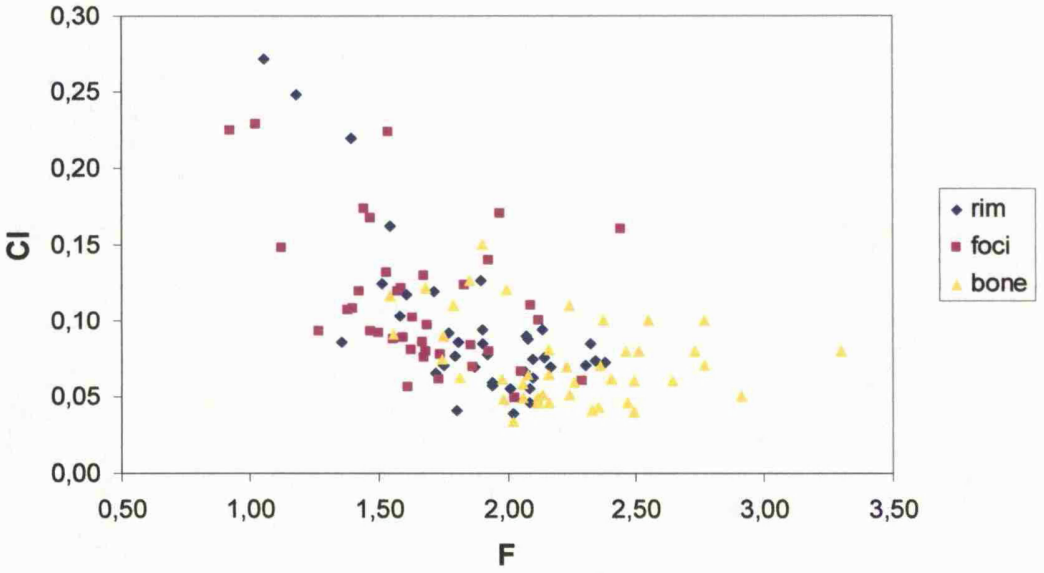

Figure 12: Plot of F vs Cl for a bone specimen from site K4 (thin section GI4a). The undamaged bone points which present the lowest Cl and highest F concentration values dominate the lower, right part of the cluster, whereas, the foci points which present the lowest F and highest Cl concentration values dominate the upper, left part of the cluster. A second bone specimen showing the general trends of F and Cl observed in the studied bone specimens

.

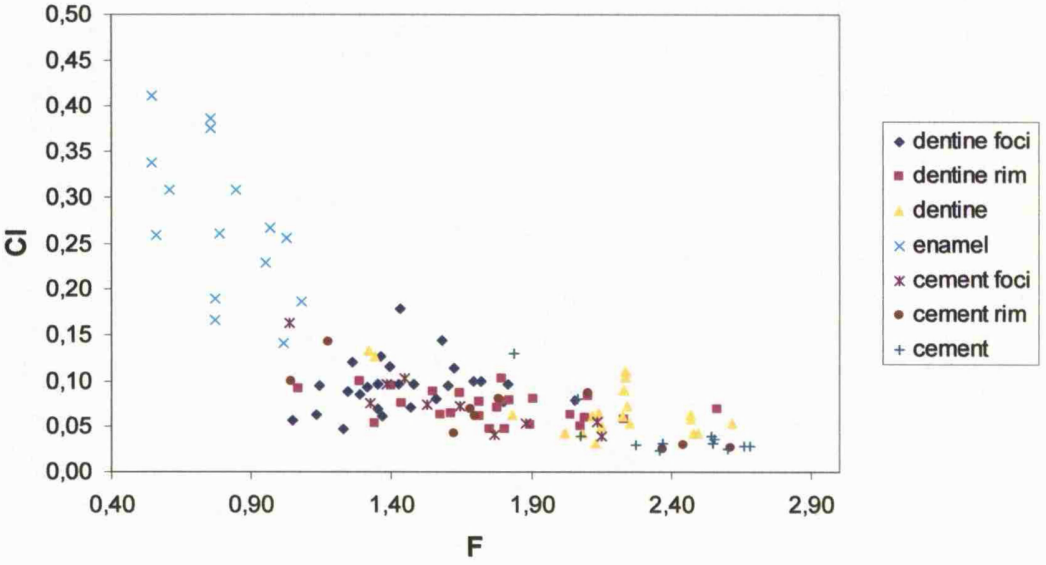

Figure 13: Plot of F vs Cl for tooth specimen K4/Δ66/3 from site K4 (thin section GI23b). The undamaged dentine and cement points with the high F concentrations dominate the lower, right part of the cluster, while the points of the foci with the low F concentrations dominate the upper, left part of the cluster. The enamel points which present the lowest F and highest Cl concentration values are clearly separated from the dentine and the cement points.

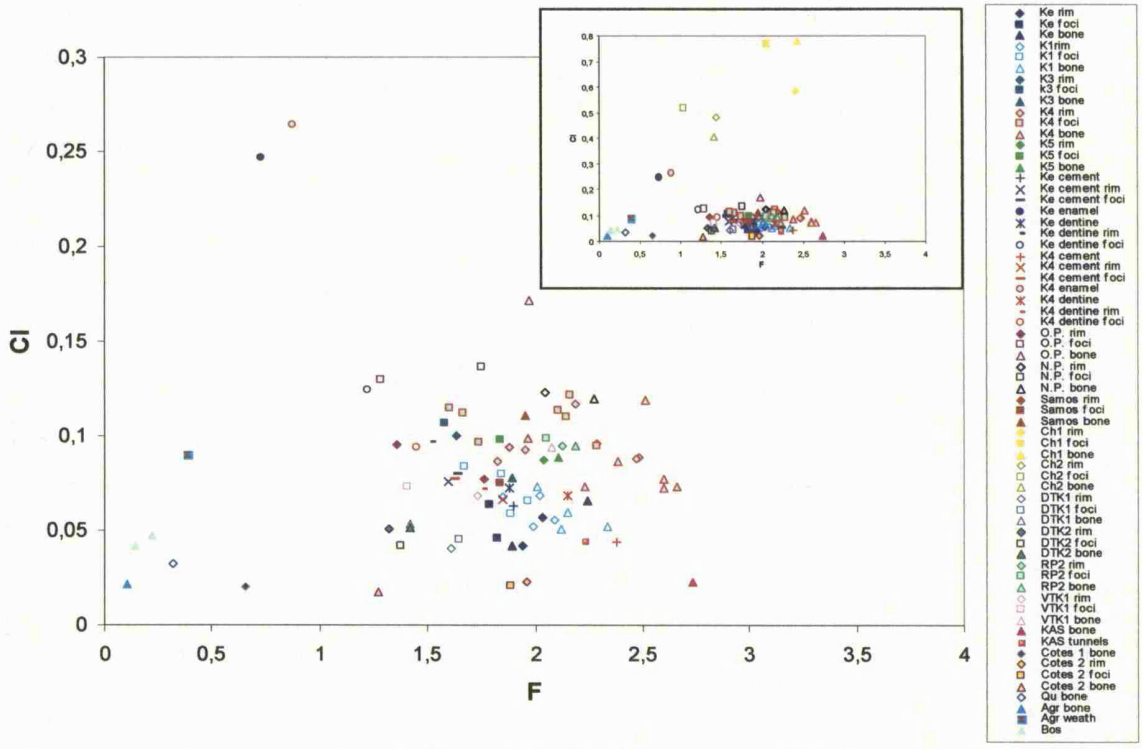

Figure 14: Plot of average values of F vs Cl for fossil bone and teeth and recent bone. The points in this plot for the fossil specimens represent the three structural areas of the bioeroded tissues (undamaged areas, foci and rims of the foci) from Kerassia and the other studied Miocene and Pleistocene localities. The small plot at the top right corner shows the extended diagram along y-axis which includes the high Cl content specimens from Chalkoutsi.

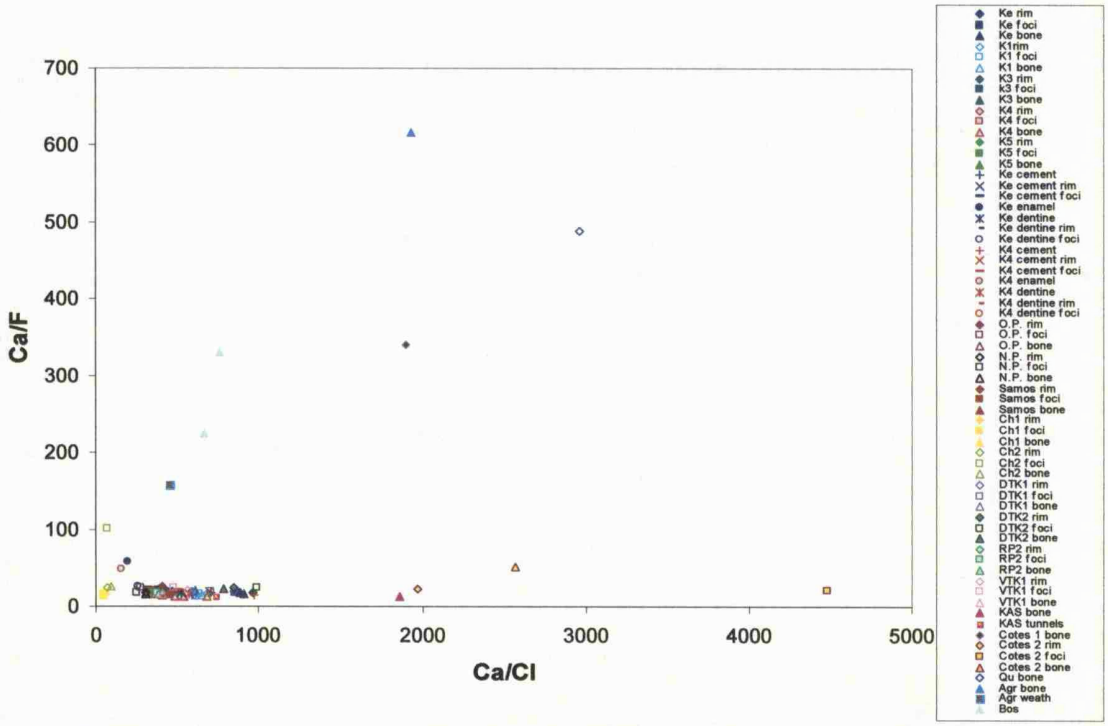

Figure 15: Plot of average values of Ca/Cl vs Ca/F for fossil bone and teeth and recent bone. The points in this plot for the fossil specimens represent the three structural areas of the bioeroded tissues (undamaged areas, foci and rims of the foci) from Kerassia and the other studied Miocene and Pleistocene localities.

(Fig. 16) linear regression of the points is not significant (the R^2 values for the rims, the foci and the undamaged areas are 0.56, 0.43 and 0.47, respectively), still there is no lack of fit in their distributions. The same trend can be observed in the rims, the foci and the undamaged areas of the dentine and the cement for the tooth sample from site K4 (Fig. 17). In sixteen out of nineteen of the examined specimens from Kerassia, and some specimens from the other localities (Samos, Kassandria, Ravin de la Plui, Ditiko 2 and one specimen from Chalkoutsi) the Mg and Na values are consistently lower in the undamaged areas (Fig. 18) and present higher concentrations in the rims, or sometimes in the foci. Conversely, in the other localities (Old Pikermi, New Pikermi, Vathylakkos 1, Cotes and the second specimen from Chalkoutsi) the Mg and Na values are consistently higher in the undamaged areas. Once again, in order to test the significance of the variation of the Mg and Na contents in the three structural areas of the damaged tissues, a two tailed t-test was employed. The null hypothesis was whether the mean Mg and Na values in one of the structural areas of the damaged bones from Kerassia were equivalent to the mean Mg and Na values in the other two. For Mg the null hypothesis was rejected for the rim-bone pair and the bone-foci pair after the mean Mg values in the bone were found to be significantly different from the mean Mg values in the foci (t=-2.24, p=0.033) and the rims (t=2.55, p=0.016) at the 0.05 level (Table 2). Conversely, the null hypothesis was not rejected for the rims-foci pair (t=-0.31, p=0.76) at the 0.05 level (Table 2). Similarly, for Na the null hypothesis was rejected for the rim-bone pair (t=2.71, p=0.011) at the 0.05 level (Table 2), and it was closely not rejected for the bone-foci pair (t=-1.81, p=0.082) at the 0.05 level (Table 2). However, the null hypothesis for the pair rim foci was clearly not rejected (t=-0.83, p=0.41) at the 0.05 level (Table 2). Therefore, this shows that also statistically the Mg and Na content in the foci (rims+foci) is significantly higher than in the undamaged areas.

It is possible that these variations in the content of Mg and Na among the three different structural areas of the hard tissues, may result from the early recrystallization of the crystallites in the foci. Despite the mobility of Na and Mg, the decreased inter-crystallite spaces restrained porewater flow and consequently the depletion of Mg and Na from the foci (rims and foci). Conversely, in the undamaged areas of the tissues the loss of collagen would increase the microporosity (Nielsen-Marsh and Hedges, 1999), and thus would gradually facilitate the flow of pore waters (Nielsen-March *et al.,* 2000) and the depletion of the mobile Mg and Na from the undamaged areas. Markedly, the less porous and compact enamel presents the highest Na and Mg values (Fig. 17).

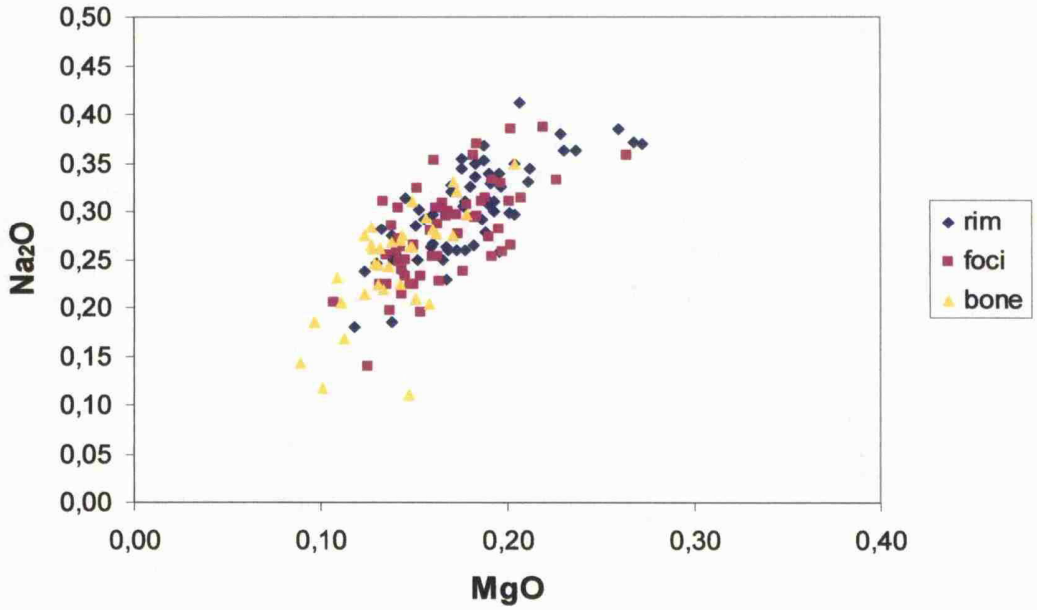

Figure 16: Plot of MgO vs Na_2O for a bone specimen from site K5 (thin section GI18a). The undamaged bone points dominate the lower part of the cluster, while the points of the rims of the foci dominate the upper part of the cluster. The selected bone specimen is one of the best examples and is representative of the general trend observed in all studied bone specimens.

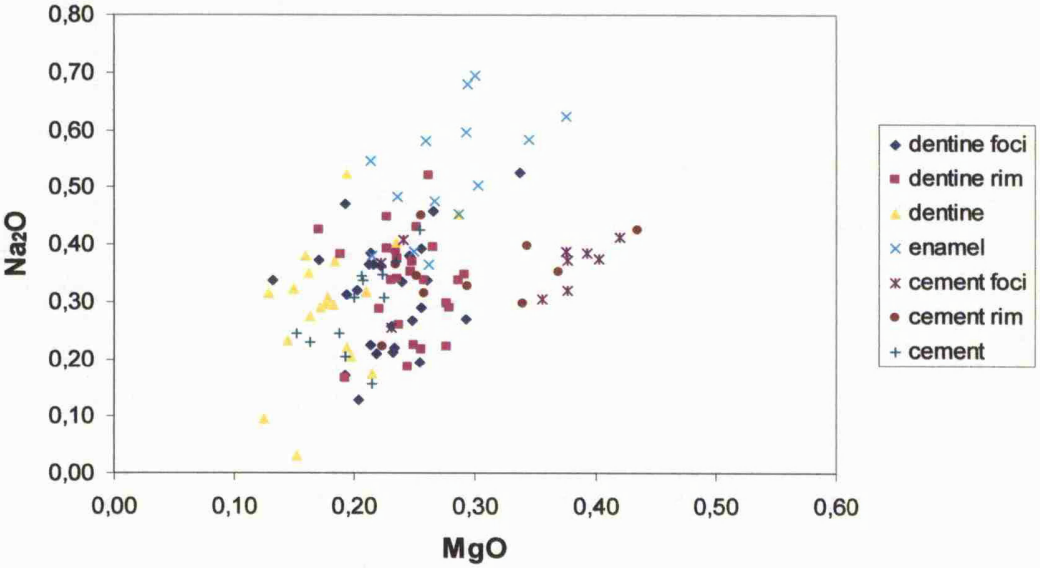

Figure 17: Plot of MgO vs Na_2O for tooth specimen K4/Δ66/3 from site K4 (thin section GI23b). The undamaged dentine and cement points which have the lowest MgO and Na_2O concentrations dominate the lower, left part of the cluster, whereas the points of the foci and the rims dominate the right part of the cluster. The enamel points which present the highest Na_2O concentration values dominate the upper part of the cluster. The selected tooth specimen is representative of the general trend observed in all studied tooth specimens

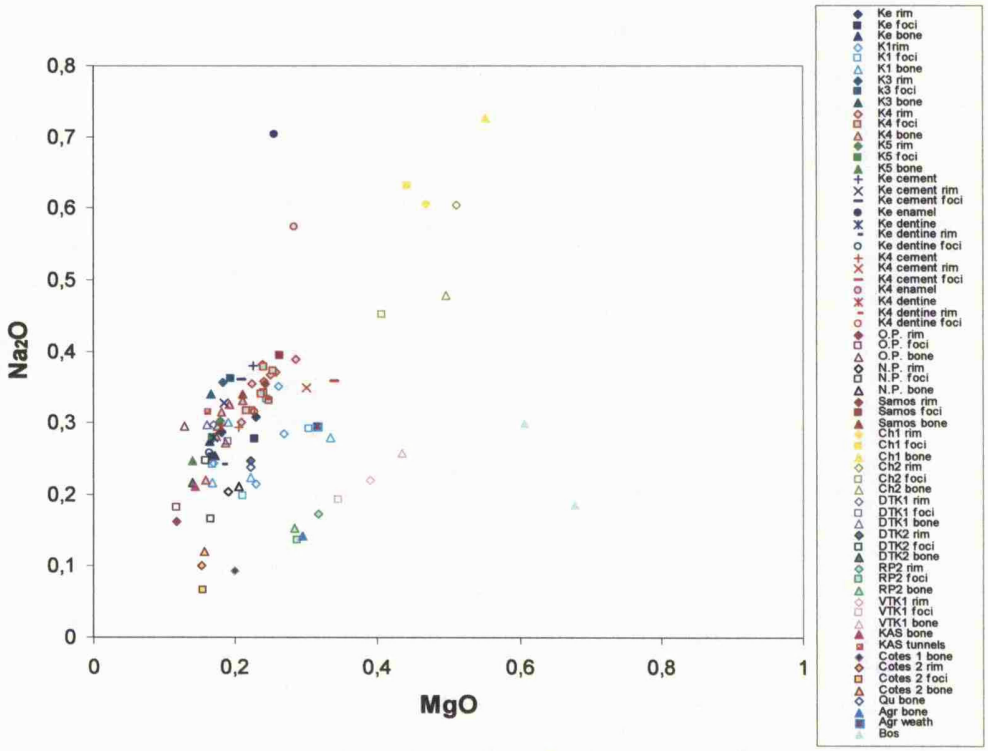

Figure 18: Plot of average values of MgO vs Na_2O for fossil bone and teeth and recent bone. The points in this plot for the fossil specimens represent the three structural areas of the bioeroded tissues (undamaged areas, foci and rims of the foci) from Kerassia and the other studied Miocene and Pleistocene localities.

Barium and Strontium

Studies in recent and archaeological bone (Grupe and Piepenbrink, 1988, 1989; Fabig and Hermann, 2002) have shown that microbial activity and consequent damage affect the concentrations of Sr and Ba in the bones. Microbes contaminate the invaded tissues with Sr and Ba and possibly with other heavy metals that they are carrying, and thus increase significantly the concentrations of these elements in the affected tissues (Grupe and Piepenbrink, 1988). According to this, one would expect to observe higher concentrations of Sr and Ba in the foci than in the undamaged areas. However, the distribution of Sr and Ba among the rims, the foci and the undamaged areas, does not present any definite and consistent distribution pattern in the studied fossil specimens, as the measured Sr and Ba concentrations for the majority of the analysed samples are below detection limit. The observed enrichment of Sr and Ba in microbially damaged bone (Grupe and Piepenbrink, 1988, 1989; Fabig and Hermann, 2002) occurs during the recrystallisation of the crystallites in the foci after the action of the microbes. Therefore, in the fossil specimens any distribution pattern caused by bacterial action among the structural areas of the tissues will probably get erased by the diffusion of Sr and Ba, which have high diffusion coefficients, during diagenesis.

CONCLUSIONS

The chemical investigation of foci and their rims, produced by bacteria, and undamaged areas of bones and teeth from Kerassia has revealed that:

- The total values of spot analyses are low due to the presence of oxides that were not analysed by the available XREMA settings, such as structurally bound CO_3 and OH and surficially located CO_2 and H_2O. The microporosity of the tissues also reduced total values. In addition, another possible reason for reduced or even biased total values is the topography of the analysed specimens
- Increased Ca/P ratios can be related to an enrichment of the tissues apatite in CO_3. Thus, Ca/P ratios may provide a measure for the relative concentration of structural CO_3 in the tissues.
- The variability of Ca/P ratios between samples probably reflects the differences in the conditions of the local burial environment and the chemistry of the local pore waters.
- Within the same sample and tissue, Ca/P ratios in the foci, the rims and the undamaged areas of bacterially damaged tissues are similar.

- The rims of the foci are usually more mineralised than the foci and undamaged areas.
- F concentrations are higher in the undamaged areas and lower in the foci. Conversely the concentrations of Cl, Mg and Na are usually higher in the foci and lower in the undamaged areas. Early rapid recrystallization that occurs in the foci possibly restrains the diagenetic F influx in the foci and protects Cl, Mg and Na from extensive depletion.
- Finally, the use of XREMA as an analytical technique for the chemical investigation of microscopic areas, as employed by this study in order to identify quantitative and qualitative elemental differences among the three different structural areas (rims, foci, undamaged areas) of microbially eroded mammal hard tissues, has been considered as inadequate and suboptimal. Although, unarguably it was possible to identify and depict such differences, there is great concern about the accuracy and the quality of the measurements. As it has been discussed above, the inability of analysing volatiles such as CO_2 and H_2O, the biased measurements caused by the extensive microporosity of the damaged and undamaged areas of the tissues and the possible topographic differences of the surfaces of the thin sections are significant disadvantages. Therefore, the desired accuracy and quality was not succeeded. In the future, techniques that will be used for detailed microanalysis of such fossilised tissues, should take into account the special structure of these tissues, the capacity of the equipment for a more complete elemental analysis (to include volatiles for example), and if possible to have lower detection limits in order to improve the accuracy and the quality of the collected data. Thus, new techniques such as Raman spectroscopy, Fourier Transform Infrared Spectroscopy (FTIR), Field Emission Auger Spectroscopy (FEAES), Secondary Ion Mass Spectrometry (SIMS), Sensitive High Resolution Ion Probe (SHRIMP) and possibly others should be tested in order to select the most suitable and adequate technique.

X-Ray Diffraction studies of Late Miocene mammal bones and teeth

INTRODUCTION

The main mineral phase of living bone and tooth tissues (enamel, dentine and cement) is a nonstoichiometric carbonated hydroxylapatite, an imperfect analogue of dahlite (Lowenstam and Weiner, 1989). A precise determination, however, of the chemical and structural composition of this apatite is not attainable. As part of living tissue, the mineral component of the hard tissues is constantly subjected to changes, maintaining equilibrium with the surrounding body fluids (Posner, 1987). Furthermore, factors such as species, tissue type, different types of bone, age, diet and isomorphous substitution are significant and contribute to this variation (Posner, 1987). Age is a crucial factor in determining the chemical and structural composition of hard tissues, as it is interrelated with the maturation of the carbonated hydroxyapatite (Handschin and Stern, 1995; Magne *et al.*, 2001). Although it is not well defined yet and there is still controversy, it is thought by many that the formation of the carbonated hydroxyapatite in all four tissues is preceded by the presence of a precursor amorphous mineral phase, such as octacalcium phosphate (OCP) (Posner, 1987; Lowenstam and Weiner, 1989; Apfelbaum *et al.,* 1990).

The size and shape of the crystallites in vertebrate hard tissues also play a fundamental role in physicochemical properties. Variation in the size of the crystallites depends on animal species, tissue type, bone type, age and even on the different areas of a single bone or tooth. Higher crystallinity in mature bone, dentine and cement and in enamel is related with larger crystallites. Crystallites in bone are plate-shaped (Weiner and Price, 1986; Epell *et al.,* 2001), while in enamel they are rod-shaped and long with a flattened hexagonal cross-section (Elliott, 2002). According to Carlson (1990) and Hilson (1986) the crystallites in dentine and cement have a similar shape and dimension to those of bone. Weiner and Price (1986) suggested that the average bone crystallite dimensions were 35-40 nm x 35-40 nm x 2.5-5 nm. Recently, the study of mature bovine bones revealed the presence of two size groups of crystallites, a small and a large one (Eppell *et al.*, 2001). The vast majority of the crystallites, approximately 98%, belong to the small size group with a thickness of less than 2 nm (Eppell *et al.,* 2001). The average dimensions of these crystallites were measured to be 12 nm x 10 nm x 0.61 nm and the length to thickness ratio was 20.3 indicating thin-plated crystallites (Eppell *et al.,* 2001). Similarly, the average dimensions of the crystallites from the large group

were 90 nm x 64 nm x 37 nm, with a length to thickness ratio of 2.7 indicating thick-plated crystallites (Eppell *et al.,* 2001). Most crystallites of the small group are accommodated in the collagen intrafibrillarly, between the fibrils' molecules, while the crystallites of the large group occupy interfibrillar spaces. The c-axis of the crystallites of both groups is parallel to the long axis of the fibre (Eppell *et al.,* 2001). Crystallites are significantly larger in enamel. Daculsi and Kerebel (1978) observed enamel crystals with an average width and thickness of 68.3 nm ± 13.4 nm and 26.3 nm ± 2.2 nm, respectively. Kohn *et al.* (1999) stated that enamel crystallites are longer than 1000 nm, nevertheless, it has been reported that they may get up to 1600 nm and even longer (Hilson, 1986; Carlson, 1990). The small size of the bone crystallites, and similarly of those in dentine and cement, and their platy shape provide them with a large surface area which renders the crystallites highly reactive (Newesely, 1989; Weiner and Price, 1986; Nielsen-Marsh *et al.*, 2000). Conversely, in enamel the larger crystallites have a smaller surface area and consequently they are less reactive.

Once collagen is lost, the small, highly reactive and unstable apatite crystallites in the hard tissues will become exposed to chemical alteration. The prevailing conditions in the burial environment, determine whether the hard tissues will undergo demineralization and dissolution, or whether they will recrystallize, turning into a more stable form and potentially becoming part of the fossil record (Trueman and Tuross, 2002). Optical properties and the histology of the fresh tissues are maintained in fossil material indicating that crystallites in the fossilized hard tissues retain their original biogenic orientation (Hubert *et al.*, 1996). According to Hubert *et al.* (1996) the crystallites, once exposed, can become the seed crystals for further apatite growth around them. The additional phosphate material needed for this growth will be provided by the dissolution of the less crystalline and thus more soluble mineral components (Weiner and Price, 1986), and of the smallest and consequently more reactive crystallites (Nielsen-Marsh *et al.,* 2000). Increase in the size of crystallites therefore indicates a subsequent increase in crystallinity. Loss of components such as Mg and HPO_4 and the incorporation of F will also contribute to this increase. In addition, the formation of larger crystals increases their stability (Nielsen-Marsh *et al.,* 2000). Crystallites, and subsequently crystallinity, will increase until groundwater is blocked either by the expansion of the crystallites occluding the intercrystallite spaces, or by the filling of the histological voids and cavities by permineralized minerals or sediment (Hubert *et al.*, 1996; Pfretzschner, 2000; Trueman and Tuross, 2002).

This chapter will first describe the mineralogy of fossil bones and teeth from a Late Miocene locality Kerassia, in Greece. In addition, it will demonstrate that crystallinity and its measure, the crystallinity index, is not related to the age but depends on the conditions of the local burial environment and the degree of recrystallization. It will also provide evidence to disprove the concept that the values of crystallinity indices for recent bone are zero (Person *et al.*, 1995; Bartsiokas and Middleton, 1992).

LOCALITY AND STRATIGRAPHY

The studied bone and tooth material was collected from a new Late Miocene (Turolian) mammal locality, Kerassia, in Greece (Fig. 1). Kerassia is situated in the largest of the three major Neogene basins of Euboea Island, the Limni-Istiea basin, located on the northern part of the island (Katsikatsos *et al.*, 1981). The rich fossiliferous outcrops occur north of the village of Kerassia. To date, seven different fossiliferous sites have been found in the locality, namely K1 to K7, where at least two fossiliferous horizons occur, an upper and a lower horizon. Sedimentological and geochemical data indicate that sites K1 and K6 belong to the upper horizon, whilst sites K2, K3, K4 and probably K5 belong to the lower horizon. The exact position of site K7, however, is still undetermined. The bone bearing layers are red brown fluvial deposits which according to Mettos *et al.* (1991) consist part of the upper stratigraphic sequence of Limni-Istiea basin. The bone assemblages were accumulated within fluvial channels. The majority of the surrounding rocks in this part of the basin are ophiolites that belong to the Lower Cretaceous tectonic nappe of the so-called Pelagonian (sensu stricto) unit (Bono, 1998). In addition, the majority of the clasts in the sediments that contain the fossil assemblages are of ophiolitic origin, indicating that the source rock of the deposits is ophiolites. Since 1993, the systematic excavations in the locality conducted by Theodorou and the University of Athens have revealed a diverse mammal fauna of Turolian age (Theodorou *et al.*, 2003). In 1982 Hans de Bruijn, Albert van der Meulen and Constantine Doukas carried out a first small scale excavation at Kerassia. The exact site of excavation was not recorded. However, information provided by Doukas (pers. comm.) and the style of preservation of the material indicate that the collection site was K1.

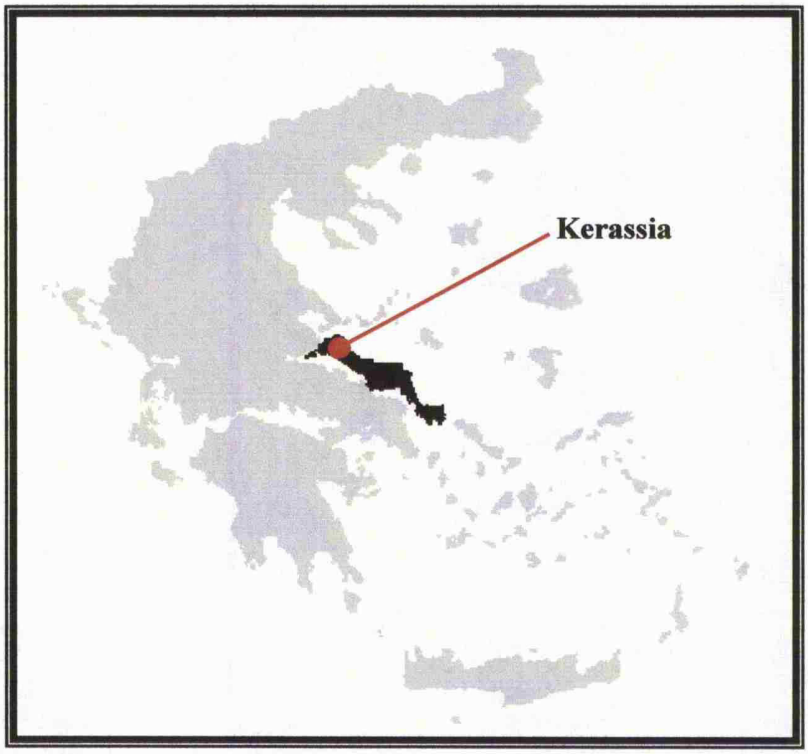

Figure 1: Sketch map of Greece showing the location of Euboea Island and Kerassia.

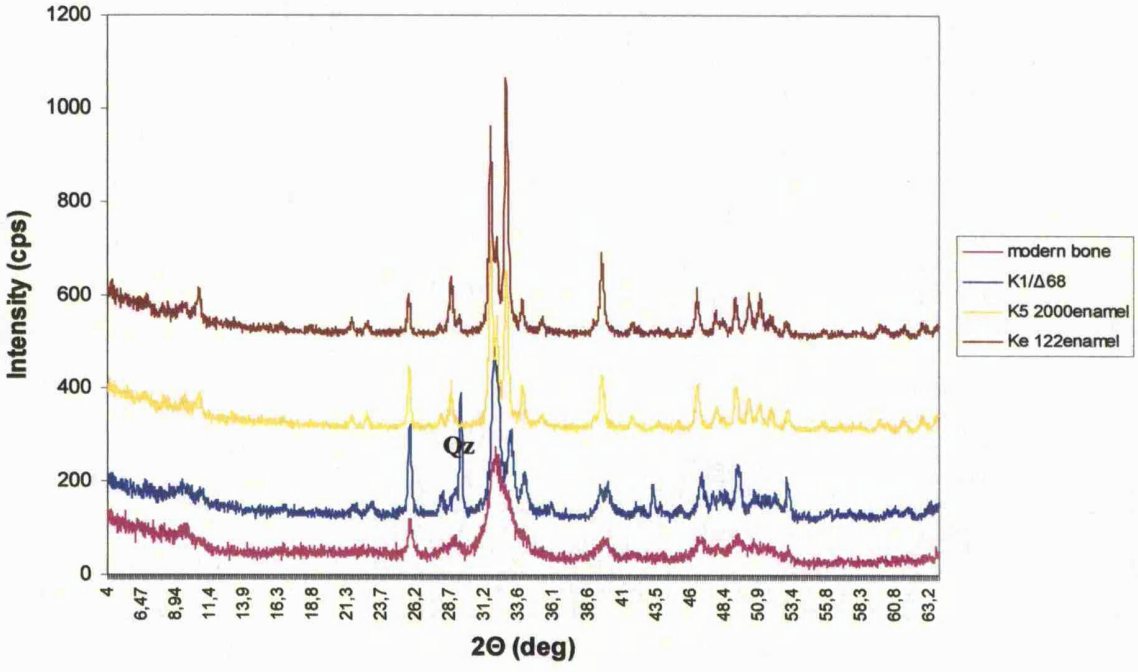

Figure 2: XRD patterns for modern bone (carbonate hydroxyapatite), fossil bone (carbonate fluorapatite) and enamel (carbonate hydroxyapatite) from gpoups A (K5 2000) and B (Ke 122). The intensity scale applies directly to the trace of modern bone. For clarity the scale of the fossil bone is displaced upwards 100 cps units and similarly the scale of the two enamel specimens are displaced 300 and 500 cps units, respectively. Qz refers to quartz peak.

MATERIAL AND METHODS

To date, the excavations in the locality of Kerassia have been focused at sites K1 and K4, thus the majority of the specimens used in this study come from these two sites. The destructive techniques utilised in this study, and the scarcity of the collected material from the other five sites restricted the number of specimens from these sites that was analysed. Fragments of fossil bone, enamel and dentine from the seven sites of Kerassia (including specimens from the 1982 excavation) were ground into fine power. 20 bone, 6 dentine and 6 enamel samples representing all seven sites of Kerassia were selected for X-ray diffraction analysis. In addition, 2 bone samples from the Miocene localities of New and Old Pikermi (Greece), 1 bone sample from the Pleistocene locality of Cotes (England) as well as two recent unweathered and one recent weathered bone samples were also similarly treated. Sediment or minerals such as calcite detected on the surface of the specimens or within cracks were removed mechanically. Sediment samples from the bone bearing sediments from all seven sites of Kerassia, as well as sediment found in bone marrow cavities from two bone specimens (K4/Δ118i and K4/Δ119i) were also ground to a fine powder, and analysed.

For the mineralogical investigation of bone and sediment samples a Phillips model PW 1730 X-ray generator, with a PW 1716 diffractometer and a PW 1050/25 detector was used. XRD spectra were obtained using a copper target in X-ray tube. The normal current operating conditions were 40kV and 30mA. 2gr of dried fine powder, was pressed into an aluminium holder in preparation for analysis. The measurement parameters were: a two theta angle range from 4° 2θ to 64° 2θ, with a step size of 0.02° 2θ at a speed of 1° per minute. For the estimation of the crystallinity index (CI), and in order to provide better and more accurate data, the bone and tooth samples were rerun at a slower speed. The measurement parameters for this run were: a two theta angle range from 30° 2θ to 38° 2θ, with a step size of 0.0192° 2θ at a speed of 0.125° per minute. The crystallinity index (CI) was calculated for all the analysed samples, using two different methods, the method of Person *et al.* (1995) (named in this study as CI_A) and the method of Bartsiokas and Middleton (1992) (named in this study as CI_B). The former is now considered to be the standard method for the calculation of CI, because it is more accurate and has the advantage of elaborating more parameters (XRD peaks) for the calculation of CI. Both methods were employed in this investigation for comparative purposes. The interplanar lattice d-spacing and the intensity values for the four major peaks on the diffractograms (211), (112), (300) and (202) were calculated from the slow X-ray runs (Fig. 3, Table 1) in order to provide more accuracy in the calculation of the

Table 1

		fossil bone			weathered	recent bone	dentine			enamel A			enamel B		
	hkl	av	min	max			av	min	max	av	min	max	av	min	max
d(Å)	211	2.8063	2.7922	2.8152	2.8070	2.8161	2.8091	2.8053	2.8186	2.8223	2.8186	2.8269	2.8244	2.8235	2.8252
	300	2.7138	2.7040	2.7240	2.7178	2.7325	2.7173	2.7132	2.7224	2.7286	2.7255	2.7317	2.7317	2.7317	2.7317
	112	2.7899	2.7685	2.7971	2.7841	2.7777	2.7897	2.7874	2.7922	2.7886	2.7857	2.7922	2.7898	2.7890	2.7906
	202	2.6337	2.6229	2.6416	2.6387	2.6547	2.6356	2.6315	2.6387	2.6376	2.6358	2.6401	2.6409	2.6401	2.6416
I/Io	211	1.00	1.00	1.00	1.00	1.00	1.00	1.00	1.00	1.00	1.00	1.00	0.90	0.87	0.93
	300	0.56	0.50	0.62	0.61	0.66	0.55	0.52	0.58	0.78	0.69	0.91	1.00	1.00	1.00
	112	0.87	0.77	0.95	0.91	0.86	0.89	0.85	0.91	0.64	0.55	0.77	0.46	0.42	0.50
	202	0.32	0.29	0.35	0.35	0.37	0.34	0.32	0.35	0.27	0.25	0.32	0.20	0.18	0.21

Table 1: X-ray diffraction data from fossil bone, dentine and enamel from both horizons of Kerassia and recent weathered and unweathered bone. The interplanar lattice values (d) and the relative intensities (I/Io) for the four major peaks of the apatite are presented.

d-spacing and intensity values, and consequently in the determination of the major mineral phase.

RESULTS

Mineral phases

X-ray diffraction patterns (Fig. 2), the characteristic interplanar lattice spacing (d) values and the relative intensities (Table 1) demonstrate that samples can generally be categorized into two groups; a group comprising bone and dentine samples and another group comprising enamel samples. Moreover, the enamel samples can be divided further into two subgroups: a group (group A) where the intensity of the (300) peak is lower than the (211) peak and a second group (group B) that contains samples Ke 122 and K4/Δ359/2 where the intensity of the (300) peak is higher than the (211) peak (Fig. 3, Table 1). Based on the data calculating d-spacing and intensity values from the slow X-ray runs (Table 1) the major mineral phase of the Miocene bone and dentine samples is carbonate fluorapatite (francolite), whereas, the major mineral phase of the enamel is carbonated hydroxyapatite (dahlite) (Table 2). In the examined Late Pleistocene bone sample from Cotes the mineral phase was identified as carbonate hydroxy-fluorapatite. In the recent bone samples, as expected, the mineral phase is carbonate hydroxyapatite.

However, in some bone and dentine samples from Kerassia, a few other minor phosphatic trace phases were traced: whiteite [$Ca(Fe,Mn)Mg_2Al_2(PO_4)_4(OH)_2.8H_2O$], lunokite [$MgMnAl(PO_4)_2(OH).4H_2O$] and jahnsite [$(Ca,Mn)Mn(Mg,Fe,Mn)_2Fe_2(PO_4)_4(OH)_2.8H_2O$]. The majority of bone, dentine and enamel samples also contained calcite. Authigenic secondary calcite is found in the fossilised tissues as a permineralised mineral in histological voids, and weathering and diagenetic cracks. Other secondary minerals detected in the fossil tissues include, magnesite [$MgCO_3$], artinite [$Mg_2CO_3(OH)_2.3H_2O$], huntite [$Mg_3Ca(CO_3)_4$] and haematite [Fe_2O_3]. In one of the two analysed recent unweathered bone samples jahnsite occurs as a secondary phase. In the weathered recent bone sample, as well as the expected carbonate hydroxyapatite, secondary farringtonite [$Mg_3(PO_4)_2$] and talc were observed.

Crystallinity index

The CI values as well as the mineral phases found in each sample are presented in Table 2. The well defined and relatively narrow peaks on the diffractograms provide evidence for an

Table 2

sample	type	CI_A	CI_B	major	trace
Ke 89	bone	0.39	6.3	CFA	calcite
Ke ii	bone	0.50	7.3	CFA	calcite, lunokite
Ke 122	dentine	0.44	6.7	CFA	calcite
Ke 122	enamel	1.17	9.1	CHA	magnesite
K1/Δ23	bone	0.46	7.0	CFA	magnesite
K1/Δ58/2	bone	0.48	7.1	CFA	whiteite, calcite, hematite
K1/Δ88	bone	0.49	7.4	CFA	whiteite, calcite
K1Δ122a	bone interior	0.50	7.2	CFA	
K1/Δ122b	bone exterior	0.47	7.2	CFA	calcite
K1/Δ68	bone	0.44	6.9	CFA	calcite
K1/A7	dentine	0.43	6.3	CFA	calcite
K1/Δ170	dentine	0.40	6.0	CFA	calcite
K1/Δ170	enamel	0.92	8.7	CHA	calcite
K1/Δ321	enamel	0.77	8.3	CHA	calcite
K2/Δ1	bone	0.47	6.8	CFA	calcite
K3 I	bone	0.44	6.9	CFA	calcite
K3/B1/10	bone	0.45	6.9	CFA	calcite
K3 105	bone	0.47	7.0	CFA	calcite
K4/Δ388 I	bone	0.43	6.5	CFA	calcite
K4/Δ90/1	bone	0.40	6.7	CFA	calcite
K4/Δ110	bone	0.42	6.5	CFA	
K4/Δ359/2	dentine	0.37	6.3	CFA	calcite, jahnsite
K4/Δ359/2	enamel	1.03	8.8	CHA	
K4/Δ25/5	enamel	0.89	8.6	CHA	calcite
K5 2000	bone	0.41	6.5	CFA	calcite
K5 i	bone	0.47	7.2	CFA	calcite
K5 I	bone	0.39	6.4	CFA	calcite, hantite
K5 2000	dentine	0.43	6.6	CFA	
K5 2000	enamel	1.03	8.8	CHA	calcite, artinite
K6/Δ1	dentine	0.42	6.1	CFA	calcite
K7 2000	bone	0.48	7.4	CFA	calcite
K7 I	bone	0.50	7.6	CFA	calcite
NPII	bone	0.37	5.6	CFA	calcite
PA 1269	bone	0.35	5.7	CFA	whiteite, calcite
Co2	bone	0.16	2.5	CHFA	
Agr	weathered bone	0.10	1.6	CHA	talc, farringtonite
BS (Bos scapula)	recent bone	0.12	1.9	CHA	jahnsite
BT (Bos tibia)	recent bone	0.12	2.1	CHA	talc

Table 2: Major and trace mineral phases of the examined bone and tooth samples and their respective crystallinity index values calculated with the method of Person *et al.* (1996) (CI_A) and the method of Bartsiokas and Middleton (1992) (CI_B). CFA= carbonate fluorapatite (francolite), CHA= carbonate hydroxyapatite (dahlite), CHFA= carbonate hydroxy-fluorapatite.

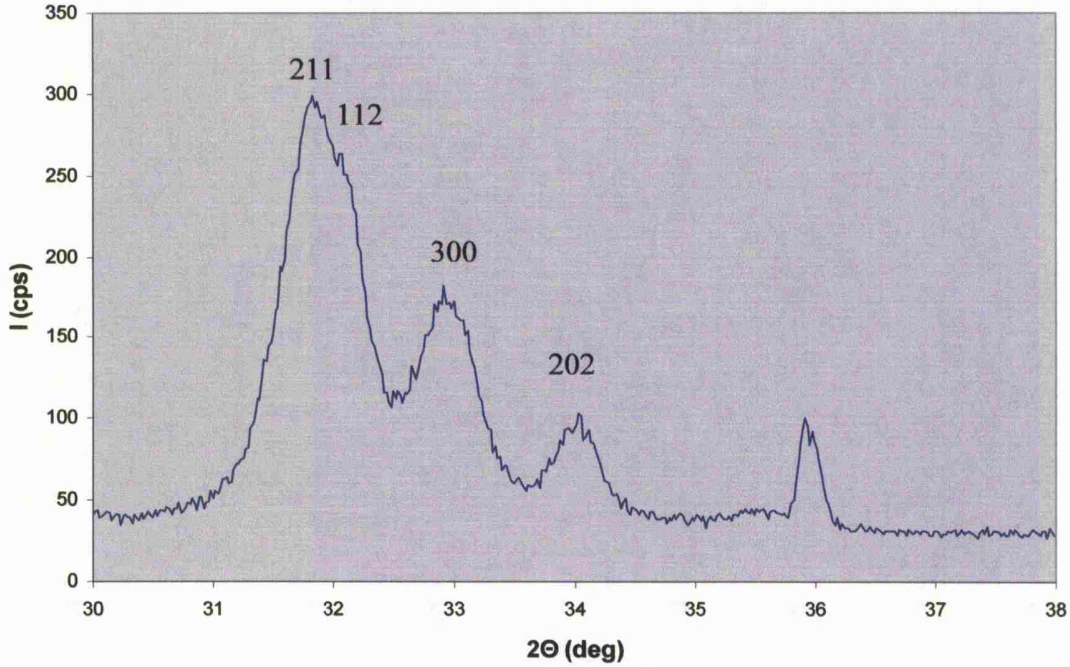

Figure 3: XRD pattern of a bone sample from site K2, run at a slow speed of 0.125° per minute for a 2θ angle ranging between 30° and 38° 2θ. The four peaks labelled with their respective Miller indices are the ones used in the calculation of CI_A and CI_B.

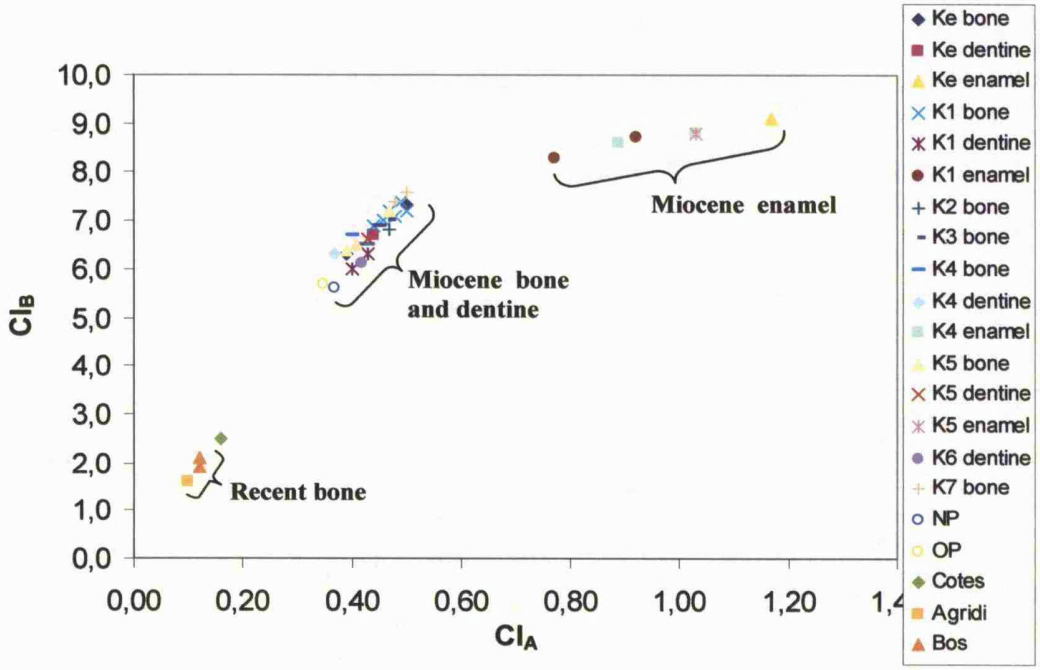

Figure 4: Plot of crystallinity index A (CI_A) (Person *et al.*, 1996) vs crystallinity index B (CI_B) (Bartsiokas and Middleton, 1992). Agridi (Agr): modern weathered bone, Bos: modern bovine bone, NP: New Pikermi, OP: Old Pikermi.

increase in the crystallinity of the mineral phase of fossil bone, dentine and enamel. This increase is reflected on the CI (Table 2). The CI calculated with the method of Person *et al.* (1995) (CI_A) for the bone samples of Kerassia ranges between 0.39-0.50 with an average value of 0.45 (n=20, standard deviation 0.04), while the CI calculated with the method of Bartsiokas and Middleton (1992) (CI_B) ranges between 6.3-7.6 with an average value of 6.94 (standard deviation 0.37). The CI_A for the dentine samples ranges between 0.37-0.44 with an average value of 0.41 (n=6, standard deviation 0.02), whereas the CI_B ranges between 6.0-6.7 with an average value of 6.33 (standard deviation 0.27). In the enamel the CI_A ranges between 0.77-1.17 with an average value of 0.97 (n=6, standard deviation 0.14) and the CI_B ranges between 8.3-9.1 with an average value of 8.72 (standard deviation 0.26). For the upper horizon at Kerassia the values of CI_A and CI_B for the bone range between 0.39-0.5 (average 0.47) and 6.3-7.4 (average 7.05) respectively, and for the dentine 0.40-0.44 (average 0.42) and 6.0-6.7 (average 6.28) respectively. Similarly, for the lower horizon the values for the bone range between 0.39-0.47 (average 0.44) and 6.4-7.2 (average 6.74) respectively, and for the dentine 0.37-0.41 (average 0.39) and 6.0-6.7 (average 6.45) respectively. Note that because of similarities in their preservation state and chemistry, the specimens from site K5 are considered to belong to the lower horizon. The CI_A and CI_B for the two bone samples from site K7 have high values (Table 2) and fall within the upper range of values of the upper horizon.

Mineralogy of the sediments

X-ray diffraction showed that the sediments which contained fossil material consist mostly of clay minerals and calcite. The clay minerals include smectite, illite, chlorite and kaolinite. Calcite always occurs along with two more carbonate minerals, magnesite and ankerite. Quartz is another common mineral, while iron-oxides and anatase are usually present. K-feldspar and albite are also detected as minor phases in a small number of samples, and probably represent unweathered grains from the original source rock. The X-ray diffraction patterns of sediment samples from the marrow cavity of two different bone specimens revealed that calcite is the major mineral phase. Clay minerals, such as smectite, illite and kaolinite, and quartz are also present as minor phases in marrow cavity sediment.

THE MINERALOGICAL COMPOSITION OF FOSSIL BONES AND TEETH FROM KERASSIA

Mineralogy of bone, dentine and enamel considering F content

The d-spacing values for the four major peaks (211), (112), (300) and (202) for the Miocene bone and dentine samples (first group, table 1), do not match with the equivalent d-spacing values reported by Jarvis (1992) for carbonate fluorapatite in phosphatic chalks and from Hubert *et al.* (1996) in Upper Jurassic dinosaur bones. All Miocene samples peaks have higher d-spacing values than those reported previously and show a consistent X-ray diffraction peak shift on the X-ray diffractograms to the left. However, data provided from X-ray emission microanalyses (XREMA) indicated that the F content in all spot analyses, regardless of their position in bioeroded bone, dentine and cement samples, always exceed 1% and in some areas F content reaches 3% (Table 1, chapter 2). Therefore, F concentrations above 1% (Hubert *et al.*, 1996; Wilson *et al.*, 1999) support and verify the determinations that the mineral phase of the bone, dentine and cement is carbonate fluorapatite (francolite), despite the difference with published d-spacing data (Jarvis, 1992; Hubert *et al.*, 1996). A proportional shift of the peaks on the X-ray diffractograms to the left also occurs in the enamel samples used in this study. XREMA data have shown that the F content in the enamel samples is consistently below 1% (Table 1, chapter 2), which indicates that the mineral phase of the enamel is carbonate hydroxyapatite (dahlite). The F content data (Table 1, chapter 2) from XREMA are consistent with the mineral determination of the Pleistocene sample from Cotes as being carbonated hydroxy-fluorapatite. The F values range between 0.31% and 3.09% verifying the presence and coexistence of both mineral phases, carbonate hydroxyapatite and carbonate fluorapatite, in the bone. Despite the obvious differences in the relative intensities between the recent bone mineral and the enamel's carbonated hydroxyapatite, the d-spacing values of the recent bone mineral are generally close to the lower range of d-spacing values of the enamel samples, evincing the similarities in their mineralogy.

Interestingly, in the recent weathered bone specimen the X-ray diffractogram peaks lie to the right of the respective recent unweathered bone peaks and thus the d-spacing values are found closer to those of the upper range of the bone carbonated fluorapatite. The F content in the unweathered part of the bone is lower than in recent, unweathered bone specimens. In the weathered part though, the F content is significantly higher than in recent unweathered bone specimens and has a maximum concentration of 1.31%. In the powdered bone sample the

whole cortex and hence both weathered and unweathered parts of the bone were used; therefore, the XRD peaks are affected by the fluorinated mineral phases of the external weathered bone.

Crystallinity index – a proxy for relative age?

As expected the well crystallised enamel presents the highest CI values, whereas the CI values for the dentine are the lowest. Despite the small number of the analysed dentine samples, it is clear that both crystallinity indices (CI_A and CI_B) indicate a higher crystallinity for the bone and dentine samples from the upper and hence the younger horizon of the two at Kerassia. However, it should be noted that the time gap between the lower and upper horizons is not known. They are separated by 6.7 metres of sediments. The small number of analysed enamel samples, and their separation into two groups which do not comply with a specific horizon, do not provide a statistically significant sample. Nevertheless, it seems that enamel samples from the upper horizon also have higher crystallinity values. However, it is obvious that both CI_A and CI_B are significantly higher in enamel group B than in enamel group A (0.9 and 8.6 for A and 1.1 and 8.95 for B), where the peak for (300) presents the highest intensity (Figure 2), and therefore suggests that these two samples are more crystallised.

The CI_A and CI_B values for the bone samples from the two Late Miocene localities of Pikermi are lower than any values from Kerassia bone (Table 2). Biostratigraphic determinations on the giraffidae and the fauna of Kerassia (Chapter 4) indicate that Kerassia belongs to MN 12 (possibly between 7.7-7.1 Ma). Bernor *et al.* (1996) suggested that Pikermi belongs to MN11/12 with a correlative age of 8.3/8.2 Ma. Thus, Kerassia is younger than Pikermi based on current data. All these observations indicate that CI values and thus crystallinity are not related with sample age, and are in agreement with the findings of Person *et al.* (1995) and Trueman (1998). The variations in the CI values, even within the same site (Table 2,) show different degrees of recrystallisation, which indicate variable burial conditions and correspond to different microenvironments. Thus, CI values depend on the degree of recrystallization and consequently on the prevailing conditions of the burial environment, therefore CI should not be used as an indicator of relative age.

Crystallinity values in recent bone

Although both Person *et al.* (1995) and Bartsiokas and Middleton (1992) considered that the values of their crystallinity indices for recent bone were zero, in this study, the CI_A and CI_B values for recent bone samples were found to be above zero (Table 2). The X-ray diffraction

data used for the calculation of the two crystallinity indices were produced by slow speed runs, and although the reflections (211), (112), (300) and (202) on the diffractograms of recent samples were not well defined they were still traceable and provided the intensity values needed for the calculation of the indices. Recent bones with crystallinity index values of zero suggest that the mineral phase in the bone tissue is totally amorphous without any structured crystals. However, the mineral phase of all the hard tissues gradually forms well-crystallised crystallites (Weiner and Price, 1986; Epell *et al.*, 2001; Kohn *et al.*, 1999), and thus with increasing age and maturation the crystallinity of the tissues will concomitantly increase (Handschin and Stern, 1995). Only at the early stages of hard tissue formation, where the mineral phase is amorphous, can it be considered that crystallinity is limited to the minimum, and that the value of any crystallinity index would be zero. Therefore, as long as there are well developed crystallites in the living bone and in other hard tissues, they would be characterised by low CI values but indisputably values greater than zero. Interestingly, the values of the CI_A and CI_B calculated for the recent weathered sample (0.1 and 1.6, respectively) are slightly lower than those of the unweathered recent samples, suggesting that weathering may have reduced the crystallinity of the bone. The Pleistocene bone sample from Cotes compared to recent bone presents a small increase in CI_A and CI_B reflecting minor changes in its crystallinity.

Comparison of CI_A and CI_B

Although, both indices are measures of crystallity, different parameters are used for their calculation. For the calculation of the CI_A (Person et al., 1995) the heights of the characteristic reflections (height between the top of the peak and adjacent valley separating it from the previous peak) of the apatite (202), (300), (112) and (211) are used (the sum of (202), (300) and (112) divided by (211)). Conversely, the calculation of CI_B (Bartsiokas and Middleton, 1992) involves the ratio between the local and general background (height) of the (300) reflection.

The intensities of these reflections and thus, the heights of these peaks and particularly of (202), (300) and (112) depend on the degree of crystallinization of the apatite crystallites in the different tissues. In modern bone these reflections are very low and not well defined, whereas in fossil bone and enamel the reflections are well defined and high (especially in enamel). In particular, reflection (300) shows significant variability (Figure 2). Its intensity in modern bone and fossil bone and dentine is lower than reflections (211) and (112), but in enamel it is always higher than reflection (112) and in enamel group B, intensity is higher even than reflection (211). These differences depend on the size and the structure of the

individual crystallites in each of these tissues. Therefore, these differences and the weight of reflection (300) in the calculation of the two indices indicate that they are not analogous. Clearly, the effect of the increase of the height of reflection (300) would be different in each of the two indices, which of course will depend on the size and the structure of the individual crystallites in each of these tissues. Thus, the CI_A vs CI_B plot (Figure 4) reflects such differences between the crystallites of modern bone, fossil bone, fossil dentine and fossil enamel.

The values of the two crystalinity indices, plotted against each other (Fig. 4), demonstrate that they are well correlated and that the enamel samples cluster is clearly separated from the bone and dentine samples cluster. The R^2 value for the regressions of enamel and bone samples are 0.97 and 0.84, respectively. No correlation exists ($R^2 = 0.1394$) among the dentine samples but this is probably due to the small number of dentine samples (n=6). However, if bone and dentine samples are considered as one homogeneous cluster, the equation for the respective regression line is $y = 10.003x + 2.364$ with $R^2 = 0.78$ and this shows that the two indices are correlated. The regression coefficient (slope) and the intercept in the bone-dentine and the bone equations have relatively close values, suggesting that bone and dentine are correctly placed in the same group. The two bone samples from the localities of Pikermi are located close to the extension of the line and seem to follow the bone and dentine samples from Kerassia. The three recent bone samples with the low CI values are located close to the centre of the axes. The sample from Cotes is situated very close to the recent bone samples. It is probable that if an array of recent bones, of different ages and thus of different degrees of maturation were analysed, the regression line of recent bones would probably cross the centre of the axes, where zero values of CI would stand for the early, immature and amorphous mineral phases.

As the overall crystallinity of a group increases, the regression coefficient (slope) of the respective regression line decreases and the intercept value increases (Figure 4). The enamel group with the highest crystallinity has the lowest regression coefficient and the highest intercept values, whereas the recent bone group presents the highest regression coefficient and the lowest intercept values. Differences in the slope of the regression line probably reflect the differences in the size and in the structural order of the mineral crystallites. The thin plate-shaped crystallites (Weiner and Price, 1986; Epell *et al.*, 2001) of living bone are not only smaller but are also different in shape from their fossil counterparts. The recrystallised crystallites of fossil bone and similarly of dentine and cement will grow freely filling the

intercrystallite spaces once occupied by collagen fibrils, forming not only larger, but also much thicker and more crystallised crystallites. In enamel and even more in fossil enamel, this effect is more enhanced than in fossil bone as the rod-shaped, hexagonal and long crystallites are well shaped and more crystallised. The observed variation in the height (intensity) of the (300) reflection in the X-ray diffraction patterns of the bone, dentine and particularly of the enamel, indicate significant differences in the size and structure of the crystallites. The XRD patterns of the enamel, and in particular those of group **B**, which are closer to the patterns of well crystallised mineral dahlite (Person *et al.*, 1996), suggest not only high crystallinities, but also optimum development and perfection of the individual crystallites. Person *et al.* (1996) after heating modern bone to temperatures above 600°C managed to reproduce XRD patterns similar to those of enamel where the (300) peak became high and thus crystallinity was improved. Michel *et al.* (1996) after employing Rietveld analysis on XRD data from modern bone and fossil bone and enamel samples from Lazaret cave, identified a similar grouping (modern bone, fossil bone, fossil enamel). They attributed the variation among the enamel, fossil and modern bone to high structural disorder and small crystallite size of bone which is clearly more emphasized in the modern bone.

CONCLUSIONS

The mineralogical study of bone, dentine and enamel samples from both fossiliferous horizons of Kerassia showed that:

- Fossil bone and dentine consist of carbonate fluorapatite and fossil enamel consists of carbonate hydroxyapatite
- Calcite is identified as a permineralizing diagenetic phase, occupying the structural and diagenetic voids of the tissues
- Crystallinity indices for bone, dentine and enamel are higher in the upper horizon and therefore crystallinity is not related to age, but to the degree of recrystallization and the local conditions of the burial environment.
- Contrary to current ideas, this study has demonstrated that the calculated crystallinity index values for recent bone were low but above zero.
- The correlation of the values of the crystallinity indices calculated with two different methods (Person *et al.*, 1996; Bartsiokas and Middleton,1992) depicts the degree of crystallinity of recent and fossil bone, dentine and enamel tissues, which is probably related to the tissues crystallite size and structure order.

GIRAFFIDAE (ARTIODACTYLA, MAMMALIA) FROM THE LATE MIOCENE OF KERASSIA, NORTHERN EUBOEA ISLAND, GREECE

INTRODUCTION

Kerassia is a newly reported Late Miocene fossil mammal locality, found in the Northern part of Euboea Island, Greece (Fig. 1). During the last two centuries, a large number of continental Neogene localities have been discovered in Greece and more specifically all around the coastline of the Aegean Sea. A large number of type species have been described from these fossil rich outcrops, including the type species of the four giraffid genera described in this study. Some of these localities are situated on Euboea Island: Limni (Cordella 1878), Achmet Aga (Woodward 1901), Achladi (Mitzopoulos 1947), Palaeovrisi (Jacobi 1982) are found in the northern part of the Island, while Aliveri and Kazarma (De Bruijn *et al.* 1979), Panagia Heria (Mitzopoulos 1947) and Halmyropotamos (Melentis 1967-69) are found in the Central part of the Island.

During fieldwork in the area of Kerassia in 1981, R.W. Kohler, a German geology student, tracked down the first fossil bone outcrop, and a year later Hans de Bruijn, Albert van der Meulen (University of Utrecht) and Constantin Doukas (University of Athens) carried out the first excavation. Since 1992, Associate Professor George Theodorou from the University of Athens has conducted systematic excavations of the locality. To date, more than 2000 specimens of large mammals have been recovered from the seven fossiliferous sites in the locality. All the excavated material (including specimens from the 1982 excavation) is stored in the collections of the Museum of Historical Geology and Palaeontology of the National and Kapodistrian University of Athens, Greece.

Although Kerassia has been excavated for twenty years, its fossil findings are only known from the brief descriptions of suids in van der Made *et al.* (1989) and Kostopoulos *et al.* (2001), as well as from the first review of the fauna and stratigraphy of the locality by Theodorou *et al.* (2003) and a study of the Carnivores by Roussiakis and Theodorou (2003).

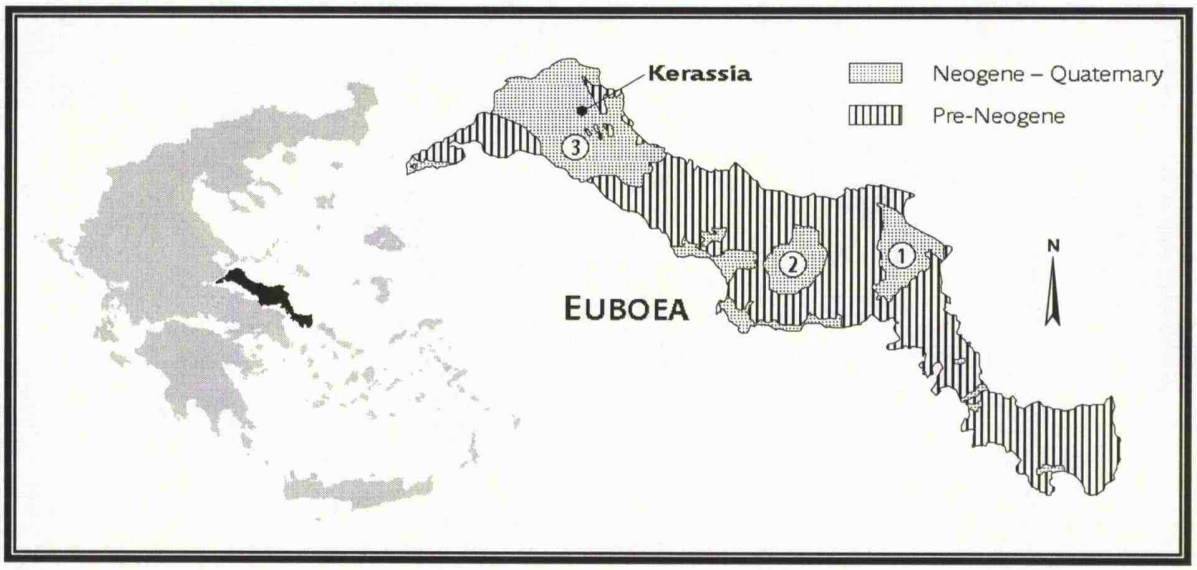

Figure 1: Location map showing Euboea Island and the locality of Kerassia. The distribution of Neogene-Quaternary and Preneogene rocks on Euboea Island, and the position of the three major Neogene basins on the island are also displayed: 1. Aliveri-Kymi basin, 2. Palioura-Gides basin, and 3. Limni-Istiea basin; adapted from Katsikatsos *et al.* (1981).

GEOLOGY AND STRATIGRAPHY

Euboea Island is situated in the central part of Greece, northeast of Athens. On the island extensive Neogene deposits, mainly of continental origin, overlie Mesozoic sedimentary and igneous rocks. The bulk of these deposits are found in the three major sedimentary basins of the island (Fig. 1): the Aliveri-Kymi basin, the Palioura-Gides basin, and the Limni-Istiea basin (Katsikatsos *et al.* 1981). In general, the three basins show a lower Early Miocene sequence of low energy, fine-grained lacustrine sediments, with lignite intercalations locally. Above lies a Late Miocene, high energy sequence of coarse grained fluvial sediments (Katsikatsos *et al.* 1981). Kerassia is found in the Limni-Istiea basin, the largest of the three basins of Euboea Island, located on the northern part of the island. According to Mettos *et al.* (1991) the basin is mostly covered by Late Miocene –Late Pliocene sediments, which have been unconformably deposited on the Early Miocene sediments.

The actual fossiliferous locality is found north of the village of Kerassia. To date, seven different fossiliferous sites have been found in the locality (namely K1 to K7) where at least two fossiliferous horizons occur, an upper and a lower one (Theodorou *et al.* 2003). The bone bearing sediments are reddish-brown, fluvial deposits that comprise the lower part of the upper sequence (Mettos *et al.* 1991), found above the sediments of the lower sequence. The substratum in this part of the basin consists of Early Cretaceous ophiolites.

The seven sites, K1-K7, all occur as roadside cuttings, found in a generally well covered, mature coniferous forest with undergrowth. The sediments generally are brown homogenous silty mud with a few scattered rounded to sub-rounded, polymict clasts. The fossil assemblages occur as dense accumulations of bones within some of the fluvial channels. Within the channels the matrix is more silty and the size and density of the clasts is greater than in the surrounding sediment. The presence of trace fossils is also evident in the sediments. Root casts as well as insect burrows, mostly ant nests and *Celliforma* (bee or wasp cells), record the maturity of the soils and the stability of the ground palaeo-surface. Sedimentological and geochemical evidence indicates that sites K1 and K6 belong to the upper horizon while K2, K3 and K4 belong to the lower one. Site K5 most probably belongs to the lower horizon, despite the differences in the sediment context of the channels' fillings (coarser clasts and large bones, mandibles and skulls with abrasion features) that suggest

higher energy environment of deposition. A definite determination is not possible yet for site K7. Note that the material from the 1982 excavation (mentioned in this study as Ke), was probably collected from site K1. Geochemical data, as well as information by Doukas (pers. comm. 2001) and a map by Kohler (1983) seem to support this hypothesis.

The prevalent orientations of the long bones in the different sites are generally northeast – southwest and northwest – southeast. Available evidence from the relative position of certain skeletal elements shows that the flow of the water in the channels was to the south. Therefore, it can be concluded that the source of the water and similarly of the sediments was north of the locality. The lack of coarse-grained material may indicate that the palaeogeographical position of the locality was at a considerable distance from the source. Consequently, these deposits most probably represent a floodplain setting.

Theodorou *et al.* (2003) gave a first account on the fauna of Kerassia, although the list is not complete as the excavations are still in progress and the material is still under preparation and study. To date, the initial determination of the material has provided the following species of large mammals: *Metailurus parvulus, Adcrocuta eximia?, Hyaenotherium wongii, Deinotherium* sp., *Choerolophodon* sp., *Microstonyx major, Gazella capricornis, Tragoportax* cf. *amalthea,* Bovidae indet., *Dorcatherium* sp., *Hipparion* sp., Rhinocerotidae indet., *Ancylotherium sp.*, and *Orycteropus* sp. which come from the upper fossiliferous horizon, whereas *Machairodus giganteus, Adcrocuta eximia, Ictitherium* cf. *pannonicum, Plioviverrops* sp., *Tetralophodon* cf. *longirostris, Gazella capricornis,* Bovidae indet., *Hipparion* sp., *Ceratotherium neumayri, Dicerorhinus* cf. *pikermiensis,* Rhinocerotidae sp. nova, *Ancylotherium sp.*, and Aves indet., are found in the lower horizon. Also, a number of specimens are attributed to the Giraffidae; four species have been identified in the upper horizon (*Palaeotragus rouenii, Samotherium major, Helladotherium duvernoyi, Bohlinia attica*) and respectively three (*Palaeotragus rouenii, Samotherium major, Helladotherium duvernoyi*) or possibly four (*Palaeotragus* sp.) in the lower one. The studied giraffid material was collected from sites K1, K3, and K4.

Abreviations: AMPG : Athens Museum of Palaeontology and Geology (Museum of Historical Geology and Palaeontology), University of Athens, Athens; NHML : Natural History Museum, London; Sedgwick : Sedgwick Museum of Earth Sciences, Cambridge; SAM : South African Museum, Cape Town; FMNH: Field Museum of Natural History, Chicago; MNHNP : Museum National d'Historie Naturelle, Paris (National Museum of Natural History, Paris).

SYSTEMATIC PALAEONTOLOGY

Order ARTIODACTYLA Owen, 1848

Family GIRAFFIDAE Gray, 1821

(Subfamily PALAEOTRAGINAE Pilgrim, 1911)

Genus PALAEOTRAGUS Gaudry, 1861

Type species. Palaeotragus rouenii Gaudry, 1861, from Pikermi, Greece

Palaeotragus rouenii Gaudry, 1861

Diagnosis. A *Palaeotragus* of small size with long and slender long bones.

Material. Left P^2-P^3 (K1/Δ82/2), left maxilla with dM^3-M^2 (K1/Δ246), part of left mandible with M_1-M_2 (Ke 306), left C (K1/Δ318), part of right mandible with M_1-M_3 (K3.181), part of left mandible with P_2-M_3 (K4/Δ111), right mandible with P_2-M_3 (K4/Δ324), left proximal part of Mc_{III+IV} (K3.335, K4/Δ119/18), right Mc_{III+IV} (K4/Δ331/5), left distal part of tibia (K1/Δ138), right proximal part of Mt_{III+IV} (K1/Δ15, K4/Δ96/1), right distal part of Mt_{III+IV} (K1/A1).

Description. The cranial elements (Appendices 1 and 2) are limited to two maxilla fragments that come from the upper fossiliferous horizon (site K1). In the first sample the two deciduous molars are molarised (Fig. 2E, F). The morphology of dM^4 is identical to that of the molars with two clearly formed and separated lobes (the terminology and orientation for the teeth used in this paper is based on Heintz (1970)). The only exception is the presence of a quite strong parastyle. In dM^3 the posterior lobe is molar like, whereas the anterior lobe looks more like a premolar with a reduction of the anterolingual region. The two lobes are separated and an lingual cingulum is present. The lingual side of the first two premolars is rounded and the external rib of the paracone-metacone is well developed. In the fossa at the posterior of the protocone a style is present. At the posterolabial side of P^2 a low but well developed additional style next to the metastyle is clear (Fig. 2D). In P^3 a folding of the enamel is visible in the posterior flange between the style and the protocone. The internal side of the labial crescent of P^3 is slightly divided into paracone and metacone. In the existing two molars of the first sample (Fig. 2E, F) the paracone is well developed, and the metacone is weaker but well defined. The parastyle and mesostyle are well developed and are inclined backwards; the

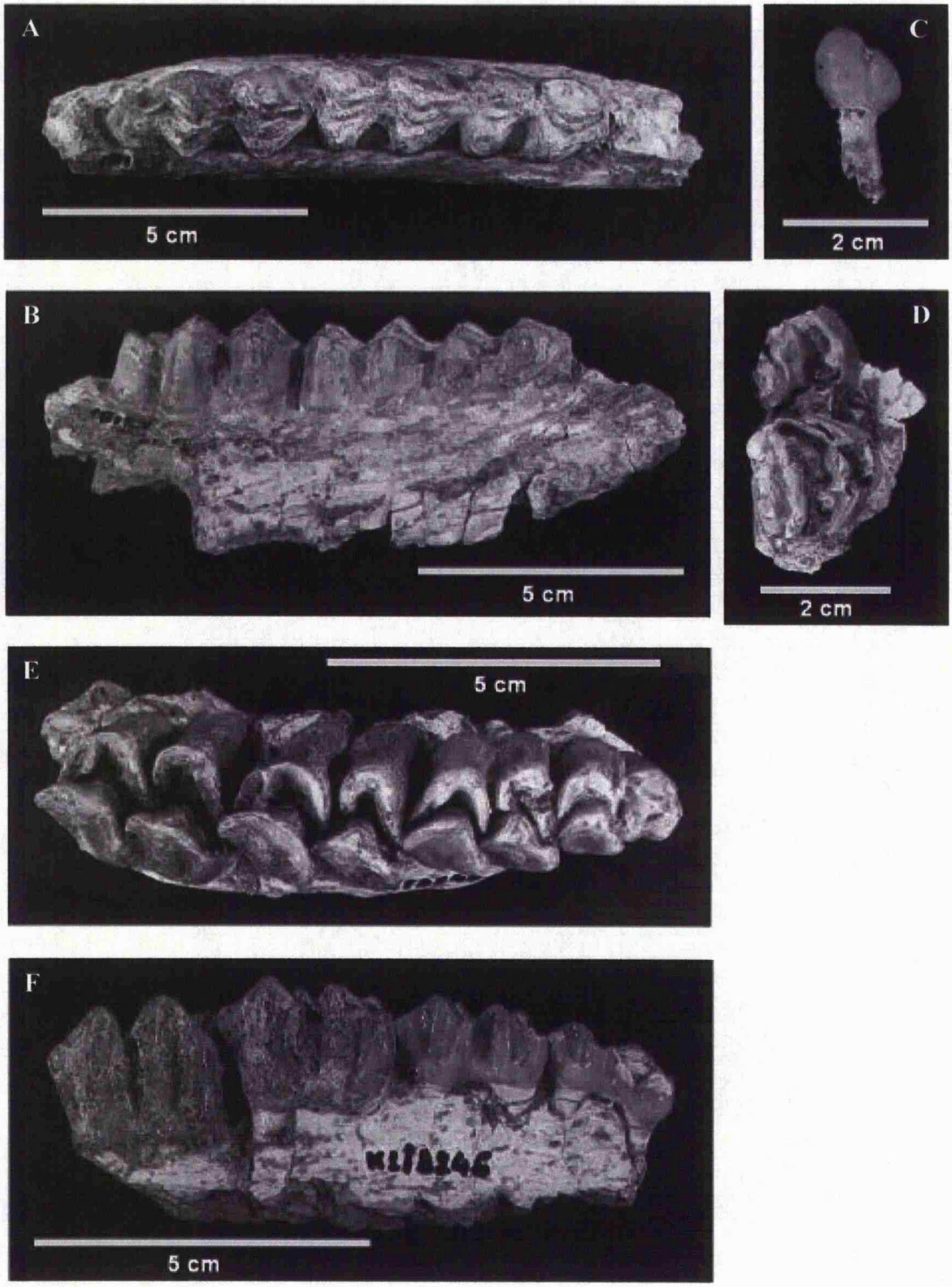

Figure 2: A. *P. rouenii*, part of left mandible with M_1-M_2, Ke 306, occlusal view. **B.** *P. rouenii*, part of left mandible with M_1-M_2, Ke 306, labial view. **C.** *P. rouenii*, left C, K1/Δ318, labial view. **D.** *P. rouenii*, left P^2-P^3, K1/Δ82/2, occlusal view. **E.** *P. rouenii*, maxilla part with dP^3-M^2, K1/Δ246, occlusal view. **F.** *P. rouenii*, maxilla part with dP^3-M^2, K1/Δ246, labial view.

metastyle is weaker but prominent. At the posterior flange of the hypocone a large enamel fold is seen, which probably corresponds to the "eperon hypoconal" of Heintz (1970). A similar, but more feeble fold can be also identified in dM^4.

Two of the mandible specimens (Fig. 3 and 4) have complete toothrows and K4/Δ324 in particular presents an almost complete ramus. The two mandibles probably belong to the same individual as the size and the degree of wear of the teeth are similar. The teeth are more worn (especially M_1), than the teeth of the other two mandible specimens (Ke 306 and K3.181) which are only slightly worn. The premolar row is considerably shorter than the molar one; the index Pm/M (P_2-$P_4 \times 100$ / M_1-M_3) for the two complete toothrows is 67.3 and 67.5, respectively and similarly the index Pm/PM (P_2-$P_4 \times 100$ / P_2-M_3) is 40.6 and 40.7, respectively. The talonid of the three premolars is reduced but well defined and separated from the trigonid with a rather deep furrow. The lower part of the labial wall of the talonid has a protuberant bulge, which is more distinct and more projected in P_3 (Fig. 3B and 4B). Although the morphology of P_2 is simple (Fig. 3A and B), P_3 and P_4 are strongly molarised. The protoconid is strong, and the parastylid is well defined and prominent. The metaconid is short and weak, whereas the entoconid is long and well developed. The hypoconid is clear and strong found at the top of the protuberant rib of the posterior region. The long posterior flange of the hypoconid is extended lingually and it is perpendicular to the axis of the tooth and parallel to the entoconid, and thus the entostylid is clearly placed lingually (Fig. 3A, B). In P_3 the protoconid is connected with the hypoconid and the entoconid. The metaconid is well developed, elongated and longitudinally oriented. Between the metaconid and the parastylid a small conid is clear, most likely a paraconid. It is almost connected with the parastylid and the elongated metaconid, forming a complete internal wall. Due to the degree of wear the metaconid is nearly connected with the protoconid. In sample K4/Δ111 the metaconid and the paraconid are broken (Fig. 4A, B). The parastylid is developed and quite prominent. The posterior flange of the hypoconid, as in P_2, is perpendicular to the axis of the tooth and is also extended up to the lingual face. The entoconid is narrow and parallel to this flange. The ribs (pillars) of the entoconid and the entostylid are found at the same level at the posterolingual side of the tooth. At the lower part of the crown they are united into a strong single tubercle, which is clearly separated from the metastylid. The protoconid in the fairly worn P_4 is connected with the metaconid and the hypoconid, and also with the entoconid (Fig. 3A, B and 4A, B). The entoconid is also connected with the metaconid, forming a closed and very molar like anterior lobe. The parastylid is feeble and the metastylid appears well developed. The lingual part of the valley that separates the metaconid and the entoconid is

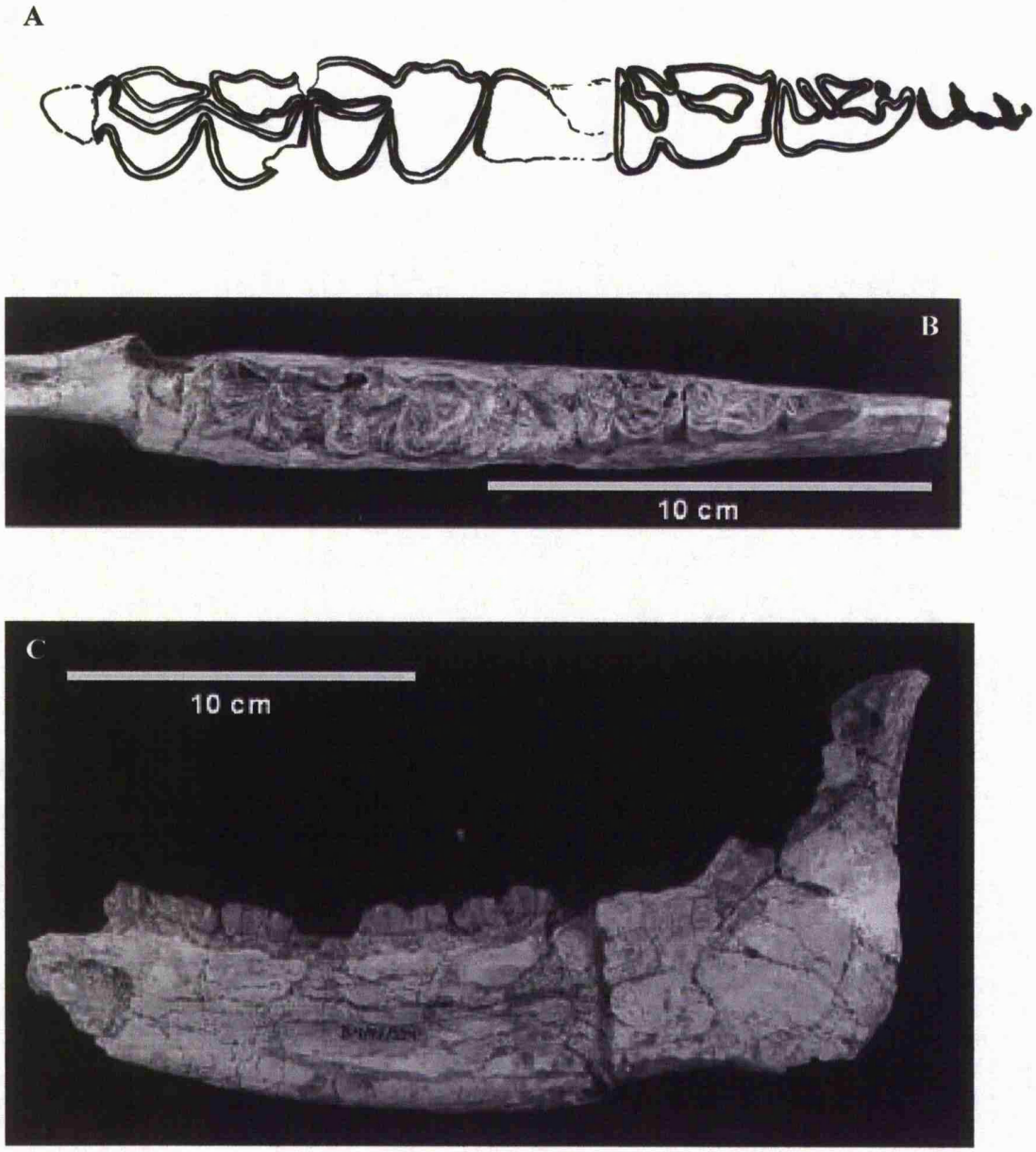

Figure 3: A. *P. rouenii*, right P_2-M_3, K4/Δ324, morphological details of the teeth, occlusal view, ×1. **B.** *P. rouenii*, right mandible with P_2-M_3, K4/Δ324, occlusal view. **C.** *P. rouenii*, right mandible with P_2-M_3, K4/Δ324, lingual view.

retained. The entostylid is narrow but well developed and is extended up to the lingual wall of the tooth, at the same level with the posterior rib of the entoconid. The antero-labial region of the tooth is reduced due to an obtuse, step-like fold between the protoconid and the protoconulid (Fig. 3A, B and 4A, B).

The morphology of the molars is simple (Fig. 2A, B, 3 and 4). The protoconid and the hypoconid are well developed. The lingual ribs (pillars) of the metaconid and the entoconid are also developed and the crescents of the metaconid and the entoconid are relatively narrow and elongated. An ectostylid is found between the two lobes, which is obviously stronger in M_1. At the anterolabial side a small fold is clear, representing a rudimentary cingulum, barely visible in M_3. The parastylid is well developed and prominent. A rather wide and deep furrow is found between the parastylid and the metaconid, closed at the lower part of the crown. The metastylid is strong, and particularly in M_3 it is well developed and projects lingually. The third lobe of M_3 is relatively small (proportionally to the other two lobes), and is separated from the second lobe at the lingual side by a deep, V-shaped furrow, open down to the base of the crown (Fig. 2A, B and 4A, B); its lingual wall is located more labially, at a considerable distance from the lingual level of the other two lobes. The shape of the labial cuspid is crescent like. A ridge (crest), which is bent anterolingually towards the entostylid, connects the cuspid with the entostylid and so closes the lingual wall. At an advanced stage of wear the cuspid is connected with the crest and is linked with the hypoconid. Although the anterior part of the mandible has not been found preserved, it is clear from the preserved mandible portions that the diastema is quite long. A loose canine from K1 presents clearly the characteristic bilobation of the giraffids (Fig. 2C). In addition, the posterior lobe is relatively long and high.

The postcranial elements (Appendices 3 – 13) attributed to this species are rather sparse and only one complete long bone is available. However, this material is enough to identify these elongated and slender limb bones as belonging to a small giraffid. The only complete long bone (Fig. 5B) is a metacarpal of great length (445mm), with a robusticity index (DTdiaphysis × 100 / length) of 8.6. This bone along with the other metacarpal specimen, a proximal part from K4, is quite robust with a fairly strong anterior ridge. The medial and lateral crests at the posterior face are strong, but fade out high in the diaphysis at a considerable distance from the lower epiphysis. The three discovered metatarsal portions present a clear sulcus at the anterior of the diaphysis which is shallow at the distal part, but wide and not well defined at the proximal part.

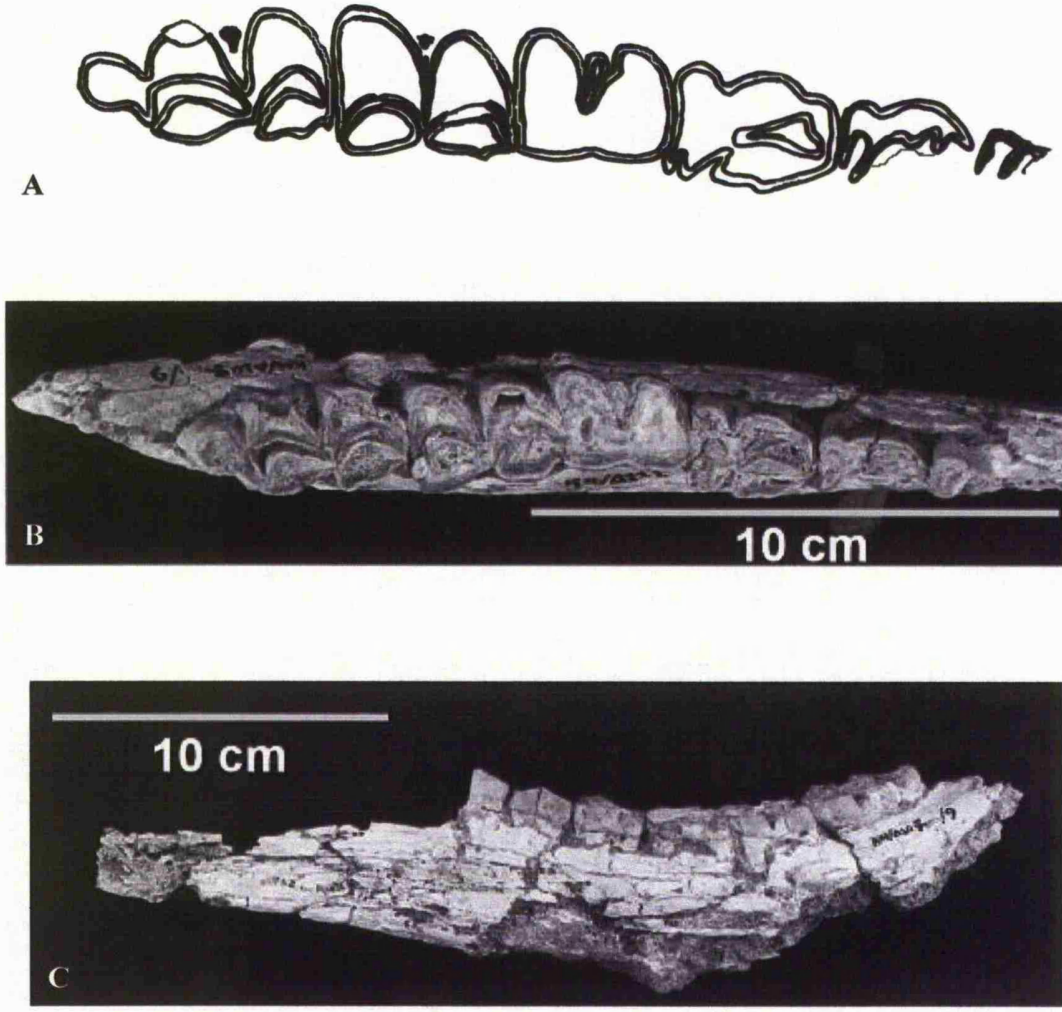

Figure 4: A. *P. rouenii*, left P_2-M_3, K4/Δ111, morphological details of the teeth, occlusal view ×1. **B.** *P. rouenii*, part of left mandible with P_2-M_3, K4/Δ111, occlusal view. **C.** *P. rouenii*, part of left mandible with P_2-M_3, K4/Δ111, lingual view.

The distal epiphysis of the tibia (Fig. 5A) is quandrangular with the lateral (external) side rounded. The medial malleolus is triangular, thin and rather narrow, and is limited to the anterior part of the medial side; its posterior edge is quite declivitous and consequently, the middle part of the external ridge of the cochlea is straight. Behind the medial malleolus the flexor digitorum longus muscle groove, which is wide and shallow, is clear, and located at the posteromedial side of the epiphysis but relatively more medially. On top of this, a significantly long imprint of the muscle is obvious at the lower part of the posterior face of the diaphysis. Close to the groove the imprint is quite wide but gradually becomes tapered towards the middle of the diaphysis. The articular surface of the malleolus at the lateral part of the epiphysis (despite the extended perforation) is narrow but long and almost extends up to the anterior ridge of the cochlea, interrupted by a feeble fibular furrow. The intercochlear crest is relatively narrow but well developed. The anterior protruding edge is strong and triangular with a fairly ample base, where a concavity is clear at its anterior surface. The posterior edge continues to the posterior face as a well developed, slanting furrow, bent towards the lateral side where the anterior ridge of the calcaneus rests.

Discussion. The dimensions and the morphology of the studied material reveal the presence of a small giraffid. A comparison with other genera of Late Miocene giraffids indicates that it represents the genus *Palaeotragus*. It is widely recognised that *Palaeotragus* is separated into two groups of species: small and large. *P. rouenii*, *P. microdon* (Koken 1885) and *P. primaevus* (Churcher 1970) are included in the small size group, which is characterized by slender and quite elongated post cranial elements. Hamilton (1978) considered that *P. rouenii* and the Chinese form *P. microdon* are synonymous. However, Bohlin (1926) and Geraads (1974, 1986) suggested that, despite their similarity, there are certain distinct differences, such as the shape of the ossicones, which are curved in *P. rouenii* but straight in *P. microdon*, and the presence of feeble ossicones in the females in *P. microdon*. Hamilton (1978) also regarded the African form *P. primaevus* as a sister group of the giraffines on the basis of the similarities in the ossicone morphology and the increased elongation and slenderness of the long limb bones. *P. coelophrys* (Rodler and Weithofer 1890), *P. expectans* (Borissiak 1914), *P. quadricornis* (Bohlin 1926), *P. borissiaki* (Alexeiev 1930) and *P. hoffstetteri* (Ozansoy 1965) are members of the large sized group, with shorter but more robust elements. Geraads (1974, 1986) stated that the differences between these species are not significant and considered them all as synonyms of *P. coelophrys*.

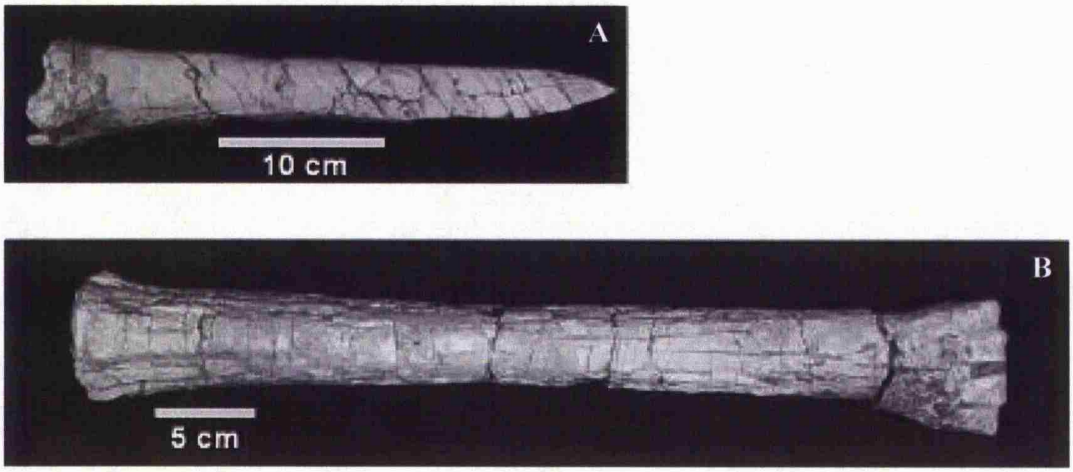

Figure 5: A. *P. rouenii*, left distal part of tibia, K1/Δ138, posterior view. **B.** *P. rouenii*, right Mc_{III+IV}, K4/Δ331/5, anterior view.

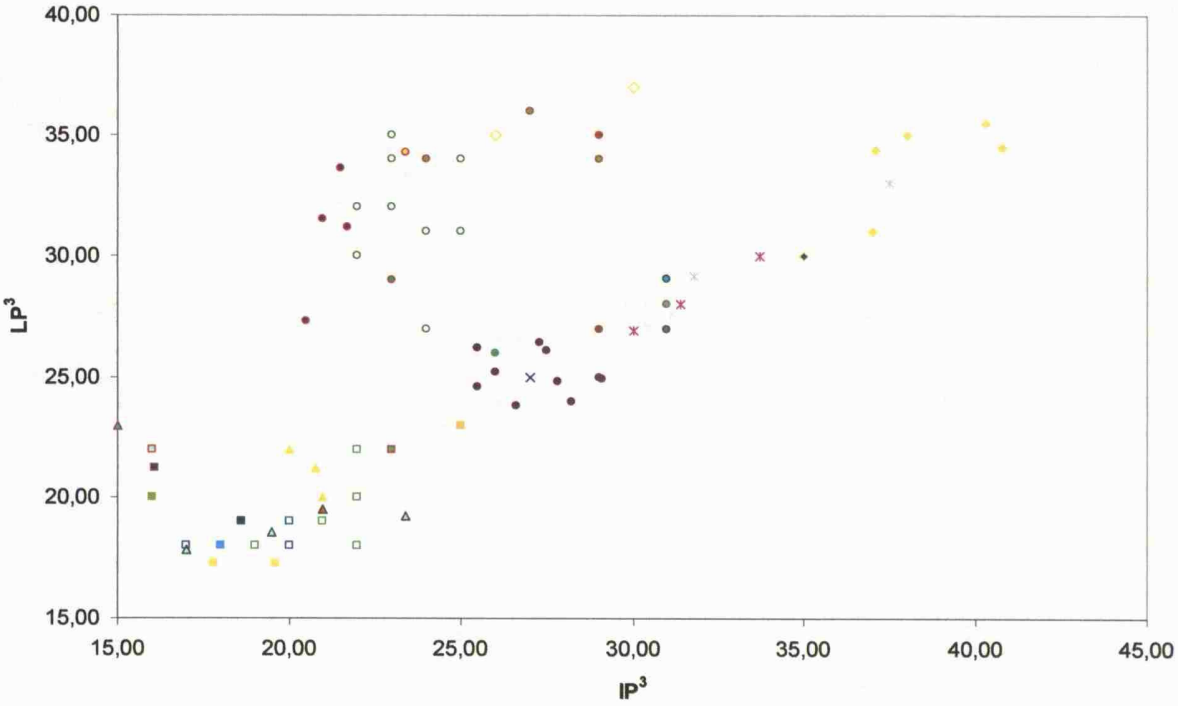

Figure 6: Plot of the upper third premolar width vs the upper third premolar length (measurements in mm). The legend for the symbols is presented in Figure 7.

Although the dimensions of some specimens from Kerassia are higher than the upper known size-range of *P. rouenii*, the overall morphology of the studied specimens indicates that they belong to this species. According to Bohlin (1926) the post cranial elements of *P. microdon* are shorter than those of *P. rouenii*, while the toothrows and the molars are slightly larger. In *Bohlinia attica* (Gaudry and Lartet 1856) the teeth and the toothrows are also slightly larger. In *P. coelophrys* the teeth are significantly larger. The two upper premolars from K1 are large enough to be related at least metrically to *B. attica* (Fig. 6). Despite the fact that they are slightly broken, it is clear that the external tubercles and the stylids are not so fully developed as in *B. attica* and in addition, their parastyle is not bifurcated. Furthermore, the lingual and labial faces of the teeth are not as bulging as in *B. attica.*

The length of the toothrow for the two complete mandibles is 133.8 mm and 136.1 mm respectively. The range of the toothrow length is 126-128.7 mm in *P. rouenii* (although it can be smaller, Roussiakis, pers. comm. 2002), 130-136 mm in *P. microdon* (Bohlin 1926), 142 mm in *B. attica* (AMPG, Roussiakis, pers. comm. 2002) and 141-170 mm in *P. coelophrys* (Hamilton 1978). Similarly, the two indices Pm/M and Pm/PM that express the relative reduction of the premolars are respectively: 72.5 and 43.1 for *P. rouenii* from Old Pikermi (specimen M8367, NHML), 62.8 and 38.9 for *P. rouenii* from Ditiko (DIT 2, Geraads 1978), 63.3 and 39.9 for *B. attica* from Pikermi (AMPG, Roussiakis, pers. comm. 2002), 65 and 38.2 for *P. coelophrys* from Maragha (De Mecquenem 1924), 62.2 and 39.7-40.1 for *P. coelophrys* from China (Bohlin 1926) and 57.1-60.0 and 36.03-37.88 for *P. microdon* from China (Bohlin 1926). The values of the two indices for the Kerassia specimens are within the range of *P. rouenii.* Although the general morphology of the teeth of *P. microdon* and *P. rouenii* is quite similar, the premolar row in *P. microdon* is relatively reduced (Fig. 8). So, despite the apparent accordance of the toothrow length of the two mandibles with *P. microdon*, the proportions of the molars and the premolars are quite different. Another striking character is the relative length of P_2 compared to the length of the premolars and the toothrow. It is considerably longer in the studied samples as well as in the other known *P. rouenii* specimens, than in *P. microdon, B. attica*, and even *P. coelophrys*. The ratios of the width against the length of P_3 and P_4 of the studied samples are similar to those of *P. rouenii.* Conversely, these ratios are higher in *P. microdon* and *P. coelophrys*, (and lower in *B. attica)* indicating that the two premolars in the first two are relatively shorter but wider (Fig. 9), (and in the latter one relatively longer). The posterior region of P_3 and P_4 is also important as it diverges in the different giraffid species and is indicative of the pattern of molarisation of the premolars (Hamilton 1978). This expansion or reduction of the posterior region can be

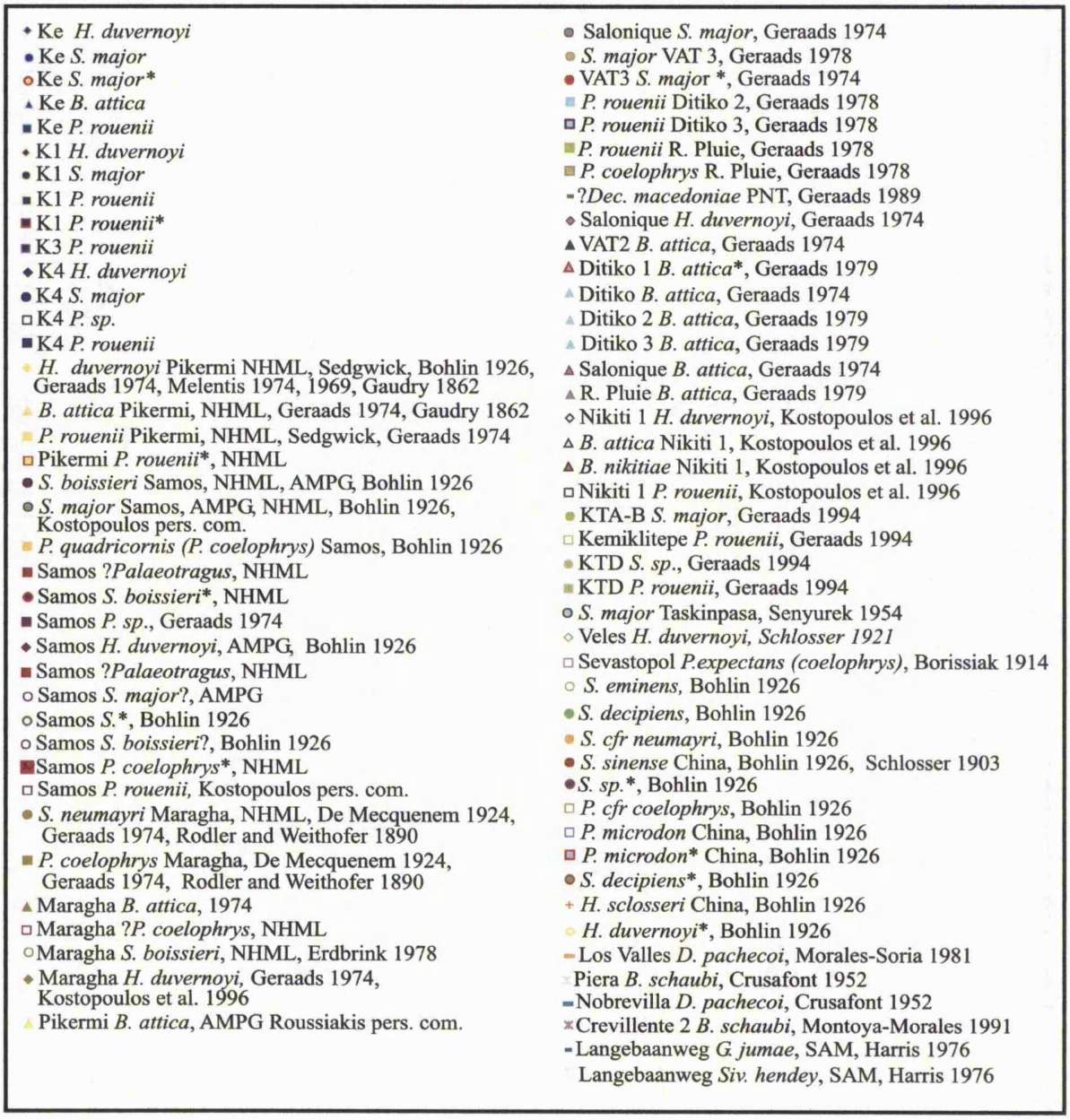

Figure 7: Legend that contains the symbols for the material from the sites of Kerassia and for all the comparative material that has been used in the plots of this study. Species names followed by a star (*) indicate juveniles. VAT = Vathylakkos, R. Pluie = Ravin de la Pluie, PNT = Pentalophos, KT = Kemikliteppe.

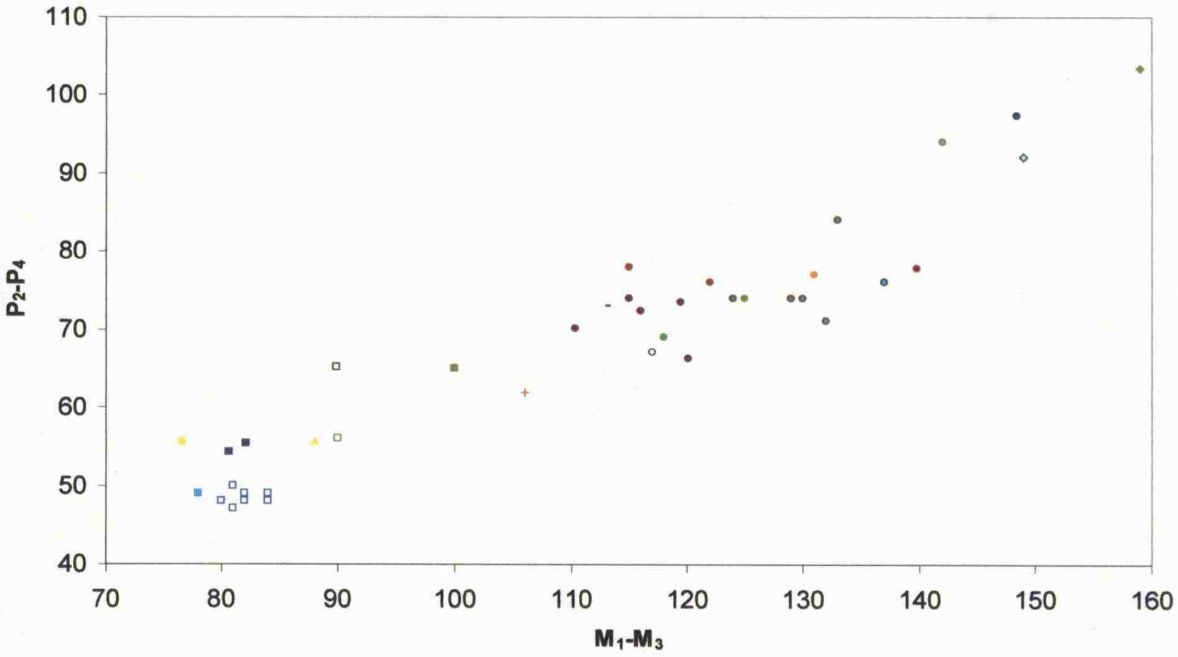

Figure 8: Plot of the length of the lower molar row vs the length of the lower premolar row (measurements in mm). The legend for the symbols is presented in Figure 7.

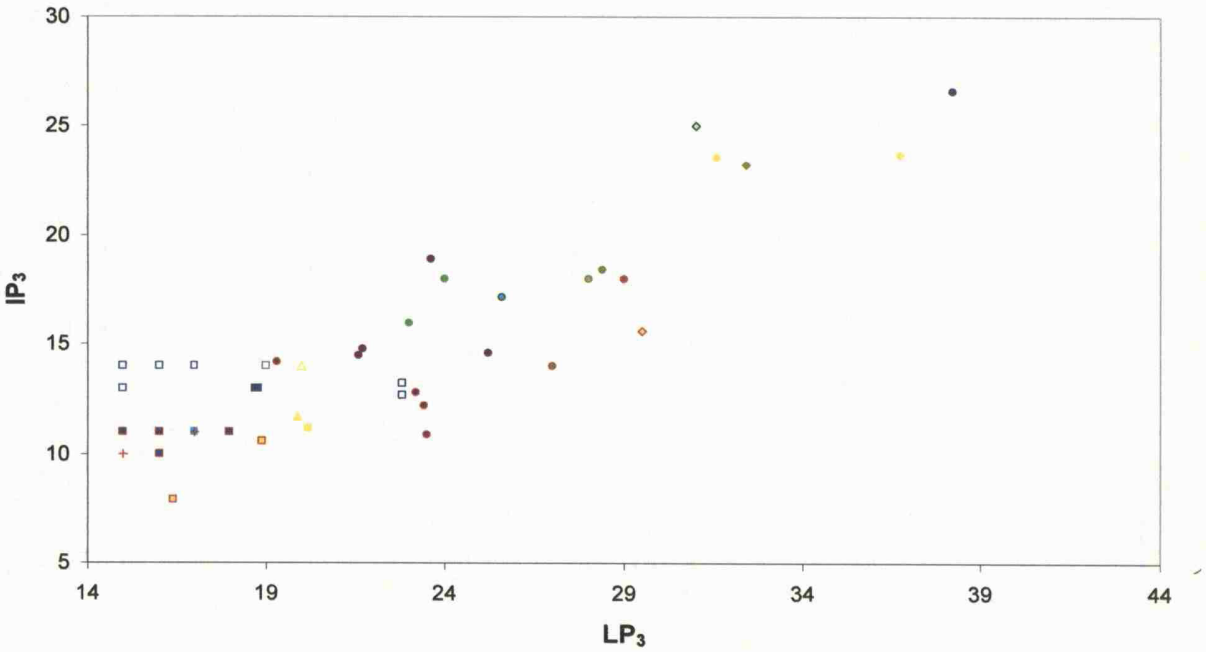

Figure 9: Plot of the lower third premolar width vs the lower third premolar length (measurements in mm). The legend for the symbols is presented in Figure 7.

expressed by the index length of posterior region/L. This index for the premolars of both mandibles is 0.31 for P_3 and 0.36 for P_4. Similarly, the index for the *P. rouenii* from the NHML is respectively 0.32 and 0.36. Both premolars are molarised. Geraads (1974), stated that the molarisation of the premolars varies from species to species in *Palaeotragus* and even within the same species. He also argued (Geraads 1986) that there is a tendency of P_3 in *P. rouenii* to molarise. The projected bulge at the posterolabial wall of the premolars (Fig. 3B, 4B) can also be identified in *P. rouenii* from Pikermi (specimen M8367, NHML). The small paraconid in P_3 is also clear. The dimensions of the molars in the specimens Ke 306 and K3.181 from Kerassia are within the range of the known *P. rouenii* specimens (Fig. 10). Although smaller they are identical with the larger molars of the two complete mandibles. Moreover, their morphology is similar with that of *P. rouenii*. The ectostylid, clearly stronger in M_1, is discernible in all three molars. Furthermore, the third lobe in M_3 is relatively small and its lingual wall is clearly separated from the second lobe. These features are quite distinctive in *P. rouenii*.

As mentioned above the postcranial elements of *P. rouenii* are quite elongated and slender. The robusticity index for the metacarpal of *P. rouenii* from Old Pikermi (specimen M11406, NHML) is 8.6 but measurements from Geraads (1974) on material from the Old Pikermi stored in MNHNP show a value of 6.21. However, measurements again from Geraads (1994) for *P. rouenii* from Kemiklitepe (KTD) indicated a value of 8.3, and also Kostopoulos *et al.* (1996) mentioned that the range of the index for the material from Nikiti (Nikiti 1) is 7.9-9.2. The range of the index for *P. coelophrys* from Maragha is 10.3-13.5 (measurements from Geraads, 1974). It is clear that the metacarpals of *P. rouenii* are longer but more gracile than those of *P. coelophrys* (Fig. 11). The robusticity index of the only complete metacarpal from K4 is within the range of *P. rouenii*, and this is probably one of the longest specimens (445mm) of the species found to date (Fig. 11). The dimensions and the gracility of the other incomplete long bones are within the range of *P. rouenii* (Fig 12 and 13). The articular surface of the malleolus in the distal tibia part from K1 is well developed, as in *P. rouenii* (Geraads 1974). The postcranial elements of *P. rouenii* are also longer than those of *P. microdon*. Until now, P. *microdon* has only been found in Eastern Asia and China.

P. rouenii has been identified in both the upper (site K1) and the lower (sites K3 and K4) horizons. The two mandibles with the longer toothrows from K4 can be associated with the long metacarpal from the same site indicating the existence of possibly one or more large and robust individuals of *P. rouenii*.

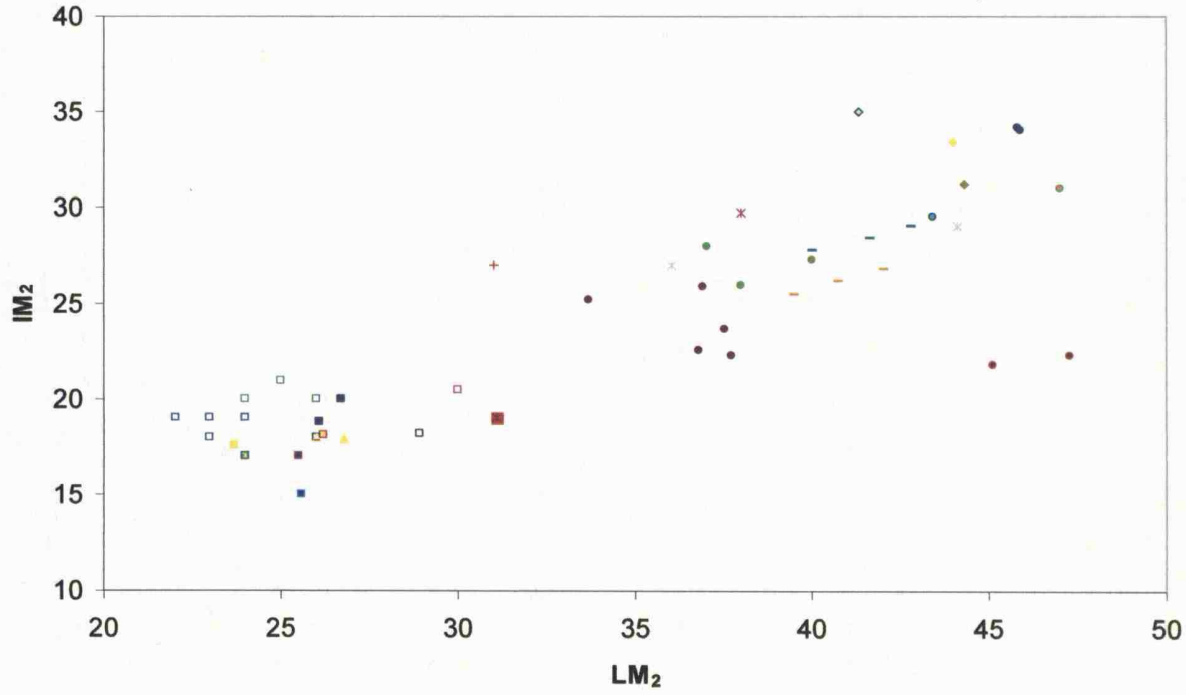

Figure 10: Plot of the lower second molar length vs the lower second molar width (measurements in mm). The legend for the symbols is presented in Figure 7.

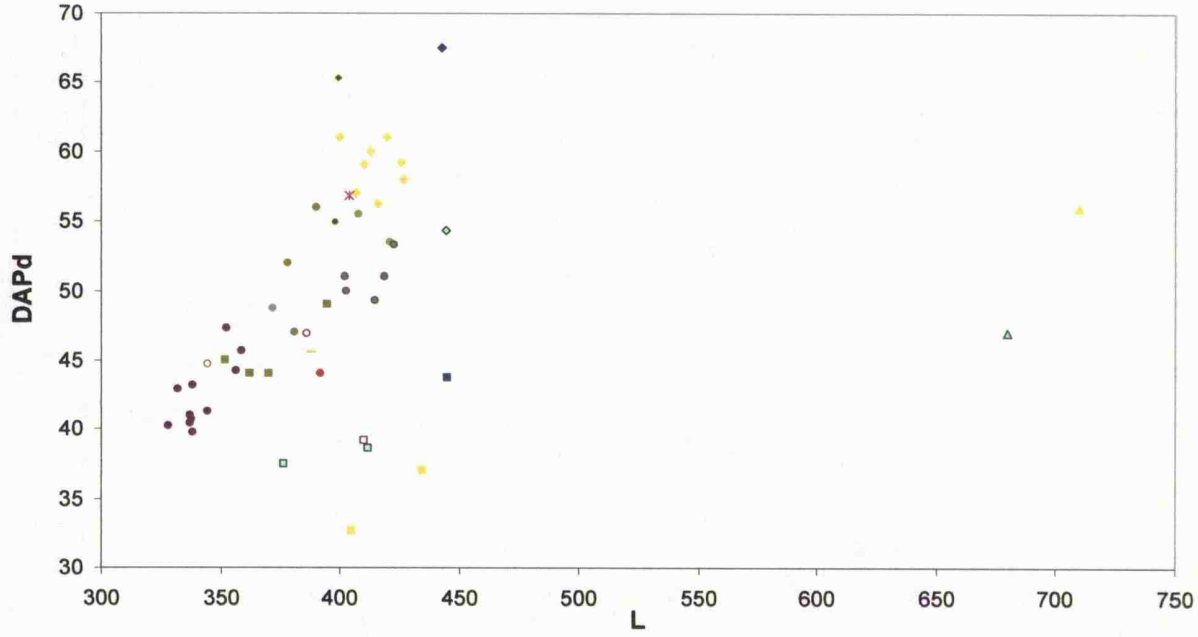

Figure 11: Plot of metacarpal length vs metacarpal distal anteroposterior diameter (measurements in mm). The legend for the symbols is presented in Figure 7.

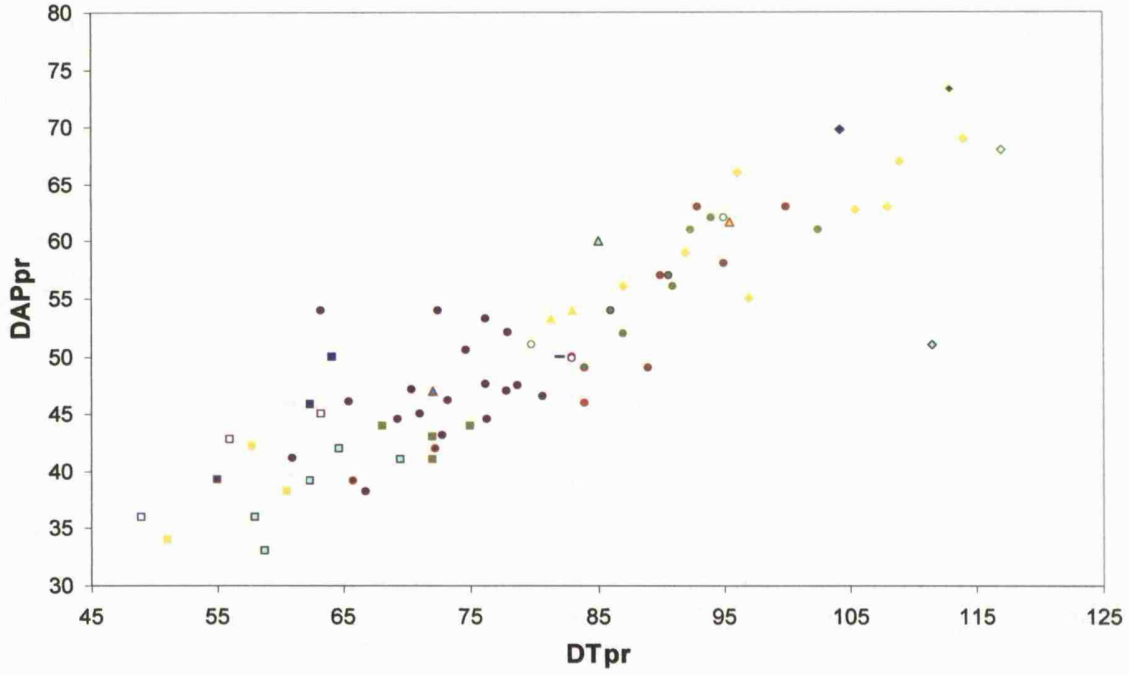

Figure 12: Plot of metacarpal proximal transverse diameter vs metacarpal proximal anteroposterior diameter (measurements in mm). The legend for the symbols is presented in Figure 7.

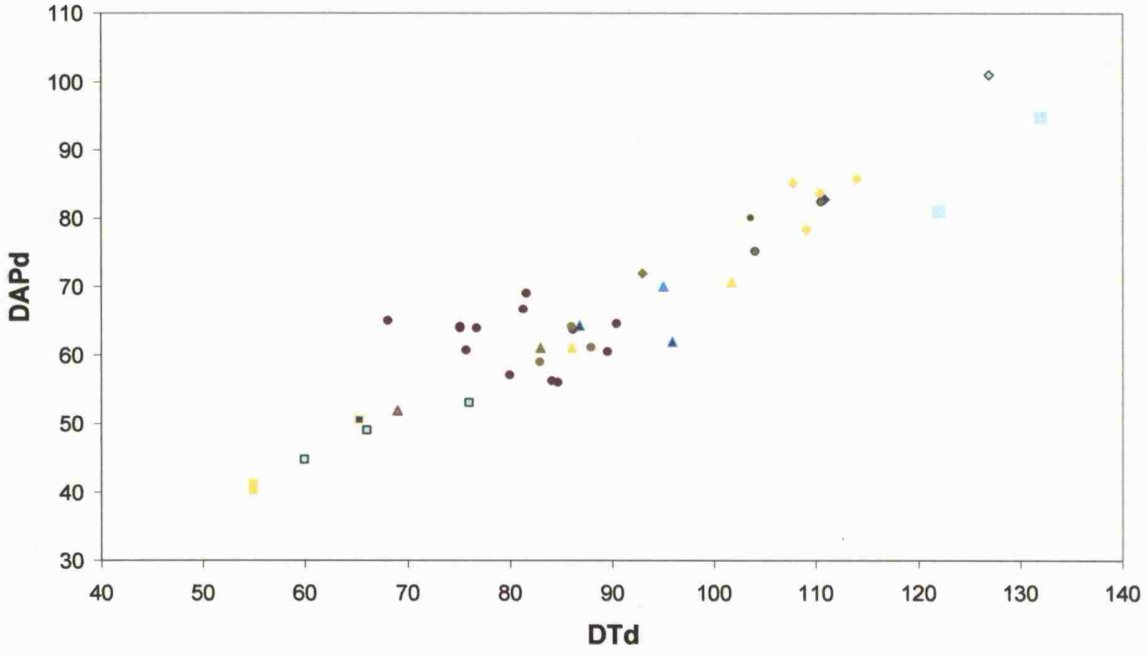

Figure 13: Plot of the tibial distal transverse diameter vs the tibial distal anteroposterior diameter (measurements in mm). The legend for the symbols is presented in Figure 7.

Palaeotragus sp.

Diagnosis. A *Palaeotragus* of possibly large size, larger than *P. rouenii* with a longer lower toothrow, elongated teeth, a molarised P_3 and a slightly molarised P_2.

Material. Part of right mandible with P_2-M_3 (K4/Δ8/1), part of left mandible with P_2-P_4 (K4/Δ8/2), right distal part of humerus (K4/Δ107/2).

Description. The toothrow (Appendix 2), in the first of the two mandible parts that most likely belong to the same individual, has been almost retained and only the anterior part of P_2 is slightly broken ((Fig. 14 A-C). In the same way the second specimen has retained the premolar row, although the posterior part of P_4 is also broken (Fig. 14 D-F). The length of the toothrow is approximately 157.3 mm. The premolar row compared to the molar row is reduced; the index Pm/M is 72.5 while the index Pm/PM is 41.5. The three premolars are molarised. A continuous lingual wall is clear at the trigonid of P_2 and although unworn, its morphology is similar to that of P_3. The talonid of the three premolars is large and well defined, and clearly separated from the trigonid with a deep labial furrow in P_4 and a shallow one in P_3 and P_2 (Fig. 14B, D). The labial wall is rather flat without any distinctive bulging. The posterior region of all the premolars is relatively increased and this is quite evident in P_4. The P_2 is elongated and narrow with a straight lingual wall and a reduced anterior end. The protoconid is very developed, and is connected with the hypoconid and the entoconid, as well as with the paraconid through the protoconulid and the parastylid. Nevertheless, the weak paraconid is connected with the strong metaconid and forms a continuous lingual wall at the trigonid. The parastylid is well defined and prominent and forms a rather deep V-shaped furrow with the paraconid. An elongated and strong ridge connects the entoconid with the protoconid and the hypoconid. The hypoconid is feeble and its posterior flange is long and narrow. Moreover, it is perpendicular to the axis of the tooth and is extended up to the lingual face of the tooth. The entoconid is longer than the posterior flange of the hypoconid. It is not parallel to the flange, as it bends slightly to the posterolingual. The entoconid together with the entostylid and the weak metastylid are united at the lower part of the crown forming a feeble bulge. In P_3 the anterior area is reduced, thus, the tooth's shape appears as triangular, with a rounded lingual wall. The protoconid is connected with the hypoconid and the entoconid, and also through the protoconulid with the crescent formed by the paraconid and the metaconid. Consequently, two valleys are formed between these three ridges. On the

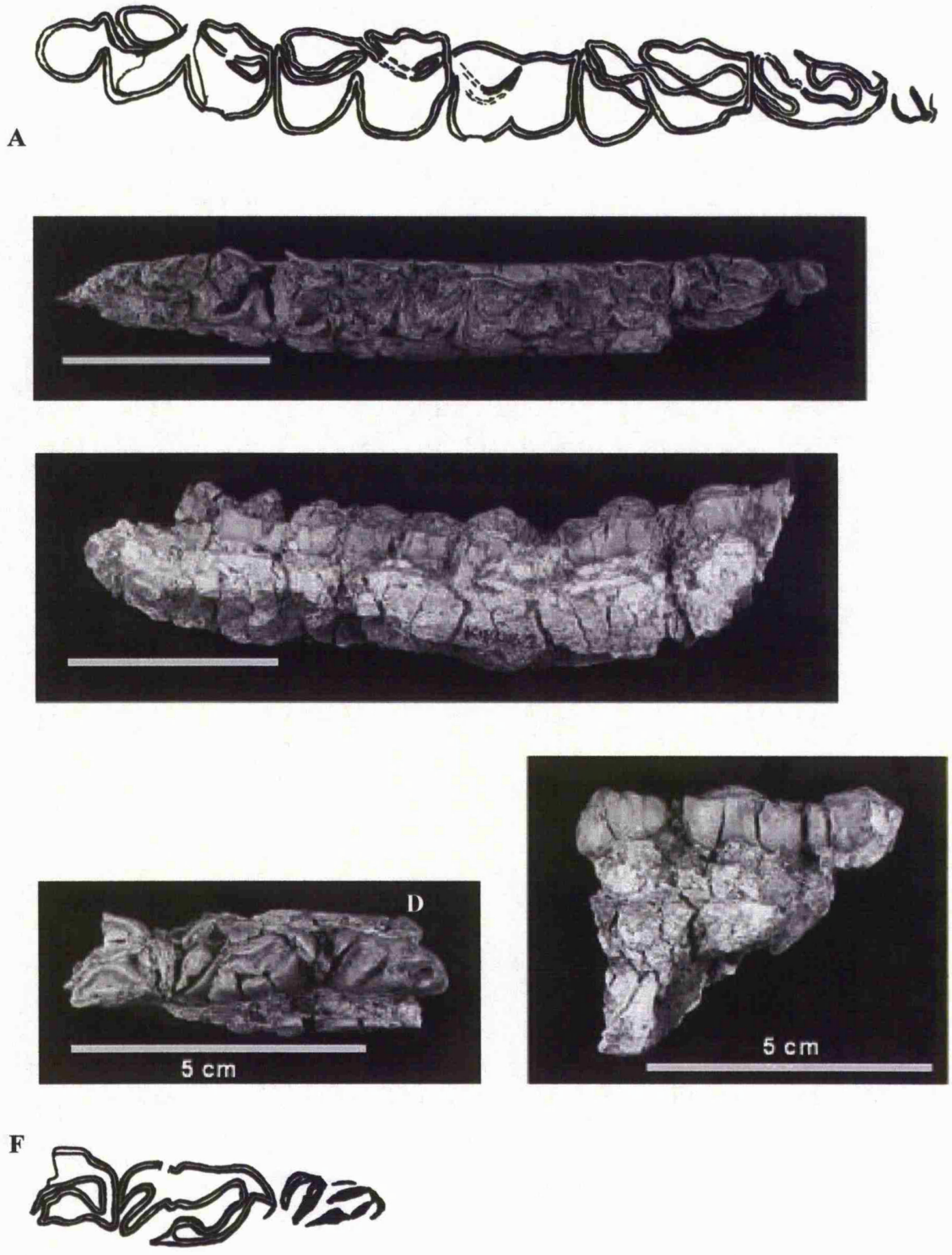

Figure 14: A. *P. sp.*, right P_2-M_3, K4/Δ8/1, morphological details of the teeth, occlusal view, ×1. **B.** *P. sp.*, part of right mandible with P_2-M_3, K4/Δ8/1, occlusal view (scale bar 5cm). **C.** *P. sp.*, part of right mandible with P_2-M_3, K4/Δ8/1, labial view (scale bar 5cm). **D.** *P. sp.*, part of left mandible with P_2-P_4, K4/Δ8/2, occlusal view. **E.** *P. sp.*, part of left mandible with P_2-P_4, K4/Δ8/2, labial view. **F.** *P. sp.*, left P_2-P_4, K4/Δ8/2, morphological details of the teeth, occlusal view, ×1.

lingual ridge the strong metaconid is clearly separated by a feeble paraconid. A well developed metastylid, bent posterolabially, is found at the posterior of the metaconid. The parastylid is developed and prominent, separated from the lingual ridge by a deep furrow, which is closed at the lower part of the crown. The protoconid is well developed and the hypoconid is narrow and elongated occupying the expanded labial side of the talonid. However, the posterior flange of the hypoconid is weak and short, and limited to the posterior of the tooth. The entoconid is elongated and narrow, bended towards the posterolabial corner of the tooth, confining the posterior valley and the entostylid (Fig. 14F). The P_4 is strongly molarised. The shape of the tooth is rectangular, with only an obtuse step-like fold at its antero-labial region (Fig. 14A, B, D). It is clearly separated into two lobes by two furrows, one at the lingual and one at the labial wall. However, the labial furrow is closed in the lower part of the crown. Although, the posterior lobe is smaller than the anterior one, the lingual wall of the tooth is identical to the lingual wall of the molars. The protoconid is well developed and oblique to the long axis of the tooth. Its posterior flange is pointing anterolingually towards the entoconid. The metaconid is also developed, elongated and longitudinally oriented, with a strong lingual rib (pillar). A transversely oriented cristid is found at the anterior of the tooth, with a prominent parastylid at its lingual end. Labially it is attached to the protoconid and lingually the parastylid is connected to the metaconid. The hypoconid is also well developed and separated from the protoconid. The posterior flange of the hypoconid is strong and is extended to the posterolingual face of the tooth. However, the posterior flange of the entoconid is extended more lingually than the entostylid (Fig. 14A, B). As for the entoconid, it is triangularly shaped, relatively well developed and also oblique with an orientation similar to that of the protoconid. In a more advanced stage of wear it seems that the protoconid would be connected with the hypoconid and the entoconid and probably with the anterior cristid.

The molars are quite worn, particularly M_1. The protoconid and the hypoconid are well developed. In M_2 a very feeble ectostylid is found between the two lobes. Conversely, in M_3 only a strong cingulum can be seen that connects the two lobes at the lower part of the crown. A small fold, obvious at the anterolabial side of M_2 and M_3, is attributed to a rudimentary cingulum. The lingual rib (pillar) of the metaconid is developed and the wall of the entoconid is almost flat. The metaconid and the entoconid in M3 are oblique and bent anterolingually. The parastylid and the metastylid are clear and prominent. The entostylid is long in M_1 and M_2, and also in M_2 it is extended to the lingual face of the tooth. In M_3, on the contrary, it is short and points to the posterior of the tooth (the third lobe). The entoconid in M_3 is relatively

small with its posterior end rounded. The third lobe is large and round, with its lingual wall found at the same level with the lingual walls of the other two lobes (Fig. 14A, B). At the anterolingual side of the lobe a short ridge is projected lingually and not towards the entoconid. Due to the advanced degree of wear the ridge is united with the lobe's labial crescent. On the lingual wall of the lobe two furrows can be identified. A small one, that separates the ridge from the entoconid and a wider, V-shaped one between the ridge and the lobe, which defines the lobe.

The only postcranial element that can be attributed to this species is a distal humerus part (Appendix 3). The trochlea and the condyle are heavily gnawed and broken. However, it is evident that the trochlea is higher than the condyle. The concave part of the trochlea is shallow and its' keel is feeble. At the anterior side of the bone a reduced coronoid fossa is limited to the lateral side of the bone, towards the supracondylar crest. At the posterior side the olecranon fossa is long and relatively narrow, and also triangularly-shaped. The epitrochlea is strong and the profile of the angle that it forms is almost vertical. Moreover, the epicondyle is shorter than the epitrochlea.

Discussion. The studied material is not sufficient to provide any definite determination, but it is clear that the three specimens belong to a rather medium sized giraffid; the overall morphology of which can probably be related with *Palaeotragus*. As mentioned above the genus *Palaeotragus* consists of a small and a large sized species. The dimensions of the three specimens are within the range of the *P. coelophrys* (Rodler and Weithofer 1890) group and to be more precise within the range of *P. coelophrys* itself. The length of the toothrow for the complete mandible is definitely within the range of *P. coelophrys*, which is 141-170 mm (Hamilton 1978). It is longer than the known range of *P. rouenii* of 126-128.7 mm and also longer than the two mandibles from Kerassia, already mentioned above and attributed to *P. rouenii* (133.8 mm and 136.1 mm, respectively). Similarly, it is longer than the Chinese *P. microdon* (Bohlin 1926). Conversely, it is shorter than the range of the toothrows of *S. boissieri* (Major 1888) from Samos stored in NHML which is 178.1-188.7 mm, or the range that Bohlin (1926) mentioned for material of *S. boissieri* also from Samos (183-195 mm). The two indices, Pm/M and Pm/PM of the complete toothrow are larger than the indices of *P. coelophrys*, *P. microdon*, *S. boissieri* (55.2-64.4 and 35.2-39.5 respectively) and also of *P. rouenii*; however, the indices for the *P. rouenii* sample from the Old Pikermi (specimen M8367, NHML) have similar values. Therefore, the premolar row of this specimen from Kerassia is longer than in the above mentioned species (Fig. 8). The dimensions and the

width/length ratios of the teeth compared with the teeth of the other species manifest that these teeth are elongated and narrow (Fig. 9). Furthermore, the posterior region of the premolars is expanded compared to the other Palaeotraginae species and compared with the *P. rouenii* specimens from Kerassia. More specifically the reduction index for P_3 and P_4 is 0.44 and 0.42 respectively (0.31 for P_3 and 0.36 for P_4 for *P. rouenii* from Kerassia). Geraads (1974) stated that the talonid of the premolars of *P. coelophrys* from Maragha is also large. The labial wall of the posterior region of the premolars in *P. rouenii* from Kerassia, as well as in *P. rouenii* in general is relatively bulged, while it is flat in the studied specimens and in *P. coelophrys*. Despite the variation of the molarisation of the premolars in the genus *Palaeotragus*, it is clear that the stage of molarisation in the studied material is advanced. Therefore, in addition to P_3 and P_4, P_2 is also molarised. The closed lingual wall is evident in both P_3 and P_2, whilst in *P. coelophrys* from Maragha (De Mecquenem 1924, pl. II, fig. 8) they are both open and in the specimen from China (Bohlin 1926, pl. III, fig. 5) it is closed in P_3 and open in P_2. Furthermore, in the sample from China a P_1 is also present. The metaconid is connected with the protoconid in the primitive P_3 and P_2 from Maragha and in the P_2 from China but not in the P_3. In the latter the posterior flange of the hypoconid is short and it is covered by the oblique and developed entoconid, as in the studied samples. In *P. rouenii* the posterior flange of the hypoconid is long and parallel with the entoconid while the valley between them is open lingually. A similar morphology is evident in the P_2 under investigation. The posterior flange of the hypoconid and the entoconid are parallel and perpendicular in *P. rouenii*, while in the studied sample the entoconid is oblique. The ectostylid, absent in the studied molars, is also absent from the molars in *P. coelophrys* while it is present in *P. rouenii*. In *P. rouenii* the third lobe of M_3 is small with a long lingual ridge that connects the lobe with the entoconid. Conversely, in the studied specimen it is large with a short lingual ridge, lingually oriented and separated clearly from the entoconid. This is also found in the third lobe of M_3 of *P. coelophrys* from Maragha (De Mecquenem 1924, pl. II, fig. 8).

The dimensions of the distal humerus part indicate a medium size animal. It is clearly larger than *P. rouenii* and closer to the lower range of *B. attica* and *S. boissieri*. In *B. attica* (specimens 11399a and 11399b, NHML) the trochlea and the condyle have similar height and the concave middle part of the trochlea is shallow with its lateral edge keel rather feeble. The epicondylar angle is obtuse, while the olecranon fossa is long, U-shaped and wide. The coronoid fossa is long and centrally placed. Similarly, in *S. boissieri* (NHML) the trochlea is higher than the condyle, the middle part is deep and the lateral keel is strong. The olecranon

fossa is short and narrow and the epicondylar angle is vertical, while the coronoid fossa is laterally placed. It is clear that the studied distal humerus part shares more characters with *S. boissieri* than with *B. attica*, indicating that it belongs to a member of the Palaeotraginae and due to some major differences like the shape and size of the olecranon fossa, and the morphology of the trochlea, it is most likely related to a large *Palaeotragus*. The lack of humerus samples attributed to *P. coelophrys* does not allow any adequate correlations with this species. Nevertheless, the dimensions of the humerus are expected to be similar to that of the studied specimen. Rodler and Weithofer (1890) reported the presence of a lower part of a humerus with a transverse diameter of the lower epiphysis of 89 mm that was related to *P. coelophrys*. Borissiak (1914) described also a lower humerus part from Sebastopol with a distal transverse diameter of 102 mm, attributed to *P. expectans* (*P. coelophrys*). The transverse diameter for the specimen from K4 is 98 mm (Fig. 15). According to his descriptions except from the similar transverse diameter the specimen from Sebastopol also presents a condyle shorter than the trochlea, a shallow trochlear concavity and an epicondyle shorter than the epitrochlea.

The dimensions of these specimens from the lower horizon (site K4) are within the range of *P. coelophrys*. However, the small number of specimens and differences in certain characters make difficult the correlation of the material with *P. coelophrys*. Therefore, a definite determination is not considered possible until more material is available.

Genus SAMOTHERIUM Major, 1888

Type species. Samotherium boissieri Major, 1888, from Samos, Greece

Samotherium major Bohlin, 1926

Text-figure 140; Plate 9, figs 8-11

1926 *Samotherium boissieri* var. *major* Bohlin, p. 87.
1954 *Samotherium majori* Bohlin; Senyurek, p. 3, figs 1-10.
1974 *Samotherium boissieri major* Bohlin; Geraads, p.16, pl. 2, figs 1-3.
1978 *Samotherium boissieri major* Bohlin; Geraads, p.271, pl. 2, figs 2-4.
1994 *Samotherium major* Bohlin; Geraads, p.161, text-fig. 1; pl.1, fig. 1.

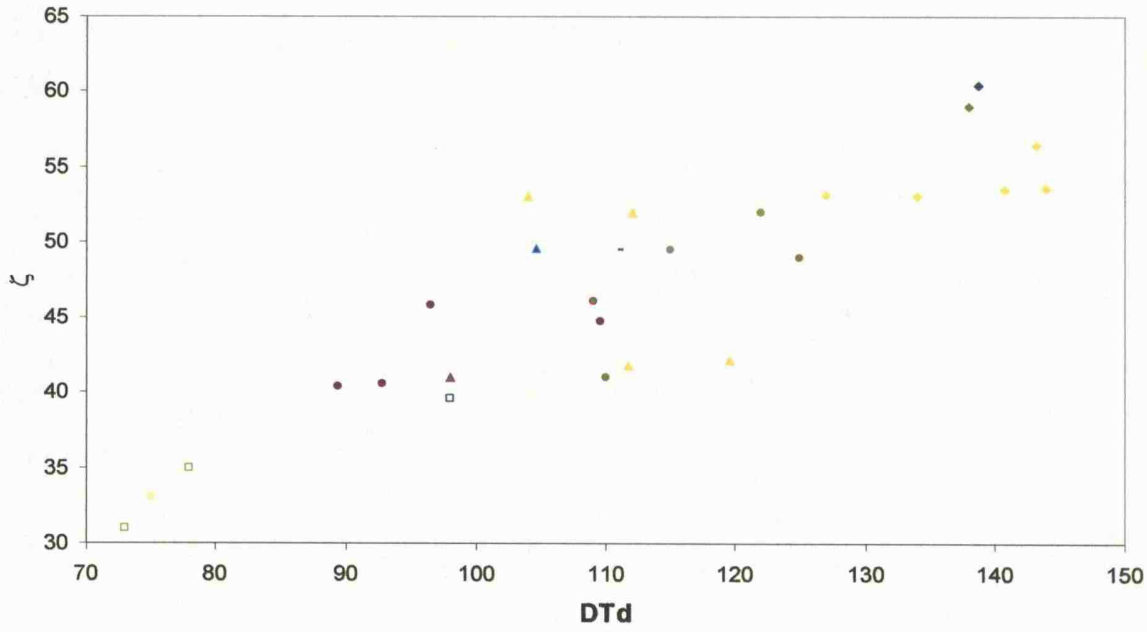

Figure 15: Plot of the humerus distal transverse diameter vs the humerus anteroposterior diameter of the trochlea measured at the intertrochlear furrow (ζ) (measurements in mm). The legend for the symbols is presented in Figure 7.

Diagnosis. A *Samotherium* of great size with long and robust long bones but less robust than *H. duvernoyi* and shorter than *S. sinence*. The orbit is located behind M^3 and P_3 is always molarised.

Material. Left maxilla part with dM^2-dM^4 (Ke 123), right mandible with P_2-M_3 (K4/Δ119/34), part of left mandible with M_2-M_3 (K4/Δ54/1), left radius (K1/Δ78), right radius (K1/Δ90), left proximal part of radius (K1/Δ89), right proximal part of radius (K1/Δ87), right proximal part of Mc_{III+IV} (?Ke 99/40), right distal part of Mc_{III+IV} (K1/A9), left Mc_{III+IV} (K1/Δ244), forelimb phalanx I (Ke 90), left tibia (K1/Δ341/1), left malleolar (K1/Δ343), left astragalus (Ke 99/49, K1/Δ342), left calcaneus (Ke 99/46, Ke 99/47), right calcaneus (K1/A2, K1/Δ243), right distal part of calcaneus (Ke 99/48), left scaphocuboideum (K1/Δ346), right scaphocuboideum (K1/Δ247/2), left intermediolateral cuneiform (K1/Δ341/2), right intermediolateral cuneiform (K1/Δ45, K1/Δ247/3), right Mt_{III+IV} (K1/Δ247/1), left Mt_{III+IV} (K1/Δ344).

Description. The only skull element consists of a partial maxilla with three deciduous molars (Fig. 17A, B, Appendix 1). The teeth are almost unworn, indicating the presence of a very young individual. The paracone is very strong and its labial rib (pillar) is remarkably developed. It is stronger in dM^2 and it gets feeble gradually more towards dM^4. Also, it is united with the strong parastyle at the lower part of the crown. The furrow between the two in the first two deciduous premolars is wider and deeper than in the third. In addition, dM^3 and dM^4 are molarised. The dM^2 is elongated, with its lingual wall rounded. The exact separation point between the long but weak protocone and the developed hypocone is not well defined. The strong paracone rib (pillar) is inclined to the posterior and the well developed, long parastyle is prominent and points to the posterolabial (Fig. 17B). The metacone is weak but distinguishable and the low metastyle is very long and is bent and extended towards the anterior. A strong and well defined posterolingual cingulum is also evident (Fig. 17A). As expected, the dM^3 is separated into two lobes, which are united at the lower part of the crown. A feeble cingulum clearly surrounds the lingual face of the tooth at the lower part of the crown. Nevertheless, it is more developed at the anterolingual and posterolingual sides of the tooth. The protocone is simple and low, with a short posterior flange. Conversely, the hypocone is well developed with symmetrical flanges that form an acute angle (Fig. 17A). At the posterior flange an "eperon hypoconal" points towards the labial side, whereas at the external face of the anterior flange a small fold or bifurcation is also clear (Fig. 17A). It is projected towards the anterior, confining the posterior flange of the protocone. The paracone rib (pillar) is inclined as in dM^2, and the parastyle is also well developed and bent (Fig. 17B).

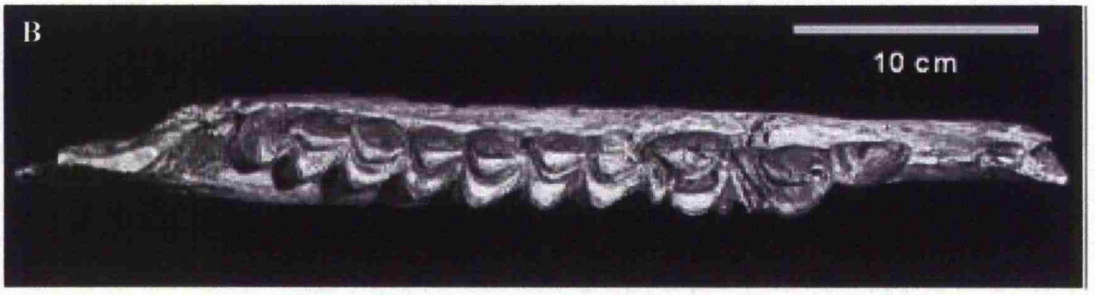

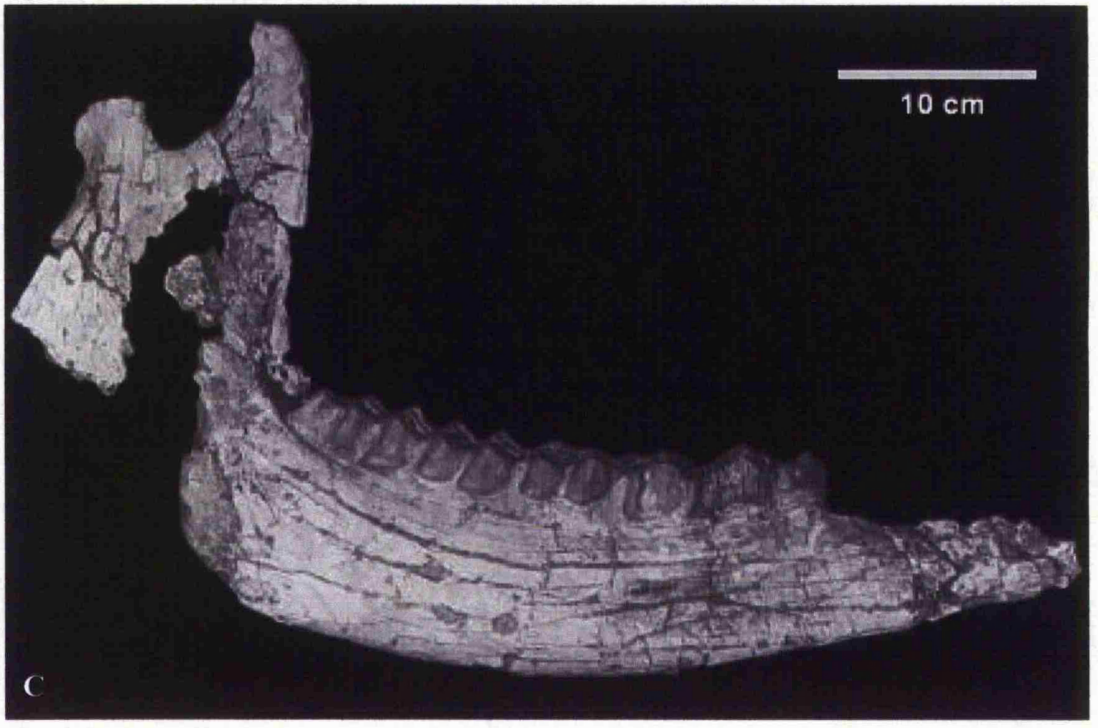

Figure 16: A. *S. major*, right P_2-M_3, K4/Δ119/34, morphological details of the teeth, occlusal view, ×1/2. **B.** *S. major*, right mandible with P_2-M_3, K4/Δ119/34, occlusal view. **C.** *S. major*, right mandible with P_2-M_3, K4/Δ119/34, labial view.

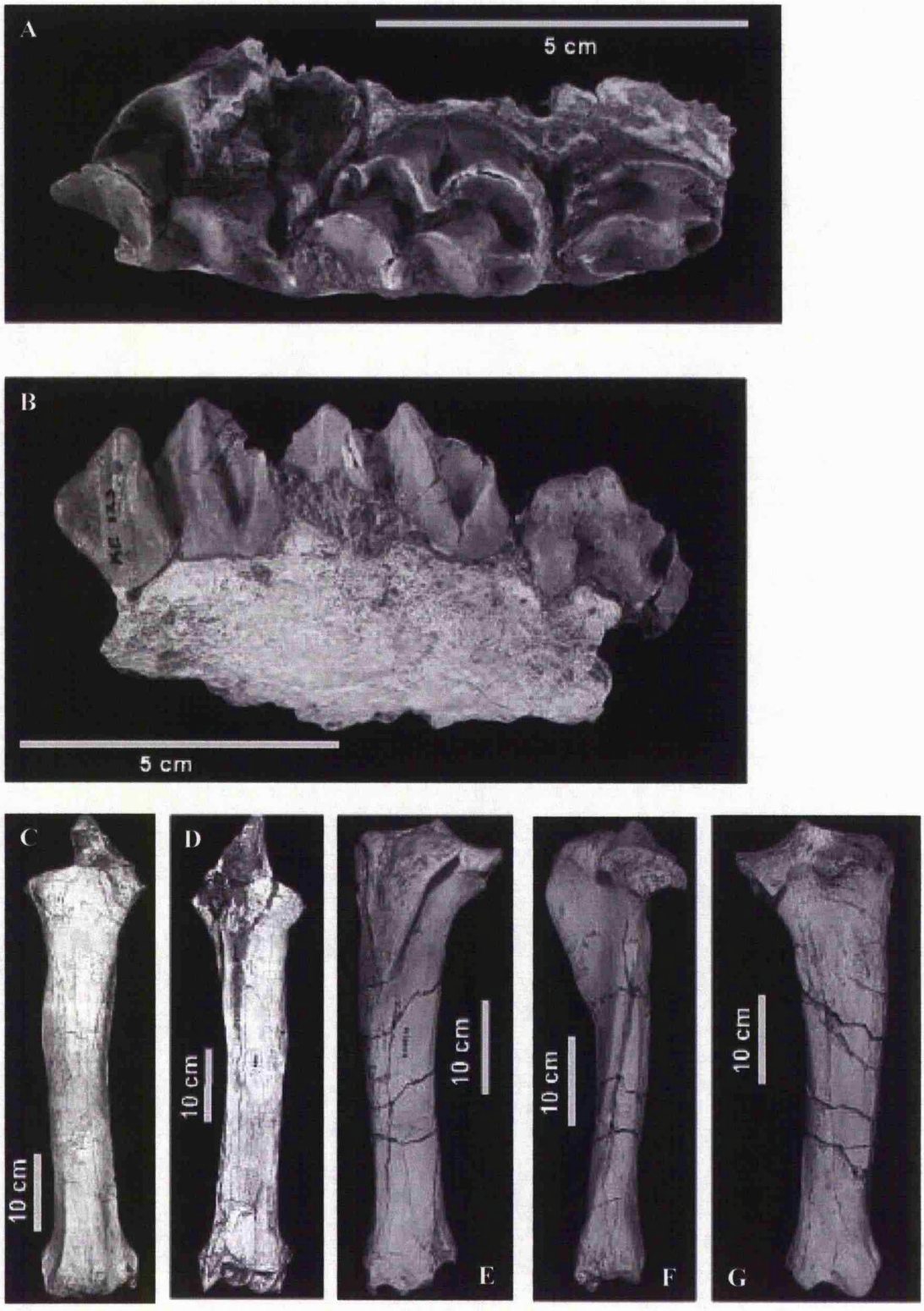

Figure 17: A. *S. major*, left maxilla part with dP^2-dP^4, Ke 123, occlusal view. **B.** *S. major*, left maxilla part with dP^2-dP^4, Ke 123, labial view. **C.** *S. major*, left radius-ulna, K1/Δ78, anterior view. **D.** *S. major*, left radius-ulna, K1/Δ78, posterior view. **E.** *S. major*, left tibia, K1/Δ341/1, anterior view. **F.** *S. major*, left tibia, K1/Δ341/1, lateral view. **G.** *S. major*, left tibia, K1/Δ341/1, posterior view.

Hence, the anterior lobe of dM^3 looks quite similar with the anterior region of dM^2. The metacone is strong with a flat and concave labial wall. The mesostyle and the metastyle are weak and projected labially. The protocone in the molar like dM^4 is broken. The hypocone is well developed with an imperceptible eperon hypoconal and a weak fold at the exterior of the anterior flange (Fig. 17A). The strong paracone rib (pillar) is vertical and the parastyle is strong but not very prominent (Fig. 17B). In addition, a style is formed at the edge of the curved posterior flange of the paracone. It is clearly not connected with the mesostyle and projects labially. The well developed labial crescent of the posterior lobe consists of a strong metacone with a weak but well defined labial rib (pillar) (Fig. 17B). Also, the labial wall is very concave. The strong mesostyle is projected labially and a long metastyle is extended to the posterolabial. Furthermore, a cingulum is retained at the posterolingual and lingual side of the hypocone, and despite the broken protocone its presence is also evident at the anterolingual side of the tooth.

The only giraffid material from the lower fossiliferous horizon that can be attributed to this species is an almost complete right mandible and a part of a left mandible, collected from site K4. Most likely the two mandible specimens (Appendix 2) belong to the same individual. In the almost complete right mandible only part of the angle of the mandible and part of the anterior of the mandible corpus are missing (Fig. 16C). The condylar process and even the largest part of the coronoid process are also preserved. The corpus is very developed with a convex lower ridge. The length of the toothrow is 245 mm, while the length of the premolar row is 97.4 mm and the length of the molar row is 148.4 mm, respectively. Therefore, it is clear that the premolar row is considerably shorter than the molar one; the indices Pm/M and Pm/ PM are 65.63 and 39.76, respectively. The talonid in the three premolars is reduced. It is well defined in P_4, as it is clearly separated from the trigonid with a deep furrow (Fig. 16A, B). Conversely, in P_2 and P_3 this labial furrow is rather imperceptible, and the labial wall is flat (Fig. 16C). However, the separation between the talonid and the trigonid is still evident. Furthermore, P_3 and P_4 are molarised. The overall shape (occlusal view) of the simple P_2 is triangular, due to a reduced anterolabial region (Fig. 16A, B). The protoconid is very developed and is connected with the entoconid, the hypoconid an also with the parastylid. The weak metaconid is attached to the protoconid, expanding the cuspid lingually. The parastylid is strong and projects anterolingually. Moreover, it is separated from the protoconid with a wide and deep valley. The well developed entoconid and the long posterior flange of the hypoconid are parallel and extend lingually (Fig. 16A, B). The fourth valley (between the entoconid and the entostylid) is long but also narrow and shallow (Fig. 16B). Conversely, the

third valley (between the protoconid and the entoconid) is short but also wide and deep (Fig. 16B). As for the hypoconid it is well defined and strong. In the elongated P_3, the protoconid is very developed and is linked with the parastylid anteriorly and with the hypoconid and the entoconid at the posterior (Fig. 16A, B). The parastylid is strong and is connected with the well developed and elongated paraconid-metaconid, forming a continuous lingual wall, where the paraconid is not clearly defined from the metaconid. The metastylid is strong and extends posteriorly (Fig. 16A, B). The entoconid is very developed and relatively long, whilst the posterior flange of the hypoconid is developed but shorter than the entoconid. They are both parallel and oblique, inclined to the posterolingual of the tooth (occlusal view). Thus, the fourth valley found in between them is closed by the anterior wall of P_4. A well defined hypoconid occupies the labial side of the prosterior region.

Of special note are the morphological features of P_4 (Fig. 16A, B). The tooth is remarkably shorter than P_3 and M_1. Its length is 33.5 mm, while the length for P_3 and M_1 is respectively 38.2 mm and 44.4 mm. The index width/length for the three teeth is 0.95 for P4, 0.70 for P3 and 0.74 for M_1. Therefore, this indicates a quadrangular shape for P_4, in contrast to the rectangular P_3 and M_1. Another striking character of this tooth is the anomalous position of the entoconid, as well as of the entoconid ridge as a whole. Normally, in the premolars the entoconid is inclined towards the posterolingual of the tooth, found next to the entostylid. Instead, in the studied tooth the entoconid bends towards the anterolingual of the tooth, and more specifically it points towards the parastylid. Despite this, it is elongated and well developed. Except from this abnormality only minor changes have occurred to adjust the structure of the tooth to this distortion. The well developed and wide protoconid is connected with the parastylid through a strong anterior flange. It is also connected with the hypoconid and the distorted entoconid. At the anterolabial side of the tooth, a large and well developed protostylid is found next to the protoconid. The parastylid is strong but not prominent at all. It is connected with the well developed and elongated paraconid-metaconid, while the metastylid ridge is strong and long extending up to M_1. Thus, the three of them form a continuous lingual wall that closes entirely the lingual side of the tooth, and even covers the fourth valley and the endostylid. The lingual surface of the wall is flat and straight. The developed hypoconid is wide and projects labially. Its anteroposterior diameter though is reduced and generally the whole tooth looks compressed. The posterior flange of the hypoconid is long, well built and perpendicular to the long axis of the tooth.

In the three molars the axes of the lobes are slightly bent towards the posterolabial. The labial walls of the lobes form acute angles (Fig. 16A, B). The protoconid and the hypoconid are well developed. The anterior flange of the protoconid is longer than the posterior and is connected with the parastylid and consequently with the long and developed metaconid. The posterior flange is pointing towards the lingual connection point of the two lobes. Conversely, in the crescent of the hypoconid of the first two molars the posterior flange is longer and extends up to the lingual wall, next to the entostylid. The anterior flange in all three molars is short and oblique, bended anterolingually towards the edge of the posterior flange of the protoconid. The metaconid and the entoconid are wide and triangularly shaped in M_1 and M_2, while in M_3 they are narrower and elongated (especially the entoconid). The ribs and the stylids of the three molars are generally weak although, there are a few exceptions. The parastylid and the metastylid in M_1 and M_2 are consequently weak but clear, however, the parastylid and the metastylid in M_3 are strong and prominent and project lingually while the posterior flange of the entoconid is long and confines the short posterior flange of the hypoconid crescent. Furthermore, a deep furrow on the lingual wall of the metaconid separates the parastylid from the rib of the metaconid. The posterior flange of the hypoconid in the first two molars is long and extends up to the lingual wall of the teeth, confining the posterior flange of the entoconid and forming a prominent entostylid. Although the lingual cuspids of the molars are generally straight, the metaconid of the M_3 is clearly crescentic (Fig. 16A, B). The third lobe of M_3 is considerably smaller than the other two lobes. It is separated from the posterior flange of the entoconid and the second lobe in general by a slit. Moreover, its lingual wall is clearly not found at the same level with the other two lobes but is placed more externally. At the labial side of the lobe a crescent is formed. The posterior part of the crescent is more developed and wide, whereas at the anterior a narrow flange confines the posterior flange of the hypoconid. A thin ridge closes the lingual side of the lobe, whereas its anterior edge is covered by the posterior flange of the entoconid.

A large number of long and robust postcranial specimens (Appendices 3 – 13), attributed to this species, have been collected at Kerassia. Despite this, only one complete radius has been recovered (K1/Δ78) (Fig. 17 C, D), whereas portions of the proximal part of the ulna, as the beak of the olecranon and the trochlear incisure, have been preserved in two specimens. The radius is long (between 502.6-538.9 mm) and quite robust, while the upper part is slightly bent towards the lateral side of the bone. The overall shape of the two epiphyses as well as of the diaphysis is generally rectangular, as their transverse diameter is considerably longer than the anteroposterior one. The upper end of the bone is wider than the shaft. The anteroposterior

diameter of the lateral part of the epiphysis is shorter than the diameter of the medial part. Furthermore, the medial wall of the epiphysis is rounded. The medial trochlear cavity is fairly large and rounded, occupying almost half the area of the proximal articular surface. It is separated from the lateral trochlear cavity by the well developed ridge of the radial part of the trochlear incisure. The lateral trochlear cavity is narrow but deep and rather oblique. A low ridge separates the lateral trochlear cavity from the narrow and shallow condylar cavity. The lateral trochlear cavity is extended anteriorly as a prominent process, which is defined laterally by two furrows on the anterior wall of the epiphysis that coincide at the rim of the articular surface with the two ridges. The lateral wall of the epiphysis is also rounded, and the lateral tuberosity is developed. Moreover, at the posterolateral of the tuberosity a small furrow is evident; probably the imprint of a muscle. The radial tuberosity is also clear and strong. The beak of the olecranon is strong, long and extends more anteriorly. The lower end of the bone is also wider than the diaphysis (Fig. 17C, D). Its lateral part projects downwards and posteriorly as the well developed ulnar styloid process. Similarly, the strong but low radial styloid process is found at the medial part. The lateral and medial ridges of the two processes are strong and prominent, and are responsible for the widening of the lower end. However, the anteroposterior diameter of the epiphysis is also increased. Furthermore, the ulnar ridge is shorter than the radial one. The medial wall of the epiphysis is rounded. The medial articular surface or the articular surface of the scaphoideum is wide and rounded, while its posterior rim is straight and inclined to the posteromedial. Conversely, in the articular surface of the semilunare the anterior part is wide but it gets narrower towards the posterior, where the rim is concave. The two oblique crests that limit this surface have a similar length, and their edges at the posterior rim are found on the same level. Their posterior parts are parallel, while the anterior part of the medial crest is bended medially. The transverse crest at the posterior of the epiphysis is very developed and prominent. Hence, the articular surface of the semilunare that continues on the crest is also developed. The third articular surface of the ulnare is relatively wide and its long axis forms a low angle with the transverse diameter of the bone. At the anterior surface of the epiphysis the deep, V-shaped groove of the extensor carpi radialis muscle is evident (Fig. 17C). The two ridges that limit the groove are acute in section, prominent and very distinct. Furthermore, the lateral ridge is much more developed and wide than the medial one. The groove is located above the medial part of the semilunare articular surface. A small and narrow but rather deep groove for the extensor digitorum communis muscle is found at the lateral part of the anterior surface, right above the lateral crest of the semilunare articular surface. Its lateral ridge is strong and as the other two ridges, it is also acute-shaped though much lower. The opening of the groove is directed anteriorly. A third

shallow groove for the abductor digiti I longus muscle is also clear at the anteromedial side of the bone, limited by the medial anterior ridge and the prominent radial styloid process. The three grooves fade out above the lower one third of the bone. A slightly concave and weak groove which probably could be referred to the flexor carpi radialis muscle is also found at the medial face of the bone.

A broken proximal part, a distal part and a complete metacarpal (Fig. 18A) are referred to this species. However, the proximal part of the latter specimen is fractured and distorted; probably due to animal trampling or postburial compaction. Thus, the dimensions of the proximal part should be considered misleading as this distortion caused a considerable widening and altered the shape of certain features. Its length is 398.2 mm, while the robusticity index due to this distortion cannot be estimated. Still, the anteromedial tuberosity is clear and developed and the ridge between the two articular surfaces of the capitatotrapezoid and the unciform is curved and more specifically it resembles an s-shape. At the posterior of the bone the two crests are strong but short and fade out at a considerable distance from the lower epiphysis. Another striking feature in the two specimens that have preserved the lower end of the bone, except from the absence of the crests at the posterior of the diaphysis, is that the transverse diameter of the diaphysis is significantly more narrow than that of the epiphysis. Furthermore, the anteroposterior diameter of the epiphysis compared to the transverse one is relatively short. Also, the lateral and medial articular eminences of the trochlea are clearly protruding laterally and medially respectively.

A long forelimb first digit (Fig. 19F) has strong and long sesamoide tuberosities, while the abaxial tuberosity presents a well developed bulge on its external side. The sagittal groove on the proximal articular surface is deep and wide. The interdigital part of the diaphysis is high but obviously it gets tapered gradually towards the abaxial side. A similar feature can be observed on the prominent external eminence of the lower articular surface.

One complete, long and very robust tibia was collected from site K1 (Fig. 17E-G). The upper part of the bone is very developed, especially along its anteroposterior diameter. At the anterior a very strong tibial crest bends laterally, forming a deep tibial sulcus with the body of the diaphysis (Fig. 17E, F). A well developed and rounded tibial tuberosity bulges out at the top of the crest. The tibial sulcus culminates at the epiphysis in a deep, V-shaped valley (groove). The posterior edge of the strong medial tuberosity projects posteriorly. Similarly, the well developed lateral tuberosity presents a prominent posterior eminence, in addition to

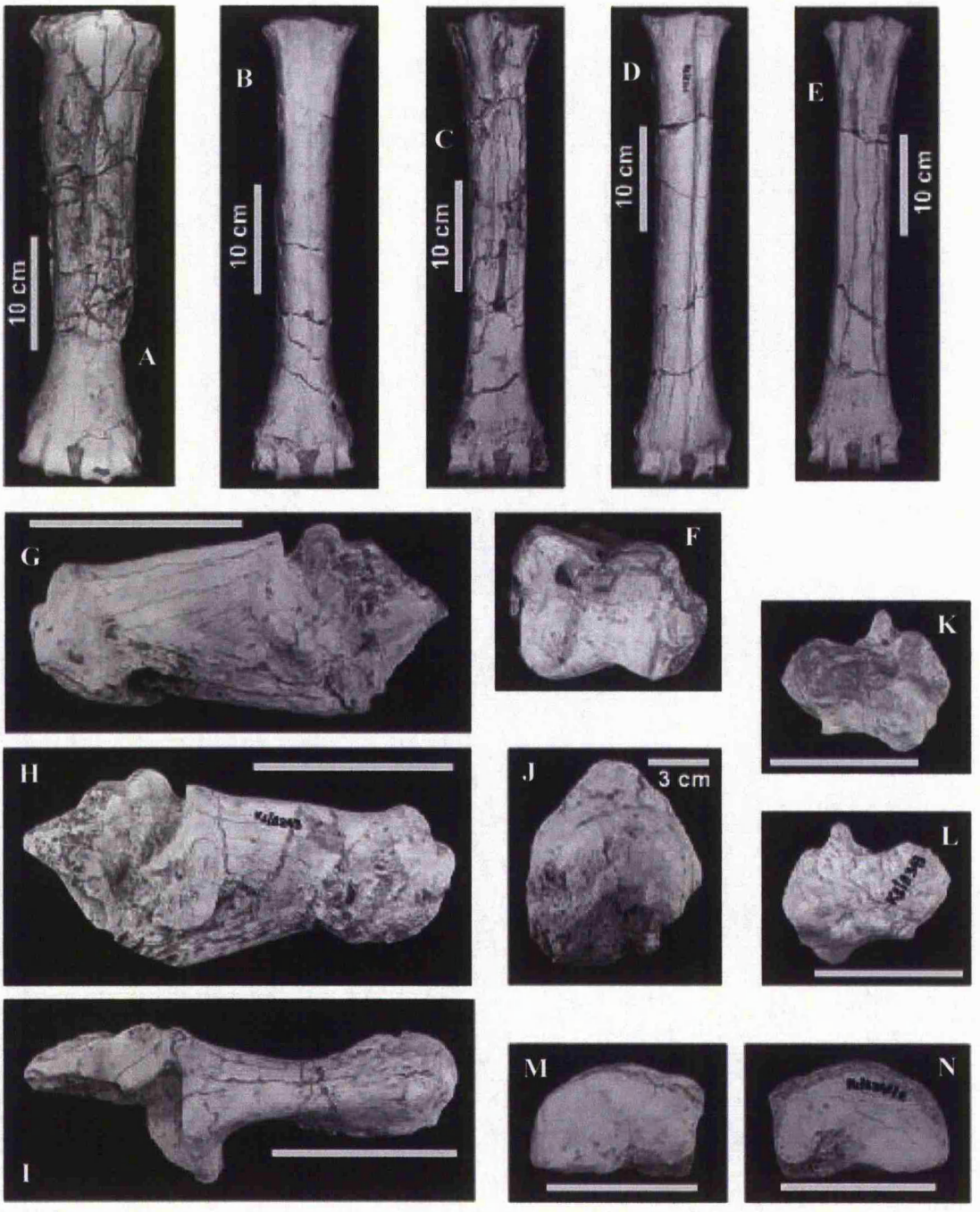

Figure 18: A. *S. major*, left Mc_{III+IV}, K1/Δ244, anterior view. **B.** *S. major*, right Mt_{III+IV}, K1/Δ247/1, anterior view. **C.** *S. major*, right Mt_{III+IV}, K1/Δ247/1, posterior view. **D.** *S. major*, left Mt_{III+IV}, K1/Δ344, anterior view. **E.** *S. major*, left Mt_{III+IV}, K1/Δ344, posterior view. **F.** *S. major*, left tibia, K1/Δ341/1, distal view (DAPd = 80mm). **G.** *S. major*, left calcaneous, Ke 99/47, medial view (scale bar: 10cm). **H.** *S. major*, right calcaneous, K1/Δ243, medial view (scale bar: 10cm). **I.** *S. major*, right calcaneous, K1/Δ243, dorsal view (scale bar: 10cm). **J.** *S. major*, right calcaneous, K1/Δ243, tuber calcanei. **K.** *S. major*, left malleolar, K1/Δ343, medial view (scale bar: 5cm). **L.** *S. major*, left malleolar, K1/Δ343, lateral view (scale bar: 5cm). **M.** *S. major*, left cuneiform, K1/Δ341/2, proximal view (scale bar: 5cm). **N.** *S. major*, left cuneiform, K1/Δ341/2, distal view (scale bar: 5cm)

the protruding lateral edge (Fig. 17F, G). These two posterior projections form a deep and relatively narrow valley (Fig. 17G) which corresponds to the indentation of the popliteus. Also, these projections are responsible for the increased length of the two articular surfaces. The overall shape of the lower epiphysis is quadrangular (Fig. 18F), with a straight medial and a relatively straight lateral wall. The medial malleolus is triangular, thin and rather wide, with a slanting posterior edge; the remaining part of the medial ridge of the cochlea is concave. The medial tuberosity at the lower part of the medial malleolus is developed but relatively short (Fig. 18F). At the posterior of the tuberosity the groove of the flexor digitorum longus muscle is evident. The groove is deep and narrow, while its position is medial and the opening of the groove is also medially oriented. The imprint of the muscle is short and is placed at the medial side of the posteromedial crest of the diaphysis. The articular surface of the malleolus is divided into two parts; a wide and well developed posterior part that continues into an anterior narrow part (Fig. 18F). The latter is limited due to the great development of the obtuse and wide fibular furrow. The length as well as the width of the two cochlear grooves is the same. Between the two cochleas the intercochlear crest is wide but low. Its anterior eminent edge is strong and triangular with a very broad base; (obviously its lateral part is much broader). A shallow and narrow concavity is clear at the anterior of this eminence, limited though only to the epiphysis. The medial part of the posterior edge is very developed and prominent, occupying the posteromesial side of the medial cochlea. The lateral part continues to the posterior as a deep but narrow furrow, which however is short and fades out at the base of the diaphysis (Fig. 17G).

A very strong malleolus was also collected (Fig. 18K, L). It is clear that the anterior part of the bone is remarkably shorter than the posterior. As a result, the anterior part of the articular surface with the tibia is shorter than the posterior. Also, the posterior part is wider than the anterior part. The fibular process is well developed, wide and high and a very prominent eminence at the anterior of the articular surface with the calcaneus increases the height of the bone to 45.4 mm (Fig. 18K, L). The upper part of the posterolateral side is very developed. A strong anterolateral tubercle is found at the lower part of the lateral surface of the bone. Another distinct feature of the articular surface with the calcaneus, except from the prominent eminence, is its wide anterior part. On the internal face of the bone the concavity of the astragalus is well marked and deep.

One complete and one slightly broken astragalus were collected (Fig. 19B,E). The lateral crest of the proximal trochlea is strong and thick, while its posterior edge also remains thick (Fig.

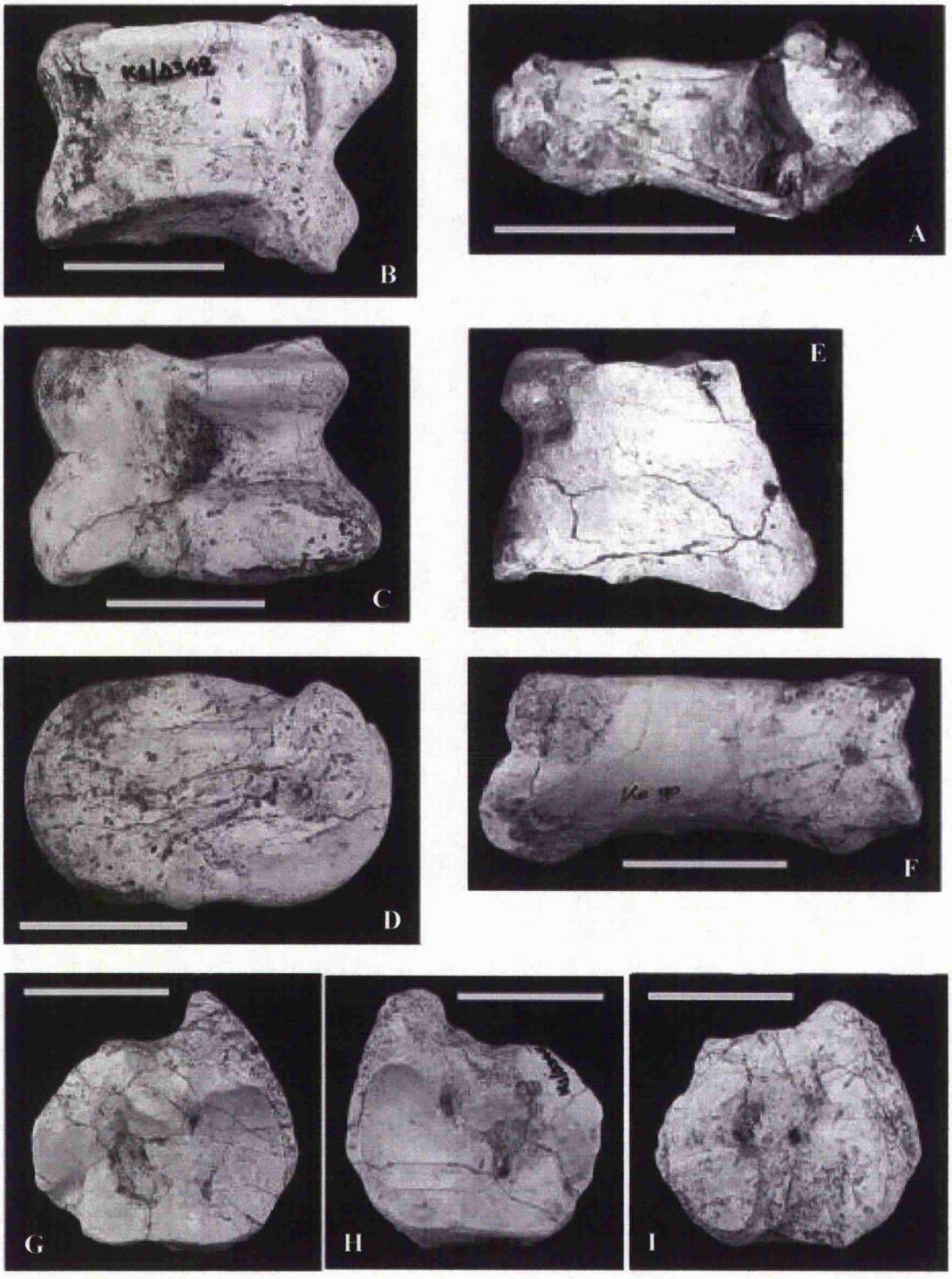

Figure 19: A. *S. major*, left calcaneous, Ke 99/46, medial view (scale bar: 10cm). **B.** *S. major*, left astragalus, K1/Δ342, posterior view (scale bar: 5cm). **C.** *S. major*, left astragalus, K1/Δ342, anterior view (scale bar: 5cm). **D.** *S. major,* left astragalus, K1/Δ342, medial view (scale bar: 5cm). **E.** *S. major*, left astragalus, Ke 99/49, posterior view (medial length 92.5 mm). **F.** *S. major*, phalanx I, Ke 90, anterior view (scale bar: 5cm). **G.** *S. major*, right scaphocuboideum, K1/Δ247/2, proximal view (scale bar: 5cm). **H.** *S. major*, left scaphocuboideum, K1/Δ346, proximal view (scale bar: 5cm). **I.** *S. major* left scaphocuboideum, K1/Δ346, distal view (scale bar: 5cm).

19C). Conversely, the medial crest is thin and its posterior edge gradually gets thicker due to a medially protruding rim (Fig. 19C). The lateral crest, although higher than the medial one, is relatively low. The proximal part of the intertrochlear groove is shallow and due to the low lateral crest its lateral side is inclined at a low angle. At the base of the lateral trochlear edge a triangular cavity is clear. The cavity continues laterally as a narrow furrow that separates the proximal trochlea from the plantar one. The surface of the plantar trochlea is fairly concave. The lateral crest is straight whilst the medial one is curved (Fig. 19B). Thus, its distal part is wider than the proximal one. The proximal edge of the medial crest is trained on the proximal intertrochlear groove. At the lateral margin of the distal part a small rounded depression is evident (Fig. 19B, E), which is most probably formed by the developed posterior edge of the lateral cochlea of the scaphocuboideum. The anteroposterior diameter of both the lateral and medial sides is increased. On the proximal part of the lateral side the furrow for the malleolus is deep. It is closed posteriorly by a low ridge that separates the furrow from a small crescentic surface, which occupies the posterolateral side of the lateral crest of the proximal trochlea. The posterolateral tubercle is strong. The furrow continues distally as the proximal articular surface of the calcaneus. A thin prominent ridge marks its lower margin. On the distal part of the lateral side, the ellipsoid facet of the distal articular surface of the calcaneus is clear. Between the ridge and the ellipsoid facet a shallow and relatively narrow concavity is clear which is open anterolaterally right above the ellipsoid facet. The crests of the distal trochlea are strong and the groove between them is relatively deep and narrow. At the anterior, the two medial crests are separated by a very shallow furrow, whereas the edges of the two lateral ones are separated by a rather deep but relatively narrow furrow. The anterior edge of the proximal medial trochlea projects slightly anteriorly as well as anteromedially (Fig. 19B, D). The anterior cavity is rounded and deep.

Five specimens of calcaneus are referred to this species. The dorsal crest is parallel with the long axis of the bone, while the plantar one is fairly oblique (Fig. 18G, H and 19A). Consequently, the latter feature is responsible for the increased height (proportionally to the length) at the base of the body of the bone as well as for the increased maximum height. Thus, the overall shape of the body of the bone is triangular. The dorsal crest is very developed, and particularly its anterior portion. The top of the beak of the crest at the anterior and the top of the articular surface of the malleolus are found at the same level (Fig. 18G, H). At the posterior of the crest, the posterodorsal tubercle is strong and high. The shape of the slightly asymmetrical tuber calcanei is triangular (Fig. 18J). The index "tuber calcanei width / tuber calcanei height" ranges between 0.79-0.89 indicating a relatively high tuber calcanei. The

lateral tubercle of the tuber is very strong and more developed than the medial one. At its posterior, the groove for the flexor digitorum superficialis muscle is deep and relatively narrow. The sustentaculum tali is thin and a well formed ridge at its side extends medially (Fig. 18G-I). The articular surface for the plantar trochlea of the astragalus is clearly concave (across the dorso-plantar axis). Across its base, the fairly deep furrow of the sinus tali is evident. The elongated articular surface for the scaphocuboideum at the anterior of the bone is concave, slightly curved, and presents a slight torsion. At its posterior the ridge formed with the sinus tali is low, whereas the anterior articular surface with the astragalus is almost flat (straight) and considerably shorter than the surface for the scaphocuboideum. On the dorsal side the posterior part of the articular surface for the malleolus is very developed and wide (Fig. 18I). It is also oblique and extends medially. The anterior part of this surface is also developed and distinctively wide with a small and rather deep concavity found on its medial side (Fig. 18I).

The medial concavities (cochleas) on the proximal side of the two complete and robust specimens of scaphocuboideum are narrower than the lateral concavities (Fig. 19G, H). The culminant plantar peak of the medial concavity is relatively low. Similarly, the plantar peak of the lateral concavity is wide and strong. The valley between the two peaks, which occupies the plantar part of the ridge of the two concavities, is fairly narrow and is located higher on the bone. The ridge between the two concavities is low and dorsally ends to a triangular acute eminence. The plantar edge of the articular surface with the calcaneus stops at the lateral side of the peak of the lateral concavity. As a result, the furrow on the plantar side between this edge and the vertical medial crest is considerably wide. Furthermore, the crest is strong and quite prominent (Fig. 19G, H). The well developed lateral tuberosity is found more centrally at the distal part of the plantar side. The slanting groove of the peroneus longus muscle across the lateral side of the bone is evident. The groove continues on the distal side of the bone where it separates the anterior articular surface of the metatarse from an elongated tuberosity (Fig. 19I). The tuberosity represents the posterior metatarse facet that is either absent or has not been formed yet. In specimen K1/Δ346 the groove is fairly deep. Another slanting groove for the tibialis cranialis muscle is found at the medial side of the bone. The groove is wide and shallow and has a very developed posterior ridge. At the internal side of the kidney shaped, anterior articular surface an indentation is present, which in specimen K1/Δ346 is deep and wide.

In the three recovered intermediolateral cuneiform specimens, the dorsal part of the lateral side of the articular surface for the scaphocuboideum bends laterally and forms a small elongated lateral facet (Fig. 18M). At the posterior of their medial wall a strong tuberosity is present, and in front of it a small indentation is also clear. Its plantar end is developed and forms a tubercle which in specimen K1/Δ247/3 is very developed and projects laterally. The indentation and the tuberosity are the places where the tibialis cranialis muscle was attached.

Two long and robust metatarsals were collected (Fig.18 B-E). The diaphysis, compared with the wide proximal and distal epiphysis, as well as with the length of the bone is relatively narrow; the values of the robusticity index for the two bones are respectively 11.95 and 12. The plantar side of the proximal epiphysis presents a few distinctive features (Fig. 32A). The medial tubercle is very developed and long, and extends plantarly. It is significantly larger and more prominent than the lateral tubercle; the two tubercles are respectively the remnants of the fifth and second metatarsals. As a result, the ellipsoid articular surface for the medial cuneiform is also enlarged. On the medial side, a furrow (valley) separates the tubercle from the rounded articular surface for the lateral cuneiform. A few centimetres down in this furrow, a small protuberance is obvious, which probably corresponds to the lost first metatarsal. Between the two tubercles a smaller tuberosity is clear, located though not in the middle but closer to the medial tubercle. It is separated from the medial tubercle by a shallow furrow and from the lateral tubercle by a fairly deep furrow. Its upper part ends to an eminent process. The well defined and strong lateral tubercle is also separated laterally from the articular surface for the scaphocuboideum by a deep and narrow furrow for the extensor digitorum lateralis muscle that continues for a few centimetres on the diaphysis and fades out. Its upper surface is not found at the same level as the rest of the articular surface, but fairly lower. Moreover, it is oblique and is directed toward the plantar-lateral of the bone. The lateral part of the epiphysis is extended laterally so that the side of the articular surface for the scaphocuboideum projects more laterally than the lateral tubercle. The dorsal sulcus is shallow and the medial crest of the diaphysis is not very developed. On the plantar side, the sulcus is also relatively shallow and U-shaped. The medial and lateral crests are not very developed, and just as in the metacarpals, they fade out high on the diaphysis. The anteroposterior diameter of the lower epiphysis is relatively small compared to the transverse diameter, while the keels of the trochleas are developed and high.

Discussion. A large and very robust species is represented in the studied material. The dimensions of the cranial as well as of the postcranial specimens are referable to two different

Late Miocene large giraffids: *Helladotherium* and *Samotherium*. In the past, the metrical similarities of their skeletal elements confused giraffid workers who provided erroneous determinations. Numerous morphological features though, suggest that this material belongs to a member of the *Samotherium* group. During the Late Miocene *Samotherium* expanded from China to eastern Asia, Anatolia and the Balkan Peninsula. Its presence was also reported in Africa (Churcher 1970, *S. africanum*), though Geraads (1974) and Hamilton (1978) considered the specimens insufficient to establish the validity of the species. In the area of the eastern Mediterranean three species of *Samotherium* have been described to date; *S. boissieri* (Major 1888), *S. neumayri* (Rodler and Weithofer 1890) and *S. major* (Bohlin 1926). The latter is considerably larger than the other two species, and its dimensions correspond to the dimensions of the other large *Samotherium* form, the Chinese *S. sinense* (Schlosser 1903). Originally, *S. major* was included in the species *S. boissieri*. The first excavations that Forsyth Major conducted on Samos Island (Greece) at the end of the 19th century took place in many different localities. The stratigraphy was not considered and the collected *Samotherium* material was attributed to one species, *S. boissieri* (Major 1888). However, in some museums' collections the material came from known localities and reflects this difference. Bohlin (1926) was the first to notice the metrical and morphological differences in the material of *Samotherium* from Samos that was stored in some European museums. He considered that the larger specimens (which in some cases were significantly larger) belonged to a new variety, *S. boissieri* var. *major* (Bohlin 1926). In 1954 Senyurek elevated the variety to the species level after the discovery of new material in Taskinpasa (Turkey). He stated that the new species could be distinguished from *S. boissieri* from the larger dimensions of the skeletal elements, the elongation of the skull and the considerably more posterior position of the orbit (Senyurek 1954). Geraads (1974, 1978) stated that the differences between *S. boissieri* and *S. major* were not so pronounced to justify the existence of two different species, and considered that the larger specimens belong to the subspecies *S. boissieri major*. Later, studying new material though from Kemiklitepe (Turkey) and considering new data about the stratigraphy of the fossiliferous localities (Solounias 1981) and the bonebeds of Samos Geraads (1994) concluded that *S. major* was indeed a different species from *S. boissieri*. In Samos the material attributed to the two species was collected from different stratigraphic levels and it is now clear that the two species never coexisted. Radiometric dating (Weidmann *et al.* 1984; Swisher III 1996) and magnetostratigraphic data (Sen and Valet 1986; Kostopoulos *et al.* 2003) plus new excavations that took place in the mid nineties (Koufos *et al.* 1997) verified this hypothesis. The derived characters that *S. major* (found in the upper fossiliferous beds or "Main Bone Beds") presents, indicate that it clearly evolved from the ancestral *S. boissieri*

(which was found in the lower beds of the sequence or "Old Mill Beds") (Geraads 1994). Solounias *et al.* (2000) suggested that feeding adaptations were probably responsible for this speciation. Bohlin (1926) suggested that *S. boissieri* and *S. neumayri* were only races of the same form. Though, differences in the proportions of their skeletal elements and in the morphology of the skull and the premolars support the validity of the two species (Geraads, 1974, Hamilton 1978). The two larger representatives of *Samotherium*, *S. major* and *S. sinense* are also two distinct species. The postcranial elements of *S. sinense* are generally longer than *S. major* (Geraads 1994), while the upper and lower toothrows are evidently longer in *S. major*.

The length of the deciduous premolars row of the only maxillar or skull part from Kerassia is 90.2 mm. This value is within the range of the deciduous premolar row of *S. major* from Samos, which is between 82-94 mm (Bohlin 1926). It is longer than the 82.3-87.7 mm of *S. boissieri* form Samos (NHML) but conversely it is shorter than the range of 96-102 mm of Bohlin's *S. sp I* from China (1926) and significantly shorter than the 108 mm of *H. duvernoyi* from Samos (Bohlin 1926). The teeth of this young calf are of course within the range of *S. major*; they are larger than those of *S. boissieri*, but smaller than those of *S. neumayri*, *S. sp I*, *S. sinense* and *H. duvernoyi* (Fig. 6). The curved posterior flange of the paracone in dM^3 and dM^4 and its labially directed edge is a feature of *Samotherium*; unlike the straight flange found in *Helladotherium* (Geraads 1974). The elongated and low metastyle of dM^2 is also evident in the dM^2 of *S. neumayri* (Rodler and Weithofer 1890, fig 1, pl. IV) and *S. sp I* (Bohlin 1926, fig. 4, Pl. VI), as well as in the three juvenile maxilla specimens of *S. boissieri* from Samos stored in the NHML (M4226, M4228, M4229) but is not present in *H. duvernoyi* (Bohlin 1926, textfig. 225). Similarly, the fold (bifurcation) on the external face of the anterior flange of the hypocone of dM^3 and dM^4 is also found in *S. neumayri* (Rodler and Weithofer 1890, fig 1, pl. IV) and *S. sp I* (Bohlin 1926, fig. 4, Pl. VI) but again it is absent in *H. duvernoyi* (Bohlin 1926, text fig. 227). In the specimen from Kerassia though, this fold in dM^4 is rather imperceptible. Thus, these two morphological features are probably diagnostic for the genus *Samotherium*. This fold (bifurcation) is not present in the dM^4 of the specimens M4228 and M4229 of *S. boissieri* from Samos, but it is clear in the two dM^4 of specimen M4226. In all specimens though, the reduced posterior flange of the protocone of the fairly worn dM^3 is connected with the anterior flange of the hypocone so that the presence of this fold in dM^3 can not be ruled out. Another feature that the four *Samotherium* species share is the strong and inclined paracone rib in dM^2 and dM^3. However, the "eperon hypoconal" in dM^3 and dM^4 only exists in the specimen from Kerassia, whereas the labially projected

metastyle of dM^3 and dM^4 can also be identified in the Maragha sample as well as in *S. boissieri*. Also, the islet at the posterior of dM^2 is only seen in *S. neumayri*. The metacone at the labial crescent of dM^2 in *S. boissieri* is strong and well defined, while, at the lingual crescent the protocone is clearly separated from the hypocone by a shallow furrow and is limited anteriorly by a deeper furrow which is followed by a well developed protoconule. None of the above characters was observed in the studied specimen. Nevertheless, the anterolingual furrow and the developed protoconule are evident in *S. sp I*. A weak and low entostyle is clear in the dM^3 of *S. boissieri* and *S. sp. I*, whereas in the studied specimen a low cingulum occupies the base of the lingual side of the tooth and closes the valley between the two lobes.

The dimensions of the two mandible specimens from Kerassia indicate the existence of a very large individual. The length of the complete toothrow is longer than the 223 mm of the *S. major* mandible from Vathilakos (VAT 3, Greece) (Geraads 1974, 1978) and the 213 mm of the mandible from Taskinpasa (Senyurek 1954). Bohlin (1926) also reports that the range of the toothrow length for *S. major* from Samos is 198- 217 mm, however, he mentions the existence of another larger specimen with a toothrow length of approximately 250 mm. Thereby, if this reference is considered valid, the studied mandible is within the range of *S. major*. The range of the toothrow length is between 178.11-188.7 mm for *S. boissieri* from Samos stored in NHML, 195 mm for *S. neumayri* from Maragha (de Mecquenem 1924), 190 mm (Schlosser 1903) and 198 mm (Bohlin 1926) for *S. sinense* from China, 240 mm for *H. duvernoyi* from Nikiti (Nikiti 2, Greece) (Kostopoulos *et al.* 1996) and 262 mm for *H. duvernoyi* from Maragha (Kostopoulos *et al.* 1996). The two indices P/M and P/PM are respectively: 66.2 and 42.2 for *S. major* from Vathylakkos, 55.5 and 35.7 for *S. major* from Taskinpasa, 53.8-63.2 and 35.9-38.7 for *S. major* from Samos, 55.2-64.4 and 35.2-39.5 for S. boissieri from Samos (NHML), 59.2 and 37.9 for *S. neumayri* from Maragha, 67.8 and 41.1 for Schlosser's (1903) and 62.3 and 38.4 for Bohlin's (1926) *S. sinense* specimen from China, 61.7 and 38.3 for *H. duvernoyi* from Nikiti (Nikiti 2, Greece) and finally 64.6 and 39.5 for *H. duvernoyi* from Maragha. The studied toothrow is considerably longer than *S. boissieri* and *S. neumayri* and it is also longer than the other large *Samotherium*, *S. sinense* (Fig. 8). Its length is not only within the range of *S. major* but it is also within the range of *H. duvernoyi*. The two indices of the studied specimen are also found within the range of *S. major*, but they do not seem to differentiate remarkably from the latter species. However, they tend to be lower than in *S. boissieri* and *S. major* indicating a relatively more reduced premolar row for these two species. Despite the accordance of the toothrow length with *H. duvernoyi*, the

morphology of the teeth and the mandible clearly coincides with *Samotherium*. The molarisation of P_3 is such a morphological feature (Fig. 16). According to Geraads (1974, 1978, 1986) the P_3 is never molarised in *H. duvernoyi*, as well as in all the other members of the Sivatheriinae. Conversely, a molarised P_3 is very often represented in the members of the Palaeotraginae, including *Samotherium* (Geraads 1974). However, in *S. major* P_3 is always molarised (Geraads 1994), and resembles P_4 strongly. The metaconid in the two premolars is never connected with the protoconid, but forms an elongated and continuous lingual wall with the paraconid, the parastylid and the metastylid. Kostopoulos *et al.* (1996) considered wrongly that the P_3 in the mandible of *H. duvernoyi* from Nikiti was molarised. In their text figure 7 it is obvious that the metaconid and the paraconid are connected with the protoconid. Moreover, the lingual wall of the tooth is not continuous as a valley clearly separates the metaconid from the paraconid. The fairly small third lobe of the M_3 is another feature of the genus *Samotherium* (Geraads 1974). In *H. duvernoyi* the third lobe is considerably larger. Its lingual wall is found at the same level with the lingual wall of the other two lobes. In *Samotherium* the lingual wall of the third lobe is located more externally. The ridge of the lingual wall in *S. boissieri* extends towards the posterior flange of the entoconid, and in an advanced stage of wear it gets connected with it and with the posterior flange of the hypoconid. In *S. major* this ridge extends anteriorly and between the posterior flanges of the entoconid and the hypoconid. Lingually its anterior part is covered by the posterior flange of the entoconid. In the studied specimen the entostylid in M_1 and M_2 as in every *Samotherium* projects lingually, while in *H. duvernoyi* is not present.

The reduction index for the two premolars of the studied mandible is 0.31 for P_3 and 0.27 for P_4. Similarly, the index for the *S. boissieri* from Samos (NHML) ranges respectively between 0.28-0.34 and 0.18-0.29. The posterior region of P_3 and P_4 in *Samotherium* is quite reduced, and generally, the posterior region of P_4 is more reduced than P3. In *Palaeotragus* and *Helladotherium* the posterior region is relatively more developed. The pattern of molarisation presented in the premolars of *Samotherium* is based on the development of the trigonid followed by a reduction of the talonid that tends to form a uni-lobe tooth (Hamilton 1978). The ratio of the width against the length for P_3 for *S. major* from Vathilakos and Taskinpasa is respectively 0.64 and 0.67, and similarly the values for P_4 are 0.82 and 0.73. The same ratios for *S. boissieri* from Samos are respectively 0.58-0.68 and 0.62-0.74, for Schlosser's (1903) *S. sinense* specimen from China are 0.63 and 0.66, whilst for *H. duvernoyi* the values are 0.75 and 0.81 for Wagner's specimen from Pikermi, 0.81 and 0.87 for the specimen from Nikiti (Nikiti 2) and equally 0.72 and 0.74 for the specimen from Maragha. Except from the extreme

ratio of P_4 of the studied specimen (0.95), the rest indicate that the premolars of *H. duvernoyi* are wider than the premolars of the three *Samotherium* species (Fig. 9). Similarly, the premolars of *S. major* compared with those of *S, boissieri* and *S. sinense* are clearly wider (Fig. 9). Furthermore, the P_4 of *S. major* presents a tendency of shortening. The dimensions of the toothrows of *S. major*, as stated above, are significantly larger and the length of the first two premolars is clearly longer than in *S. boissieri*, *S. neumayri* and *S. sinense*. Therefore, a proportional length for the P_4 would be expected. Instead, the P_4 is either shorter (as in the mandibles from Vathilakos and Taskinpasa) than the P_4 of the three other *Samotherium* species, or as in the larger specimen from Kerassia shorter than its P_3. The two ratios LP_4/LP_3 and LP_3/LP_2 (Appendix 2) indicate the relative elongation / shortening of the three premolars. It is evident that the values for the specimens from Vathilakos and Taskinpasa are lower compared to the other species. Hence, their P_3 and P_4 are relatively shorter. Kerassia's specimen though presents an even lower LP_4/LP_3 indicating a much shortened P_4 and a much higher LP_3/LP_2 for the elongated P_3.

The extreme and fairly abnormal shortening of the studied P_4 along with the distortion of its morphological structure, possibly indicate a pathological cause. The tooth is significantly compressed anteroposteriorly. The anomalous position of the entostylid and the wide and fairly short hypoconid clearly demonstrate this compression. In the specimen from Vathilakos as well as in other *Samotherium* species the entostylid is oblique, pointing towards the posterolingual side of the tooth, and the hypoconid is narrow. Also, the anomalous position of the entoconid evinces that this compression caused the abnormal development of the tooth which happened during the early stages of its eruption. In ruminants the P_4 erupts after the P_3 (Getty 1975). In this case the eruption of the tooth was probably further delayed, giving the opportunity to the P_3 to develop freely and elongate. When the eruption of P_4 started the space between P_3 and M_1 was already considerably confined, restraining the even development of the tooth. Thus, in order to fit in the existing gap the tooth was distorted and shortened. A similar condition was observed in the type species specimen of *S. boissieri* from Samos (NHML, specimen M 4215). The values of LP_3/LP_2 and LP_4/LP_3 for the premolars of the right mandible are respectively 1.32 and 0.94, indicating a similar shortening of P_4 and elongation of P_3. Unfortunately, the mandible is still attached to the skull, so the observation of the occlusal surface and of the morphology of the tooth is not possible. Another notable feature of the studied P_4 is the strong anterolabial protostylid. The premolars of *Samotherium* do not usually present stylids. Except from Kerassia's specimen, in a mandible of *S. boissieri* from Samos (NHML, specimen M 4235) a strong posterolabial stylid is present in all the three

premolars. The presence of this stylid increases significantly the width of the first two premolars.

The dimensions of the long and robust skeletal elements are within the range of *S. major*. Obviously, these elements are longer and more massive than those of *S. boissieri* and most of them are longer than those of *S. neumayri*. Most of them though are shorter than those of *S. sinense*. The length of some elements coincides with the range of *H. duvernoyi* elements; however, the latter are clearly more robust.

The rounded medial and lateral walls of the proximal epiphysis and the arrangement of the articular surfaces of the distal epiphysis of the radius in the studied specimens evidence the presence of *Samotherium* (Geraads 1974). They are longer than *S. boissieri*, and shorter than *S. sinense* and *H. duvernoyi*, while they are within the range of *S. major* and *S. neumayri* (K1/Δ78) or relatively shorter (K1/Δ90) (Fig. 20). Nevertheless, the anteroposterior diameter of their proximal and distal epiphyses (Fig. 21) seems to be larger than *S. neumayri* and even *S. sinence*. At the proximal epiphysis the anterior rim of the lateral trochlear cavity is less prominent in *S. boissieri*, whereas it is more developed and confined by deeper furrows in *S. sinense* (Bohlin 1926, text figure 78). Conversely, the anterior wall of the epiphysis in *H. duvernoyi* is straight. The position and the shape of the muscle grooves and their ridges at the anterior of the distal epiphysis is another distinctive feature. In *Samotherium* the ridges are high and acute shaped, while in *Helladotherium* they are low and rounded with shallow grooves between them. In the studied specimens the ridges are very developed and especially the lateral ridge of the deep groove of the extensor carpi radialis muscle. In *S. boissieri* this ridge is not considerably higher than the medial one and the muscle groove is shallow. Although the lateral ridge is very developed in *S. sinense* (Bohlin 1926, text figure 80), the medial one is low and the muscle groove is also shallow. The groove of the extensor digitorum communis muscle is deep in *S. sinense* as in Kerassia's specimens but it is relatively shallow in *S. boissieri*. In *H. duvernoyi* the groove is shallow and its opening is oriented more laterally. The transverse crest at the posterior of the epiphysis is more developed in *S. sinense* than in *S. boissieri* and Kerassia specimens, and it is very low in *H. duvernoyi*. The two crests of the semilunare surface in *Samotherium* have a similar length, while in *Helladotherium* the lateral is shorter than the medial one and also they are both more oblique (Geraads, 1974).

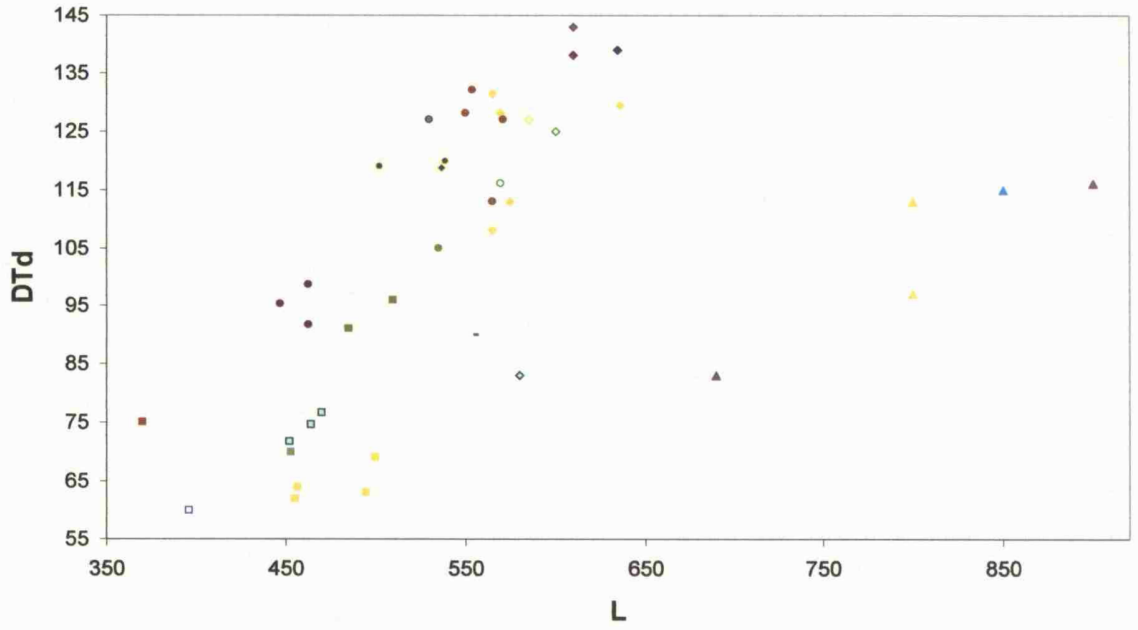

Figure 20: Plot of length vs distal transverse diameter of the radius (measurements in mm). The legend for the symbols is presented in Figure 7.

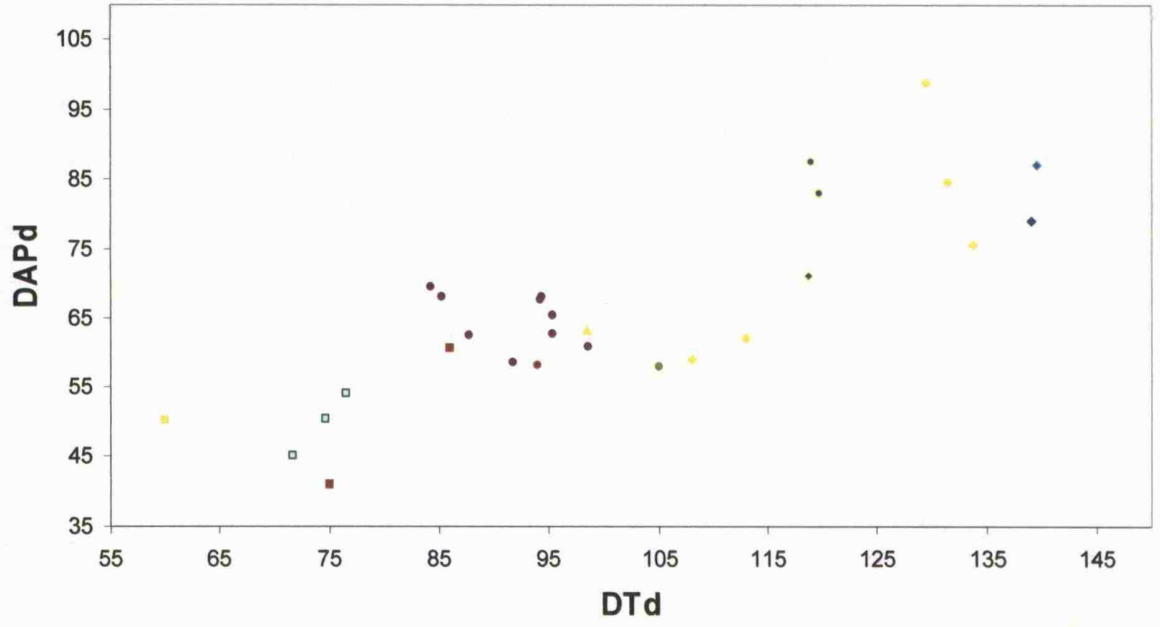

Figure 21: Plot of distal transverse diameter vs distal anteroposterior diameter of the radius (measurements in mm). The legend for the symbols is presented in Figure 7.

The range of the length of the metacarpal is 402-419 mm for *S. major* from Salonica (Greece) (Geraads 1974) and 408-421 mm for *S. major* from Kemiklitepe (Geraads 1994), while the length of a specimen from Samos (P.10 1963), stored in the collections of AMPG that most likely belongs to *S. major*, is 386 mm. Similarly, the range for *S. boissieri* from Samos (NHML) is 327.8-358.7 mm, for *S. neumayri* from Maragha is 378-390 mm (Geraads 1974), for *S. sinense* from China is 425-466 mm (Bohlin 1926), for *H. duvernoyi* from Pikermi is 400-427 (Geraads 1974; Melentis 1974, 1969; author's measurements NHML) and for *H. duvernoyi* from Nikiti 1 is 444.5 mm (Kostopoulos *et al.* 1996). The length of the only complete specimen from K1 is within the range of *S. major* (Fig. 11). It is clearly longer than *S. boissieri*, slightly longer than *S. neumayri*, clearly shorter than *S. sinense* and slightly shorter than *H. duvernoyi*. However, the distinction from *H. duvernoyi* is obvious. The two crests at the palmar side of the bone are limited to the diaphysis as in *Samotherium*, while in *Helladotherium* the crests are retained up to the lower epiphysis (Geraads 1974). The widened lower epiphysis with the relatively shortened anteroposterior diameter and the evidently narrow diaphysis is another feature of *Samotherium* (Fig. 22).

The length of the studied tibia from Kerassia is 517.5 mm. It is within the range of *S. major* from Samos and Kemiklitepe; 510-550 mm (Geraads 1994). Whilst, it is longer than *S. boissieri*, *S. neumayri* and *S. sinense*, and shorter than *H. duvernoyi* and *B. attica* (Fig.23). The distinction between *Samotherium* and *Bohlinia* is very clear and due to the great length and the gracility of the tibia of the latter. The well developed tibial crest with the strong tibial tuberosity and the deep and wide tibial sulcus indicate a *Samotherium*. The posterior ridge of the proximal epiphysis is relatively straight in *S. boissieri* and *S. sinense* (Bohlin1926, text figure 113). In the studied specimen, however, the medial and lateral tuberosities project significantly to the posterior, forming clearly between them a deep valley. In *H. duvernoyi* only a lateral projection exists, limited to the very lateral edge of the epiphysis. At the lower epiphysis the reduced anterior part of the malleolar articular surface characterizes *Samotherium* and differentiates it clearly from *Helladotherium*. In *S. sinense* though, the anterior surface is wider than the other *Samotherium* species (Geraads 1974). The fibular furrow in *S. boissieri* and *S. neumayri* is wide and shallow, while in the studied specimen it is clearly deeper. However, in *S. sinense* it is narrow (Bohlin 1926, text figure 115), as it is also narrow in *H. duvernoyi*. In the latter the opening of the furrow is oriented laterally and is located at the middle of the lateral wall. Another striking feature is the short imprint of the flexor digitorum longus muscle at the posterior of the lower epiphysis, and its position. In *B. attica* the imprint is very long and extends high in the diaphysis, and is located at the medial

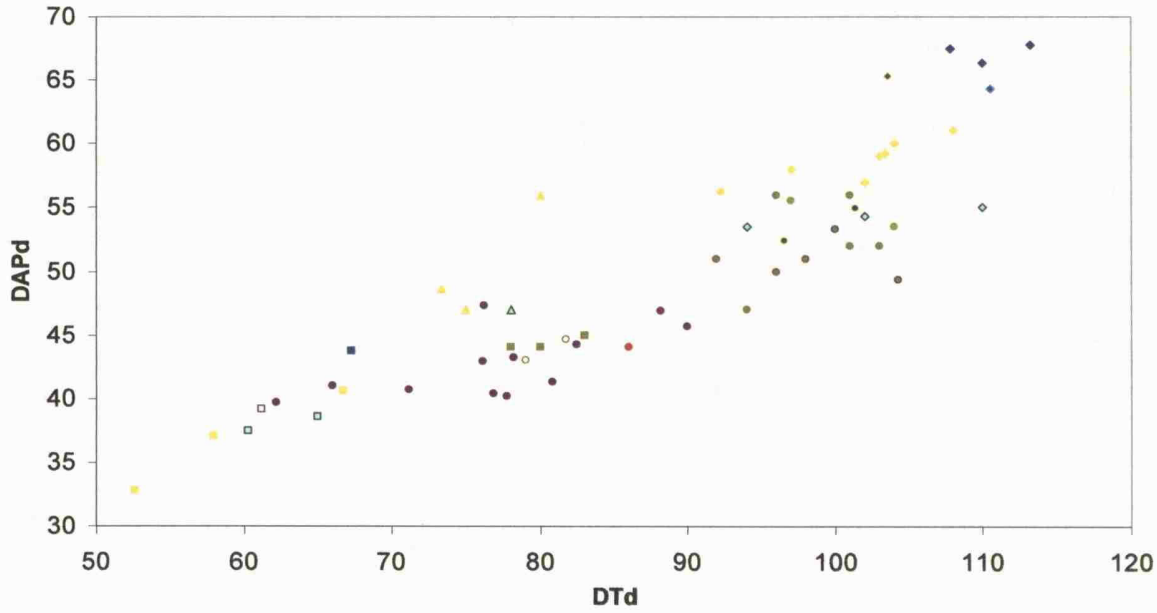

Figure 22: Plot of distal transverse diameter vs distal anteroposterior diameter of the metacarpal (measurements in mm). The legend for the symbols is presented in Figure 7.

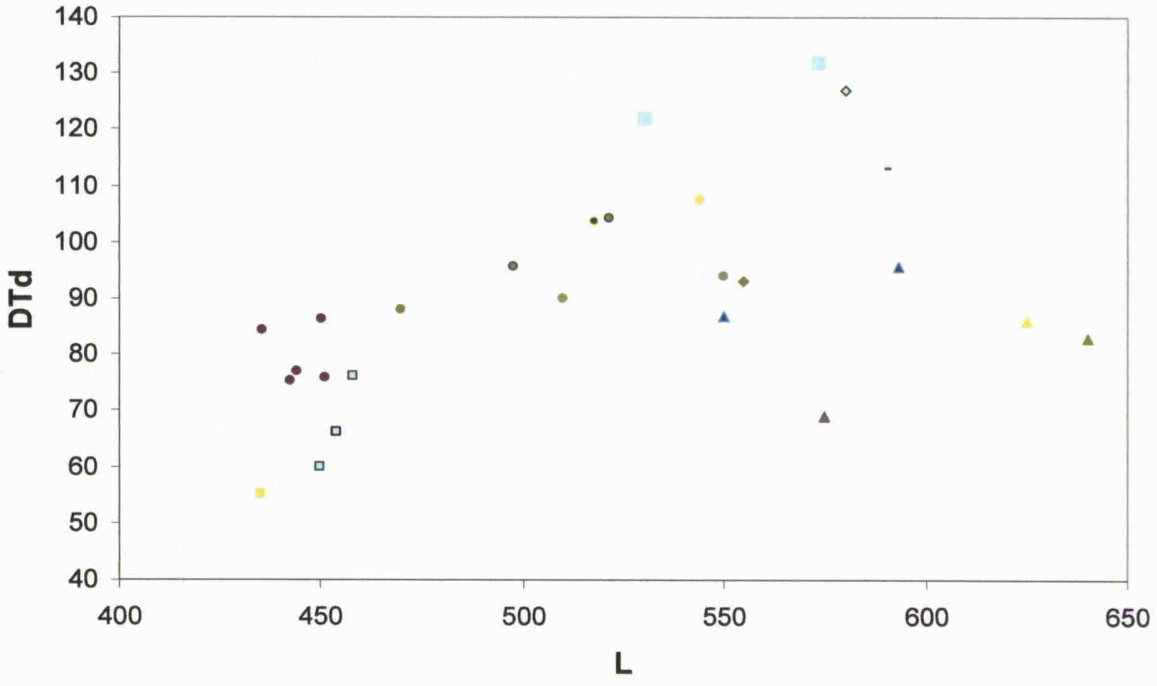

Figure 23: Plot of length vs distal transverse diameter of the tibia (measurements in mm). The legend for the symbols is presented in Figure 7.

edge of the posterior side of the bone. In *H. duvernoyi* the imprint of the muscle is short but longer than in *Samotherium*, and is similarly located at the posterior of the bone. In the studied specimen as well as in *S. boissieri*, the short imprint is located at the posterior part of the medial side of the bone. Therefore, the muscle's groove at the epiphysis in the two species as well as in *S. neumayri* (de Mecquenem 1924, plate II figure 5) is found more medially than in *Bohlinia* and *Helladotherium*.

Until now it has been considered (Bohlin 1926; Geraads 1994) that the *Samotherium* material from Samos stored in the NHML was homogenous, came from the lower horizons, and was represented only by *S. boissieri*. However, the presence of specimen M5432 (a right tibia, with the distal epiphysis not fully fused, articulated with the tarsal bones and the proximal part of the metatarsal) with a length of 521.2 which is within the range of *S. major*, denotes the presence of *S. major* in the material. The darker colour of the bones also indicates that it was probably collected from another locality and most likely from the upper horizons of Samos. Thus, the collections in the NHML possibly contain other specimens from the upper horizons.

The malleolus is clearly distinct from *H. duvernoyi* as the anterior part of the bone is clearly reduced. In addition the anterior part of the articular surface with the tibia is shorter and narrower, indicating a *Samotherium*. The anteroposterior and transverse diameters of the bone are larger than *S. boissieri*, shorter than *S. sinense* and similar to *S. neumayri* (Fig. 24). However, its height is considerably increased, due to the long fibular process and the very eminent anterior part of the distal articular surface; the ratio height/DAP is 0.82 for the specimen from Kerassia, 0.68-0.79 for *S. boissieri* from Samos (NHML), 0.61-0.75 for *S. neumayri* from Maragha, 0.51-0.55 for *S. sinense* form China and 0.61-0.66 for *H. duvernoyi* from Pikermi.

The absence of the notch from the medial ridge of the plantar trochlea of the astragalus and the shallow proximal intertrochlear groove differentiate the studied material from *H. duvernoyi*. Nevertheless, the presence of a rounded depression at the base of the lateral margin of the plantar trochlea is indicative of *Samotherium*. This rounded depression does not exist in *B. attica*. In addition, in *Samotherium* the plantar trochlea becomes narrower towards the top and is clearly separated from the proximal trochlea with a groove, while in *B. attica* the proximal part of the plantar trochlea widens to the top and its medial edge is directed towards the medial proximal trochlea forming with the medial trochlea a continuous

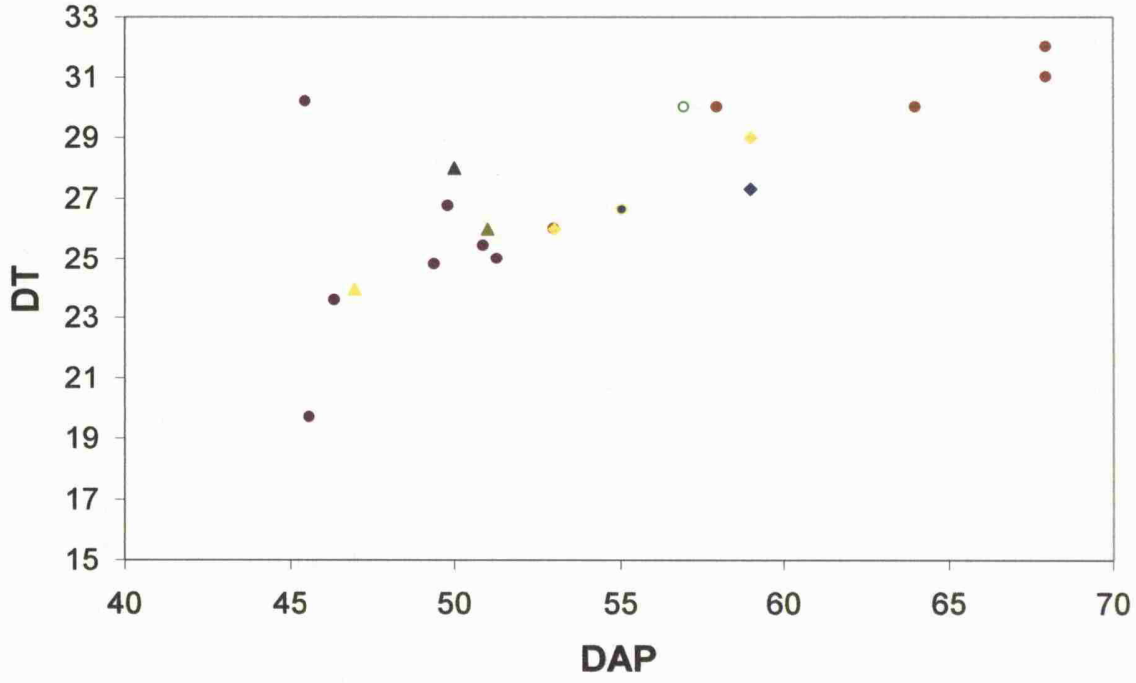

Figure 24: Plot of anteroposterior diameter vs transverse diameter of the malleolus (measurements in mm). The legend for the symbols is presented in Figure 7.

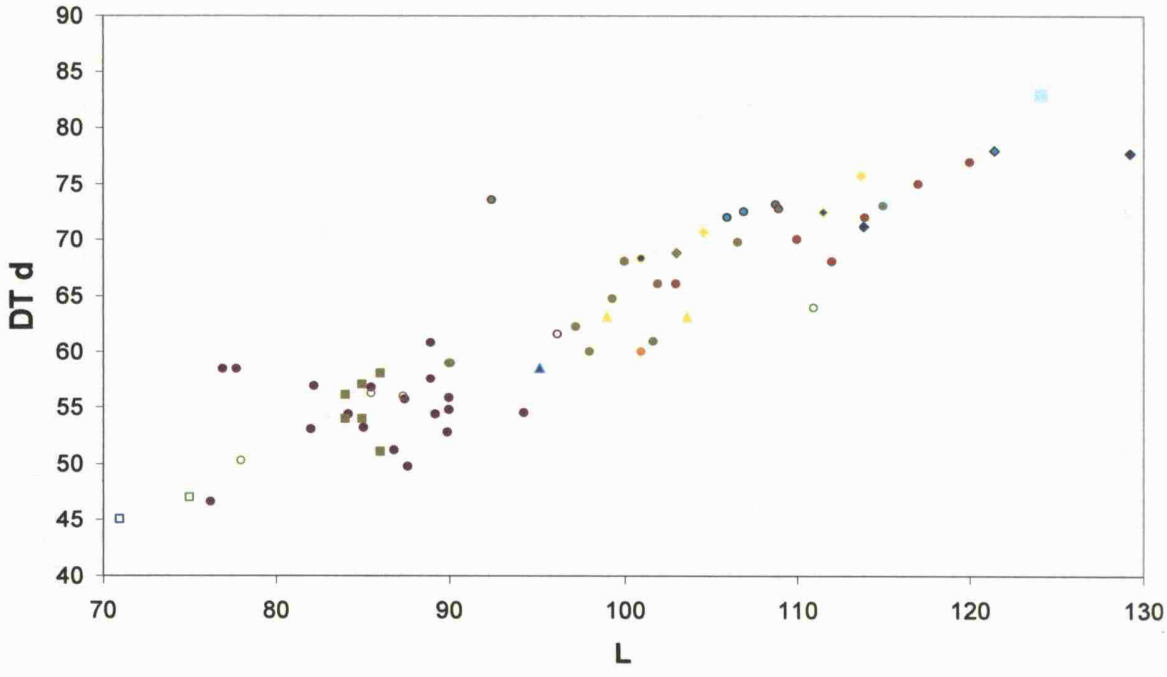

Figure 25: Plot of maximum (lateral) length vs distal transverse diameter of the astragalus (measurements in mm). The legend for the symbols is presented in Figure 7.

posteromedial ridge. The prominent rim of the medial proximal trochlea is present in the studied specimen but was not recognised in *S. sinense* (Bohlin 1926, table IX, figures 3, 4). The studied specimens are longer and more robust than *S. boissieri*, but they are shorter than *S. sinense* (Fig. 25, 26). They are within the upper range of 94-102 mm of *S. neumayri* from Maragha (Rodler and Weithofer 1890) and the 97.2-106.6 mm range of the five specimens under the number M3876 stored in the collections of NHML that most likely belong to *S. neumayri*. Although they are shorter from the two specimens of *S. major* from Taskinpasa (106 and 107 mm; Senyurek 1954) and also from the two specimens of *S. major* from Samos stored in AMPG (12/88 PG 102 and 12/88 PG 106, 109 and 108.8 mm respectively), they are slightly longer than the 100 mm of the large *Samotherium* specimen from Samos described by Schlosser (1904).

The distinctive triangular shape of the body of the five calcaneus and the wide anterior part of the malleolar articular surface evinces the presence of *Samotherium*. In *H. duvernoyi* the body of the calcaneus is clearly rectangular, as the dorsal and plantar crests are parallel and the anterior part of the malleolar surface is relatively narrow. Although the length of *B. attica* is compatible with the length of *S. major* and *S. neumayri*, the gracility as well as the shorter proportions of the other measurements make the distinction from *Samotherium* species obvious (Fig. 27). The five calcaneus are longer and more massive than those of *S. boissieri*. They are slightly shorter than *S. sinense* and they are within the range of *S. major* and *S. neumayri*. The strongly asymmetric tuber calcanei of *S. sinense* (Bohlin 1926) is clearly different from the symmetric tuber of *S. neumayri* and *S. boissieri* (Geraads 1974) or the slightly asymmetric tuber in the studied specimens (Fig. 18J, 28). The latter though are also clearly separated from *S. boissieri* and *S. neumayri* as at the medial side of the anterior part of the malleolar articular surface they present a deep concavity, which is not found in the other two. In the collections of the NHML except from the already mentioned articulated hindlimb specimens M5432, specimen M4282(311) from Samos is also larger than the other *S. boissieri* specimens and therefore it probably belongs to *S. major*. Similarly the three specimens under the number M3888 and two under the number M7433 from Maragha most likely belong to *S. neumayri*.

The great width of the scaphocuboideum of *H. duvernoyi* is a first diagnostic feature for the distinction from *Samotherium*. The relatively low plantar peak of the medial concavity is a feature of *Samotherium*. The plantar end of the articular surface of the calcaneus stops at the lateral side of the peak of the lateral concavity while in *H. duvernoyi* and *B. attica* it turns

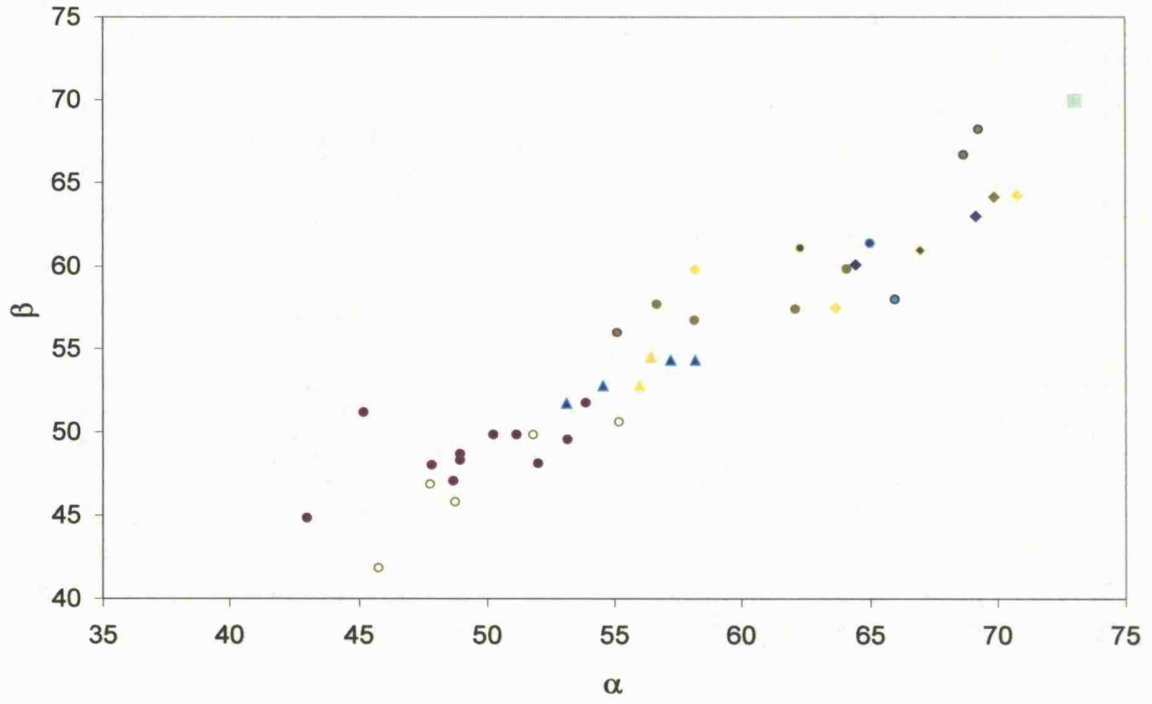

Figure 26: Plot of maximum medial anteroposterior diameter (α) vs maximum lateral anteroposterior diameter (β) of the astragalus (measurements in mm). The legend for the symbols is presented in Figure 7.

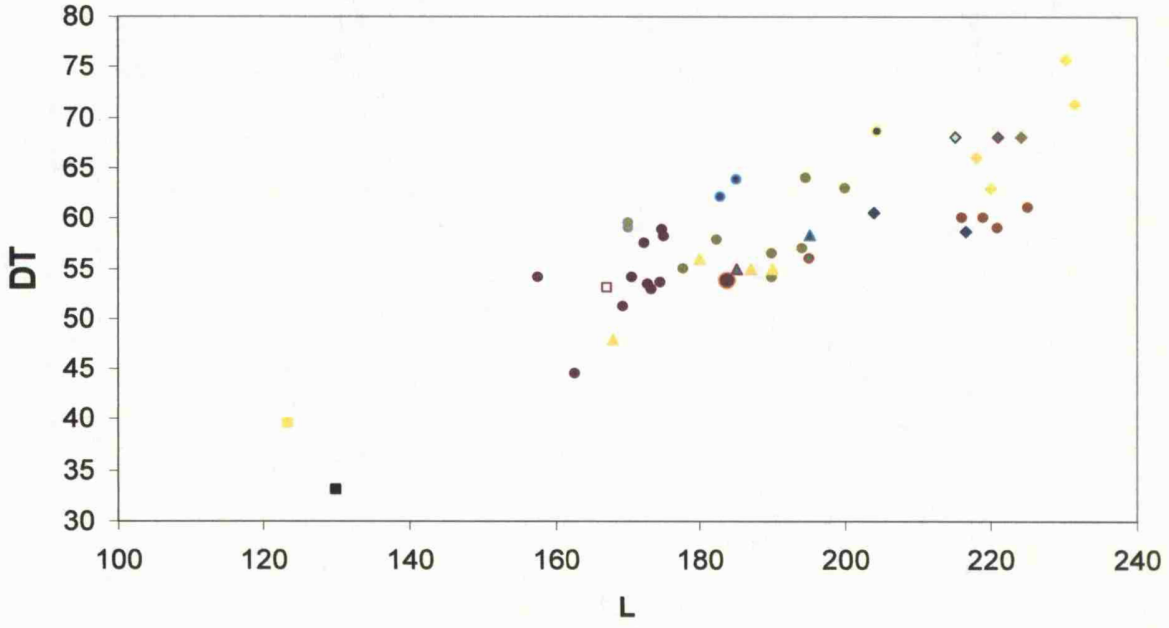

Figure 27: Plot of length vs maximum transverse diameter at the sustentaculum tali of the calcaneous (measurements in mm). The legend for the symbols is presented in Figure 7. The large purple dot with the orange rim belongs to specimen M4282(311) from the NHML collections of Samos that is grouped with the calcanei of *S. boissieri.* Metrically though, as it is clear from this and the following plot, it fits with the dimensions of *B. attica.*

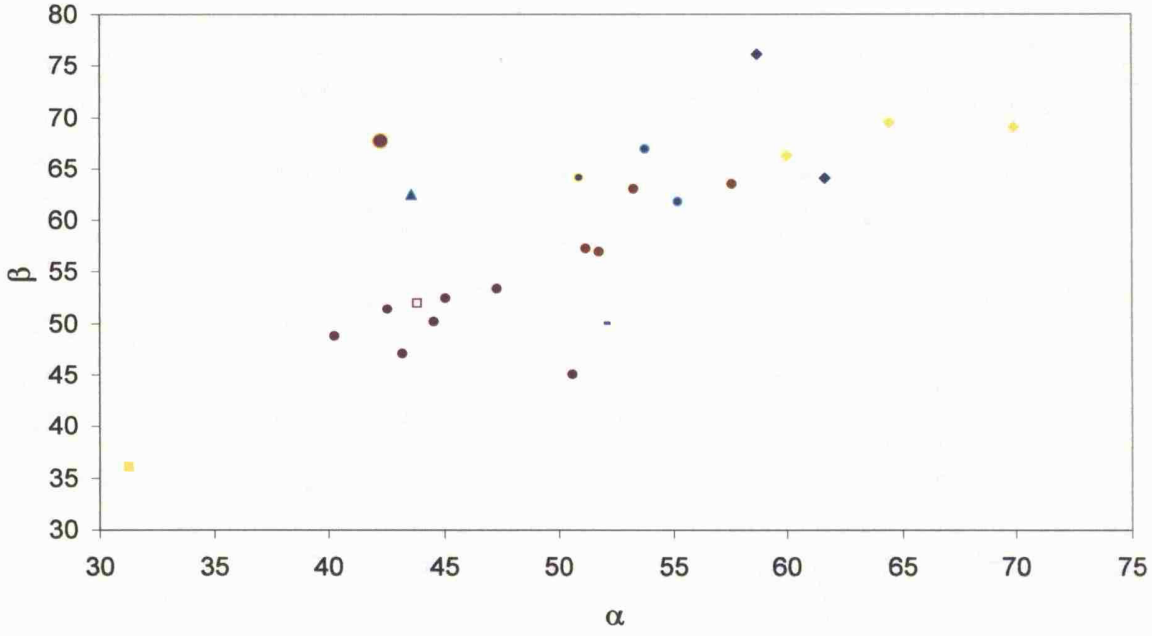

Figure 28: Plot of transverse diameter (α) vs anteroposterior diameter (β) of the tuber calcanei (measurements in mm). The legend for the symbols is presented in Figure 7. The large purple dot with the orange rim as in figure 27.

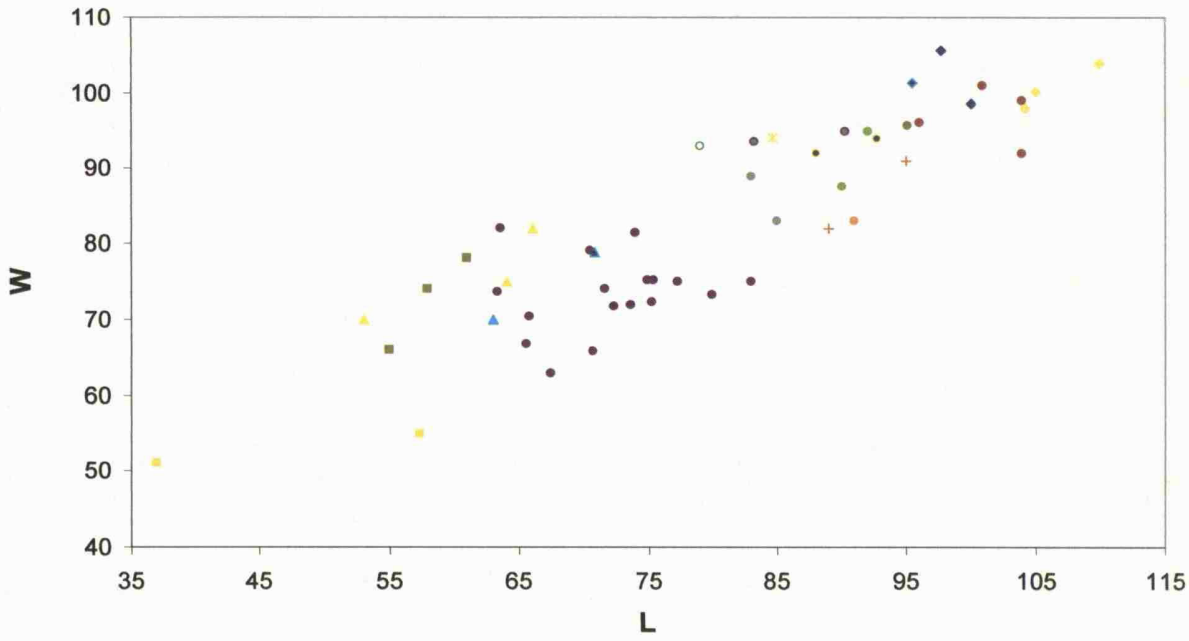

Figure 29: Plot of length vs maximum maximum width of scaphocuboideum (measurements in mm). The legend for the symbols is presented in Figure 7.

around the peak. As a result the furrow on the plantar side of the bone is wider in *Samotherium*. The studied specimens are within the range of *S. major*, they are larger than *S. boissieri* and *B. attica*, and shorter than *S. sinense* (Fig. 29). Besides, the elongated anteroposterior diameter is one of the distinctive characters of the latter. Another feature used for the distinction is the contact of the distal apophysis of the plantar ridge with the metatarsal, which was not observed in specimen K1/Δ247/2 which was found articulated with a metatarsal. As for *S. neumayri* the lack of compatible measurements in the literature did not allow the metrical correlation. However, in the collections of NHML specimen M3877 from Maragha could be attributed to *S. neumayri*. Metrically it coincides with *S. major* and the studied specimens. The complete absence though of the posterior metatarsal facet (Geraads 1974) and in addition the reduced medial ridge and the reduced lateral tuberosity differentiate it from the studied specimens and *S. major*.

The dimensions of the three large intermediolateral cuneiform specimens from K1 are clearly larger than *S. boissieri* and also clearly smaller than *S. sinense* (Fig. 30); their anteroposterior and transverse diameters are similar with those of *H. duvernoyi*, however, the thickness in *H. duvernoyi* is greater.

The length of the two metatarsal bones from Kerassia is 417.6 and 426.7 mm and their robusticity indices are 11.9 and 12 respectively. The range of the length of the metatarsals of *H. duvernoyi* from Pikermi is 433-465 mm (Melentis 1974; Geraads 1974; Gaudry 1862; Bohlin 1926; collections of NHML) and equally the robusticity index ranges 10.4-14.1, while in *H. duvernoyi* from Nikiti this is respectively 457.6-460mm and 10.4-11.4. Equally the values for *S. sinense* from China are 495-540 mm (Bohlin 1926; Geraads 1974) and 9.44, for *S. neumayri* from Maragha are 402-444 mm (Geraads 1974; Rodler and Weithofer 1890) and 10.7-13.7, for *S. boissieri* from Samos (NHML) are 349.9-412.2 and 10-12.7, while for *S. major* from Kemiklitepe the values are 462 mm (Geraads 1994) and 11.7, and for *S. major* from Vathilakos the length is 455 mm (Geraads 1974). It is clear that the studied metatarsals are longer and more robust (Fig. 31) than those of *S. boissieri*, although there is the exception of specimen M4289(81) from Samos that is remarkably robust. It is also clear that they are shorter than the robust metatarsals of *H. duvernoyi* and considerably shorter than the elongated and thus slender metatarsals of *S. sinense* (Fig. 31). They are within the range of *S. neumayri*, but they are shorter than the two known specimens of *S. major*. However, after comparing the wider range of values of the other species, one can conclude that the length of the metatarsal specimens of *S. major* most likely had a wider range of values. The seemingly

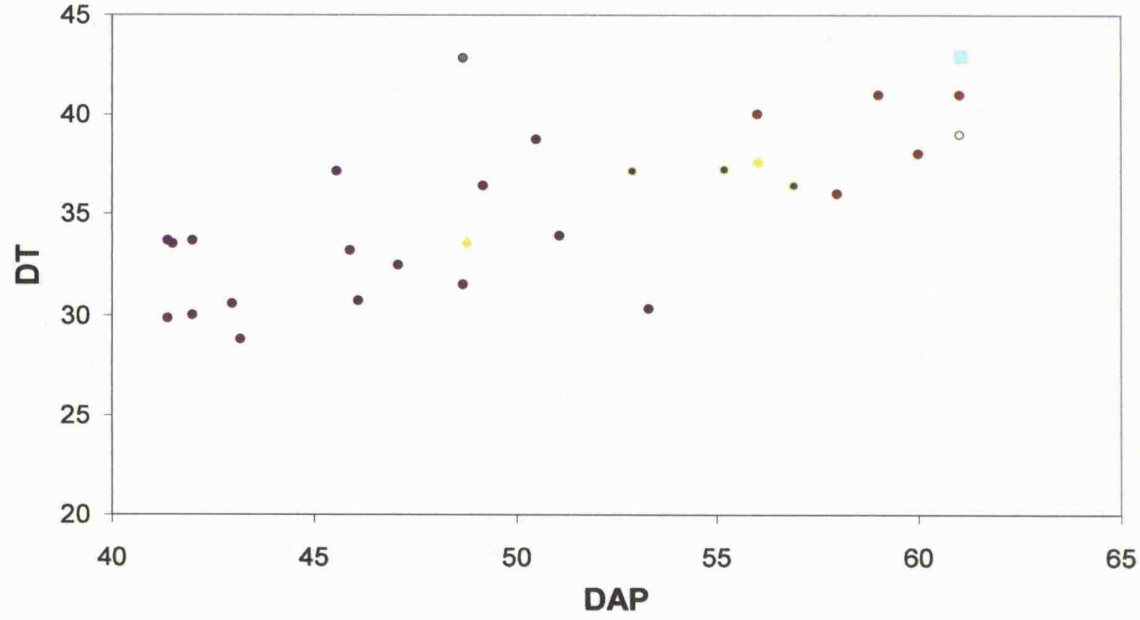

Figure 30: Plot of anteroposterior diameter vs transverse diameter of the intermediolateral cuneiforme (measurements in mm). The legend for the symbols is presented in Figure 7.

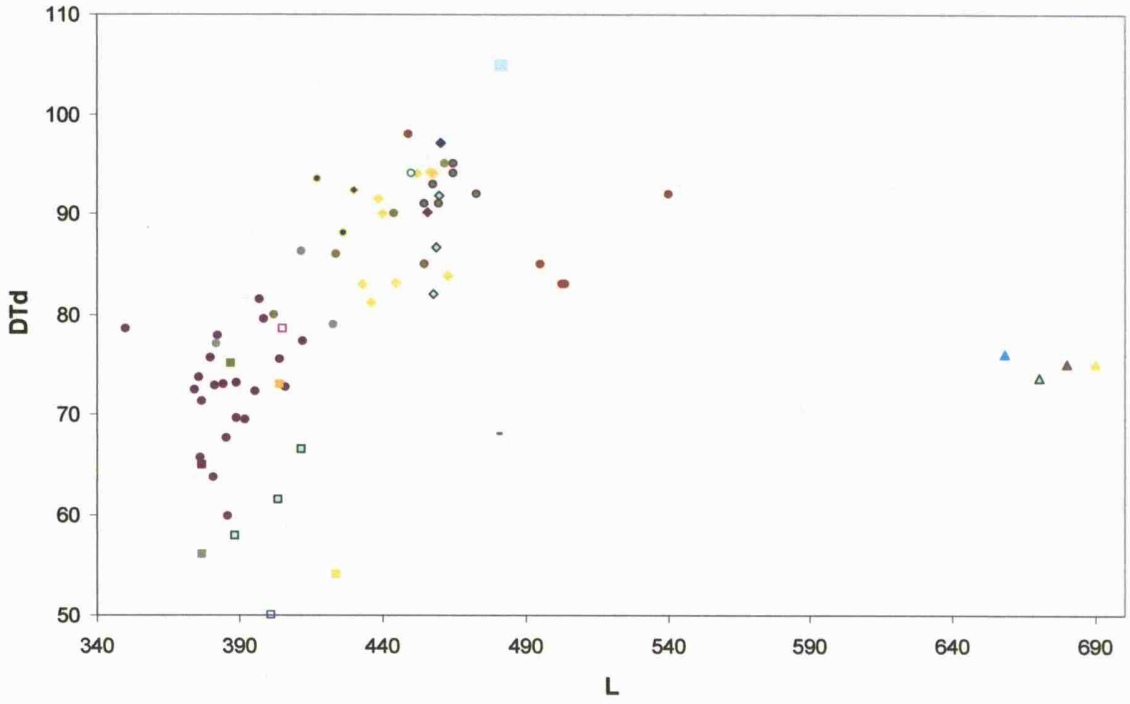

Figure 31: Plot of length vs distal transverse diameter of the metatarsal (measurements in mm). The legend for the symbols is presented in Figure 7.

narrow range may reflect the small number of discovered bones or the lack of data from the literature. In addition to the relative slenderness of the metatarsals of *Samotherium* species the following makes the distinction from *H. duvernoyi* clear: the very developed and prominent medial tubercle at the plantar side of the bone with the small protuberance in the medial furrow of the bone, and the tubercle found between the medial and the lateral ones, with the eminent process at the top (Fig. 32A, C). In *H. duvernoyi* the medial and lateral tubercles are found at the same level and are connected by a thin ridge (Fig. 32D). Also, the small protuberance found in the medial furrow in front of the medial tubercle in *Samotherium*, remnant of the first metatarsal, is not present in *H. duvernoyi*. The great length and the very prominent medial tubercle plus the fairly reduced lateral tubercle differentiate *S. sinense* from the other *Samotherium* species. Similarly, the shorter metatarsals of *S. boissieri* can be easily distinguished from the other *Samotherium* species. Moreover, the medial tubercle is less prominent and the lateral one more developed (Fig. 32C). (Among the material of *S. boissieri* from Samos stored in NHML there are a few specimens with their proximal articular surface distorted.) The well defined and strong lateral tubercle (present in the studied specimens) is probably one of the distinctive features for *S. major*, as well as the deep furrow that confine it laterally (Fig. 32A). This tubercle is not so developed and the lateral furrow is shallower than in the other *Samotherium* species.

The studied material from Kerassia belongs to a large *Samotherium*, *S. major*. It was identified in both horizons and more specifically in sites K1 and K4. Nevertheless, its presence in the lower horizon is marked only by two mandible specimens. For the moment, among the prepared material from the lower horizon there is no postcranial material that could be associated with the two mandibles, which most likely belong to the same individual, or with *S. major* in general. Articulated and associated specimens have been found in site K1. The right metatarsal K1/Δ247/1 was found articulated with the scaphocuboideum K1/Δ247/2 and the cuneiform K1/Δ247/3 and probably is associated with the right calcaneus that was found nearby. Similarly, the left tibia (K1/Δ341/1), the left astragalus (K1/Δ342), the left scaphocuboideum (K1/Δ346) and the left cuneiform (K1/Δ341/2) were collected from the same area and are also associated with each other. Probably other bones could belong to the same individuals. The skeletal material from site K1 belongs at least to three individuals. To date, *S. major*, except from Kerassia, has been reported in only four other localities, namely Samos (Bohlin, 1926), Taskinpasa (Senyurek 1954), Vathylakkos (Geraads 1974, 1978), and Kemiklitepe (Geraads 1994). These localities are found all around the Aegean Sea. With the addition of the Kerassia specimens the presence of *S. major* is to date limited to this relatively

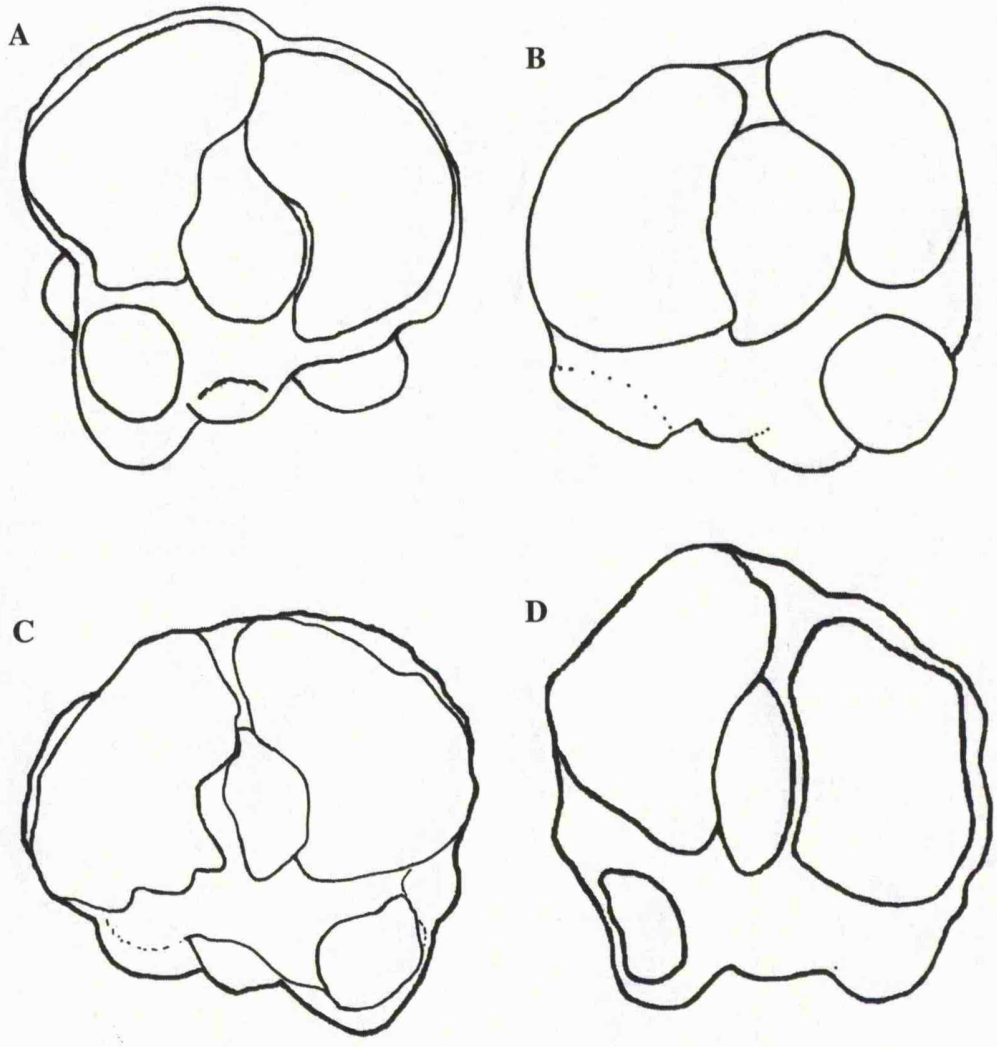

Figure 32: A. *S. major*, right Mt $_{III+IV}$, K1/Δ247/1, proximal articular surface. **B.** *B. attica*, left Mt $_{III+IV}$, Ke 163, proximal articular surface. **C.** *S. boissieri* (Samos, NHML), left Mt $_{III+IV}$, proximal articular surface. **D.** *H. duvernoyi*, right Mt $_{III+IV}$, K1/Δ83, proximal articular surface.

small palaeogeographic area. If this is a reflection of *S. major's* true range certain palaeoenvironmental and/or palaeoclimatological conditions did not allow *S. major* to migrate and expand further.

(Subfamily SIVATHERIINAE Zittel, 1893)

Genus HELLADOTHERIUM Gaudry, 1860

Type species. Helladotherium duvernoyi Gaudry, 1860, from Pikermi, Greece

Helladotherium duvernoyi Gaudry, 1860

Diagnosis. A Sivatherine of great size with long and fairly robust long bones and relatively long upper and lower premolar rows. P_3 is always not molarised.

Material. Right maxilla part with P^2-M^3 (K1/Δ75/1), left I_3 (K4/Δ350), left humerus (K4/Δ110/7), right radius (K1/Δ155, K4/Δ110/2), right distal part of radius (Ke 164), left proximal part of radius (K4/Δ133/6), left Mc_{III+IV} (K1/Δ82, K4/Δ119/33), left distal part of Mc_{III+IV} (K4/Δ86/1, K4/Δ340/11), right distal part of Mc_{III+IV} (Ke 99/41), forelimb phalanx I (K3.4), right distal part of tibia (K4/Δ81), left malleolar (K4/Δ314/6), right astragalus (K1/Δ22, K4/Δ6/1, K4/Δ314/2,7), left calcaneus (K4/Δ62, K4/Δ331/2) right distal part of calcaneus (K4/Δ314/6), left scaphocuboideum (Ke 99/43, K4.8), right scaphocuboideum (K4/Δ314/1), right Mt_{III+IV} (K1/Δ83, K4/Δ331/1), left proximal part of right Mt_{III+IV} (K1/Δ153), right proximal part of Mt_{III+IV} (K4/Δ388/6), hindlimb phalanx I (K4/Δ354).

Description. The cranial material (Appendix 1) is limited to a maxilla part with P^2-M^3 from site K1 (Fig. 33A, B) and an I_3 from K4 (Fig. 33C). Among the six teeth of the maxilla only M^3 is intact. Unfortunately, this specimen was exposed on the surface of the roadside cutting wall and was badly damaged by erosion before its collection. Despite this, most of the M2 and the lingual parts of M^1, P^3 and P^2 have been preserved (Fig. 33A, B). The preservation of a significant part of P^2 allowed the almost accurate measurement of the length of the toothrow which is 214 mm. The accurate measurement of the length of the molar and the premolar row was not possible as the labial part of M^1 and P^4 were destroyed. However, approximate measurements were taken in order to provide values for the estimation of indices and

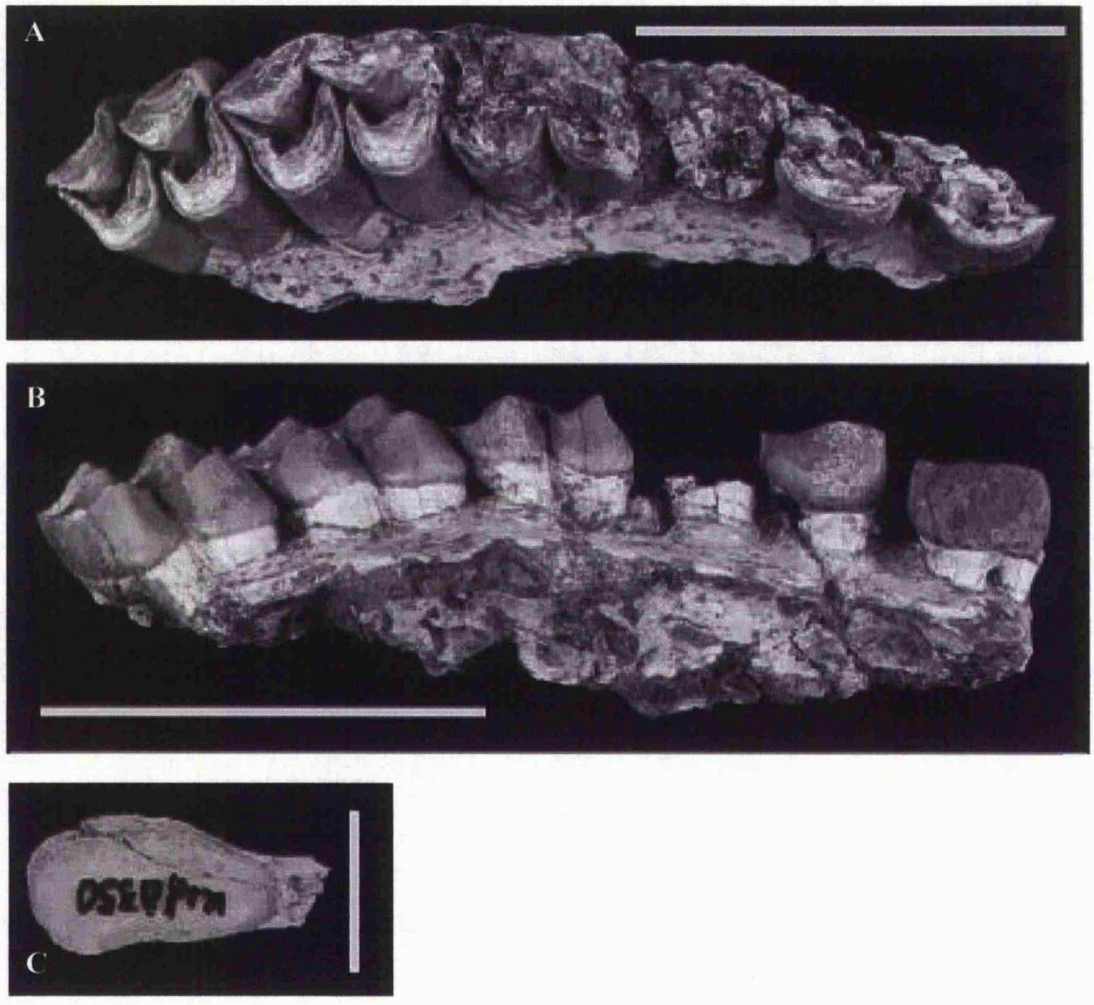

Figure 33: A. *H. duvernoyi*, right maxilla part with P^2-M^3, K1/Δ75/1, occlusal view (scale bar 10cm). **B.** *H. duvernoyi*, right maxilla part with P^2-M^3, K1/Δ75/1, lingual view (scale bar 10cm). **C.** *H. duvernoyi,* left I_3, K4/Δ350, labial view (scale bar 2cm).

correlations. For the same reason the damaged teeth were measured, measuring the borders of alveolar cavities when the walls of the teeth were not available. Hence, the actual dimensions of these teeth would be larger. So, the approximate lengths of the premolar and molar toothrows are respectively 94.9 and 127.5 mm. The indices P/M and P/PM are respectively 74.4 and 44.4, and thus indicate a relative shortening of the premolar row. From the remaining lingual portions of the first two premolars it is rather clear that their lingual crescents are fairly elongated and furthermore P^2 is probably longer than $P^3$and P^4. In the preserved lingual parts of the three molars it is clear that the lingual wall of the lobes is rounded. The protocone in M^3 and M^2 is very developed and fairly wider than the hypocone. The short posterior flange of the protocone has a transverse position and is directed labially and not towards the anterior flange of the hypocone. The anterior flange of the protocone in M^3 is connected with the parastyle. The anterior flange of the hypocone is long and is directed towards the paracone. However, it does not confine the posterior flange of the protocone. The posterior flange of the hypocone is connected with the metastyle, and on its internal wall a feeble enamel fold is clear that corresponds to an "eperon hypoconal". It is obvious that the labial crescents of the molars are significantly higher than their lingual ones. The paracone is very strong and a developed rib is found on its labial wall. A fairly developed parastyle is found at its anterior, while its posterior flange is straight and not connected to the mesostyle. The latter is also developed and fairly prominent, covering lingually the posterior flange of the paracone. The metacone is not very developed and its imperceptible rib forms a relatively flat lingual wall. In addition the metastyle is strong, and thus the lingual wall is concave. A very robust third incisor was found in site K4; its length is 16.5 mm, its width is 14.8 mm and its height is 29.9 mm. The general shape of the tooth is triangular. It is wide at the top of the crown but gradually it gets more narrow towards the root at the base of the tooth. In addition, the external side is considerably wider than the internal side.

Among the long and robust long bones attributed to this species (Appendices 3 – 13), an almost complete humerus is present; the head and part of the trochiter are broken (Fig. 34A, B). At the posterolateral of the upper part of the bone the tricipital ridge is clear and strong. The ridge continues to the anterolateral side of the bone as a strong but not very prominent deltoid tuberosity. The transverse diameter of the proximal part of the bone is increased and thus the bone is fairly wide, whilst it is narrow across its anteroposterior diameter. At the distal epiphysis the trochlea is higher than the condyle. The concave surface of the lateral trochlea is deep and wide and is limited laterally from the condyle with a strong keel. The triangular coronoid fossa has a wide base. The supracondylar crest is very developed and is

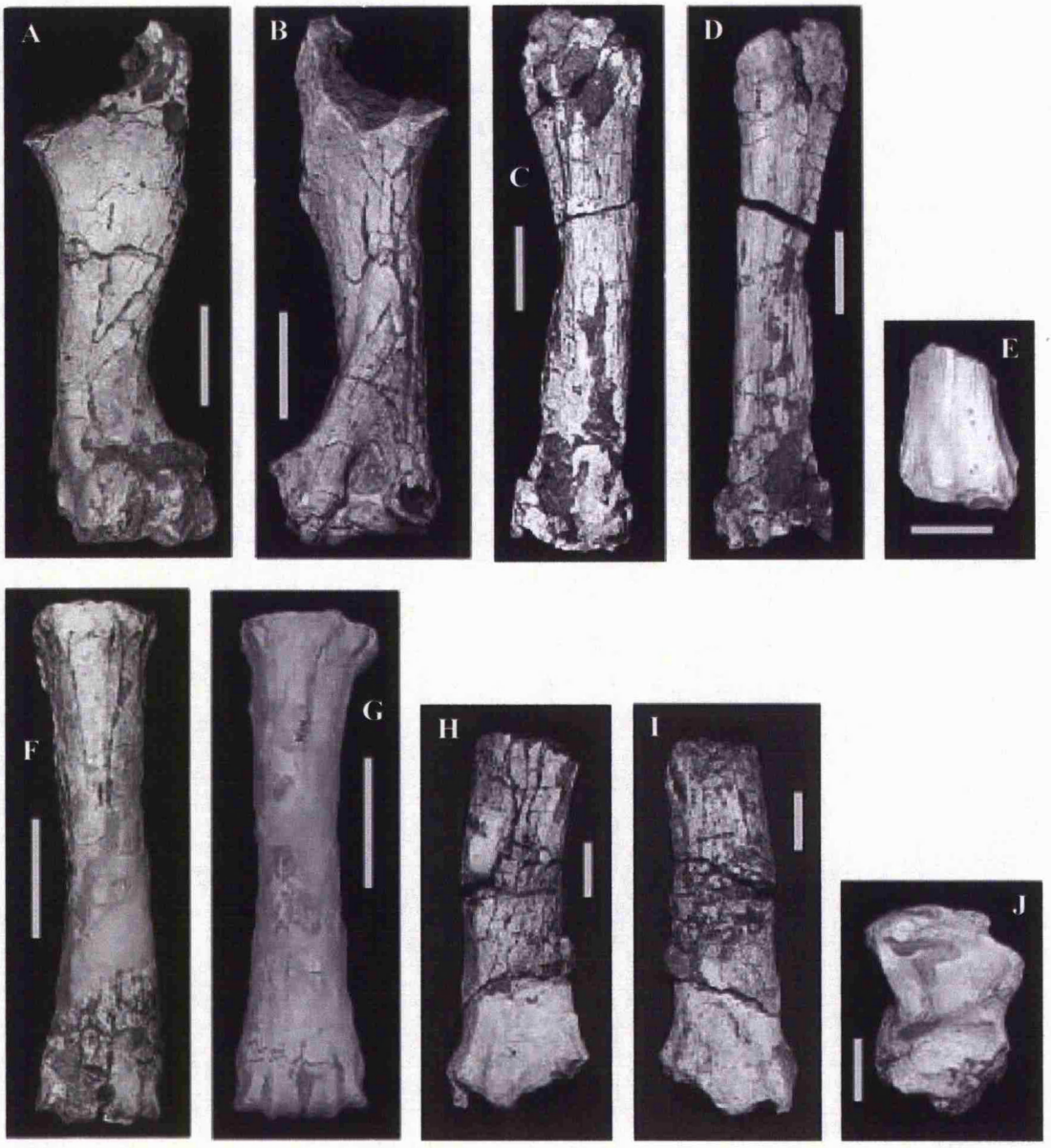

Figure 34: A. *H. duvernoyi*, left humerus, K4/Δ110/7, anterior view (scale bar 10cm). **B.** *H. duvernoyi*, left humerus, K4/Δ110/7, posterior view (scale bar 10cm). **C.** *H. duvernoyi*, right radius, K4/Δ110/2, anterior view (scale bar 10cm). **D.** *H. duvernoyi*, right radius, K4/Δ110/2, posterior view (scale bar 10cm). **E.** *H. duvernoyi*, right distal part of radius, Ke 164, anterior view (scale bar 10cm). **F.** *H. duvernoyi*, left Mc_{III+IV}, K4/Δ119/33, anterior view (scale bar 10cm). **G.** *H. duvernoyi*, left Mc_{III+IV}, K1/Δ82, anterior view (scale bar 10cm). **H.** *H. duvernoyi*, right distal part of tibia, K4/Δ81, posterior view (scale bar 5cm). **I.** *H. duvernoyi*, right distal part of tibia, K4/Δ81, anterior view (scale bar 5cm). **J.** *H. duvernoyi*, right distal part of tibia, K4/Δ81, distal view (scale bar 5cm).

expanded laterally following the development and the widening of the lower epiphysis. The epicondyle and the epitrochlea are slightly gnawed; however, it is clear that the strong epitrochlea is longer than the epicondyle. The profile of the epitrochlear angle is slightly obtuse. The olecranon fossa is U-shaped, relatively long and wide (Fig. 34B). Its proximal end is not well defined as it continues in the diaphysis as a shallow concavity.

From the four specimens of radius that were collected from sites K1 and K4 only one is complete; a very long and robust specimen (K4/Δ110/2) with a length of 634.4 mm (Fig. 34C, D). Also, in another specimen from K1 with a channelled diaphysis and proximal part the length is approximately 536.4 mm. The overall shape of the bone is rectangular and the epiphyses are wider than the diaphysis. However, the widening is not sharp but the upper and lower parts of the diaphysis gradually get wider. The medial wall of the upper epiphysis is rather rectangular. The anteroposterior diameter of the lateral part of the epiphysis is significantly shorter than the diameter of the medial part. The anterior rim of the deep and concave lateral trochlea is also concave. Nevertheless, the anterior wall of the epiphysis is straight. The lateral tuberosity as well as the bicipital tuberosity is feeble. At the lower epiphysis, the ulnar and radial styloid processes are well developed and prominent (Fig. 34D). The articular surface for the scaphoideum is wide and rounded but it gets gradually narrower towards the posterior where the rim is concave and is directed towards the posterior. Similarly, the anterior part of the articular surface for the semilunare is wide and becomes very narrow towards the posterior, where it presents a concave posterior rim. The medial crest of the semilunare is longer than the lateral one. As a result, the strong and fairly prominent posterior edge of the medial crest is considerably higher than the lateral crest. Also, the two crests do not seem to be parallel, and the transverse crest at the posterior of the epiphysis is not very developed. The articular surface for the ulnare is wide and the whole distal surface of the ulnar styloid process is long. In addition, the ulnar styloid process is laterally placed, which also indicates a relative widening of the lower epiphysis. The groove of the extensor carpi radialis muscle at the anterior of the epiphysis is very wide, shallow and U-shaped (Fig. 34E). The two ridges are strong, rounded and have a similar height despite the fact that the lateral one is slightly stronger. The groove is located above the medial semilunare ridge and the lateral part of the articular surface of the scaphoideum. The groove for the extensor digitorum communis muscle is also shallow and relatively wide with a rounded lateral ridge; its opening is directed anterolaterally. In the same regard the groove for the abductor digiti I longus muscle is shallow and relatively narrow and is located more medially at the anteromedial side of the bone. The lower epiphysis presents a relative widening of the

transverse diameter and a reduction of the anteroposterior diameter; the latter probably due to the low anterior ridges.

Two complete specimens and three distal parts of very robust metacarpals were collected from both horizons (sites K1 and K4). The specimen from site K4 is comparatively very long (Fig. 34F), whereas the specimen from site K1 is considerably shorter (Fig. 34G). The length of the specimen from K4 is 442.7 mm and from K1 is 399.5 mm respectively. Similarly the robusticity index for the two specimens is 15.4 and 16.3 respectively, indicating some very robust metacarpals with very wide diaphysis. Despite this significant difference in the length, the other dimensions are relatively close and in particular the DAP and DT of the proximal epiphysis are greater in the second specimen from K1. The overall shape of the proximal epiphysis is triangular as the DAP of its lateral part is considerably shorter than the DAP of the medial part. This smooth reduction is mirrored on the anterior wall of the bone. The ridge that separates the two articular surfaces is straight or slightly curved as in K1/Δ82 and is attached to the lateral side of the broad synovial fossa. In specimen K4/Δ119/33 at the posteromedial and posterolateral sides two small elongated bones are obvious. Possibly these two bones represent the remaining second and fifth metacarpals. The posterior sulcus is deep and U-shaped, and the two crests are strong and they are retained until the lower epiphysis. The keels at the lower epiphysis are very prominent and strong. The anteroposterior diameter in both the lower and upper epiphysis is increased in the studied specimens.

A robust distal part is the only tibia specimen that could be referred to this species (Fig. 34H-J). The preserved portion of the diaphysis is fairly wide. The shape of the lower epiphysis is generally quandrangular, despite the fact that the medial cochlea is longer than the lateral one. In addition it is wider, whereas its anterior part becomes very narrow and continues almost to the anterior of the epiphysis where it is confined by a low and thin ridge. The medial malleolus is triangular, strong and fairly thick, with a very slanting posterior edge and a relatively long and straight remaining medial ridge. The medial tuberosity is very developed and long (Fig. 34J). The groove for the flexor digitorum longus muscle is deep and relatively wide, while its opening is clearly directed posteriorly (Fig. 34H). The imprint of the muscle is short and it tapers and fades in the lower part of the diaphysis (Fig. 34H). Its position is at the posterior of the posteromedial crest of the bone. Although the posterior part of the articular surface of the malleolus is broken, it is still clear that the surface is strong and well developed. The anterior part, confined by a wide and rather shallow fibular furrow, is narrow but fairly long. The intertrochlear crest is narrow and relatively high. The eminent edge at its anterior is

triangular and it is also very developed and very wide (Fig. 34I). The peak of the eminence is not acute but is more trapezoid and broad. A wide, fairly deep and obtuse V-shaped concavity is located at the anterior wall of this eminence; the concavity is long and fades away in the diaphysis (Fig. 34I, J). The posterior edge of the crest continues medially as a strong and fairly prominent process, and laterally as a wide, shallow and very short furrow.

A malleolus articulated with the calcaneus and the astragalus was collected from site K4. Due to this articulation and the damaged proximal part of the bone, it was not possible to examine certain features. Despite this, the very long anteroposterior diameter of the bone, as well as the fairly long and relatively narrow anterior part of the proximal articular surface, are still evident.

Three long specimens of astragalus are referred to this species. The prominent posterior edge of the lateral crest of the proximal trochlea is well developed, triangular shaped and has a rather acute peak (Fig. 35A, D). Furthermore, it is fairly high and in particular significantly higher than the medial crest of the trochlea. The proximal part of the latter is strong and thick; this is also due to a strong tubercle found on the medial wall of the crest. However, the anterior part of the crest becomes gradually very thin, while conversely the anterior part of the lateral crest becomes thicker (Fig. 35B). The intertrochlea groove is deep and fairly wide both proximally and anteriorly. As a result the mesial wall of the lateral trochlea crest is steep. The furrow that separates the proximal trochlea from the plantar one is not continuous but is clearly separated into an oblique, shallow and wide medial one, and a triangular shaped and wide (deep also in specimen K1/Δ22) lateral one (Fig. 35A, D). This triangular shaped furrow continues laterally upon the prominent posterolateral tubercle. The plantar trochlea is slightly concave, while, the medial crest is more lifted up than the lateral crest. The two crests of the trochlea are straight and parallel (Fig. 35A, D). However, the distal part of the medial crest is interrupted by a very developed notch. The notch sections the medial crest forming a triangular oblique imprint (Fig.35C); in specimen K1/Δ22 this is accompanied by a shallow furrow. This notch is created by the sliding of the posteromedial eminent peak of the scaphocuboideum of the astragalus. This sliding surface is clear at the distal part of the crest below the triangular notch. The lateral wall of the distal part of the lateral crest is also interrupted by a concavity. The anteroposterior diameter of the medial side of the bone is considerably longer than the lateral one. The furrow for the malleolus at the lateral side of the bone is shallow. A very low ridge separates it from the proximal articular surface of the calcaneus. Between the ridge and the distal ellipsoid facet the concavity is deep and wide. The

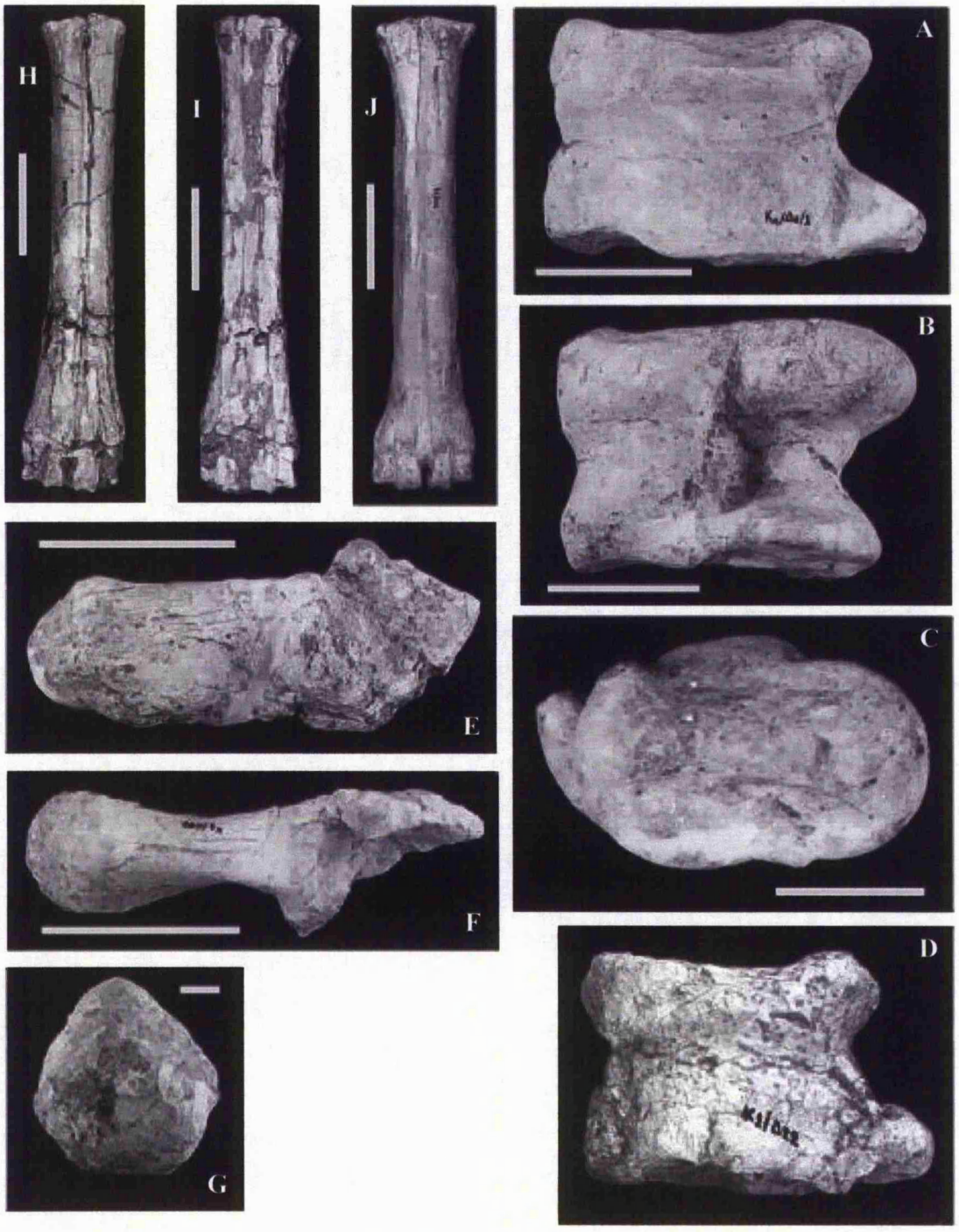

Figure 35: A. *H. duvernoyi*, right astragalus, K4/Δ6/1, posterior view (scale bar 5cm). **B.** *H. duvernoyi*, right astragalus, K4/Δ6/1, anterior view (scale bar 5cm). **C.** *H. duvernoyi*, right astragalus, K4/Δ6/1, medial view (scale bar 5cm). **D.** *H. duvernoyi*, right astragalus, K1/Δ22, posterior view (maximum length 111.5mm). **E.** *H. duvernoyi*, left calcaneus, K4/Δ62, medial view (scale bar 10cm). **F.** *H. duvernoyi*, left calcaneus, K4/Δ62, dorsal view (scale bar 10cm). **G.** *H. duvernoyi*, left calcaneus, K4/Δ62, tuber calcanei (scale bar 2cm). **H.** *H. duvernoyi*, right Mt $_{III+IV}$, K4/Δ331/1, anterior view (scale bar 10cm). **I.** *H. duvernoyi*, right Mt $_{III+IV}$, K4/Δ331/1, posterior view (scale bar 10cm). **J.** *H. duvernoyi*, right Mt $_{III+IV}$, K1/Δ83, anterior view (scale bar 10cm).

crests of the distal trochlea are strong and the lateral one in particular is strong and wide. The intertrochlear groove is wide. At the anterior the distal trochlea is separated from the proximal one with a narrow, shallow but continuous furrow (Fig. 35B). The anterior edge of the proximal medial trochlear crest is fairly prominent and projects medially (Fig. 35B). The anterior cavity is very wide and deep (Fig. 35B).

One complete and two broken robust specimens of calcaneus were found in site K4. The length of the complete specimen is 216.46 mm (Fig. 35E-G). The dorsal and plantar crests of the bone are parallel and the overall shape of the body of the bone is rectangular. The top of the articular surface of the malleolus is considerably higher than the top of the beak of the dorsal crest (Fig. 35E). The posterodorsal tubercle is strong but low. The triangular tuber calcanei is very strong and asymmetrical as its medial part is more developed (Fig. 35G). The index "tuber calcanei width / tuber calcanei height" for the complete specimen is 0.96 indicating a significantly wide tuber. The groove for the flexor digitorum superficialis is shallow and wide. The sustentaculum tali is strong and wide, while the articular surface for the plantar trochlea of the astragalus is slightly concave. The furrow of the sinus tali is shallow and is limited plantarly by strong and high ridge. On the surface the distal articular facet for the astragalus is short and limited to the anterior of the surface. The articular surface for the scaphocuboideum is long and curved. The posterior part of the articular surface for the malleolus is wide and strong, while the axis of the cylinder is inclined towards the medial of the bone (Fig. 35F). Conversely, the anterior part is very narrow and short (Fig. 35F).

Three complete or slightly damaged robust specimens of scaphocuboideum from sites K1 and K4 are inferred to this species. The medial concavity is longer and wider than the lateral one. The culminant peak of the medial concavity is fairly high and acute, while the plantar peak of the lateral concavity is weak and relatively low (Fig. 36C). The valley between the two peaks is wide but shallow and is found at the same level with the articular surface for the calcaneus. The ridge between the two concavities is low and its dorsal end is a strong triangular eminence. The articular surface for the calcaneus continues plantarly behind the peak of the lateral concavity (Fig. 36A, C). At the plantar side (Fig. 36B, C), the valley between the peaks continues as a wide furrow that maintains its width from top to bottom. The medial vertical crest is strong and prominent. The lateral tuberosity is weak and is located at the plantar part of the lateral wall. On the lateral side of the bone, the shallow, oblique groove of the peroneus longus muscle continues on the distal side of the bone where it gets deeper and wider. It separates the anterior articular surface for the metatarsal from an elongated and narrow facet

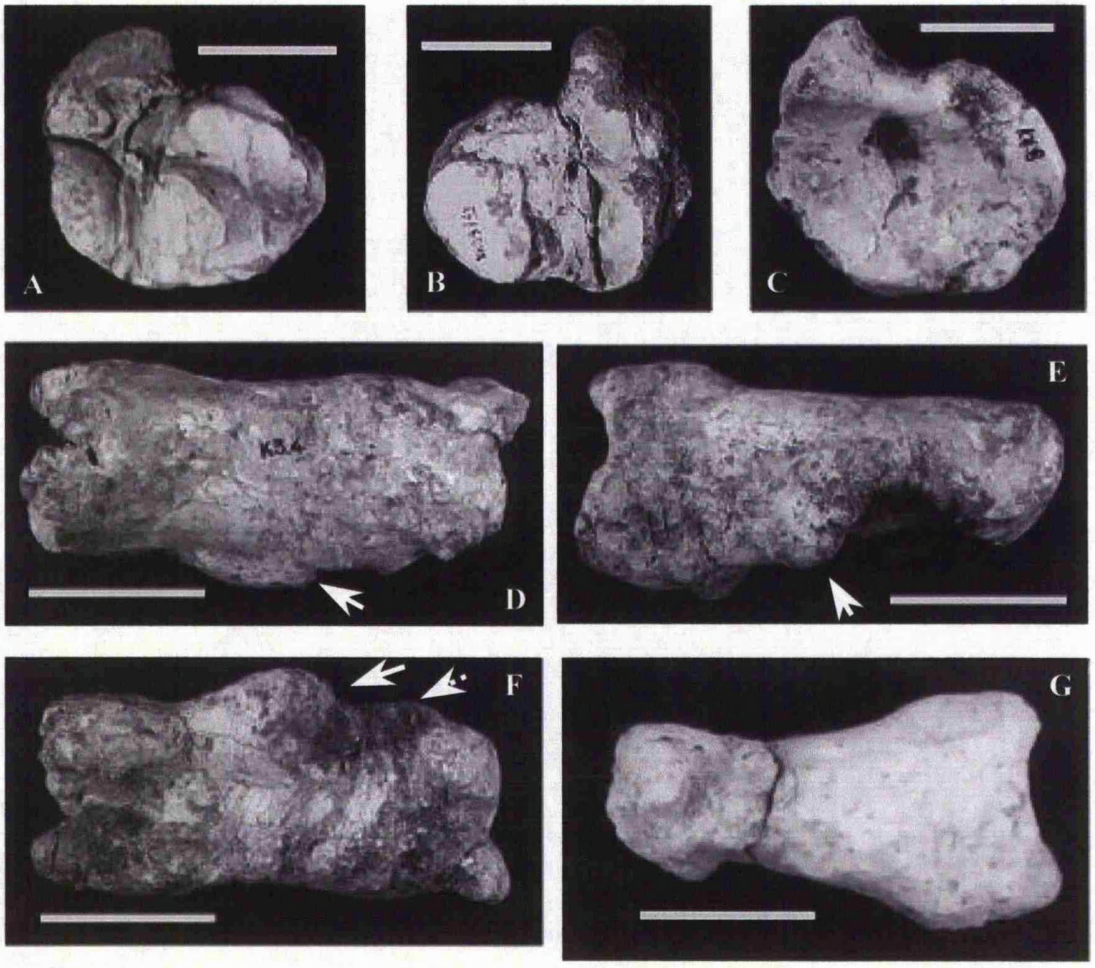

Figure 36: A. *H. duvernoyi*, left scaphocuboideum, Ke 99/43, proximal view (scale bar 5cm). **B.** *H. duvernoyi*, left scaphocuboideum, Ke 99/43, distal view (scale bar 5cm). **C.** *H. duvernoyi*, left scaphocuboideum, K4.8, proximal view (scale bar 5cm). **D.** *H. duvernoyi*, phalanx I, K3.4, anterior view (scale bar 5cm). **E.** *H. duvernoyi*, phalanx I, K3.4, abaxial view (scale bar 5cm). **F.** *H. duvernoyi*, phalanx I, K3.4, posterior view (scale bar 5cm). **G.** *H. duvernoyi*, phalanx I, K4/Δ354, axial view (scale bar 5cm). The arrows in figures D, E and F show the osseous growth on the abaxial side of the phalange. The dashed line arrow in figure F shows the position of a minor osseous growth and the healed infected lesion.

for the posterior metatarse facet. The narrowness of the facet explains the weakness of the lateral tuberosity. On the medial wall of the bone the groove for the tibialis cranialis muscle is not only shallow and wide but it is also curved. Its plantar ridge is very developed and forms a very prominent protuberance.

The metatarsal bones are represented by two complete specimens and two proximal parts. The length for the specimen from K1 is 429.8 mm (Fig. 35J) and for the longer one from K4 460.3 mm (Fig. 35 H). Their robusticity indices are respectively 13.7 and 13.5, indicating some very robust animals. At the plantar side the lateral and medial tubercles of the proximal epiphysis are slightly prominent and are both found at the same level, despite the fact that the medial tubercle is fairly more developed than the medial one. At the anterior of the lateral tubercle only a shallow imperceptible furrow is present, but conversely a furrow is not observed at the medial wall. The two tubercles at the plantar face of the epiphysis are connected with a transverse, narrow and eminent ridge. In the middle, the ridge is higher and bulges slightly plantarly, forming two imperceptible furrows medially and laterally with the two tubercles. At the anterior, the medial crest of the bone is more developed and considerably more prominent than the lateral one. A V-shaped valley is found between the two crests at the upper part of the bone, which continues distally as the anterior sulcus. The posterior sulcus is wide and both crests are strong and they continue down to the distal epiphysis (Fig. 35I). The DAP of the distal epiphysis, compared with the DT is relatively increased. The lower part of the diaphysis widens gradually towards the wide lower epiphysis.

Two robust and long first phalanges are also referred to this species. According to Geraads (1974) the shape of the proximal articular surface of the forelimb digits in giraffidae is more quandrangular, in contrast to the clearly rectangular shape of the digits of the hindlimb. So, the specimen from site K4 (a quandrangular shaped one) is probably a very robust forelimb digit (Fig. 36G). The sagittal groove at the proximal articular surface is deep and fairly wide. The dorsal wall of the articular surface is bulging and prominent, with a small indentation at the upper part. The sesamoid tuberosities at the posterior of the bone are very strong and thick but they are also relatively short. The sulcus between the two tuberosities is wide. Another distinctive feature is the high abaxial wall of the diaphysis. The second specimen from site K3 comprises a very long and very robust second digit, which, similarly can be attributed due to its rectangular shape to a hindlimb one (Fig. 36D-G). The cochlea is long and deep but fairly narrow and the dorsal and plantar edges of the two articular surfaces end to eminent peaks. The dorsal wall of the articular surface also presents a strong and prominent bulge, but not as

strong as in the forelimb digit, with an indentation at the upper part. The axial sesamoid tuberosity is long and narrow with a strong protuberance at its distal part, whereas the abaxial tuberosity is short but very thick. Moreover, the sulcus between the two tuberosities is narrow. The most interesting aspect though in this digit is its distorted abaxial wall and the osseous growths in the middle of the diaphysis and the dorso-abaxial part of the distal epiphysis (Fig. 36D-G). It is evident that the transverse diameter of the diaphysal part of the bone has been widened by the increment of the distorted abaxial wall (Fig. 36G, F). A large triangular shaped tubercle, which probably represents a co-ossified bone flake (splinter), is seen projecting abaxially just bellow the abaxial sesamoid tuberosity (Fig. 36F, G). Its distal part is connected with the proximal edge of the abaxial part of the distal trochlea. Another small tubercle projects abaxially at the dorsal edge of the abaxial part of the distal trochlea. Also, an unusual bulging is found at the distal part of the axial wall of the diaphysis.

Discussion. In the studied material, a second large but more robust species than *S. major* is represented. As mentioned above numerous morphological features of the skeletal elements diversify the two large giraffid genera of Late Miocene: *Helladotherium* and *Samotherium*. Features such as the very robust long bones and the elongation of the premolar row indicate the presence of *Helladotherium*. *Helladotherium* is a very common representative of the Late Miocene faunas in Eurasia. Its presence has been reported in a large number of localities across Europe and West Asia. To date only two species of *Helladotherium* are generally accepted: *H. duvernoyi* and *H. grande* (Lydekker 1883). The latter, which is generally larger than *H. duvernoyi*, has only been identified in the localities of Siwalik (Pakistan). A third species, *H. gaudryi* that was established by De Mecquenem in 1924 was later considered a synonym of *H. duvernoyi* (Geraads 1974).

Although *H. duvernoyi* is considered to be a very common finding in the Late Miocene localities across Eurasia, the lack of cranial material is striking. Only a small number of cranial specimens has been discovered, and therefore the number of complete specimens is even smaller. Only a complete skull without ossicones has been found in Pikermi attributed to a female individual and described by Gaudry (1862-67), plus a few more maxilla parts. Five more specimens of complete or almost complete mandibles make up the list. Unfortunately, the right maxilla part collected from site K1 was damaged by erosion, and thus invaluable information has been lost. However, the preserved M^2 and M^3, as well as the preserved portions of the other teeth were enough for the determination and the approximate metrical correlation of the specimen. Thus, from the dimensions of the toothrow and the teeth

individually, the studied specimen unquestionably belongs to a large giraffid. The length of the toothrow for *H. duvernoyi* from Pikermi is 215 mm (cast AMPG), for *S. boissieri* from Samos stored in NHML ranges between 160-180.5 mm, for *S. neumayri* from Maragha is 200 mm (de Mecquenem 1924), for *S. sinense* from China is 190 mm (Bohlin 1926), for *S. major* from Vathylakkos is 210 mm (Geraads 1978), for *S. major* from Taskinpasa is 205 mm (Senyurek 1954), for *S. major* from Kemiklitepe is 210 (Geraads 1994) and for *S. major* from Samos it ranges between 195-208 mm (Bohlin 1926). In another specimen from a young individual that Gaudry found in Pikermi the P^4 is not fully erupted (1862-67, Pl. XLI, fig. 2 and Pl. XLII, fig. 2) and the length of the toothrow is 207 mm (Bohlin 1926). Similarly, the two indices P/M and P/PM are respectively: 80.2 and 47 for the left and 77.2 and 45.2 for the right toothrow for the skull of *H. duvernoyi* from Pikermi, 67.6-73.2 and 40.4-44.1 for *S. boissieri* from Samos, 60 and 37.5 for *S. neumayri*, 68.1 and 41.6 for *S. sinense*, 64.9 and 40.5 for *S. major* from Vathylakkos, 68 and 41.9 for *S. major* from Taskinpasa, 66.7 and 40.9 for *S. major* from Kemiklitepe, 69.4-72.9 and 42.6-44.1 for *S. major* from Samos and 71.9 and 44.4 for the young *H. duvernoyi* from Pikermi. The measured lengths of the toothrow for the studied specimen, as well as for the specimens of *H. duvernoyi* from Pikermi, are slightly larger than the toothrows of the other large giraffid, *S. major* (Fig. 37). However, the two indices P/M and P/PM make the distinction between the two species evident. The premolar row in *H. duvernoyi* is considerably longer than in *S. major* (Fig. 37). Even the minimised measurement of the broken premolar row in the studied specimen is longer than the longer toothrow of *S. major*. The smaller values for the two indices, though for the young individual from Pikermi must be attributed to the incomplete eruption of P^4. Also, the presence of a feeble "eperon hypoconal" in the preserved two molars differentiate the studied specimen from *Samotherium*. According to Geraads (1974) an "eperon hypoconal" is never present in the upper molars of *Samotherium*. The labial crescents of the molars are higher than the lingual ones in *Helladotherium*. This is another distinctive feature, as well as the elongated lingual crescent of the premolars; in *Samotherium* the premolars are rounded (Geraads 1974). In *Helladotherium* P^2 is elongated and is always longer than P^4, while in *Samotherium* it is usually shorter. In the studied specimen despite the damage in the premolars this trend seems to be valid. The triangular shape and the great size of the third incisor suggest that most likely it belongs to *H. duvernoyi*. According to Geraads (1974), the incisors in *Samotherium* are rectangular. A mandible part of *S. neumayri* from Maragha (Rodler and Weithofer 1890, Pl. IV, fig. 2) and an anterior part of a mandible with all the incisors and the canines of *S. major* from Vathylakkos (Geraads 1978, pl. II, fig. 4) also demonstrate a rectangular shape for their incisors.

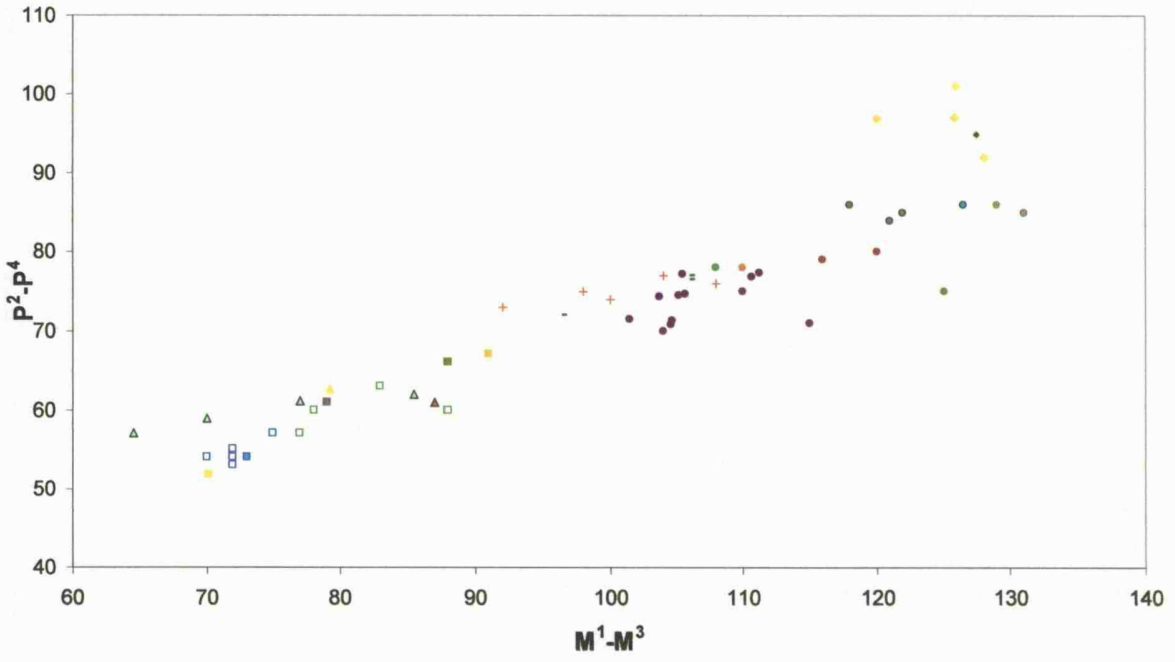

Figure 37: Plot of the length of the upper molar row vs the length of the upper premolar row (measurements in mm). The legend for the symbols is presented in Figure 7.

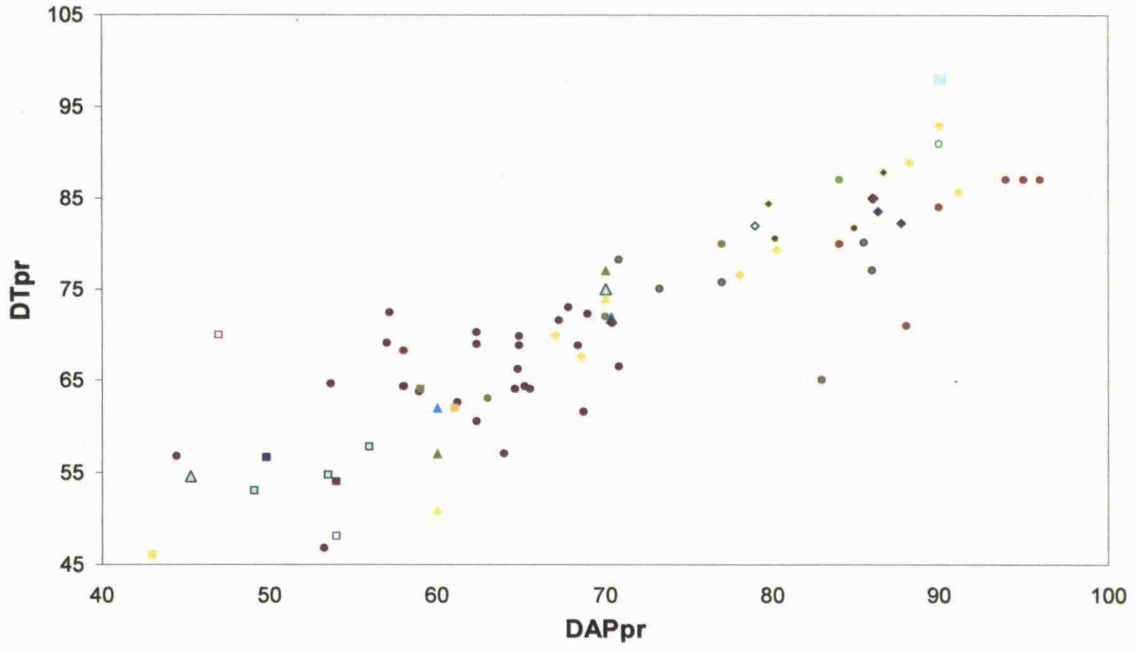

Figure 38: Plot of proximal anteroposterior diameter vs proximal transverse diameter of the metatarsal (measurements in mm). The legend for the symbols is presented in Figure 7.

Despite the similarities in the length of some elements with *S. major*, the robusticity of the post cranial material makes this distinction clear. The robust humerus (Fig. 15) is obviously longer than in *S. major* (the length of the preserved part is about 515 mm), indicating the presence of *H. duvernoyi*. The more anterior position of the deltoid tuberosity (lateral in *Samotherium*) (Geraads 1974) and the relatively smaller keel of the lateral trochlea (Geraads 1994) are two more features. The olecranon fossa, in contrast to the short and narrow fossa in *Samotherium* (Geraads 1974), is wide and long. In addition, the epicondyle is very thick and shorter than the epitrochlea, while in *Samotherium* it is thinner and is relatively equal to the epitrochlea. The generally greater length and the robusticity of the bone characterize the radius of *H. duvernoyi*.

The length of the radius of *H. duvernoyi* ranges between 565-636 mm. The specimen from site K4 is within the uppermost part of this range (Fig. 20, 21). However, the length of the specimen from site K1 (536.4 mm) is significantly shorter than the range of the specimens found todate (Fig. 20). The morphological features that differentiate *H. duvernoyi* from *Samotherium*, as discussed above in detail, were identified in both specimens. The rectangular shape and the straight anterior wall of the proximal epiphysis and the rounded and low ridges that define the shallow muscle grooves at the anterior wall of the distal epiphysis are present in the studied specimens.

A fairly long metacarpal from site K4 and a relatively short one from site K1 are practically found in the two limits of the range of *H. duvernoyi* (Fig. 11). The short one is also included within the range of *S. major*, while the long one is within the range of *S. sinense*. The robusticity index for *H. duvernoyi* from Pikermi ranges 13.4-17.5, for *H. duvernoyi* from Nikiti (Nikiti 1) is 17, for *S. boissieri* from Samos is 10.8-12.9, for *S. neumayri* from Maragha is 13.4-14.8, for *S. major* from Kemiklitepe is 12.4-13.3, for *S. major* from Saloniki 12.2-13.7 and for *S. major* from Vathylakkos is 10.7; unfortunately no measurements for the diaphysis of *S. sinense* are available, but the values of the index are expected to be similar to the other *Samotherium* species. The high robusticity index of the two specimens denotes without any doubt their association with *H. duvernoyi*. The retention of the two crests at the plantar side of the bone until the lower epiphysis is another indicative feature. The relatively increased anteroposterior diameter of the lower epiphysis (Fig. 22) as well as the fairly reduced anteroposterior diameter of the lateral part of the proximal epiphysis (Fig. 12) are two more features of *H. duvernoyi*. In *Samotherium* (as well as in *Palaeotragus* and *Bohlinia*) this reduction is less and the lateral wall of the epiphysis is relatively higher than *Helladotherium*.

The dimensions of the distal tibia part are clearly larger than the dimensions of *Bohlinia* and *S. sinense*, they are generally slightly larger than *S. major* and within the range of *H. duvernoyi* (Fig. 13). The long anterior part of the malleolar articular surface, however, rules out the association with *S. major* (Geraads 1974, 1994). The medial malleolus is also noticeably thicker than in *Samotherium* and *Bohlinia*. The imprint of the flexor digitorum longus muscle is shorter than in *Bohlinia* and longer than in *S. major*, and as discussed above it is located in a different position in *S. major* but shares the same position with *Bohlinia* at the posterior of the posterolateral crest of the bone. Another distinctive feature of *H. duvernoyi* is the deep and elongated concavity at the anterior of the epiphysis which is feeble in *Bohlinia* and is limited to the epiphysis wall in *S. major*.

The presence of the notch at the medial ridge of the plantar trochlea of the astragalus and the great size of the bone (Fig. 25, 26) are indicative of *H. duvernoyi* and clearly distinguish it from the large *Samotherium* species and *Bohlinia attica*. The robusticity and the size of the studied calcanei are definitely greater than *Bohlinia* (Fig. 27, 28). They are within the range of *H. duvernoyi* and as noted above the rectangular shape of the body of the bone rules out the association with the triangular shaped body of *Samotherium*. The well developed and asymmetric tuber calcanei is another discriminating feature (Fig. 28). The great width and the high culminant peak of the medial concavity of the scaphocuboideum are clearly associated with *H. duvernoyi* (Fig. 29). The low valley between the two peaks at the proximal side of the bone as well as the elongated and narrow facet at the plantarolateral of the distal side for the posterior metarsial facet are also diagnostic of *H. duvernoyi*.

As it was also observed in the metacarpals the longer of the two complete metatarsals comes from site K4 and the short one comes from site K1 (Fig. 31). The length of the former is close to the upper limit of the range of *H. duvernoyi* whereas the length of the latter is slightly lower than the lower limit. The lengths of the two specimens are also within the range of *S. major* and the shorter one is even found within the range of *S. neumayri*. However, the high robusticity index and the morphology of the bones suggest that the studied specimens belong to *H. duvernoyi* (Fig. 38). As in *H. duvernoyi* the two tubercles at the plantar side of the proximal epiphysis are found in the same level and are connected by a narrow transverse ridge, the crests at the plantar side are retained, as in the metacarpals, down to the lower epiphysis (Geraads 1974) and the anteroposterior diameter of the lower epiphysis is relatively increased.

Between the two robust and long phalanges, of particular interest is the long forelimb one that presents osseous growths at its abaxial wall. Without any doubt the origin of these abnormalities is either a pathologic or a traumatic cause. Except from the osteophytic growths, bulgings are present at the lower part of both the axial and abaxial sides of the bone. This might be the outcome of, a callus from the healing of a fracture or some other traumatic injury. However, there is no evident displacement in the lower part of the bone to support with certainty a fracturing of the animal's digit. In the case of fracturing one would expect a displacement and deformation of the bone. Therefore, either an injury that caused an infection to the bone or a pathologic condition such as a bone disease is more likely responsible for these osteophytic increments. If the originating cause was a disease one would expect to find either strong deformation of the bones and/or of the articular surfaces, or presence of tubercles and osteophytic growths in a large area of the bone, or an irregular and damaged bone surface (as in arthritis, tuberculosis, bone tumors, etc.) that would extend over a large area or all over the bone and would probably indicate chronic conditions, cancer or infectious diseases (Steinbock 1976). The obvious signs of healing around the triangular tubercle and all around the infected area (Fig. 36 G), the overall good condition of the bone and the bone surfaces, and the intact and unquestionably healthy articular surfaces strongly support the traumatic cause. Therefore, the limited area of the infection and the localised lesion probably suggests an injury that caused an inflammation to the bone. This is possibly a good diagnostic indication for "acute pyogenic osteomyelitis by direct infection" (Steinbock 1976). According to Steinbock (1976) osteomyelitis is literally a generic term for the description of bone infection by various pathogenic microorganisms. However, its exact definition stands for the inflammation of the marrow cavity, while the inflammation of the periosteum is called periostitis and similarly the inflammation of the compact bone osteitis. Even an injury like a blow (Sigerist 1951) or a muscle infection or tenontitis can cause minor cases of periostitis.

The osteophytic growths though, suggest a more acute case. A sharp object was probably responsible for the animal's injury, which caused a deep penetrating wound that affected the surface of the bone. The wound was exposed and became infected by microorganisms. The animals defence reaction to the injury and the infection caused the inflammation of the infected bone. The triangular tubercle was probably the part of the bone that was separated from the living bone due either to splintering or to sequestration. In the first case it could be assumed that the impact and/or the sharpness of the injuring medium was enough to detach a splinter from the bone. In the latter, due to the infection a piece of bone might have been deprived from blood supply (necrosis) and subsequently died. The dead portion was then

detached (Steinbock 1976) from the living bone. The healing of the bone and the formation of new bone followed. The triangular tubercle was co-ossified with the bone and osteophytic growths developed around the infected area and around the abaxial side of the distal epiphysis, and thus this may have caused the abaxial expansion of the bone. A sinus cavity at the plantar side of the main osteophytic growth probably indicates the area where the infection started and persisted for longer before the full healing of the bone. The presence of the sinus cavity strongly suggests that the causal microorganisms were pyogenic bacteria (Steinbock 1976). The open wound probably provided drainage for the pus and thus prevented the expansion of the infection. However, at the early stages of the infection there is a possibility that pus might have penetrated and concentrated around the periosteum lifting it and formed the bulging seen at the axial side of the bone. The infection was probably limited to the periosteum and the compact bone and therefore it can be well described as periostitis and/or osteitis. The healing of the bone would definitely have taken several months, especially because the animal would have had to move frequently in search of food and to keep away from predators. Also, the fact that the injured bone was a digit, which had to support the weight of such a large animal like *H. duvernoyi*, would retard the healing even further. Such a deep injury and the inflammation that followed would have caused intense pain and lameness that would have limited the mobility of the animal and thus, would have made it vulnerable. Acute osteomyelitis may last for a very long period of time before healing and in severe cases it may became chronic (Steinbock 1976). According to Sigerist (1951) osteomyelitis has frequently been recognised not only in human remains but also in fossil animals. Moodie (1923a, 1923b, 1926) mentioned several examples of osteomyelitis from the fossil record; he identified osteomyelitis in the dorsal processes of the vertebrae of a Permian *Dimetrodon*, in several Jurassic and Cretaceous dinosaurs and a number of Pleistocene mammals (bisons, bears, lions, wolves).

H. duvernoyi has also been identified in both fossiliferous horizons (sites K1, K3 and K4) and it is well represented in both of them. The outstanding consistency in the length of some complete long bones from sites K1 and K4 probably indicate that they are associated and belong either to two specific individuals or to individuals with the same size. In site K1 the lengths of a right radius, a left metacarpal and a right metatarsal are just slightly lower than the lower limit of the known ranges of *H. duvernoyi* and thus, they probably belong to one individual. Similarly, in site K4 the lengths of a right radius, a left metacarpal, a left metatarsal and of a broken but very long left humerus, are close to the upper limit of the known ranges and therefore they should also belong to the same individual. Moreover, the

collected material from the two sites corresponds to at least two individuals in each site. The lack of cranial material as well as of cranial material with ossicones that could be related with a male individual has caused scepticism concerning the taxonomic relations of the species (Matthew 1929; Hamilton 1978). However, the unmolarised P_3 (Geraads, 1986), and among others the size and robusticity of the skeletal elements favour the direct relation with the Sivatheriinae.

(Subfamily GIRAFFINAE Zittel, 1893)

Genus BOHLINIA Matthew, 1929

Type species. Bohlinia attica Gaudry et Lartet, 1856, from Pikermi, Greece

Bohlinia attica Gaudry et Lartet, 1856

Diagnosis. A Giraffine of large size with a long neck and very long but slender long bones.

Material. Left humerus distal part (Ke 302), forelimb Phalanx I (Ke 131), left tibia (Ke 87, Ke 162), right distal part of tibia (Ke 89), left astragalus (Ke 156, Ke 99/50), left astragalus proximal part (Ke 99/52), right astragalus (Ke 99/51), left calcaneus (Ke 99/45), left scaphocuboideum (Ke 99/44), left proximal part of Mt_{III+IV} (Ke 163).

Description. To date, no cranial elements that could be attributed to this species have been discovered. However, a significant number of gracile postcranial elements (Appendices 3 – 13) are known, that were collected during the 1982 excavation, and thus they possibly came from site K1. Among them there is a distal part of a humerus with a broken epicondyle. The overall shape of the articular surface is rectangular as the heights of the trochlea and the condyle are almost the same. The epitrochlea is fairly long and its profile forms a slightly obtuse angle. The concave surface of the lateral trochlea is shallow and is confined laterally by a strong but low and rather wide keel. At the anterior side of the bone a shallow coronoid fossa is located in the middle of the bone approximately above the lateral trochlea. At the medial side, next to the coronoid fossa and just above the medial trochlea a relatively large, elongated and rounded articular facet can be easily distinguished. The supracondylar ridge

projects slightly laterally. The U-shaped olecranon fossa is wide, fairly deep and relatively long, with a well defined and sharp proximal end.

A long and gracile forelimb digit is also included in this species (Fig. 40C,D). The sagittal groove at the proximal extremity is wide and deep. The dorsal wall of the bone is straight without any bulging at the proximal part; however the dorsal narrow part of the distal articular surface is developed and protrudes dorsally. The abaxial wall is relatively steep. The abaxial-palmar eminence of the distal articular surface is very prominent as the abaxial crest of the palmar side fades away and disappears at the base of the eminence. At the palmar side of the proximal extremity the abaxial tuberosity is broken as well as the distal part of the axial one. Despite this the depression at the upper part of the groove between the two tuberosities is obviously fairly deep.

Two complete, very long but rather gracile specimens (Fig. 39A-D) and one distal part of a tibia are attributed to this species. The proximal part of the bone is not very developed. The tibial crest is weak and thin but fairly prominent and is accompanied by an equally weak and thin tuberosity. The tibial sulcus is shallow and forms an obtuse ankle with the tibial crest at the top of the epiphysis. The medial and lateral tuberosities at the posterior are weak and slightly prominent (Fig. 39B). However, a third prominent tuberosity is evident between the two tuberosities which confines the indentation of the popliteus (Fig. 39B). The upper part at the posterior of the bone under the epiphysis is concave. The slender diaphysis is curved along its longitudinal axis presenting a slight concave anteroposterior curve in the middle of the diaphysis (Fig. 39C) as well as two more transverse oriented curves (Fig. 39A, B, D); the first one is found at the proximal lateral side of the bone and the second one at the distal medial side. The overall shape of the lower epiphysis is quandrangular (Fig. 39F); however, its lateral wall is rounded. The medial malleolus is triangular, thin, with a wide base that extends towards the posterior, due to a gently slanting posterior edge. The medial tuberosity is long but low. At its posterior the groove of the flexor digitorum longus muscle is shallow but wide, with the opening of the groove directed posteriorly. The imprint of the muscle is long and tapers towards the diaphysis, and it is located at the posterior of the posteromedial crest of the bone (Fig. 39B). The anterior part of the articular surface for the malleolus is short and narrow. Conversely the posterior part is developed and although wide its lateral rim is rounded. The fibular furrow is relatively wide and shallow. The intercochlear crest is very developed and is wide and high (Fig. 39F). The medial cochlea is longer and more narrow than the lateral one. The long anterior eminent edge of the crest is narrow, triangularly

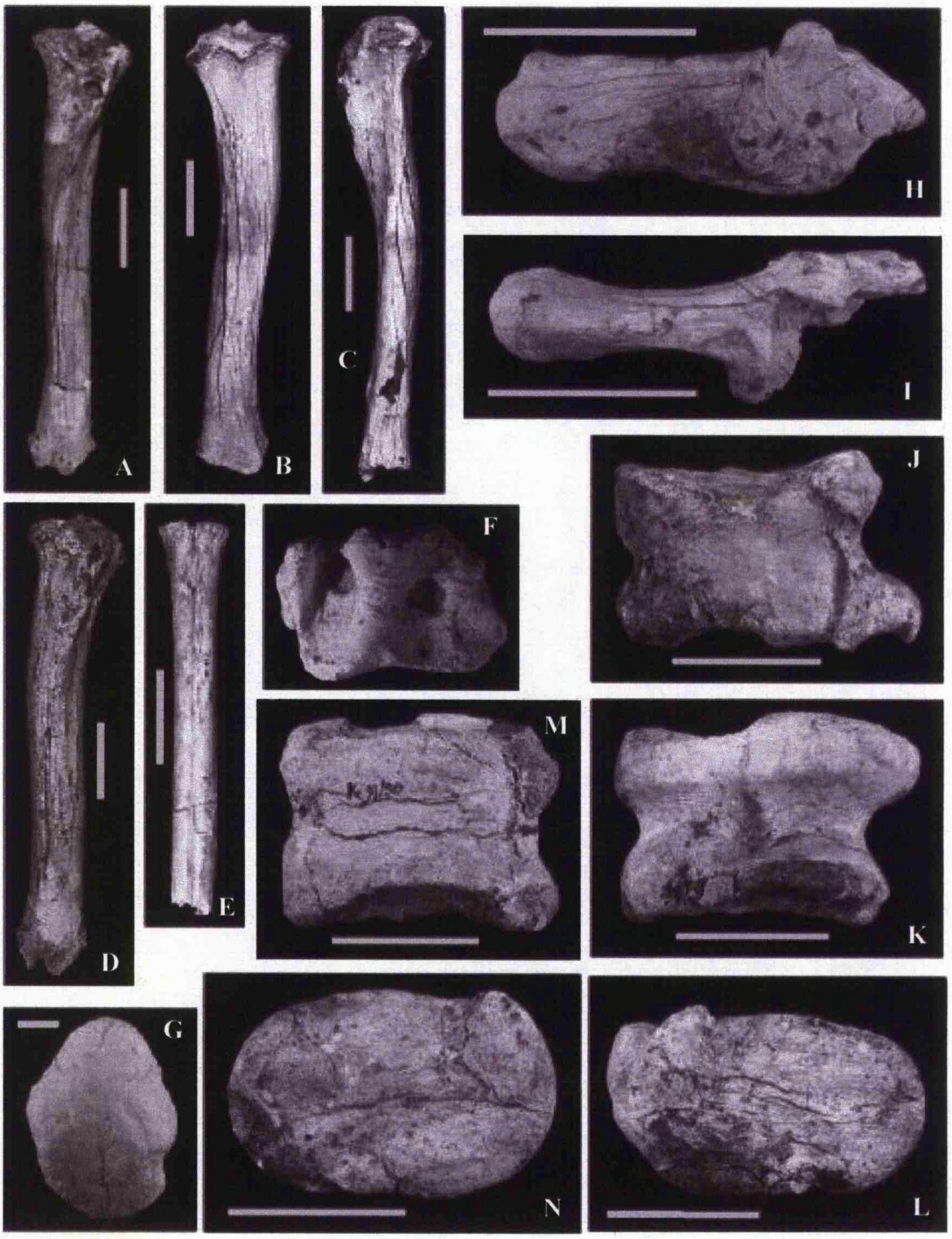

Figure 39: A. *B. attica*, left tibia, Ke 162, anterior view (scale bar 10cm). **B.** *B. attica*, left tibia, Ke 87, posterior view (scale bar 10cm). **C.** *B. attica*, left tibia, Ke 87, lateral view (scale bar 10cm). **D.** *B. attica*, left tibia, Ke 87, anterior view (scale bar 10cm). **E.** *B. attica*, left proximal part of Mt_{III+IV} Ke 163, anterior view (scale bar 10cm). **F.** *B. attica*, left tibia, Ke 87, distal view (transverse diameter 95.7mm). **G.** *B. attica*, left calcaneus, Ke 99/45, tuber calcanei (scale bar 2cm). **H.** *B. attica*, left calcaneus, Ke 99/45, medial view (scale bar 10cm). **I.** *B. attica*, left calcaneus, Ke 99/45, dorsal view (scale bar 10cm). **J.** *B. attica*, right astragalus, Ke 99/51, posterior view (scale bar 5cm). **K.** *B. attica*, right astragalus, Ke 99/51, anterior view (scale bar 5cm). **L.** *B. attica*, right astragalus, Ke 99/51, medial view (scale bar 5cm). **M.** *B. attica*, right astragalus, Ke 99/51, posterior view (scale bar 5cm). **N.** *B. attica*, right astragalus, Ke 99/51, medial view (scale bar 5cm).

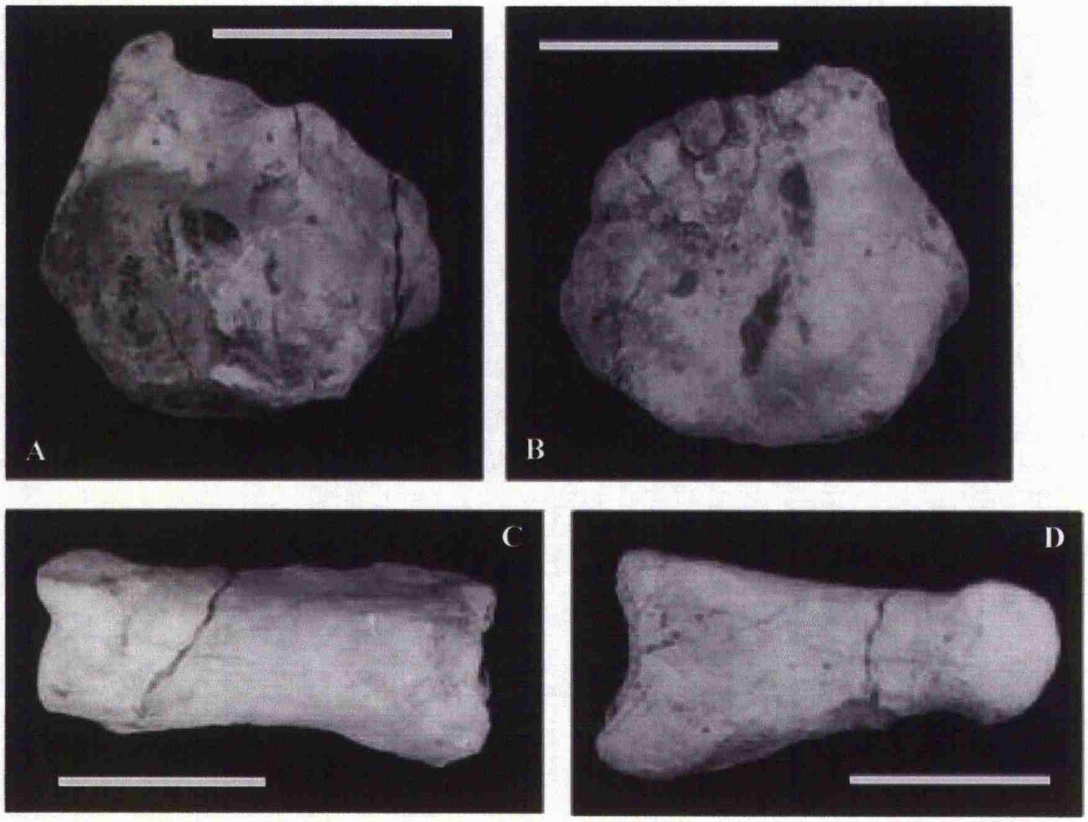

Figure 40: A. *B. attica*, left scaphocuboideum, Ke 99/44, proximal view (scale bar 5cm). **B.** *B. attica*, left scaphocuboideum, Ke 99/44, distal view (scale bar 5cm). **C.** *B. attica*, Phalanx I, Ke 131, anterior view (scale bar 5cm). **D.** *B. attica*, Phalanx I, Ke 131, axial view (scale bar 5cm).

shaped, with a rather acute peak. At the anterior of the eminence a feeble, narrow, short and shallow concavity is present. At the posterior the medial eminence is well developed and long. At its lateral side, the furrow at the posterior of the intertrochlear crest is shallow and short.

Four astragali are attributed to this species, of which two are complete and two are broken. With a first look on the specimens one can easily separate them into two different forms: one robust and wide form (specimens Ke 156 and Ke 99/51) (Fig. 39J-L) and a second one more gracile and narrow (specimens Ke 99/50 and Ke 99/52) (Fig. 39M, N). Despite this, the overall morphology is identical. The strong and thick lateral crest of the proximal trochlea ends to the posterior to an equally strong and triangular shaped edge. The anterior of the medial crest is thin but gradually it thickens towards the posterior due to a medially protruding rim (Fig. 39K). Its posteriormost edge is prominent and projects towards the posterior. The anterior part of the lateral crest projects laterally, while the anterior prominent edge of the medial crest projects medially. The intertrochlear groove is wide, however, in the gracile form the proximal part of the groove becomes narrower. The furrow that separates the proximal from the plantar trochlea is continuous (Fig. 39J). It is wide at the base of the lateral trochlear edge forming a cavity and it becomes very narrow towards the medial trochlear edge. The rims of the former project laterally, forming a very prominent posterolateral tubercle. The plantar trochlea is slightly concave. The two crests of the trochlea are found at the same level and although the medial one presents a concave curve they can be considered as parallel (Fig. 39J, M). The proximal edge of the medial curved crest points medially towards the posterior edge of the medial proximal trochlear crest, where they almost contact. Owing to this a concave surface is formed at the posterior part of the medial side of the bone. At the distal part of the medial crest a feeble notch is just discernable as well as the sliding surface of the medial concavity of the scaphocuboideum. At the lateral side of the bone, the proximal part of the furrow for the malleolus is very shallow. Its posterior part and also lateral side of the proximal lateral trochlear crest is open laterally forming a short but very wide groove, where the lateral tubercle comprises its distal ridge and the thin prominent rim of the trochlear crest its proximal ridge. Distally the furrow ends in a deep rounded depression. A strong ridge separates it from the deep concavity of the sinus calcanei. The sinus is open anteriorly. The ellipsoid facet at the bottom is small. The two crests of the distal trochlea are strong. The intertrochlear groove is wide and shallow in the wide form (Fig. 39M) but it is narrow and deep in the narrow form (Fig. 39J). A relatively wide and deep furrow separates

the two medial trochleas at the anterior. The anterior cavity is wide and it is deeper in the narrow form.

A long complete calcaneus from site K1 is another specimen of this species (Fig. 39G-I). The body of this gracile bone is rectangular. The top of the articular surface for the malleolus is found higher than the beak of the dorsal crest. The posterodorsal tubercle is strong. The triangular tuber calcanei is fairly symmetrical (Fig. 39G). The index "tuber calcanei width / tuber calcanei height" is 0.70 indicating a fairly narrow tuber. The groove for the flexor digitorum superficialis is very shallow and relatively wide. The sustentaculum tali is strong and wide with the articular surface for the astragalus being slightly concave (Fig. 39H, I). The furrow of the sinus tali is almost imperceptible. At its plantar side a strong and high ridge is clear. The articular facet for the astragalus is concave and slightly shorter than the articular surface for the scaphocuboideum. The posterior part of the articular surface for the malleolus is wide and strong, while the anterior part is wide and relatively long. The articular surface for the scaphocuboideum is curved, concave and presents a slight torsion.

Only one specimen of scaphocuboideum was related to this species (Fig. 40A, B). The plantar peak of the medial concavity is strong and high. It is turned dorsally so that the concavity forms a deeper curve. The plantar peak of the lateral concavity is developed and relatively high but narrow. Therefore, the part of the concavity at the dorsal side of the peak is much narrower than at the main part. The valley between the two peaks is wide and is found relatively high in the bone. The lateral concavity is significantly shorter than the medial one. The ridge between the two concavities is developed and high. Dorsally, it culminates to a very developed, wide and high triangular eminence. At the plantar side the ridge is confined by a large and deep indentation. The plantar edge of the articular surface for the calcaneus stops behind the peak of the lateral concavity (Fig. 40A). At the plantar side of the bone two grooves are easily identified: a major wide groove next to the medial prominent vertical crest as a succession of the valley between the two peaks and a second, narrow but well defined one next to the latter that starts at the plantar end of the calcaneus articular surface and ends to the large foramen in the middle of the plantar side of the bone. The lateral tuberosity is developed and its position is fairly lateral. The groove for the peroneus longus muscle at the lateral side is very weak, however, it gets narrow and deep at its distal part. It continues at the distal side where it separates the ellipsoid and wide posterior metatarse facet from the anterior articular surface. Also, another distinct feature at the distal side is the deepening of the plantar part of the articular surface for the medial cuneiform (Fig. 40B). Therefore, the plantar part of

the surface is found below the level of the posteromedial part of the bone. At the medial side of the bone the groove for the tibialis cranialis muscle is wide and shallow. Its plantar ridge is very developed and forms a distinct and strong tuberosity.

A proximal part of a gracile metatarsal which appears to be fairly elongated has been also collected (Fig. 39 E). The medial and lateral tubercles at the plantar side of the proximal epiphysis are slightly prominent and are found approximately at the same level (Fig. 32B). However the medial tubercle, which contains the large rounded articular surface of the medial cuneiform, is more developed and also it projects slightly medially. A third well developed and fairly prominent tubercle is found between the two tubercles and it is situated closer to the medial tubercle. At its upper surface an eminent ridge is clear. A deep and wide furrow separates it from the lateral tubercle and a narrow and shallow furrow from the medial tubercle. The groove for the peroneus longus muscle at the lateral part of the articular surface is long and fairly deep. At the anterior the medial crest is more developed and the sulcus starts relatively high in the bone almost below the rim of the epiphysis. The preserved portion of the diaphysis is narrow (transverse diameter) and slender. The posterior sulcus is narrow and relatively shallow.

Discussion. Among the material, the presence of a large sized, gracile species with elongated and slender limb bones is evident. The elongated and slender limb bones suggest that this species belongs to the giraffines, and to be more precise to the late Miocene representative of the subfamily, *Bohlinia*. Unlike the previously mentioned late Miocene giraffid genera, the presence of *Bohlinia* is limited in a relatively restricted palaeogeographic area. To date, *Bohlinia* has been reported in a number of localities across Greece, South Bulgaria, Turkey and Iran. It is generally accepted that all the material discovered until now and associated with this genus is attributed to only one species, *B. attica*. However, a number of authors considered the existence of a second species of *Bohlinia*, found in the same localities as *B. attica* (Pikermi, Ravin de la Pluie, Kalimanci, Maragha, Nikiti) and actually coexisting with it. A small number of smaller and very slender bones that were recovered from Pikermi, Ravin de la Pluie, Kalimanci, and Maragha and were associated with *Bohlinia* were attributed to the species *B. sp.* (Geraads 1974) or the synonym given by Gaudry (1862-67) *Camelopardalis* (*Orasius*) *speciosa*? (Geraads 1974; Gaudry 1862-67; Kojumdgieva *et al.* 1982). The values of the dimensions in some of the postcranial material (Geraads 1974) shows that the metrical differences of these specimens with the largest of the specimens of *B. attica* is always less than 20%. This difference between the largest specimens belonging to

males and the smaller female ones in modern giraffes, *Giraffa camelopardalis* (Linnaeus 1758), can be over 20% (measurements by the author, FMNH and Harris 1976). Therefore, it is clear that possibly all the material belongs to one species of *Bohlinia* and the difference in size can be attributed to sexual dimorphism. Thus, the smaller bones represent gracile female individuals. Kostopoulos *et al.* (1996) also proposed the existence of another new species of *Bohlinia*, *B. nikitiae* from Nikiti (Nikiti 1). Their determination was based on an incomplete and deformed skull, shorter than *B. attica* with a generally longer toothrow. According to the authors the toothrow is metrically closer to the hornless skull of *P. coelophrys* from Ravin de la Pluie, and furthermore, the two skulls share a number of similar morphological characters. Hence, they considered that the sample from Ravin de la Pluie possibly represents a female individual of *B. nikitiae*. The existence of only one specimen makes questionable the validity of this species. The similarities with *P. coelophrys* may possibly indicate that the Nikiti specimen represents a male individual of *P. coelophrys*. Therefore for the time being, only the presence of one species of *Bohlinia* can be accepted with confidence, namely *B. attica*.

Unfortunately, to date cranial and teeth specimens are absent from the available material. However, the slenderness and elongation of the postcranial material is a very distinctive feature of *B. attica*. The dimensions of the distal humerus part are within the range of *B. attica* (Fig. 15). The distal transverse diameter ranges in *B. attica* from Pikermi, Maragha and the localities of Axios Valey between 90-124 mm (NHML authors measurements; Geraads 1974, 1979; deMecquenem 1924). The range of *S. boissieri* from Samos (NHML) is 84.5-109.6 mm, while the diameter in *P. coelophrys* from Maragha is 89 mm (Rodler and Weithofer 1890), in *P. expectans* (*P. coelophrys*) from Sebastopol is 102 mm and in *P. sp* from site K4 98 mm. It is clear that the distal DT of the studied specimen is within the range of *B. attica*, but also within the range of *S. boissieri* and close to the value of *P. sp.* (Fig. 15). However, the morphology of the of the bone leaves no doubt that the specimen belongs to *B. attica*. The rectangular shape of the trochlea with the shallow trochlear furrow and the low lateral trochlea keel characterise *Bohlinia*. Conversely, the higher trochlea, the deep furrow and the high keel are typical in *Palaeotragus* and *Samotherium*. The mesial position of the coronoid fossa and the presence of the ellipsoid facet above the medial trochlea at the anterior of the bone are two more features of *B. attica*. The latter has been also identified in the two humerus samples of *B. attica* from Pikermi stored in the collections of NHML. The same character is also present and was recognised in modern giraffe (*G. camelopardalis*) humerus specimens stored in the zoological collections of FMNH. This feature was not found in the humerus of other giraffid taxa that were examined by the author; *Helladotherium*, *Samotherium*,

Palaeotragus, *Sivatherium*, and modern Okapi (*Okapia johnstoni*, Sclatter 1901). Also it is not present in *Decennatherium pachecoi* (Crusafont 1952) according to a drawing of a distal humerus part from Los Valles de Fuentiduena (Spain) featured by Morales and Soria (text fig. 11, 1981). It seems that this character is present only in the tall giraffines which own very elongated limb bones. Probably, when a *B. attica* (or a *G. camelopardalis*) had to bend its fore limbs in order to lie down on the ground or even more to access something with the mouth at the level of the ground (or even lower), its long limbs would not make this an easy task. Despite the long neck, modern giraffes (and probably their distant ancestors *B. attica* too) cannot reach the ground without bending their fore limbs. It has been observed and it is well known, that when giraffes drink water (Solounias and Moelleken 1993) and especially when the water level is below the level of the bank of the lake/river/pond they need quite some effort to bend their fore limbs to reach the water. They even spread apart their fore and hind limbs to get their bodies even closer to the ground. During bending, the humerus-radius joints would then have to support most of the animal's weight. The two bones would then come in contact. These contact points are: for the humerus the medial part above the medial trochlea, and for the radius, the anterior rim of the medial trochlear cavity. The regular contact of the two bones has formed this facet.

As expected the slenderness of the first forelimb digit is a very distinctive feature for *B. attica*. The digits of *H .duvernoyi* and *S. major* are more robust especially at their proximal part. In *H. duvernoyi* the proximal part of the dorsal wall presents a strong bulging, which is more feeble in *S. major*. In this specimen the dorsal wall is straight except for the dorsal part of the distal epiphysis which projects dorsally. The dimensions of the bone are within the range of *B. attica*.

The range of the length of the tibia of *B. attica* from Pikermi is 600-625 mm (Gaudry 1862-67; Geraads 1974) and in the specimens from Salonica it is 575 mm and from Maragha it is 640 mm (Geraads 1974). Similarly, the range of the tibia of *H. duvernoyi* from the localities of Pikermi, Nikiti 1 and Maragha is between 490-580 mm (authors measurements NHML; Gaudry 1862-67; Geraads 1974; Kostopoulos et al. 1996). It is clear that the tibiae of *B. attica* are generally longer than *H. duvernoyi* and clearly longer than S. *major* (Fig. 23). The length of specimen Ke 87 is found within the range of *B. attica*, whereas in specimen Ke 162 it is noticeably shorter and is found within the range of *H. duvernoyi* and even that of *S. major*. However, the slenderness of both specimens clearly differentiates them from both species and thus indicates their association with *B. attica*. Moreover, the presence of a mesial tubercle

between the medial and lateral tubercles at the posterior of the proximal epiphysis is another indication that they belong to *B. attica* (Geraads 1974). In contrast to the well developed proximal part in *H. duvernoyi* and *S. major*, the weakness of this part of the bone in *B. attica* is obvious. The curved diaphysis, the long imprint of the flexor digitorum muscle and its position are two more distinctive features. At the lower epiphysis the wide medial malleolus, the narrow anterior eminence of the intercochlear crest, the short and narrow anterior articular surface for the malleolus and the rounded lateral wall of the epiphysis also characterise *B. attica*. Although the short Ke 162 is significantly shorter than other known tibia specimens of *B. attica*, its morphology strongly indicates that it belongs to this species and most likely represents a gracile female individual. It is only 14.1% shorter than the longest known specimen from Maragha, and it is within the difference percentage that is observed as discussed above in recent giraffes.

Even a cursory examination of the four astragalus specimens is enough to realise the presence of two distinct forms. Despite the overall morphological similarity the metrical differences are obvious. The clear distinction between the two groups is also verified by the diagrams of the various metrical parameters (Fig. 26). Except from the size difference it seems that the larger specimens are relatively wider and the furrows of the proximal and distal trochleas in the small form are relatively deeper. Both forms are larger than *S. boissieri* and clearly smaller than *H. duvernoyi*. Also, in *H. duvernoyi* the well developed and deep notch at the medial crest of the plantar trochlea is another distinctive feature. Geraads (1974, 1979) suggested that this notch is not present in *B. attica* but that a profound one is only found in *Giraffa*. However, a feeble and very shallow notch was identified in all four astragalus specimens. The overall size and in particular some dimensions of the large form like the proximal and distal widths are similar with *S. major* as well as with *S. neumayri*. The presence of a rounded depression at the distal lateral margin of the plantar trochlea, the absence of the notch and increased anteroposterior diameter in *Samotherium* differentiates it clearly from *B. attica*. Furthermore, the direction of the proximal edge of the medial crest of the plantar trochlea in *B. attica* is directed towards the posterior edge of the medial crest of the proximal trochlea, whereas in *Samotherium* it is directed towards the groove of the trochlea. The two forms probably indicate the existence of sexual dimorphism in the skeleton and therefore represent male and female individuals. The largest difference between the larger and the smaller specimen was observed for the distal transverse diameter and was 12%.

The gracility and the rectangular shape of the body of the calcaneus make evident the association with *B. attica* and the distinction from *H. duvernoyi* and *Samotherium* (Fig. 27). The symmetricity of the tuber calcanei is another distinctive character (Geraads, 1974). Also, the low value of its "width/height" index is considerably lower than the other two taxa and suggests a narrower and relatively longer tuber (Fig. 28). The relatively long articular facet for the astragalus at the anterior is another feature. The only specimen of scaphocuboideum that is related to this species can be correlated at least metrically with the gracile astragalus group. It is considerably smaller than *H. duvernoyi* and *S. major* and its dimensions are within the range of *B. attica* and *S. boissieri* (Fig. 29). Although the valley between the two peaks is found relatively high as in *Samotherium*, the lateral concavity is shorter than the lateral one and the posterior edge of the articular surface for the calcaneus is found at the plantar side of the lateral peak, indicating the association of the specimen with *B. attica*. The well developed dorsal eminence of the ridge between the concavities and the existence of two muscle grooves at the plantar side of the bone are probably features of the *B. attica* as well. Also, the relatively long posterior articular facet for the metatarsal is according to Geraads (1974, 1979) another diagnostic character for *B. attica*. This facet as mentioned above is also found in *H. duvernoyi* but it is relatively smaller.

The gracile proximal metatarsal part is smaller than the two studied large giraffid taxa and it is found within the upper range of *S. boissieri* (Fig. 38). However, its morphology shows that it is different from both *Samotherium* and *Helladotherium*. The medial and lateral tubercles at the plantar side of the bone are found in the same level as in *H. duvernoyi* (Fig. 32B). However, the third tubercle in the middle is well developed and prominent located closer to the medial one. Contrary, in *H. duvernoyi* the tubercle is weak with a mesial position. The relatively narrow diaphysis and the narrow and shallow posterior sulcus are also indicative of *B. attica*.

All the available material that has been attributed to *B. attica* was collected during the 1982 excavations. Unfortunately, the recovery of more material during later excavations was not possible. As it has been argued above, the material from the 1982 excavations was most likely collected from site K1. The other three giraffid species described above and found in site K1 are also present in the material from 1982 excavations, as well as other taxa such as the suids. Therefore, it is clear that the presence of *B. attica* has been only certified in the upper horizon. Among the studied material at least three individuals are represented, of which 2 probably belonged to females. The sexual dimorphism in *B. attica* as with modern *G. camelopardalis*,

must be very strong. Specimens with significant size difference, and as it was observed in the case of the astragalus even with a slight morphological difference, probably indicate the presence of small and gracile females and of larger and more robust males. Two forms or groups were identified in more than one skeletal element, the tibia, the astragalus and also the correlation of the gracile scaphocuboideum with the small size group was also possible. This exhibits some sort of noticeable consistency. Diagrams also, demonstrated this clear separation. Inserting in the diagrams values of specimens from other localities the picture not only remained the same but it became clearer. Even the specimens that were attributed to *B. sp.* (Geraads 1974) do fit, as it has been shown, in a smaller female group.

SEXUAL DIMORPHISM

As it has been noted above the post cranial elements of *B. attica*, present differences in the size and as in the case of the astragalus, even minor differences in the morphology. These differences can be attributed to sexual dimorphism. The presence or absence of cranial appendages in ruminants has always been considered as a diagnostic feature for the distinction of males and females. Nevertheless, there are examples where both males and females retain them, such as in the modern cattle and even in modern *G. camelopardalis*, although their size in the males is considerably larger than in females. Skulls without ossicones such as the complete skull of *H. duvernoyi* from Pikermi (Gaudry 1862-1867), the skull of *S. major* from Taskinpasa (Senyurek 1954), the skull of *P. coelophrys* from Ravin de la Pluie (Geraads 1978) were thus interpreted as female individuals. However, complete skulls or ossicones have not been unearthed from Kerassia yet. Except from the presence and size of the cranial appendages, the distinction of males from females can be based on their size and their robusticity. The body mass and the size of the skeletal elements are usually significantly higher in males. Hence, the post cranial elements are expected to be longer and more robust in males.

The examination of skeletal material from modern *G. camelopardalis* and *O. johnstoni* (FMNH) revealed a marked sexual dimorphism in both species. The dimorphism in the post cranial material is expressed as a difference in the size (length or height) and the robusticity of the skeletal elements. Wilson (1982) stated that generally the limb bones of males in cattle are slightly longer and a lot broader than in females. In addition there was great overlap in the length values while the dimorphism was more marked in the breadth values (Wilson 1982).

specimen number	species	locality	sex	length	DTdia	Robusticity index
127878	*G. camelopardalis*	modern (FMNH)	male	750,00	61,20	8,10
104906	*G. camelopardalis*	modern (FMNH)	female	620,00	42,90	6,90
127880	*G. camelopardalis*	modern (FMNH)	female	700,00	46,20	6,60
26066	*O. johnstoni*	modern (FMNH)	male	320,00	31,80	9,90
58839	*O. johnstoni*	modern (FMNH)	female	315,00	28,10	8,90
max	*S. boissieri*	Samos (NHML)		412,20	48,30	11,78
min	*S. boissieri*	Samos (NHML)		370,90	33,70	8,84
max	*H. duvernoyi*			462,70	61,90	14,05
min	*H. duvernoyi*			429,80	47,60	10,40

Table 1: The length, the transverse diameter in the middle of the diaphysis and the robusticity index of metatarsals for male and female individuals of modern *G. camelopardalis* and *O. johnstoni*, and the respective minimum and maximum values of metatarsals of *S. boissieri* from Samos (NHML) and *H. duvernoyi* from a number of different Late Miocene localities.

Usually, the numbers of specimens of single elements collected from one locality are not enough to provide sexual dimorphism correlations. However, some collections, like the one of *S. boissieri* from the lower horizons of Samos in the NHML, contain enough specimens for some of the skeletal elements to provide such correlations. In most scatter diagrams it is obvious that the range of the values is very wide, and especially in diagrams where the robusticity is presented against length where sometimes, there is an obvious separation in two groups. Also, if the specimens of the same species from different localities are represented in the same diagram the same things are observed: wide range of values and separation into two groups. Even with the paucity of single elements of the different species from Kerassia it was clear that sometimes two size groups were represented in a certain species. This has been noted not only in *B. attica* but also in *P. rouenii*, *S. major* and *H. duvernoyi*; two large mandibles and a long metacarpal are found in the upper size range of *P. rouenii*, two sizes of long bones that represent the two extreme size limits of *H. duvernoyi*, and the very large mandible of *S. major* from site K4.

It is not within the scope of this paper to study the sexual dimorphism of the giraffids but only to point out the presence of sexual dimorphism in the skeletal elements and in particular in the limb bones of the giraffes from Kerassia. To show sexual dimorphism the following discussion will be restricted in only one element, the metatarsal bone. Table 1 includes the length, the transverse diameter of the diaphysis and the robusticity index values of male and female individuals of the two modern giraffe species plus the minimum and maximum (that probably represent male and female) values of *S. boissieri* from Samos and *H. duvernoyi* from Kerassia and other late Miocene localities. Although the number of measured specimens is low, however it is still clear that the difference between males and females (or maximum and minimum values) is far more marked between the transverse diameters and the robusticity indices of the specimens, than between their lengths. The difference between the transverse diameters in *S. boissieri* and *H. duvernoyi* is three times more than between the lengths. This seems to agree with the Wilson (1982) that sexual dimorphism in cattle is more marked in the breadth values. Parameters that indicate the robusticity of long bones are possibly more suitable to be used for the discrimination between males and females. The two column diagrams in figures 41A and 42A depict the distribution of the transverse diameters of the diaphysis in *S. boissieri* and *H. duvernoyi*. It is clear in both plots that there are two groups. It can be assumed that the boundary between the two groups and therefore between males and females is found between 39 and 41 mm for *S. boissieri* and between 52 and 55 mm for *H. duvernoyi*. Similarly, in figures 41B and 42 B the distributions of the robusticity indices for

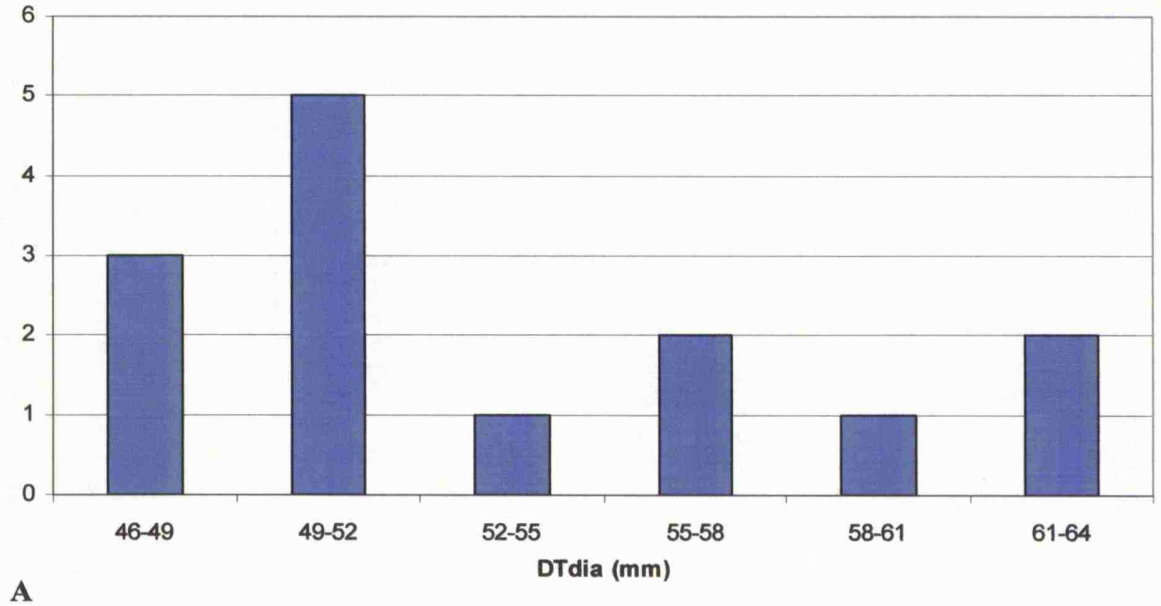

A

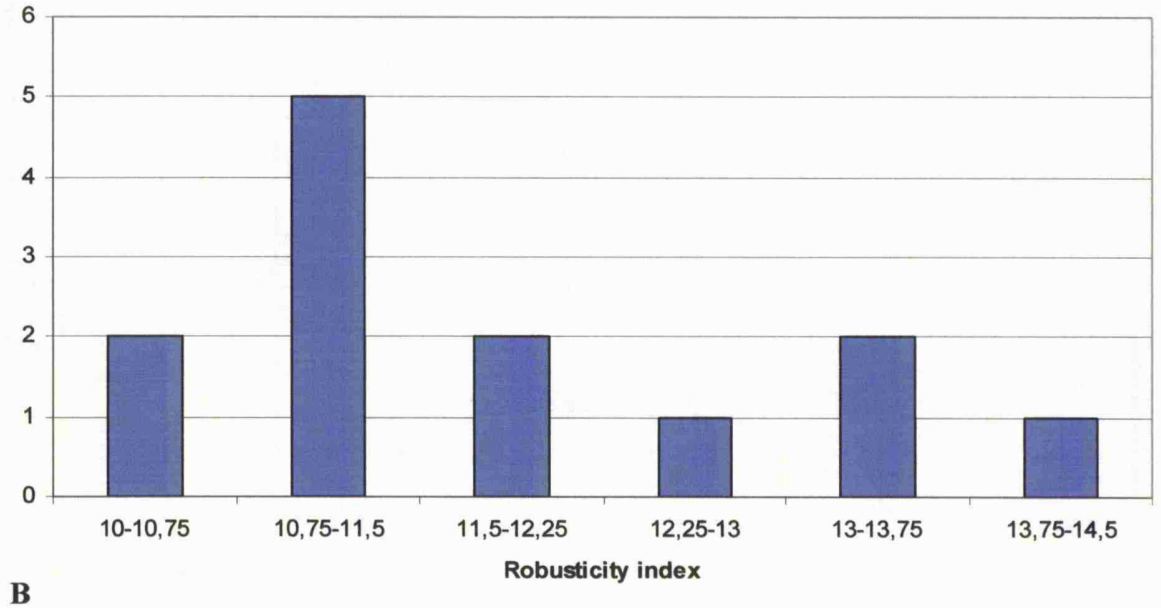

B

Figure 41: Two histograms of **A.** a set of 14 values of transverse diameters in the middle of the diaphysis and **B.** a set of 13 values of robusticity indices for the metatarsals of *H. duvernoyi* from different Late Miocene localities. In both histograms the presence of two groups is evident, which is attributed to sexual dimorphism.

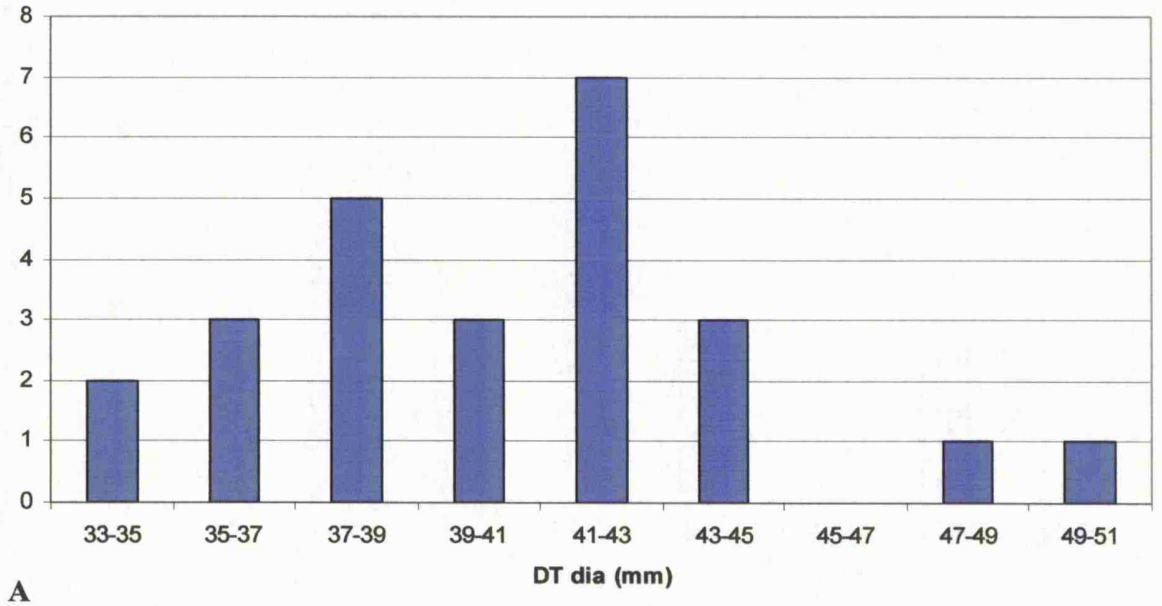

A

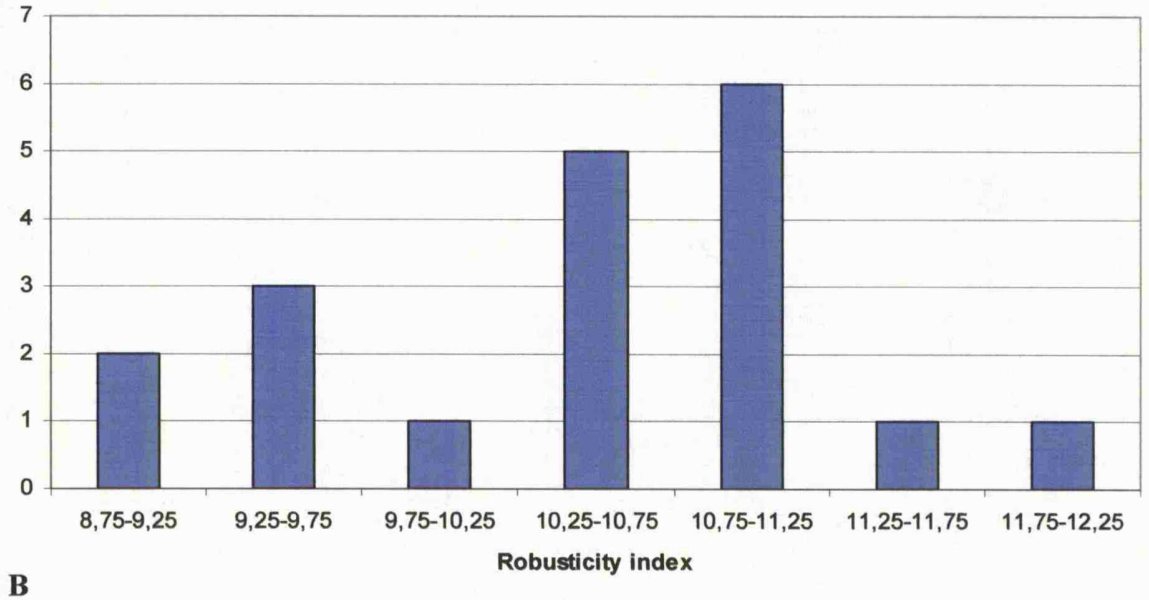

B

Figure 42: Two histograms of **A.** a set of 23 values of transverse diameters of the middle of the diaphysis and **B.** a set of 19 values of robusticity indices for the metatarsals of *S. boissieri* from the lower fossiliferous layers (Old Mill Beds) of Samos stored in NHML. In both histograms the presence of two groups is evident, which again is attributed to sexual dimorphism.

the two species also depict the presence of two groups; of gracile females and robust males. The collection of more data and statistical analysis plus the correlation with the other skeletal elements will provide more sufficient and compelling results about the sexual dimorphism of fossil and extant giraffidae.

BIOCHRONOLOGY AND BIOGEOGRAPHY

The study of the locality of Kerassia is still at the initial stages, therefore, a complete picture of the fauna and its interrelations with other late Miocene localities is still not clear. This paper is a contribution towards this aim. A significant number of giraffids, which are present in the two fossiliferous horizons, provide an insight into the biochronological position of Kerassia. Stratigraphically, the lower horizon is situated 7 meters below the upper one. In total, five species have been identified in the two fossiliferous horizons; *P. rouenii*, *P. sp.*, *S. major* and *H. duvernoyi* were found in the lower horizon, and *P. rouenii*, *S. major*, *H. duvernoyi* and *B. attica* in the upper one.

The comparison of these species from both horizons with giraffid taxa from other late Miocene Eurasian localities suggests a Turolian age for the locality of Kerassia. The European Land Mammal Zones can provide a more accurate estimation of the age of Kerassia as the chronostratigraphic range for most of the above species is well defined. Gentry and Heizmann (1996) and Gentry *et al.* (1999) gave detailed biochronologic attributions for the listed species. In the former paper the range for *P. rouenii* was considered as MN9-MN12 (Mammal Neogene), while in the latter paper as MN10-MN13. However, its presence in Ditiko 2 supports the MN13 extension (Geraads 1978; Bonis et Koufos 1999). Both papers agree that the age range for *B. attica* is MN10-MN13 and for *H. duvernoyi* the age range is MN11-MN13. According to Bonis and Koufos (1999) the presence of *H. duvernoyi* in Nikiti 1 suggests also a late MN10 age for this species. The range for *P. coelophrys*, if *P. sp.* is indeed associated with it, is MN9-MN12. All these species have a wide biostratigraphic range and they cannot provide any other more precise dating for Kerassia than Turolian. However, the presence of *S. major* provides more accuracy. As mentioned above, in Samos *S. major* is only found in the upper fossiliferous layers or Main Bone Beds, while *S. boissieri* is found in the lower layers or Old Mill Beds. It is generally accepted now that the Old Mill Beds characterise the Early Turolian (MN11), whereas the Main Bone beds characterise Middle Turolian (MN12) (Steininger *et al.* 1996; Bernor *et al.* 1996; Koufos *et al.* 1997; Kostopoulos

et al. 2003). Therefore, it can be assumed that *S. boissieri* characterises MN11 or Early Turolian, while *S. major* is characteristic for MN12 or Middle Turolian. In Kerassia *S. major* was identified in both fossiliferous horizons indicating that the age of Kerassia is Middle Turolian or MN12.

S. major has been also identified in Vathylakkos 3, Kemikliteppe A-B and Taskinpasa. This probably suggests that the faunas in these five localities were synchronous and were represented in the MN12. However, Vathylakkos (Kostopoulos *et al.* 2003; Kostopoulos pers. comm.) according to magnetostratigraphic data and the presence of taxa that exhibit characters from MN11, such as *Nisidorcas planicornis*, indicates a slightly older age; it has been attributed to MN11/12 (Bonis and Koufos 1999; Kostopoulos *et al.* 2003). In Samos a long stratigraphic sequence and the availability of good radiometric and magnetostratigraphic data provide a good reference locality with an age span from MN11 to the base of MN13. Swisher III (1996) provided more precise radiometric dating data for the different fossiliferous beds of Samos; the age for the Old Mill Beds was estimated to 8.33 ±0.05 Ma, the estimated age for the rich upper Main Bone Beds was ≥7.1 Ma, while the maximum age for the lower Main Bone Beds and more specifically for Brown's site Q4 (Solounias 1981) was estimated as being 7.7 Ma. Magnetostratigraphic data from Kemiklitepe (Sen *et al.* 1994) seem to correlate well with Samos and it is rather clear that Kemiklitepe A-B can be related with the upper Main Bone Beds. Although magnetostratigraphic or other dating data are not available for Kerassia, it can be assumed that at least the upper horizon can be also related with Kemiklitepe A-B and the upper Main Bone Beds of Samos. Possibly the slightly older Vathylakkos 3 can be related to the lower Main Bone Beds of Samos, and similarly, the lower horizon from Kerassia could also be related with them despite the small stratigraphic difference between the two fossiliferous horizons at Kerassia. In Kemiklitepe the upper horizon is fifteen meters above the lower one, nevertheless Sen *et al.* (1994) suggested that the lower horizon has an MN11 and respectively the upper one a MN12 age. They considered that this was prior to sedimentary gaps and a low sedimentation rate. Such a hypothesis can also be a possible scenario for Kerassia; a relatively low sedimentation rate, and gaps in the sedimentation. The latter can be easily observed as some of the contacts of the beds between the two horizons were sharp, without any significant change in their lithology, and others indicated mature paleosols; and thus this evinces periods with minor or no sedimentation and possible erosion.

A problem, however, arises with the calibration of the chronological boundary between MN11 and MN12. Steininger (1999) suggested that the boundary between the two zones should be calibrated according to palaeomagnetic calculations from Opdyke *et al.* (1997) from Neogene localities in Eastern Spain, to 8 Ma. Conversely, Krijgsman *et al.* (1996), Sen (1996, 1997), Agusti *et al.* (2001), Kostopoulos *et al.* (2003) suggested a calibration of the boundary at 7.5 Ma. A number of authors in the last few years have expressed their concern about the use of mammal Neogene (MN) units and their boundaries and raised the problems of correlating the different faunas and localities (Agusti 1999; van Dam *et al.* 2001; Sen 2001). The MN units were originally established (Mein 1975) to serve as a common resultant for the correlation of the European terrestrial record. They were based on Western European localities and faunas and more specifically on Spanish ones without considering faunal differences in space and time (Agusti 1999). This becomes more evident in the comparisons with the different faunas and localities from the Eastern Mediterranean (Sen 2001). However, as Sen (2001) pointed out for the moment there is no other mammal zonation and the need for a common language between mammal workers supports its use. Although there are problems with the MN unit zonation, it is considered here appropriate to use Sen's magnetostratigraphic data and calibrations, as his data come from the Eastern Meditarranean. Thus, the MN11/MN12 boundary will be considered as 7.5 Ma. Kerassia's upper horizon, Kemiklitepe A-B and the upper Main Bone Beds of Samos correspond to an early MN12 age, while Kerassia's lower horizon, Vathylakkos 3 and the lower upper Main Bone Beds of Samos are placed around the boundary MN11/MN12. These results are in agreement with previous work on Kerassia, for example, Made and Moya-Sola (1989) in their study of the suid material from the upper horizon (site K1) suggested a late MN12 age for Kerassia. Conversely, in their study Kostopoulos *et al.* (2001) considered that the suid material presented some primitive characters and suggested an MN11-MN12 age. Roussiakis *et al.* (2003) in their study of the carnivores of Kerassia and Theodorou *et al.* (2003) in their preliminary report on the locality and the fauna also suggested an MN11-MN12 age. The study of the fauna and especially of the hipparions and the bovids will provide clear and more accurate correlations. For the moment, the presence of *S. major* in Kerassia indicates a MN12 age, and most likely an early MN12 age. The two horizons of Kerassia seem to correlate well with the Main Bone Beds of Samos, and more specifically the upper horizon with the upper Main Bone Beds of Samos dated at /7.1 Ma and the lower one with the lower Main Bone Beds of Samos dated at the maximum of 7.7 Ma (Swisher 1996).

As it has been already mentioned two of the four genera found in Kerassia during the late Miocene were widely spread across Eurasia. *Palaeotragus* expanded from China to Spain, while *Samotherium* did not extend beyond the southern Balkans. The other two, as it has been also noted, were limited to western Eurasia. At the species level, the palaeogeographic area that the four species (or five if *P. sp.* is associated with *P. coelophrys*) occupied was more restricted. With the exception of *S. major* the other four species are very common representatives of the late Miocene and particularly of the late Vallesian and Turolian of the Southeastern Europe and Southwestern Asia including the southern territories of the former Soviet republics. *P. rouenii* has been recognised in a number of localities from Afganistan to the southern Balkans and more specifically as far west as Tito Veles (FYROM, Former Yucoslavic Republic of Macedonia) (Schlosser 1921). The large form of *Palaeotragus*, *P. coelophrys* expanded from the localities of Maragha (Iran) to Ravin de la Pluie (Greece), although its presence has been also reported in Chinese localities (Bohlin 1926). *H. duvernoyi* has been also identified in a great number of localities from Maragha to Tito Veles, however it has been also reported in the French Turolian (MN12) locality of Luberon and in the late Turolian (MN13) localities of Polgardi (Hungary). Conversely, *B. attica* occupied a smaller area, from Maragha to Tito Veles, but was limited northwards, as it has not been reported further north than Kalimanci (Bulgaria) (Bakalov 1953). *S. major*, ranges from the east part of the Greek mainland to the west part of Turkey. This indicates that *S. major* was a localised representative of the giraffidae in the late Miocene, with a limited expansion in space as well as in time.

PALAEOENVIRONMENT AND PALAEOECOLOGY

The striking differences in the faunal content between localities across Eurasia during the Late Miocene have been widely recognised. However, the presence of rich and diverse ungulate faunas with hipparions, rhinoceroses, bovids, giraffes and others distinguishes the special character of these Pikermian faunas. The term Pikermian fauna was coined by Crusafont-Pairo (1951) to describe these rich late Miocene faunas. Kurten (1952) used the term hipparion faunas to characterise the abundance of the three toed equids in these faunas. Recently, Solounias *et al.* (1999) suggested the term Pikermian biome so as to include also the respective flora. These localities present certain faunal and floral characters that allow their separation into distinct groups with specific geographical and environmental boundaries. A number of authors have subdivided Eurasia into provinces and designated their boundaries

(Tobien 1967; Bernor 1978, 1983, 1984; Bonis *et al.* 1979; Bonis *et al.* 1992; Fortelius *et al.* 1996). Although there are different opinions concerning the number and the boundaries of the provinces, there is mutual agreement about the existence and the boundaries of an eastern Mediterranean-southwest Asian (Bernor 1978), or sub-Paratethyan (Bernor 1983), or Greco-Irano-Afganian (Bonis *et al.* 1992), or East block (Fortelius *et al.* 1996) province. Briefly, the other late Miocene Eurasian provinces according to the previously mentioned authors would be: a west European, a Chinese, an Indopakistan and, as some authors consider, a North African one.

In western Eurasia two different faunal associations were defined: a Central European one with a woodland/forest character and secondly a perimediterranean one with a dominant steppe/savannah character (Koenigswald 1929; Crusafont and Villalta 1954; Tobien 1967). Originally, the concept of a savannah was used to describe the palaeoecological settings of a perimediterranean fauna and was suggested by early palaeontologists on account of the systematic affinities with the modern African savannah faunas (Gaudry 1862-67; Osborn 1910; Abel 1927). Later on, other workers provided further evidence in support of the savannah hypothesis. Hypsodonty is considered to be such a striking character, indicative for the interpretation of herbivore animals as grazers and thus as savannah dwellers. This tendency has been observed in the late Miocene ungulates and has been interpreted as a grazing adaptation and thus as a savannah or an open environment adaptation (Kurten 1952; Janis 1982, 1989; Webb 1983). Thus, savannah environments are associated with overall warm and arid conditions. Bonis *et al.* (1992), after using taxonomic comparisons and statistical analysis to compare late Miocene faunas with recent ones, came to the conclusion that except from Ditiko the other studied "Greco-Irano-Afganian" faunas represented open environments. Also, it is well known that during the late Miocene the expansion of the C4 grasslands took place (Cerling *et al.* 1989; Cerling and Quade 1990; Quade *et al.* 1994; Cerling *et al.* 1997; Cerling 2001).

However, during the last two decades new data has been used to an alternative scenario where sclerophyllous evergreen woodlands dominated the Pikermian biome (Bernor *et al.* 1979; Ioakim and Solounias 1985; Solounias and Dawson-Saunders 1988; Bernor *et al.* 1988; Solounias and Moelleken 1992; Quade *et al.* 1994; Solounias *et al.* 1995; Solounias *et al.* 1999). New methods for the determination of the palaeodietary adaptations of the late Miocene ungulates were employed, such as: isotopes from teeth enamel (Quade *et al.* 1994), masticatory morphology (Solounias *et al.* 1988; Solounias and Dawson-Saunders 1988;

Solounias and Moelleken 1993; Solounias *et al.* 1995) and tooth microwear (Hayek *et al.* 1992; Solounias and Moelleken 1992; Solounias *et al.* 2000). These methods have revealed interesting and sometimes quite unexpected results about the animals' feeding habits. Palaeobotanical data (Axelrod 1973, 1975; Guernet *et al.* 1976; Sauvage 1977; Ioakim and Solounias 1985; Knobloch and Velitzelos 1987; Gregor and Velitzelos 1987; Solounias and Dawson-Saunders 1988; Bernor *et al.* 1988; Solounias and Moelleken 1992; Kloosterboer van Hoeve 2000; Ivanov *et al.* 2002) and the isotopic composition of soil carbonates and tooth enamel (Cerling *et al.* 1989; Cerling and Quade 1990; Quade *et al.* 1994; Cerling 2001) have supported the presence of a C3 dominated vegetation and thus the presence of extensive woodlands with undergrowth. Despite their successful expansion in the rest of the world, it seems that C4 grasses never managed to expand in Western Eurasia. All these data suggest warm and humid enough conditions during the late Miocene that allowed the development of such a flora and supported the formation of soil carbonates.

But what does Kerassia and its giraffids reveal about the palaeoecology and the palaeoenvironmental settings of the North Euboea Island in the middle Turolian? First of all, geographically Kerassia is situated within the boundaries of the "Greco-irano-afganian" province; the west boundary is Tito Veles and the eastern one the Molayan localities in east Afganistan. This palaeogeographic province is characterised mainly by the abundance of bovids and giraffids (Bonis *et al.* 1992). In Kerassia such diversity was also observed as a significant number of bovids and five species of giraffids are present. At Kerassia, four of these species coexisted in the lower and four coexisted in the upper fossiliferous horizon. In addition to giraffids and bovids, hipparions (at least two species), rhinoceroses, proboscideans, and other herbivores thrived and are preserved in both horizons. Although the study of the fauna has not been yet completed, the preliminary data of the excavated material have suggested that at least fifteen different herbivore species coexisted in each horizon. Therefore, the four giraffid species would have had to compete not only with each other but also with the other herbivores. Such abundance and diversity of herbivores, as well as of giraffid species, indicates a habitat with a combination of climate and vegetation that could support them. *H. duvernoyi*, *S. major* and *B. attica* were very large animals, and even the smaller of the five species *P. rouenii* was larger than most of the other ungulate species. This means that they would need daily a considerable amount of food to survive and it is therefore unlikely that they competed for the same food sources. It would be more reasonable if the different species of giraffes occupied different niches and also had different feeding habits. During the last fifteen years Solounias, with a number of different co-workers, has used and

developed a number of different methods (as stated above) trying to depict the diet and feeding habits of late Miocene ungulates, and in particular those that came from the "Greco-Irano-Afganian" province. Their methods and results provided new data about the feeding habits of late Miocene giraffes as well as of other ungulates. The material for these studies came mostly from Pikermi and Samos. From the study of its tooth microwear *H. duvernoyi* was interpreted as a browser (Solounias *et al.* 2000). The tooth microwear method (Teaford and Walker 1984) is based on the identification and counting of enamel wear patterns, such as pits and scratches on its wear surface. The numbers of pits and scratches found were similar as those of the extant *G. camelopardalis*. *B. attica* was also characterised as a browser from its masticatory morphology and tooth microwear (Solounias *et al.* 1999; Solounias *et al.* 2000). The numbers of pits and scratches though are significantly higher than *H. duvernoyi* and *G. camelopardalis*. Although the masticatory morphology indicated a browser, the tooth microwear consistently showed that *P. coelophrys* was a grazer and therefore it was characterised as a grazer (Solounias and Moelleken 1988; Solounias *et al.* 1999; Solounias *et al.* 2000). *P. rouenii* on the other hand presents a masticatory morphology of a browser-mixed feeder and tooth microwear of a mixed feeder, and was interpreted as a seasonal mixed feeder (Solounias *et al.* 1999; Solounias *et al.* 2000). The wear pattern values suggest that *P. rouenii* is closer to the browsing mode, and thus these animals would turn to grazing seasonally when the opportunity for browsing became less rewarding, as in winter or summer. Their size would also limit the animal from accessing the higher parts of the trees, and grazing would be a possible solution. Finally, *S. major* was interpreted as a grazer. Both masticatory morphology and tooth microwear clearly indicated grazing (Solounias and Moelleken 1988; Solounias *et al.* 1999; Solounias *et al.* 2000). The orbit, as described by Senyurek (1954) for the skull of *S. major* from Taskinpasa, is clearly located behind M3; hence this according to Solounias and Dawson-Saunders (1988) also suggests that *S. major* was a grazer. Furthermore, stable carbon analysis showed much enriched values of $\delta^{13}C$ which indicated that C4 grasses were probably part of *S. major's* diet. In one of the cases also the very high number of pits and scratches indicated mountain grazing (Solounias *et al.* 2000). The similarities in the microwear pattern between *H. duvernoyi* and *G. camelopardalis* might indicate that *H. duvernoyi* was a specialised browser like *G. camelopardalis* (*G. camelopardalis* feeds only on Acacia leaves). In the same regard it can be presumed that *B. attica*, due the higher number of pits and scratches on the enamel, could be considered as a generalised browser. These interpretations verify the hypothesis that the four species of giraffes in order to coexist had to exploit different food resources. Browsing and even seasonal mixed feeding suggest that there was enough tree coverage to provide the necessary

food. And this is in accordance with the evergreen sclerophylous woodland scenario that was mentioned above.

The phalange from site K3 revealed a pathologic condition for the *H. duvernoyi* individual that it belonged to. The animal suffered acute pyogenic osteomyelitis and this condition probably required a period of several months until it was fully healed (Karamitsos (veterinary surgeon), pers. com.). Pain and lameness would affect its mobility and thus the animal would be an easy target for predators. Also, the open wound and the pus from the inflammation would provide a strong and distinct odour that could easily attract predators. Therefore, the animal in order to survive would have to hide in a place that would provide it with cover and plenty of food and available water so that the animal would not have to move a lot. Such a protected habitat could possibly be a forest or dense woodland. Conversely, in an open environment the animal despite its size would have less possibility to survive.

Some striking differences found in the morphology of the lower epiphysis of the radius between *S. major* and *H. duvernoyi*, probably indicate different functional morphologies for the radiuses of the two animals and thus different modes of locomotion. As noted above the lower epiphysis of *H. duvernoyi* is wider with a shorter anteroposterior diameter than *S. major*. This probably suggests that *H. duvernoyi* was adapted for a life in a close environment such as a forest or dense woodland. The wide epiphysis would provide it with the ability to perform swift manoeuvres in such an environment. Conversely, the narrower but longer anteroposterior diameter and thus more robust epiphysis in *S. major* suggests an animal that is better adapted for a life in an open environment, with the ability to run. The deep muscle grooves at the anterior of the epiphysis also support this hypothesis and indicate strong and powerful muscles that enhanced the animal's ability to run faster.

If the area was covered by savannahs or extensive seasonal grasslands, it would mean that the animals would have to migrate during the dry season to find new food resources. The fossil record, however, does not indicate such major seasonal migrations. *B. attica* and *S. major* are relatively localised taxa, limited in the southwest part of the province. Especially this is clear for *S. major* a dedicated grazer which was limited in an even smaller palaeogeographic area than *B. attica*. During the Turolian there were two possible pathways for the giraffes of Kerassia to migrate: north and east. *B. attica* has not been found north of Kalimanci and east of Maragha, whereas *S. major* has not been found north of Vathylakkos and east of Taskinpasa. Therefore, it can be assumed that during the latest Vallesian -Turolian in the

central Greco-Anatolian territory there was enough grass cover, and enough rainfall and/or waterbodies that could support it all year long. The presence of areas covered with woodlands and/or forests would be essential to support these large browsing animals. There is enough palaeobotanical evidence to support this. Macrofossils and pollen from a number of late Miocene localities in the Greco-Irano-Afganian province indicate the presence of sclerophylous hardwood floras (conifers, oaks etc.) accompanied by significant chaparral undergrowth (Axelrod 1973, 1975; Guernet *et al.* 1976; Sauvage 1977; Orgetta 1979; Ioakim and Solounias 1985; Knobloch and Velitzelos 1987; Gregor and Velitzelos 1987; Solounias and Dawson-Saunders 1988; Bernor *et al.* 1988; Solounias and Moelleken 1992; Kloosterboer van Hoeve 2000; Ivanov *et al.* 2002). The abundance of soil carbonates is similar to that found in other late Miocene Greek localities by Quade *et al.* (1994). It indicates an annual precipitation of under approximately 1000 mm/yr. This agrees with recent precipitation data for the late Miocene of NW Bulgaria (Ivanov *et al.* 2001). Evidence also from extensive bacterial damage in bones and teeth from Kerassia, and also from other late Miocene Greek localities suggest a temperate to warm and moist climate for the late Miocene of the Northeastern Mediterranean (Iliopoulos 2002, 2003). The presence of wetland components, like *Taxodium* and *Glyptostrobus* in floral remains (Velitzelos and Gregor 1986; Orgetta 1979), and lignites (Symeonidis and Marcopoulou-Diacantoni 1977; Kloosterboer van Hoeve 2000) suggest wet enough conditions to maintain waterbodies such as lakes and marshes with no winter frost. Agusti and Anton (2002) suggested that the climatic changes that took place in the late Vallesian in Europe did not have a dramatic effect on the fauna. They considered that the new seasonal conditions affected mostly the plants, not by the expansion of grasslands but by the prevalence of deciduous trees. Seasonality disrupted fruit plants and this in return had an effect on omnivore and frugivore animals with a significant fruit component in their diet. Therefore, a seasonal, temperate to warm and moist climate must be implied for the late Miocene of Kerassia, with probably temperate and wet winters and warm and relatively dry summers.

Kerassia's giraffes in both horizons lived in a diverse environment that consisted of a mosaic of different ecologic habitats that ranged from open areas with C3 grasslands, rivers, woodlands, and forests and possibly even with some wetland facies and facies of different altitudes. *S. major* and *P. coelophrys* (*P. sp.*) lived close to open areas with enough C3 dominated grass to graze on, *H. duvernoyi* and *B. attica* lived in woodlands or forested areas, while *P. rouenii* lived probably in more open woodlands and fed seasonally on the available browsing or grazing (tree undergrowth or grasses close to waterbodies). The presence of

possibly two grazers and one browser in the lower horizon and conversely of one grazer and two browsers in the upper horizons, indicate that it is probable that the upper horizon represented more forested (more tree coverage) habitats than the lower one. This is also supported by the presence of some forest dwellers like *Microstonyx major* and *Dorcatherium sp.* in the upper horizon and which are absent from the lower one. This might also indicate a general trend towards a change to more forested conditions during the middle Turolian, or it might just represent a localised event without any further general climatic or environmental meaning.

Appendix 1: Upper teeth

Specimen number	Species	Locality	Museum / author	P^2-P^4	M^1-M^3	P^2-M^3	LP^2	IP^2	LP^3	IP^3	LP^4	IP^4
Ke 123*	*Samotherium major*	Kerassia	AMPG	90.2			25.6	18.7	34.3	23.4	35.2	29.7
K1/Δ75/1	*Helladotherium duvernoyi*	Kerassia	AMPG	94.9	127.5	214.0	32.5	33.6	30.0	35.0	29.0	37.5
K1/Δ82/2	*Palaeotragus rouenii*	Kerassia	AMPG				17.4	15.6	19.0	18.6		
K1/Δ246*	*Palaeotragus rouenii*	Kerassia	AMPG						21.2	16.1	21.0	19.1
(cast Holotype)	*Helladotherium duvernoyi*	Pikermi	AMPG(MHNP)	97.1	125.8	214.8	34.4	35.4	34.5	40.8	33.9	43.7
	Helladotherium duvernoyi	Pikermi	AMPG(MHNP)	101.0	125.9	215.0	35.8	35.3	35.5	40.3	31.6	46.8
M4065 (cast)	*Helladotherium duvernoyi*	Pikermi	NHML (SPGM)		124.8						34.4	37.1
M4066 (cast)	*Bohlinia attica*	Pikermi	NHML (SPGM)	62.7	79.2	139.1	22.3	20.2	21.2	20.8	21.4	23.6
M11419a	*Palaeotragus rouenii*	Pikermi	NHML	51.9	70.1	118.2	15.2	15.3	17.3	17.8	16.2	19.3
M11419b	*Palaeotragus rouenii*	Pikermi	NHML		67.4				17.3	19.6	16.3	19.5
M11419c	*Palaeotragus rouenii*	Pikermi	NHML								16.6	21.0
M11419d	*Palaeotragus rouenii*	Pikermi	NHML		64.5							
M4216fem	*Samotherium boissieri*	Samos	NHML	71.2	104.7	168.0	23.3	21.0	26.2	25.5	24.7	28.8
	Samotherium boissieri	Samos	NHML		111.7				24.6	25.5	25.6	28.2
M4219	*Samotherium boissieri*	Samos	NHML	74.5	105.2	174.9	24.4		26.3		25.9	
	Samotherium boissieri	Samos	NHML	74.6	105.6	176.2	23.9	22.5	26.4	27.3	24.6	30.6
M4226	*Samotherium boissieri*	Samos	NHML	77.2	105.5	174.9	26.2	25.1	24.9	29.1	24.2	30.2
	Samotherium boissieri	Samos	NHML	77.3	111.2	176.0	25.7	25.0	26.1	27.5	24.4	30.2
M4221	*Samotherium boissieri*	Samos	NHML		111.3				25.2	26.0	21.7	27.6
M4228*	*Samotherium boissieri*	Samos	NHML	82.3			24.9	18.4	33.6	21.5	34.2	29.2
M4225	*Samotherium boissieri*	Samos	NHML	74.3	103.7	171.2	24.7	24.6	24.8	27.8	22.4	27.7
268	*Samotherium boissieri*	Samos	NHML		102.6	160.0			22.8		21.9	
M4229*	*Samotherium boissieri*	Samos	NHML	88.9			24.9	15.5	27.3	20.5	31.5	26.4
M4226*	*Samotherium boissieri*	Samos	NHML	87.0			22.3	14.6	31.5	21.0	33.3	27.0
*	*Samotherium boissieri*	Samos	NHML	87.7			22.4	15.7	31.2	21.7	33.5	27.6
M4215male	*Samotherium boissieri*	Samos	NHML		113.9				26.4		25.6	
	Samotherium boissieri	Samos	NHML	76.9	110.7	180.5	26.6		27.6		25.0	
M4224	*Samotherium boissieri*	Samos	NHML	70.7	104.6	175.1	19.1	22.1	23.8	26.6	22.4	26.3
M4223	*Samotherium boissieri*	Samos	NHML	71.4	101.5	163.3	15.8	24.7	24.0	28.2	21.2	28.3
M3868	*Samotherium neumayri*	Maragha	NHML		104.1						23.8	31.0
M3868	*Samotherium neumayri*	Maragha	NHML		104.6							
M3867a	*Bohlinia attica*	Maragha	NHML		88.0							
DIT 2	*Palaeotragus rouenii*	Ditiko 2	(Geraads, 1978)	54.0	73.0	121.0	18.0	14.0	18.0	18.0	18.0	21.0
DIT 3	*Palaeotragus rouenii*	Ditiko 2	(Geraads, 1978)								18.0	23.0
R.Pl. 89	*Palaeotragus rouenii*	Ravin de la pluie	(Geraads, 1978)						20.0	16.0	19.0	21.0
R.Pl. 91	*Palaeotragus coelophrys*	Ravin de la pluie	(Geraads, 1978)	61.0	79.0	140.0	21.0	20.0	22.0	23.0	19.0	26.0
VAT 3	*Samotherium boissieri?*	Vathylakkos 3	(Geraads, 1978)	85.0	131.0	210.0	29.0	27.0	28.0	31.0	26.0	34.0
PNT 136	*?Decenatherium macedoniae*	Pentalophos	(Geraads, 1989)		101.0	172.0						33.0
PNT112	*?Decenatherium macedoniae*	Pentalophos	(Geraads, 1989)	72.0	96.5	166.0						31.0
PNT 145	*?Decenatherium macedoniae*	Pentalophos	(Geraads, 1989)	76.5	106.0	177.0						31.0
PNT 325	*?Decenatherium macedoniae*	Pentalophos	(Geraads, 1989)	77.0	106.0	176.0						30.5
DTK 186*	*Bohlinia attica*	Ditiko1	(Geraads, 1979)				18.5	12.0	23.0	15.0	24.0	20.0

Appendix 1: Upper teeth

Specimen number	Species	Locality	Museum / author	P^2-P^4	M^1-M^3	P^2-M^3	LP^2	IP^2	LP^3	IP^3	LP^4	IP^4
KTB1	*Samotherium major*	Kemiklitepe	Geraads, 1994	86.0	129.0	210.0						
NTK 52	*Bohlinia attica*	Nikiti 1	(Kostopoulos et al.1996)	57.0	64.5	119.0						
NTK 145	*Bohlinia attica*	Nikiti 1	(Kostopoulos et al.1996)	59.0	70.0	125.0						
NTK 148	*Bohlinia attica*	Nikiti 1	(Kostopoulos et al.1996)	61.2	77.0	136.5						
NTK 172	*Bohlinia attica*	Nikiti 1	(Kostopoulos et al.1996)	62.0	85.5	146.5						
NTK 147	*Bohlinia nikitiae*	Nikiti 1	(Kostopoulos et al.1996)	61.0	87.0	149.0	19.5	17.0	19.5	21.0	19.0	27.4
NTK min	*Bohlinia attica*	Nikiti 1	(Kostopoulos et al.1996)				17.1	14.1	17.8	17.0	16.5	19.4
NTK max	*Bohlinia attica*	Nikiti 1	(Kostopoulos et al.1996)				19.7	18.7	19.2	23.4	20.6	26.0
NTK mean	*Bohlinia attica*	Nikiti 1	(Kostopoulos et al.1996)				18.4	16.3	18.6	19.5	18.3	22.4
Wagner "Orasius"	*Bohlinia attica*	Pikermi	Bohlin 1926				21.0	17.0	22.0	20.0	20.0	24.0
Wagner "C. vetusta"	*Bohlinia attica*	Pikermi	Bohlin 1926						20.0	21.0	22.0	23.0
Wagner "C. vetusta"	*Bohlinia attica*	Pikermi	Bohlin 1926									
Wagner "C. vetusta"	*Bohlinia attica*	Pikermi	Bohlin 1926								21.0	22.0
	Bohlinia attica	Salonique	Arambourg & Piveteau, 1929				20.0	19.0	21.0			
Gaudry	*Bohlinia attica*	Pikermi	Geraads 1974						22.0	20.0	20.0	22.0
Gaudry	*Palaeotragus rouenii*	Pikermi	Gaudry, 1862								18.0	25.0
Gaudry	*Palaeotragus rouenii*	Pikermi	Gaudry, 1862				19.0	17.0	18.0		18.0	21.0
	Samotherium neumayri	Maragha	De Mecquenem, 1924	75.0	125.0	200.0						
	Palaeotragus coelophrys	Maragha	De Mecquenem, 1924	66.0	88.0	146.0						
*	*Samotherium neumayri*	Maragha	Rodler & Weithofer, 1890				27.0	18.0	31.0	23.0	36.0	30.0
schadel	*Samotherium neumayri*	Maragha	Rodler & Weithofer, 1890				23.0		25.0		26.0	29.0
a	*Samotherium neumayri*	Maragha	Rodler & Weithofer, 1890				23.0		26.0		27.0	31.5
b	*Samotherium neumayri*	Maragha	Rodler & Weithofer, 1890								28.0	
c	*Samotherium neumayri*	Maragha	Rodler & Weithofer, 1890									
d	*Samotherium neumayri*	Maragha	Rodler & Weithofer, 1890				24.0		24.0		24.5	28.0
e	*Samotherium neumayri*	Maragha	Rodler & Weithofer, 1890				26.0		27.0		28.0	29.0
schadel	*Palaeotragus coelophrys*	Maragha	Rodler & Weithofer, 1890				20.0		19.0		18.0	
zahnreiche	*Palaeotragus coelophrys*	Maragha	Rodler & Weithofer, 1890				23.0		21.0		21.0	
116*	*Palaeotragus microdon juv*	Kansu	Bohlin 1926	60.0				12.0	22.0	16.0	23.0	21.0
49*	*Palaeotragus microdon juv*	Shansi	Bohlin 1926	59.0			18.0	12.0	22.0	16.0	23.0	21.0
108*	*Palaeotragus microdon juv*	Shansi	Bohlin 1926	59.0			16.0	12.0	22.0	16.0	23.0	20.0
a	*Palaeotragus microdon*	China	Bohlin 1926		75.0						18.0	21.0
b	*Palaeotragus microdon*	China	Bohlin 1926	53.0	72.0	121.0						
c	*Palaeotragus microdon*	China	Bohlin 1926	54.0	70.0	120.0	17.0	18.0	19.0	21.0	18.0	23.0
d	*Palaeotragus microdon*	China	Bohlin 1926	54.0	72.0	122.0	18.0		18.0	20.0	18.0	23.0
e	*Palaeotragus microdon*	China	Bohlin 1926	55.0	72.0	122.0	18.0	18.0	19.0	20.0	18.0	23.0
f	*Palaeotragus microdon*	China	Bohlin 1926		68.0							
g	*Palaeotragus microdon*	China	Bohlin 1926		67.0							
h	*Palaeotragus microdon*	China	Bohlin 1926	55.0	72.0	125.0						
I	*Palaeotragus microdon*	China	Bohlin 1926	54.0	73.0	125.0						
j	*Palaeotragus microdon*	China	Bohlin 1926	57.0	75.0	129.0	18.0		18.0	17.0	18.0	20.0
A	*Palaeotragus cfr. coelophrys*		Bohlin 1926	60.0	88.0	141.0	18.0	17.0	19.0	21.0	20.0	24.0
B	*Palaeotragus cfr. coelophrys*		Bohlin 1926	60.0	78.0	134.0	19.0	18.0	20.0	22.0	19.0	27.0

Appendix 1: Upper teeth

Specimen number	Species	Locality	Museum / author	P^2-P^4	M^1-M^3	P^2-M^3	LP^2	IP^2	LP^3	IP^3	LP^4	IP^4
C	*Palaeotragus cfr. coelophrys*		Bohlin 1926	63.0	83.0	139.0	19.0	19.0	22.0	22.0	20.0	26.0
D	*Palaeotragus cfr. coelophrys*		Bohlin 1926	57.0	77.0	131.0	17.0	17.0	18.0	19.0	19.0	22.0
E	*Palaeotragus cfr. coelophrys*		Bohlin 1926	60.0	81.0	133.0	18.0	19.0	18.0	22.0	19.0	
*	*Palaeotragus decipiens*		Bohlin, 1926	84.0			23.0	18.0	29.0	23.0	32.0	28.0
	Palaeotragus decipiens		Bohlin, 1926	78.0	108.0	178.0	22.0	23.0	26.0	26.0	25.0	35.0
	Palaeotragus quadricornis	Samos	Bohlin, 1926	67.0	91.0	155.0	23.0	22.0	23.0	25.0	21.0	27.0
*	*Samotherium cfr. neumayri*		Bohlin, 1926				27.0	19.0	34.0	25.0		
	Samotherium cfr. neumayri		Bohlin, 1926	78.0	110.0	180.0	26.0	24.0	0.0	26.0	26.0	32.0
1*	*Samotherium sp.*	30	Bohlin, 1926	96.0			26.0	18.0	34.0	24.0	38.0	32.0
4*	*Samotherium sp.*	30	Bohlin, 1926	100.0					34.0	29.0	43.0	38.0
6*	*Samotherium sp.*	30	Bohlin, 1926	102.0			27.0	18.0	36.0	27.0	40.0	33.0
S.79	*Samotherium sp.*	30	Bohlin, 1926	89.0	134.0	223.0	23.0	27.0	29.0	32.0	32.0	37.0
	Samotherium sinense	115	Bohlin, 1926	79.0	116.0	190.0	24.0	22.0	27.0	29.0	25.0	34.0
S.48*	*Samotherium sinense*		Bohlin, 1926				25.0	21.0	35.0	29.0	38.0	35.0
	Samotherium sinense	China	Schlosser, 1903	80.0	120.0	190.0	26.0	27.0	29.0	28.5	27.0	31.0
	Samotherium major	Taskinpasa	Senyurek, 1954	86.0	126.5	205.0	28.6	28.0	29.1	31.0	29.1	33.5
3fem	*Samotherium boissieri*	Samos	Bohlin, 1926	70.0	104.0	168.0						
c	*Samotherium boissieri*	Samos	Bohlin, 1926	71.0	115.0	180.0						
d	*Samotherium boissieri*	Samos	Bohlin, 1926		118.0							
e	*Samotherium boissieri*	Samos	Bohlin, 1926			171.0						
f	*Samotherium boissieri*	Samos	Bohlin, 1926	75.0	110.0	179.0	24.0	25.0	25.0	29.0	25.0	31.0
4fem	*Samotherium major*	Samos	Bohlin, 1926		125.0	205.0						
9 (Samos 29) fem	*Samotherium major*	Samos	Bohlin, 1926	84.0	121.0	197.0						
10male	*Samotherium major*	Samos	Bohlin, 1926		128.0	208.0						
11fem	*Samotherium major*	Samos	Bohlin, 1926	85.0	122.0	198.0	25.0	29.0	27.0	31.0	27.0	31.0
A	*Samotherium major*	Samos	Bohlin, 1926	86.0	118.0	195.0						
*1	*Samotherium*	Samos	Bohlin, 1926	82.0			26.0	18.0	32.0	22.0	32.0	29.0
*2	*Samotherium*	Samos	Bohlin, 1926	83.0			24.0	19.0	27.0	24.0	32.0	28.0
*3	*Samotherium*	Samos	Bohlin, 1926	89.0			28.0	18.0	35.0	23.0	36.0	30.0
*5	*Samotherium*	Samos	Bohlin, 1926	89.0			24.0	17.0	30.0	22.0	34.0	28.0
*6	*Samotherium*	Samos	Bohlin, 1926	92.0			26.0	20.0	31.0	25.0	35.0	30.0
*7	*Samotherium*	Samos	Bohlin, 1926	91.0			26.0	19.0	34.0	23.0	36.0	27.0
*8	*Samotherium*	Samos	Bohlin, 1926	94.0			26.0	19.0	34.0	25.0	37.0	30.0
*9	*Samotherium*	Samos	Bohlin, 1926	91.0			25.0	18.0	32.0	23.0	35.0	28.0
*10, 265	*Samotherium*	Samos	Bohlin, 1926	92.0			27.0	18.0	31.0	24.0	35.0	31.0
a	*Honanotherium schlosseri*		Bohlin, 1926	74.0	100.0	168.0						
b	*Honanotherium schlosseri*	11	Bohlin, 1926	77.0	104.0	176.0				28.0		32.0
c	*Honanotherium schlosseri*	Sung-Tsun	Bohlin, 1926		98.0	169.0						
d	*Honanotherium schlosseri*	13	Bohlin, 1926	75.0	98.0	166.0					23.0	34.0
e	*Honanotherium schlosseri*		Bohlin, 1926	73.0	92.0	161.0						
f	*Honanotherium schlosseri*	29	Bohlin, 1926		100.0							
g	*Honanotherium schlosseri*	51	Bohlin, 1926	76.0	108.0	169.0	25.0	24.0	25.0	27.0	25.0	33.0
h	*Honanotherium schlosseri*	70	Bohlin, 1926		101.0						22.0	28.0

Appendix 1: Upper teeth

Specimen number	Species	Locality	Museum / author	P^2-P^4	M^1-M^3	P^2-M^3	LP^2	IP^2	LP^3	IP^3	LP^4	IP^4
M2443*	*Helladotherium*	Pikermi?	Bohlin, 1926	108.0			29.0	25.0	37.0	30.0	40.0	39.0
M2440-2*	*Helladotherium*	Pikermi?	Bohlin, 1926				28.0	19.0	35.0	26.0	36.0	30.0
*	*Helladotherium*	Maragha	Bohlin, 1926						35.0	26.0	36.0	33.0
gaudryi, tafXLII, fig2	*Helladotherium duvernoyi*	Pikermi	Bohlin 1926	97.0	120.0	214.0	34.0	34.0	35.0	38.0	31.0	43.0
gaudryi, tafXLI, fig2	*Helladotherium duvernoyi*	Pikermi	Bohlin 1926	92.0	128.0	207.0	31.0		31.0	37.0	32.0	40.0
4	*Birgerbohlinia schaubi*	Piera	Crusafont 1952	92.5			33.8	32.2	33.0	37.5	29.9	40.0
260	*Birgerbohlinia schaubi*	Piera	Crusafont 1952	76.2	104.5	180.5	30.0	26.5	29.2	31.8	26.4	36.6
min	*Birgerbohlinia schaubi*	Crevillente 2	Montoya-Morales 1991				31.0	26.8	26.9	30.0	25.7	31.5
average	*Birgerbohlinia schaubi*	Crevillente 2	Montoya-Morales 1991				31.9	29.6	28.0	31.4	27.6	35.2
max	*Birgerbohlinia schaubi*	Crevillente 2	Montoya-Morales 1991				32.7	32.5	30.0	33.7	28.5	38.0
average	*Decennatherium pachecoi*	Nombrevilla	Crusafont 1952				30.0		33.0		27.8	33.8
LVF316	*Decennatherium pachecoi*	Los Valles	Morales and Soria, 1981									

Notes

L = occlusal length

l = maximum width

specimens with a star (*) characterize deciduous teeth

AMPG(MHNP) in parenthesis the museum where the original specimen is stored

NHML (SPGM) in parenthesis the museum where the original specimen is stored

SPGM : Sammlung fur Palaontologie und Historische Geologie, Munchen

Appendix 1: Upper teeth

Specimen number	Species	Locality	LM^1	IM^1	LM^2	IM^2	LM^3	IM^3	Pm/M	Pm/PM
Ke 123*	*Samotherium major*	Kerassia								
K1/Δ75/1	*Helladotherium duvernoyi*	Kerassia	43.4	44.0	46.4	44.8	45.8	43.5	74.4	44.3
K1/Δ82/2	*Palaeotragus rouenii*	Kerassia								
K1/Δ246*	*Palaeotragus rouenii*	Kerassia	24.6	22.9	25.8	23.6				
(cast Holotype)	*Helladotherium duvernoyi*	Pikermi	40.0	43.9	47.3	51.4	45.7	45.6	77.2	45.2
	Helladotherium duvernoyi	Pikermi	39.9	52.4	49.7	54.1	45.0	45.6	80.2	47.0
M4065 (cast)	*Helladotherium duvernoyi*	Pikermi	42.8	38.7	44.9	43.7	43.9	41.3		
M4066 (cast)	*Bohlinia attica*	Pikermi	26.7	25.0	25.2	28.3	33.4	26.4	79.2	45.1
M11419a	*Palaeotragus rouenii*	Pikermi	23.5	23.2	26.6	23.9	24.7	23.9	74.0	43.9
M11419b	*Palaeotragus rouenii*	Pikermi	20.0	21.4	23.3	23.5	23.5	22.3		
M11419c	*Palaeotragus rouenii*	Pikermi	23.7	22.3	25.8	24.6				
M11419d	*Palaeotragus rouenii*	Pikermi	16.0		24.1	22.7	26.0	23.8		
M4216fem	*Samotherium boissieri*	Samos	36.4	35.5	39.4	38.0	34.9	34.5	68.0	42.4
	Samotherium boissieri	Samos	36.8	34.3	39.0	37.6	34.6	34.0		
M4219	*Samotherium boissieri*	Samos	32.8	34.2	38.9	39.5	38.2	35.1	70.8	42.6
	Samotherium boissieri	Samos	32.5	34.4	37.4		36.8	36.4	70.6	42.3
M4226	*Samotherium boissieri*	Samos	32.3		40.3	38.3	38.7	38.2	73.2	44.1
	Samotherium boissieri	Samos	35.9	34.9	41.3		39.3	38.4	69.5	43.9
M4221	*Samotherium boissieri*	Samos	27.5	33.9	30.4	36.6	34.4			
M4228*	*Samotherium boissieri*	Samos	40.8							
M4225	*Samotherium boissieri*	Samos	35.2	34.7	37.4	38.5	34.0	37.2	71.6	43.4
268	*Samotherium boissieri*	Samos	31.7		40.0	38.4	37.1	33.3		
M4229*	*Samotherium boissieri*	Samos	37.0							
M4226*	*Samotherium boissieri*	Samos								
*	*Samotherium boissieri*	Samos								
M4215male	*Samotherium boissieri*	Samos	34.0		42.2		42.4			
	Samotherium boissieri	Samos	33.5		42.0		42.5		69.5	42.6
M4224	*Samotherium boissieri*	Samos	34.4	33.2	37.0	36.0	33.8	30.3	67.6	40.4
M4223	*Samotherium boissieri*	Samos	26.0	35.5	32.5	38.4	35.1	34.8	70.3	43.7
M3868	*Samotherium neumayri*	Maragha	28.2	37.0	36.4	40.6	40.2	41.1		
M3868	*Samotherium neumayri*	Maragha	27.3	37.1	39.5	40.6	42.1	41.8		
M3867a	*Bohlinia attica*	Maragha	31.7	33.1	33.7	36.4	32.3	30.8		
DIT 2	*Palaeotragus rouenii*	Ditiko 2	23.0	25.0	27.0	28.0	26.0	28.0	74.0	44.6
DIT 3	*Palaeotragus rouenii*	Ditiko 2	26.0	27.0	27.0	28.0	26.0	27.0		
R.Pl. 89	*Palaeotragus rouenii*	Ravin de la pluie	24.0	26.0	26.0	28.0	26.0	28.0		
R.Pl. 91	*Palaeotragus coelophrys*	Ravin de la pluie	24.0	28.0	28.0	30.0	28.0	29.0	77.2	43.6
VAT 3	*Samotherium boissieri?*	Vathylakkos 3	38.0	42.0	46.0	47.0	43.0	42.0	64.9	40.5
PNT 136	*?Decenatherium macedoniae*	Pentalophos		32.4						
PNT112	*?Decenatherium macedoniae*	Pentalophos		31.0					74.6	43.4
PNT 145	*?Decenatherium macedoniae*	Pentalophos		31.5					72.2	43.2
PNT 325	*?Decenatherium macedoniae*	Pentalophos		33.0					72.6	43.8
DTK 186*	*Bohlinia attica*	Ditiko1	27.0	26.5						

Appendix 1: Upper teeth

Specimen number	Species	Locality	LM^1	IM^1	LM^2	IM^2	LM^3	IM^3	Pm/M	Pm/PM
KTB1	*Samotherium major*	Kemikliteppe							66.7	41.0
NTK 52	*Bohlinia attica*	Nikiti 1							88.4	47.9
NTK 145	*Bohlinia attica*	Nikiti 1							84.3	47.2
NTK 148	*Bohlinia attica*	Nikiti 1							79.5	44.8
NTK 172	*Bohlinia attica*	Nikiti 1							72.5	42.3
NTK 147	*Bohlinia nikitiae*	Nikiti 1	25.4	27.5	29.1	29.5	29.6	30.0	70.1	40.9
NTK min	*Bohlinia attica*	Nikiti 1	23.8	24.0	22.8	25.6	25.7	26.0		
NTK max	*Bohlinia attica*	Nikiti 1	26.3	27.4	30.2	33.2	31.0	30.0		
NTK mean	*Bohlinia attica*	Nikiti 1	25.1	25.2	26.7	28.2	27.5	27.6		
Wagner "Orasius"	*Bohlinia attica*	Pikermi	26.0	26.0	28.0	27.0	33.0	27.0		
Wagner "C. vetusta"	*Bohlinia attica*	Pikermi								
Wagner "C. vetusta"	*Bohlinia attica*	Pikermi			31.0	30.0	29.0	27.0		
Wagner "C. vetusta"	*Bohlinia attica*	Pikermi	27.0	28.0	28.0	28.0	28.0	28.0		
	Bohlinia attica	Salonique			29.0	30.0	29.0	29.0		
Gaudry	*Bohlinia attica*	Pikermi	29.0	27.0	30.0	30.0	30.0	28.0		
Gaudry	*Palaeotragus rouenii*	Pikermi	21.0	24.0	24.0	26.0				
Gaudry	*Palaeotragus rouenii*	Pikermi	24.0		26.0	25.0	25.0			
	Samotherium neumayri	Maragha							60.0	37.5
	Palaeotragus coelophrys	Maragha							75.0	45.2
*	*Samotherium neumayri*	Maragha								
schadel	*Samotherium neumayri*	Maragha	39.0		42.0	44.0	41.0			
a	*Samotherium neumayri*	Maragha	42.0		45.0	40.0				
b	*Samotherium neumayri*	Maragha	38.0		46.0	41.0	44.0			
c	*Samotherium neumayri*	Maragha	38.0		43.0		43.0			
d	*Samotherium neumayri*	Maragha	35.0							
e	*Samotherium neumayri*	Maragha								
schadel	*Palaeotragus coelophrys*	Maragha	25.5		27.0		26.0			
zahnreiche	*Palaeotragus coelophrys*	Maragha	30.0		31.0		29.0			
116*	*Palaeotragus microdon juv*	Kansu								
49*	*Palaeotragus microdon juv*	Shansi								
108*	*Palaeotragus microdon juv*	Shansi								
a	*Palaeotragus microdon*	China	24.0		28.0	26.0	27.0	25.0		
b	*Palaeotragus microdon*	China							73.6	43.8
c	*Palaeotragus microdon*	China	21.0	26.0	24.0	28.0	26.0	28.0	77.1	45.0
d	*Palaeotragus microdon*	China	23.0	27.0	26.0	30.0	25.0	27.0	75.0	44.3
e	*Palaeotragus microdon*	China	22.0	25.0	26.0	28.0	28.0	29.0	76.4	45.1
f	*Palaeotragus microdon*	China								
g	*Palaeotragus microdon*	China	21.0	24.0	23.0	26.0	24.0	25.0		
h	*Palaeotragus microdon*	China							76.4	44.0
I	*Palaeotragus microdon*	China							74.0	43.2
j	*Palaeotragus microdon*	China	24.0	25.0	27.0	27.0	27.0	25.0	76.0	44.2
A	*Palaeotragus cfr. coelophrys*		29.0	28.0	31.0	31.0	30.0	30.0	68.2	42.6
B	*Palaeotragus cfr. coelophrys*		25.0	29.0	29.0	32.0	28.0	30.0	76.9	44.8

Appendix 1: Upper teeth

Specimen number	Species	Locality	LM^1	lM^1	LM^2	lM^2	LM^3	lM^3	Pm/M	Pm/PM
C	*Palaeotragus cfr. coelophrys*		27.0	30.0	30.0	33.0	31.0	31.0	75.9	45.3
D	*Palaeotragus cfr. coelophrys*		25.0	26.0	28.0	28.0	27.0	26.0	74.0	43.5
E	*Palaeotragus cfr. coelophrys*		27.0	29.0	28.0	29.0	30.0	29.0	74.1	45.1
*	*Palaeotragus decipiens*									
	Palaeotragus decipiens		33.0	42.0	41.0	44.0	35.0	40.0	72.2	43.8
	Palaeotragus quadricornis	Samos							73.6	43.2
*	*Samotherium cfr. neumayri*									
	Samotherium cfr. neumayri		34.0	38.0	40.0	42.0	38.0	35.0	70.9	43.3
1*	*Samotherium sp.*	30	47.0							
4*	*Samotherium sp.*	30	49.0	44.0	52.0	50.0				
6*	*Samotherium sp.*	30								
S.79	*Samotherium sp.*	30	45.0	45.0	48.0	48.0	41.0	43.0	66.4	39.9
	Samotherium sinense	115	39.0	43.0	40.0	46.0	39.0	40.0	68.1	41.6
S.48*	*Samotherium sinense*									
	Samotherium sinense	China	37.0	34.0	42.0	40.0	45.0	42.0	66.7	
	Samotherium major	Taskinpasa	35.2	40.0	46.5	44.5	49.2	39.5	68.0	42.0
3fem	*Samotherium boissieri*	Samos							67.3	41.7
c	*Samotherium boissieri*	Samos							61.7	39.4
d	*Samotherium boissieri*	Samos								
e	*Samotherium boissieri*	Samos								
f	*Samotherium boissieri*	Samos	34.0	36.0	41.0	39.0	40.0	38.0	68.2	41.9
4fem	*Samotherium major*	Samos								
9 (Samos 29) fem	*Samotherium major*	Samos							69.4	42.6
10male	*Samotherium major*	Samos								
11fem	*Samotherium major*	Samos	38.0	42.0	44.0	45.0	46.0	41.0	69.7	42.9
A	*Samotherium major*	Samos							72.9	44.1
*1	*Samotherium*	Samos								
*2	*Samotherium*	Samos								
*3	*Samotherium*	Samos								
*5	*Samotherium*	Samos								
*6	*Samotherium*	Samos								
*7	*Samotherium*	Samos								
*8	*Samotherium*	Samos								
*9	*Samotherium*	Samos								
*10, 265	*Samotherium*	Samos								
a	*Honanotherium schlosseri*								74.0	44.0
b	*Honanotherium schlosseri*	11	36.0	40.0	39.0	41.0	37.0	40.0	74.0	43.8
c	*Honanotherium schlosseri*	Sung-Tsun			39.0	43.0	36.0	40.0		
d	*Honanotherium schlosseri*	13	37.0	40.0	36.0	40.0	35.0	40.0	76.5	45.2
e	*Honanotherium schlosseri*								79.3	45.3
f	*Honanotherium schlosseri*	29	34.0		36.0	41.0	37.0	41.0		
g	*Honanotherium schlosseri*	51	38.0	40.0	42.0	43.0		41.0	70.4	45.0
h	*Honanotherium schlosseri*	70	34.0	34.0	36.0	38.0	33.0	35.0		

Appendix 1: Upper teeth

Specimen number	Species	Locality	LM^1	lM^1	LM^2	lM^2	LM^3	lM^3	Pm/M	Pm/PM
M2443*	*Helladotherium*	Pikermi?	50.0	46.0						
M2440-2*	*Helladotherium*	Pikermi?								
*	*Helladotherium*	Maragha								
gaudryi, tafXLII, fig2	*Helladotherium duvernoyi*	Pikermi	38.0	46.0	47.0	52.0	46.0	46.0	80.8	45.3
gaudryi, tafXLI, fig2	*Helladotherium duvernoyi*	Pikermi	43.0	41.0	45.0	48.0	42.0		71.9	44.4
4	*Birgerbohlinia schaubi*	Piera	33.0	39.0						
260	*Birgerbohlinia schaubi*	Piera	32.1	36.9	35.3	40.7	38.3	40.7		
min	*Birgerbohlinia schaubi*	Crevillente 2	31.9	37.5	35.1	42.0	34.3	37.8		
average	*Birgerbohlinia schaubi*	Crevillente 2	34.0	39.5	38.4	43.3	36.7	40.0		
max	*Birgerbohlinia schaubi*	Crevillente 2	36.3	41.1	41.7	46.6	40.5	43.6		
average	*Decennatherium pachecoi*	Nombrevilla	39.0		44.0	41.5	41.5	37.7		
LVF316	*Decennatherium pachecoi*	Los Valles			36.7	34.2	36.0	34.5		

Notes

L = occlusal length

l = maximum width

specimens with a star (*) characterize deciduous teeth

AMPG(MHNP) in parenthesis the museum where the original specimen is store

NHML (SPGM) in parenthesis the museum where the original specimen is store

SPGM : Sammlung fur Palaontologie und Historische Geologie, Munchen

Appendix 2: Mandibles and lower teeth

Specimen number	Species	Locality	Museum / author	hp	Wmax	P_2-P_4	M_1-M_3	P_2-M_3	LP_2	IP_2	LP_3	IP_3	LP_4	IP_4	LM_1
Ke 306	*Palaeotragus rouenii*	Kerassia	AMPG		24.2										22.5
K3.181	*Palaeotragus rouenii*	Kerassia	AMPG		22.8		82.8								24.6
K4/Δ8/1 d	*Palaeotragus sp.*	Kerassia	AMPG			65.2	89.9	157.3		10.3	22.8	13.2	24.3	15.5	23.7
K4/Δ8/2 s	*Palaeotragus sp.*	Kerassia	AMPG						19.6	9.4	22.8	12.7		14.9	
K4/Δ111	*Palaeotragus rouenii*	Kerassia	AMPG	36.8	24.4	54.3	80.7	133.8	15.4	10.2	18.7	13.0	20.9	15.3	22.2
K4/Δ119/34 d	*Samotherium major*	Kerassia	AMPG	62.5	44.7	97.4	148.4	245.0	30.3	18.6	38.2	26.6	33.5	31.9	44.4
K4/Δ54/1 s	*Samotherium major*	Kerassia	AMPG												
K4/Δ107/9	*Palaeotragus rouenii*	Kerassia	AMPG												
K4/Δ324	*Palaeotragus rouenii*	Kerassia	AMPG	35.3	24.7	55.4	82.1	136.1	16.3	9.1	18.8	13.0	21.1	15.6	19.8
K4/Δ350	*Helladotherium duvernoyi*	Kerassia	AMPG												
K1/Δ 318	*Palaeotragus rouenii*	Kerassia	AMPG												
M8367 (+M13063)	*Palaeotragus rouenii*	Pikermi (O)	NHML	34.2	22.3	55.5	76.6	128.7	16.2	8.7	20.2	11.2	22.2	14.2	23.0
*without number	*Palaeotragus rouenii*	Pikermi (O)	NHML	32.0							18.9	10.6	23.4	12.5	
*M13062	*Palaeotragus rouenii*	Pikermi (O)	NHML	27.0		54.6			10.5		16.4	7.9	26.4	10.7	23.5
M11453	*Palaeotragus rouenii*	Pikermi (O)	NHML		22.5										24.6
M11397	*Helladotherium duvernoyi*	Pikermi (O)	NHML	55.6					27.9	17.3	36.7	23.7			
*M11496	*Helladotherium duvernoyi*	Pikermi (O)	NHML								29.5	15.6	49.0	18.7	
M4067 (cast)	*Helladotherium duvernoyi*	Pikermi (O)	NHML (SPGM)		40.6		135.8				31.6	23.6	35.1	28.5	43.3
M4215 (Hol)	*Samotherium boissieri*	Samos	NHML												
M4215	*Samotherium boissieri*	Samos	NHML	46.8		75.4			20.4		27.0		25.3		34.1
*M4237	*Samotherium boissieri*	Samos	NHML	36.2							19.3	14.2	39.5	18.8	41.8
M4236 (169)	*Samotherium boissieri*	Samos	NHML			70.1	110.3	178.1	21.3	11.2	21.7	14.8	26.0	18.6	31.6
M4235a (162)	*Samotherium boissieri*	Samos	NHML	41.3	41.8	72.4	116.0	183.1	19.2	15.8	23.6	18.9	30.3	21.9	33.3
M4235b (161)	*Samotherium boissieri*	Samos	NHML	41.0	38.1	74.0	115.0	188.7	19.8		23.0		30.2	21.0	34.8
M4234 (159)	*Samotherium boissieri*	Samos	NHML	45.4	30.7	66.3	120.1	188.5	18.8		21.6	14.5	25.9	19.2	35.8
M4224 (158)	*Samotherium boissieri*	Samos	NHML	45.2	29.3	73.5	119.4	187.2	19.4	11.7	25.2	14.6	30.2	18.8	36.0
*M4239	*Samotherium boissieri*	Samos	NHML	31.3		84.1			20.0	8.9	23.2	12.8	41.0	18.8	
*4238a	*Samotherium boissieri*	Samos	NHML								23.5	10.9	38.9	14.7	
*4240	*Samotherium boissieri*	Samos	NHML		23.9						23.4	12.2	40.6	18.1	
*4237	*Samotherium boissieri*	Samos	NHML	42.6	36.4	77.8	139.8	211.2					41.1	20.3	41.7
*4238b	*Samotherium boissieri*	Samos	NHML									9.5	39.1	13.2	
M4242a	*Samotherium boissieri*	Samos	NHML						22.7	13.7					
*M4242e(149)	*Palaeotragus coelophrys*	Samos	NHML		25.1									19.7	29.5
M3873a	*Samotherium neumayri*	Maragha	NHML												
M3873b	*Samotherium neumayri*	Maragha	NHML												
M3873c	*Samotherium neumayri*	Maragha	NHML								28.4	18.4			
without number	*Bohlinia attica*	Pikermi (O)	AMPG Roussiakis pers. com.	46.3	24.5	55.7	88.0	142.0	13.1	9.3	19.9	11.7	21.6	14.8	27.0
DIT 2	*Palaeotragus rouenii*	Ditiko 2	(Geraads, 1978)			49.0	78.0	126.0	13.0	9.0	17.0	11.0	20.0	14.0	22.0
R.Pl. 104	*Palaeotrgus coelophrys*	Ravin de la Pluie	(Geraads, 1978)				86.0								
VAT 3	*Samotherium boissieri (major)*	Vathilakkos 3	(Geraads, 1978)			94.0	142.0	223.0	26.0	14.0	28.0	18.0	28.0	23.0	39.0
PNT 111	*?Decenatherium macedoniae*	Pentalophos	(Geraads, 1989)			73.0	113.0	187.0							
PNT 137	*?Decenatherium macedoniae*	Pentalophos	(Geraads, 1989)				101.0	170.0							
NIK 1	*Helladotherium duvernoyi*	Nikiti 1	(Kostopoulos et al.1996)			92.0	149.0	240.0	25.5	14.4	31.0	25.0	36.0	31.2	36.5
MAR 882	*Helladotherium duvernoyi*	Maragha	(Kostopoulos et al.1996)			103.5	159.0	262.0	26.4	17.2	32.4	23.2	35.7	26.3	
*	*Helladotherium duvernoyi*	Pikermi	(Gaudry, 1862)						21.0		29.0		46.0		43.0
	Palaeotragus rouenii	Pikermi	(Gaudry, 1862)	34.0					16.0		16.0		18.0		20.0
	Samotherium neumayeri	Maragha	De Mecquenem, 1924			74.0	125.0	195.0							

Appendix 2: Mandibles and lower teeth

Specimen number	Species	Locality	Museum / author	hp	Wmax	P_2-P_4	M_1-M_3	P_2-M_3	LP_2	IP_2	LP_3	IP_3	LP_4	IP_4	LM_1
	Palaeotragus coelophrys	Maragha	De Mecquenem, 1924			65.0	100.0	170.0							
a	*Samotherium neumayri*	Maragha	Rodler & Weithofer, 1890										29.0		37.0
b	*Samotherium neumayri*	Maragha	Rodler & Weithofer, 1890										31.0		37.0
c	*Samotherium neumayri*	Maragha	Rodler & Weithofer, 1890												38.0
d	*Samotherium neumayri*	Maragha	Rodler & Weithofer, 1890										28.0		33.0
e	*Samotherium neumayri*	Maragha	Rodler & Weithofer, 1890						15.0		20.0		21.5		24.0
f	*Samotherium neumayri*	Maragha	Rodler & Weithofer, 1890												36.0
g	*Samotherium neumayri*	Maragha	Rodler & Weithofer, 1890						20.0		25.0		29.0		
	Palaeotragus coelophrys	Maragha	Rodler & Weithofer, 1890												
	Palaeotragus coelophrys	Maragha	Rodler & Weithofer, 1890												
XIII*	*Palaeotragus microdon*	116 Kansu	Bohlin, 1926			56.0			11.0	7.0	16.0	11.0	25.0	15.0	
XIV*	*Palaeotragus microdon*	114 Shansi	Bohlin, 1926			60.0			13.0	8.0	18.0	11.0	28.0	16.0	
XV*	*Palaeotragus microdon*	49 Shansi	Bohlin, 1926			54.0			11.0	8.0	15.0	11.0	24.0	16.0	
XVI*	*Palaeotragus microdon*	115 Kansu	Bohlin, 1926			59.0			11.0	6.0	16.0	10.0	26.0	15.0	
5*	*Palaeotragus cfr. coelophrys?*	70	Bohlin, 1926			57.0					15.0	10.0	27.0	16.0	
9*	*Palaeotragus cfr. coelophrys?*	31	Bohlin, 1926			56.0			11.0	7.0	17.0	11.0	25.0	15.0	
I	*Palaeotragus microdon*	116 Kansu	Bohlin, 1926			48.0	80.0	131.0		10.0	15.0	13.0	18.0	15.0	
II	*Palaeotragus microdon*	116 Kansu	Bohlin, 1926			47.0	81.0	130.0	12.0	10.0	15.0	13.0	18.0	15.0	
III	*Palaeotragus microdon*	116 Kansu	Bohlin, 1926			49.0	82.0	132.0			15.0	14.0	18.0	15.0	
IV	*Palaeotragus microdon*	116 Kansu	Bohlin, 1926			49.0	84.0	136.0							
V	*Palaeotragus microdon*	116 Kansu	Bohlin, 1926			48.0	82.0	130.0	12.0	10.0	16.0	14.0		15.0	
VI	*Palaeotragus microdon*	116 Kansu	Bohlin, 1926			48.0	84.0	131.0	12.0	11.0	16.0		18.0	17.0	
VII	*Palaeotragus microdon*	108 Shansi	Bohlin, 1926			50.0		134.0			15.0	13.0	18.0	15.0	22.0
VIII	*Palaeotragus microdon*	114 Shansi	Bohlin, 1926				93.0							16.0	24.0
IX	*Palaeotragus microdon*	30 Shansi	Bohlin, 1926			50.0	81.0	132.0	13.0	10.0	17.0	14.0	18.0	15.0	
X	*Palaeotragus microdon*	109 Shansi	Bohlin, 1926				84.0						17.0	14.0	21.0
XI	*Palaeotragus microdon?*	49 Shansi	Bohlin, 1926				84.0				17.0	14.0	19.0	15.0	
1	*Palaeotragus cfr. coelophrys*	108 Shansi	Bohlin, 1926			55.0					17.0	14.0	19.0	15.0	24.0
2	*Palaeotragus cfr. coelophrys*	70	Bohlin, 1926			59.0		147.0							
3	*Palaeotragus cfr. coelophrys*	43	Bohlin, 1926				87.0								24.0
4	*Palaeotragus cfr. coelophrys?*	With P1	Bohlin, 1926			56.0	90.0	141.0	13.0	11.0	19.0	14.0	20.0	16.0	
Ex1	*Palaeotragus decipiens*		Bohlin, 1926			74.0	124.0	198.0	20.0	12.0	24.0	18.0	26.0	22.0	
Ex2	*Palaeotragus decipiens*		Bohlin, 1926			69.0	118.0	187.0	17.0	15.0	23.0	16.0	27.0	22.0	33.0
Ex I*	*Samotherium cfr. neumayri*		Bohlin, 1926			93.0			22.0	10.0	27.0	14.0	49.0	22.0	
	Samotherium cfr. neumayri		Bohlin, 1926			77.0	131.0	209.0							
Ex.2*	*Samotherium sinense*		Bohlin, 1926			101.0			21.0	12.0	29.0	18.0	52.0	22.0	
	Samotherium sinense		Bohlin, 1926			76.0	122.0	198.0		15.0		22.0		25.0	
	Samotherium sinense	China	Schlosser, 1903			78.0	115.0	190.0	23.5	14.0	27.0	17.0	32.0	21.0	33.0
	Samotherium major	Taskinpasa	Senyurek, 1954			76.0	137.0	213.0	23.6	14.2	25.6	17.2	27.8	20.4	36.4
M3868	*Samotherium boissieri ?*	Samos	Bohlin, 1926			74.0	124.0	195.0							
	Samotherium boissieri ?	Samos	Bohlin, 1926			67.0	117.0	183.0							
M2439	*Samotherium major*	Samos	Bohlin, 1926			74.0	130.0	201.0							
	Samotherium major	Samos	Bohlin, 1926			84.0	133.0	217.0							
	Samotherium major	Samos	Bohlin, 1926					250.0							
13	*Samotherium major*	Samos	Bohlin, 1926			74.0	129.0	203.0							
	Samotherium major	Samos	Bohlin, 1926			71.0	132.0	198.0							
	Samotherium major	Samos	Bohlin, 1926					213.0							

Appendix 2: Mandibles and lower teeth

Specimen number	Species	Locality	Museum / author	hp	Wmax	P_2-P_4	M_1-M_3	P_2-M_3	LP_2	lP_2	LP_3	lP_3	LP_4	lP_4	LM_1
*	*Samotherium*	Samos	Bohlin, 1926			75.0			17.0	9.0	21.0	12.0	38.0	16.0	
*	*Samotherium*	Samos	Bohlin, 1926			80.0			18.0	8.0	24.0	11.0	41.0	19.0	
*	*Samotherium major?*	Samos	Bohlin, 1926			91.0			21.0	11.0	27.0	15.0	46.0	21.0	
2	*Honanotherium schlosseri*	29	Bohlin, 1926				115.0								
3	*Honanotherium schlosseri*	29	Bohlin, 1926			75.0					26.0	20.0	27.0	23.0	
7	*Honanotherium schlosseri*	73	Bohlin, 1926			62.0	106.0	173.0	18.0	14.0	23.0	18.0	26.0	21.0	
Wagner "Orasius"	*Bohlinia attica*	Pikermi	Bohlin, 1926								20.0	14.0	22.0	17.0	26.0
*	*Helladotherium sp.*	Samos	Bohlin, 1926			92.0			23.0	13.0	30.0	18.0	45.0	24.0	40.0
1	*Birgerbohlinia schaubi*	Piera	Crusafont 1952				128.4								31.5
261	*Birgerbohlinia schaubi*	Piera	Crusafont 1952				137.5						33.0	21.0	38.2
CR2-215	*Birgerbohlinia schaubi*	Crevillente 2	Montoya-Morales 1991						25.0	16.4	31.1	20.0	33.8	22.2	37.9
min	*Decennatherium pachecoi*	Nombrevilla	Crusafont 1952						24.0	13.2	28.7	16.5	32.0	20.0	34.5
av	*Decennatherium pachecoi*	Nombrevilla	Crusafont 1952						26.4	14.3	30.3	18.4	33.1	21.8	37.2
max	*Decennatherium pachecoi*	Nombrevilla	Crusafont 1952						27.5	16.4	31.6	21.3	35.0	23.7	38.4
min	*Decennatherium pachecoi*	Los Valles	Morales and Soria, 1981						22.5	13.0	27.6	16.9	28.0	20.5	33.0
av	*Decennatherium pachecoi*	Los Valles	Morales and Soria, 1981						24.6	14.1	29.0	17.9	31.4	22.5	36.1
max	*Decennatherium pachecoi*	Los Valles	Morales and Soria, 1981						27.0	14.8	31.4	19.2	35.0	23.9	37.7
L9161	*Sivatherium hendeyi*	Langebaanweg	Harris, 1976								38.9	27.1	42.5	29.3	46.1
L31137	*Sivatherium hendeyi*	Langebaanweg	Harris, 1976						27.5	17.4	39.7	26.3	44.5	31.9	44.4
KTB 16*	*Samotherium major*	Kemikliteppe	Geraads, 1994			87.0			19.2	9.0	25.8	13.7	44.2	18.5	
KTD 54*	*Samotherium major*	Kemikliteppe	Geraads, 1994								26.7	13.6	45.5	20.0	
Sans (KTA?)*	*Samotherium major*	Kemikliteppe	Geraads, 1994								26.7	13.6	48.6	19.7	
KTA 141*	*Samotherium major*	Kemikliteppe	Geraads, 1994								27.0	13.5			
I 190	*Palaeotragus expectans (coelophrys)*	Sebastopol	Borissiak 1914						18.0	11.0	21.0	14.0	24.0	16.0	
I 126*	*Palaeotragus expectans (coelophrys)*	Sebastopol	Borissiak 1914						15.0	8.0	19.0	11.0	30.0	13.0	27.0
I 125*	*Palaeotragus expectans (coelophrys)*	Sebastopol	Borissiak 1914						15.0	8.0	22.0	11.0	29.0	14.0	26.5
I 123*	*Palaeotragus expectans (coelophrys)*	Sebastopol	Borissiak 1914						14.0	7.0	19.0	10.0	32.5	15.0	28.0

Notes

L = occlusal length

l = maximum width

hp = height of the mandible in front of P_2

Wmax = maximum width of the mandible

Lpost = length of the posterior region of the premolars

specimens with a star (*) characterize deciduous teeth

NHML (SPGM) in parenthesis the museum where the original specimen is stored

SPGM : Sammlung fur Palaontologie und Historische Geologie, Munchen

Appendix 2: Mandibles and lower teeth

Specimen number	Species	Locality	IM_1	LM_2	IM_2	LM_3	IM_3	Pm/M	Pm/PM	P3 Lpost/L	P4 Lpost/L	IP3/LP3	IP4/LP4	IM1/LM1	LP3/LP2	LP4/LP3
Ke 306	*Palaeotragus rouenii*	Kerassia	15.2	25.6	15.0									0.68		
K3.181	*Palaeotragus rouenii*	Kerassia	16.1	25.5	17.0	34.5	16.6							0.65		
K4/Δ8/1 d	*Palaeotragus sp.*	Kerassia	17.3	28.9	18.2	38.2	17.7	72.5	41.4	0.44	0.42	0.58	0.64	0.73		1.07
K4/Δ8/2 s	*Palaeotragus sp.*	Kerassia								0.43		0.56			1.16	
K4/Δ111	*Palaeotragus rouenii*	Kerassia	17.9	26.7	20.0	35.9	17.6	67.3	40.6	0.31	0.36	0.70	0.73	0.81	1.21	1.12
K4/Δ119/34 d	*Samotherium major*	Kerassia	32.8	45.8	34.2	59.0	33.2	65.6	39.8	0.31	0.27	0.70	0.95	0.74	1.26	0.88
K4/Δ54/1 s	*Samotherium major*	Kerassia		45.9	34.0	60.1	33.0									
K4/Δ107/9	*Palaeotragus rouenii*	Kerassia				35.9	17.6									
K4/Δ324	*Palaeotragus rouenii*	Kerassia	15.5	26.1	18.8	36.0	18.7	67.5	40.7	0.31	0.36	0.69	0.74	0.78	1.15	1.12
K4/Δ350	*Helladotherium duvernoyi*	Kerassia														
K1/Δ 318	*Palaeotragus rouenii*	Kerassia														
M8367 (+M13063)	*Palaeotragus rouenii*	Pikermi (O)	15.5	23.7	17.6	31.4	15.4	72.5	43.1	0.32	0.36	0.55	0.64	0.67	1.25	1.10
*without number	*Palaeotragus rouenii*	Pikermi (O)										0.56	0.53			1.24
*M13062	*Palaeotragus rouenii*	Pikermi (O)	13.4	26.2	18.1							0.48	0.41	0.57	1.56	1.61
M11453	*Palaeotragus rouenii*	Pikermi (O)	17.5											0.71		
M11397	*Helladotherium duvernoyi*	Pikermi (O)								0.31		0.65			1.32	
*M11496	*Helladotherium duvernoyi*	Pikermi (O)										0.53	0.38			1.66
M4067 (cast)	*Helladotherium duvernoyi*	Pikermi (O)	31.9	44.0	33.4	52.9	31.5			0.37	0.34	0.75	0.81	0.74		1.11
M4215 (Hol)	*Samotherium boissieri*	Samos		36.9		49.3										
M4215	*Samotherium boissieri*	Samos													1.32	0.94
*M4237	*Samotherium boissieri*	Samos	25.9	47.3	22.3							0.74	0.48	0.62		2.05
M4236 (169)	*Samotherium boissieri*	Samos	23.7	36.8	22.6	46.0	21.0	63.6	39.4	0.34	0.24	0.68	0.72	0.75	1.02	1.20
M4235a (162)	*Samotherium boissieri*	Samos	24.5	36.9	25.9	48.2	24.4	62.4	39.5	0.28	0.18	0.80	0.72	0.74	1.23	1.28
M4235b (161)	*Samotherium boissieri*	Samos		33.7	25.2	47.7	24.1	64.3	39.2		0.20		0.70	0.00	1.16	1.31
M4234 (159)	*Samotherium boissieri*	Samos	23.6	37.5	23.7	47.8	23.1	55.2	35.2	0.33	0.29	0.67	0.74	0.66	1.15	1.20
M4224 (158)	*Samotherium boissieri*	Samos	22.5	37.7	22.3	47.2	22.6	61.6	39.3	0.31	0.25	0.58	0.62	0.63	1.30	1.20
*M4239	*Samotherium boissieri*	Samos										0.55	0.46		1.16	1.77
*4238a	*Samotherium boissieri*	Samos										0.46	0.38			1.66
*4240	*Samotherium boissieri*	Samos										0.52	0.45			1.74
*4237	*Samotherium boissieri*	Samos	24.7	45.1	21.8			55.7	36.8				0.49	0.59		
*4238b	*Samotherium boissieri*	Samos											0.34			
M4242a	*Samotherium boissieri*	Samos														
*M4242e(149)	*Palaeotragus coelophrys*	Samos	19.6	31.1	19.0									0.66		
M3873a	*Samotherium neumayri*	Maragha				54.3	24.8									
M3873b	*Samotherium neumayri*	Maragha		40.0	27.3											
M3873c	*Samotherium neumayri*	Maragha											0.65			
without number	*Bohlinia attica*	Pikermi (O)	16.8	26.8	17.9	35.9	18.8	63.3	39.2	0.36	0.38	0.59	0.69	0.62	1.52	1.09
DIT 2	*Palaeotragus rouenii*	Ditiko 2	16.0	24.0	17.0	33.0	17.0	62.8	38.9			0.65	0.70	0.73	1.31	1.18
R.Pl. 104	*Palaeotrgus coelophrys*	Ravin de la Pluie														
VAT 3	*Samotherium boissieri (major)*	Vathilakkos 3	30.0	47.0	31.0	55.0	28.0	66.2	42.2			0.64	0.82	0.77	1.08	1.00
PNT 111	*?Decenatherium macedoniae*	Pentalophos						64.6	39.0							
PNT 137	*?Decenatherium macedoniae*	Pentalophos														
NIK 1	*Helladotherium duvernoyi*	Nikiti 1	33.5	41.3	35.0	65.8	35.0	61.7	38.3			0.81	0.87	0.92	1.22	1.16
MAR 882	*Helladotherium duvernoyi*	Maragha		44.3	31.2	66.0	33.3	65.1	39.5			0.72	0.74		1.23	1.10
*	*Helladotherium duvernoyi*	Pikermi	28.0	45.0										0.65	1.38	1.59
	Palaeotragus rouenii	Pikermi		24.0	17.0	32.0									1.00	1.13
	Samotherium neumayeri	Maragha						59.2	37.9							

Appendix 2: Mandibles and lower teeth

Specimen number	Species	Locality	IM_1	LM_2	IM_2	LM_3	IM_3	Pm/M	Pm/PM	P3 Lpost/L	P4 Lpost/L	IP3/LP3	IP4/LP4	IM1/LM1	LP3/LP2	LP4/LP3
	Palaeotragus coelophrys	Maragha						65.0	38.2							
a	*Samotherium neumayri*	Maragha		42.0		55.0										
b	*Samotherium neumayri*	Maragha		42.0		55.0										
c	*Samotherium neumayri*	Maragha		42.0		53.0										
d	*Samotherium neumayri*	Maragha		39.0		57.0										
e	*Samotherium neumayri*	Maragha		28.0		45.0									1.33	1.08
f	*Samotherium neumayri*	Maragha		41.0		49.0										
g	*Samotherium neumayri*	Maragha													1.25	1.16
	Palaeotragus coelophrys	Maragha		32.5		36.0										
	Palaeotragus coelophrys	Maragha		29.0		39.0										
XIII*	*Palaeotragus microdon*	116 Kansu										0.69	0.60		1.45	1.56
XIV*	*Palaeotragus microdon*	114 Shansi										0.61	0.57		1.38	1.56
XV*	*Palaeotragus microdon*	49 Shansi										0.73	0.67		1.36	1.60
XVI*	*Palaeotragus microdon*	115 Kansu										0.63	0.58		1.45	1.63
5*	*Palaeotragus cfr. coelophrys?*	70										0.67	0.59			1.80
9*	*Palaeotragus cfr. coelophrys?*	31										0.65	0.60		1.55	1.47
I	*Palaeotragus microdon*	116 Kansu	17.0	23.0	18.0	36.0	18.0	60.0	36.6			0.87	0.83			1.20
II	*Palaeotragus microdon*	116 Kansu	18.0	23.0	18.0	37.0	18.0	58.0	36.2			0.87	0.83		1.25	1.20
III	*Palaeotragus microdon*	116 Kansu	19.0	23.0	19.0	34.0	19.0	59.8	37.1			0.93	0.83			1.20
IV	*Palaeotragus microdon*	116 Kansu		23.0	19.0	38.0	19.0	58.3	36.0							
V	*Palaeotragus microdon*	116 Kansu	19.0	24.0	19.0	37.0	18.0	58.5	36.9			0.88			1.33	
VI	*Palaeotragus microdon*	116 Kansu	21.0					57.1	36.6				0.94		1.33	1.13
VII	*Palaeotragus microdon*	108 Shansi	18.0	22.0	19.0				37.3			0.87	0.83	0.82		1.20
VIII	*Palaeotragus microdon*	114 Shansi	20.0											0.83		
IX	*Palaeotragus microdon*	30 Shansi	18.0	26.0	18.0		18.0	61.7	37.9			0.82	0.83			
X	*Palaeotragus microdon*	109 Shansi	17.0	24.0	17.0	35.0	15.0						0.82	0.81		
XI	*Palaeotragus microdon?*	49 Shansi	18.0	24.0	19.0	35.0	18.0					0.82	0.79			1.12
1	*Palaeotragus cfr. coelophrys*	108 Shansi	20.0	24.0	20.0							0.82	0.79	0.83		1.12
2	*Palaeotragus cfr. coelophrys*	70			23.0	40.0			40.1							
3	*Palaeotragus cfr. coelophrys*	43		25.0	21.0	37.0	20.0									
4	*Palaeotragus cfr. coelophrys?*	With P1	20.0	26.0	20.0	40.0	21.0	62.2	39.7			0.74	0.80		1.46	1.05
Ex1	*Palaeotragus decipiens*		29.0	38.0	26.0	52.0	26.0	59.7	37.4			0.75	0.85		1.20	1.08
Ex2	*Palaeotragus decipiens*		26.0	37.0	28.0	48.0	24.0	58.5	36.9			0.70	0.81	0.79	1.35	1.17
Ex I*	*Samotherium cfr. neumayri*											0.52	0.45		1.23	1.81
	Samotherium cfr. neumayri							58.8	36.8							
Ex.2*	*Samotherium sinense*											0.62	0.42		1.38	1.79
	Samotherium sinense		31.0		30.0		26.0	62.3	38.4							
	Samotherium sinense	China	22.0	38.0	26.0	51.0	27.0	67.8	41.1			0.63	0.66	0.67	1.15	1.19
	Samotherium major	Taskinpasa	27.3	43.4	29.5	59.2	28.6	55.5	35.7			0.67	0.73	0.75	1.08	1.09
M3868	*Samotherium boissieri ?*	Samos						59.7	37.9							
	Samotherium boissieri ?	Samos						57.3	36.6							
M2439	*Samotherium major*	Samos						56.9	36.8							
	Samotherium major	Samos						63.2	38.7							
	Samotherium major	Samos														
13	*Samotherium major*	Samos						57.4	36.5							
	Samotherium major	Samos						53.8	35.9							
	Samotherium major	Samos														

Appendix 2: Mandibles and lower teeth

Specimen number	Species	Locality	IM_1	LM_2	IM_2	LM_3	IM_3	Pm/M	Pm/PM	P3 Lpost/L	P4 Lpost/L	IP3/LP3	IP4/LP4	IM1/LM1	LP3/LP2	LP4/LP3
*	*Samotherium*	Samos										0.57	0.42		1.24	1.81
*	*Samotherium*	Samos										0.46	0.46		1.33	1.71
*	*Samotherium major?*	Samos										0.56	0.46		1.29	1.70
2	*Honanotherium schlosseri*	29				48.0	28.0									
3	*Honanotherium schlosseri*	29										0.77	0.85			1.04
7	*Honanotherium schlosseri*	73		31.0	27.0	47.0	25.0	58.5	35.8			0.78	0.81		1.28	1.13
Wagner "Orasius"	*Bohlinia attica*	Pikermi	17.0	26.0	18.0	36.0	19.0					0.70	0.77	0.65		1.10
*	*Helladotherium sp.*	Samos	30.0									0.60	0.53	0.75	1.30	1.50
1	*Birgerbohlinia schaubi*	Piera	24.0	36.0	27.0	58.5	28.0							0.76		
261	*Birgerbohlinia schaubi*	Piera	25.8	44.1	29.0	57.2	29.0						0.64	0.68		
CR2-215	*Birgerbohlinia schaubi*	Crevillente 2	27.1	38.0	29.7	54.5	28.0					0.64	0.66	0.72	1.24	1.09
min	*Decennatherium pachecoi*	Nombrevilla	25.0	40.0	27.8	50.0	24.3					0.57	0.63	0.72	1.20	1.11
av	*Decennatherium pachecoi*	Nombrevilla	26.4	41.6	28.4	54.3	26.2					0.61	0.66	0.71	1.15	1.09
max	*Decennatherium pachecoi*	Nombrevilla	28.5	42.8	29.0	56.6	28.7					0.67	0.68	0.74	1.15	1.11
min	*Decennatherium pachecoi*	Los Valles	23.0	39.5	25.5							0.61	0.73	0.70	1.23	1.01
av	*Decennatherium pachecoi*	Los Valles	25.2	40.8	26.2	53.0	22.8					0.62	0.72	0.70	1.18	1.08
max	*Decennatherium pachecoi*	Los Valles	27.0	42.0	26.8							0.61	0.68	0.72	1.16	1.11
L9161	*Sivatherium hendeyi*	Langebaanweg	30.6	50.6	36.7	71.5	34.7					0.70	0.69	0.66		1.09
L31137	*Sivatherium hendeyi*	Langebaanweg	33.8			64.2	33.1					0.66	0.72	0.76	1.44	1.12
KTB 16*	*Samotherium major*	Kemikliteppe										0.53	0.42		1.34	1.71
KTD 54*	*Samotherium major*	Kemikliteppe										0.51	0.44			1.70
Sans (KTA?)*	*Samotherium major*	Kemikliteppe										0.51	0.41			1.82
KTA 141*	*Samotherium major*	Kemikliteppe										0.50				0.00
I 190	*Palaeotragus expectans (coelophrys)*	Sebastopol														
I 126*	*Palaeotragus expectans (coelophrys)*	Sebastopol	19.0	30.0	20.5	37.5										
I 125*	*Palaeotragus expectans (coelophrys)*	Sebastopol	17.0													
I 123*	*Palaeotragus expectans (coelophrys)*	Sebastopol	19.0													

Appendix 3: Humerus

Specimen number	Species	Locality	Museum / author	L1	L2	DTpr	DTd	α	β	γ	δ	ε	στ	ζ	η	υ	ι	ια	ιβ	ιγ
Ke 302	*Bohlinia attica*	Kerassia	AMPG				104.6		49.0	109.7			48.0	49.6						
K4/Δ110/7	*Helladotherium duvernoyi*	Kerassia	AMPG	>520			138.8		86.2	137.5	78.4	99.2	65.4	60.4	127.0	51.9	88.8	87.7	103.6	55.4
K4/Δ107/2	*Palaeotragus sp.*	Kerassia	AMPG				98.0		50.4	79.3	46.1	59.5	40.2	39.6			55.4	55.1		
M48288	*Palaeotragus rouenii*	Pikermi	NHML			105.2		70.2							76.2	33.0				
M11399a	*Bohlinia attica*	Pikermi	NHML				119.6		67.0		61.0	78.7	49.1	42.1	103.9	33.2	64.2	57.4	84.5	44.8
M11399b	*Bohlinia attica*	Pikermi	NHML				111.7		57.2	88.0	54.9	74.9	43.2	41.8			61.7	53.5		43.7
M11370	*Helladotherium duvernoyi*	Pikermi	NHML	521.1	479.3	174.2	144.0	130.0	81.9	110.6	68.1	91.3	52.3	53.6	126.6	60.1	77.5	73.3	98.2	67.0
M11371a	*Helladotherium duvernoyi*	Pikermi	NHML				140.8		80.0	111.3	68.2	90.5	52.8	53.5			75.0	75.0	94.2	70.0
M11371b	*Helladotherium duvernoyi*	Pikermi	NHML				143.2		80.1	118.9	71.5	96.7	55.3	56.4	130.1	72.0	84.1	83.6	95.5	78.2
M48291	*Helladotherium duvernoyi*	Pikermi	NHML				127.0		76.6	111.6	64.2	90.7	51.2	53.1			67.0	67.5	82.8	62.8
M4256a(190)	*Samotherium boissieri*	Samos	NHML				102.2		52.5	79.6	51.7	77.2	38.5				51.0	60.8		
M4253a	*Samotherium boissieri*	Samos	NHML				104.3		61.3	69.5					112.0	53.5	63.5	73.7	87.0	56.0
M4253b	*Samotherium boissieri*	Samos	NHML						65.2	104.8							63.5	70.8	87.8	62.4
M4256b(183)	*Samotherium boissieri*	Samos	NHML				89.4		52.5	90.3		78.9		40.4	89.3	53.3	53.3	64.2	80.5	53.7
M4255a	*Samotherium boissieri*	Samos	NHML				109.6		56.5	76.3	55.3		40.8	44.7			55.5	70.8		
M4255b	*Samotherium boissieri*	Samos	NHML																	
M4256c	*Samotherium boissieri*	Samos	NHML				92.8		57.7		52.0		40.9	40.5			54.5	62.2		
M4254	*Samotherium boissieri*	Samos	NHML			102.9		133.4							99.8	51.3			85.6	52.7
M4252	*Samotherium boissieri*	Samos	NHML	390.2	345.2	122.1	96.5	138.6	55.9	105.5	59.5	94.9	40.4	45.8	96.8	66.6	57.1	72.0	87.2	68.2
M4257a(376)	*Samotherium boissieri*	Samos	NHML				84.5		42.8	108.2	49.7	80.1	33.6				45.4	63.1		
M4257b	*Samotherium boissieri*	Samos	NHML				92.4		56.9	93.5		76.9	37.9							
M4258	*Samotherium boissieri*	Samos	NHML				97.7		51.5	96.9		83.5					48.6	62.7		
KTA 93	*Samotherium major*	Kemiklitepe	Geraads, 1994											54.0						
KTA 102	*Samotherium major*	Kemiklitepe	Geraads, 1994																	
KTA 137	*Samotherium major*	Kemiklitepe	Geraads, 1994	430?										54.0						
KTB 49	*Samotherium major*	Kemiklitepe	Geraads, 1994	410?			122.0							52.0						
	Samotherium major	Samos	Geraads, 1994	410?			116.0													
KTD 48	*Samotherium ?sp.*	Kemiklitepe	Geraads, 1994	373.0			115.0							49.5						
KTA 113	*Palaeotragus rouenii*	Kemiklitepe	Geraads, 1994				73.0							31.0						
KTD 17a	*Palaeotragus rouenii*	Kemiklitepe	Geraads, 1994				78.0							35.0						
I 198	*Palaeotragus coelophrys (expectans)*	Sebastopol	Borissiak, 1914				102.0													
PNT 113	*?Decenatherium macedoniae*	Pentalophos	(Geraads, 1989)				111.0							49.5						
R.Pl. 105	*Bohlinia attica*	Ravin de la Pluie	(Geraads, 1979)	480.0			116.0													
DIT 1	*Bohlinia attica*	Ditiko 2	(Geraads, 1979)	445.0			124.0													
DIT 9	*Bohlinia attica*	Ditiko 3	(Geraads, 1979)	410.0			90.0													
MAR 544	*Samotherium neumayri*	Maragha	(Geraads, 1974)	380.0			110.0							41.0						
547b	*Samotherium neumayri*	Maragha	(Geraads, 1974)	400.0			125.0							49.0						
Slq	*Samotherium boissieri*	Salonique	(Geraads, 1974)	390.0			109.0							46.0						
	Samotherium boissieri		Bohlin 1926	455.0			112.0													
	Samotherium sinense		Bohlin 1926	494.0	427.0	154.0	122.0	176?												
	Samotherium eminens		Bohlin 1926	485.0		183.0	124.0	118.0												
1506	*Helladotherium duvernoyi*	Pikermi	(Geraads, 1974)	460.0			134.0							53.0						
919	*Helladotherium duvernoyi*	Maragha	Geraads, 1974				138.0							59.0						
	Palaeotragus coelophrys	Maragha	Rodler & Weithofer 1890				89.0													
PIK 1681	*Palaeotragus rouenii*	Pikermi	(Geraads, 1974)	320.0			75.0							33.0						
108(1)	*Palaeotragus microdon*		Bohlin 1926	314.0	285.0		80.0													
116(1)	*Palaeotragus microdon*		Bohlin 1926		295.0		85.0													
PIK 1617	*Bohlinia attica*	Pikermi	(Geraads, 1974)				104.0							53.0						
PIK 1618	*Bohlinia attica*	Pikermi	(Geraads, 1974)				106.0													
PIK 1619	*Bohlinia attica*	Pikermi	(Geraads, 1974)				112.0							52.0						
Slq 678	*Bohlinia attica*	Salonique	(Geraads, 1974)				98.0							41.0						
	Bohlinia attica	Pikermi	(Gaudry, 1862)	500.0			105.0													
	Helladotherium duvernoyi	Pikermi	(Gaudry, 1862)	490.0			131.0													
	Bohlinia attica	Maragha	Mecquenem, 1924				100.0													
	Bohlinia attica	Maragha	Mecquenem, 1924				110.0													

Appendix 3: Humerus

Notes

L1 = maximum length measured at the top of the major tubercle of the trochiter
L2 = length measured at the top of the head
DTpr =proximal transverse diameter
DTd = distal transverse diameter
α = anteroposterior diameter of the head
β = maximum height of the medial trochlea
γ = anteroposterior diameter of the trochlea-epitrochlea
δ = maximum height of the lateral trochlea
ε = anteroposterior diameter of the condyle-epicondyle
στ = height of the intertrochlear furrow
ζ = anteroposterior diameter of the intertrochlear furrow
η = transverse diameter of the diaphysis at the level of the deltoid tuberosity
θ = anteroposterior diameter of the diaphysis at the level of the deltoid tuberosity
ι = the minimum transverse diameter of the diaphysis at its lower part
ια = the respective anteroposterior diameter of the above
ιβ = transverse diameter in the middle of the diaphysis
ιγ = anteroposterior diameter in the middle of the diaphysis

Appendix 4: Radius-Ulna

Specimen number	Species	Locality	Museum / author	L	DAPpr	DTpr	DAPd	DTd	DAPdia	DTdia	d
Ke 164	*Helladotherium duvernoyi*	Kerassia	AMPG				87.0	139.5			
K1/Δ78	*Samotherium major*	Kerassia	AMPG	538.9	83.5	148.6	83.0	119.8	49.4	73.2	42.7
K1/Δ85	*? Palaeotragus rouenii*	Kerassia	AMPG						34.8	49.6	
K1/Δ87	*Samotherium major*	Kerassia	AMPG		78.3	136.0			48.0	85.6	39.0
K1/Δ89	*Samotherium major*	Kerassia	AMPG		78.8	135.6					
K1/Δ90	*Samotherium major*	Kerassia	AMPG	502.6			87.5	119.0	50.0	83.6	
K1/Δ155	*Helladotherium duvernoyi*	Kerassia	AMPG	536.4			71.0	118.8			
K4/Δ110/2	*Helladotherium duvernoyi*	Kerassia	AMPG	634.4	81.2		79.0	139.0	57.5	88.0	
K4/Δ133/6	*Helladotherium duvernoyi*	Kerassia	AMPG		81.0	167.0					
M11405	*Palaeotragus rouenii*	Pikermi	NHML				50.1	60.0	31.0	46.4	
M11400	*Bohlinia attica*	Pikermi	NHML				63.2	98.5	42.1	67.6	
M11372	*Helladotherium duvernoyi*	Pikermi	NHML	636.0	85.2	154.6	99.0	129.5	64.0	88.5	50.3
M11373	*Helladotherium duvernoyi*	Pikermi	NHML	565.4	78.5		84.5	131.5	54.2	81.7	
M11374a	*Helladotherium duvernoyi*	Pikermi	NHML		81.8	143.5			45.8	76.2	49.6
M11374b	*Helladotherium duvernoyi*	Pikermi	NHML				75.5	133.8			
M11374c*	*Helladotherium duvernoyi*	Pikermi	NHML				77.3	123.5			
M11374d*	*Helladotherium duvernoyi*	Pikermi	NHML				80.0	116.0			
M4257a(376)	*Samotherium boissieri*	Samos	NHML		64.4	96.3					
M4257b	*Samotherium boissieri*	Samos	NHML		57.3	108.9					
M4258	*Samotherium boissieri*	Samos	NHML		61.6	113.8				51.1	
M4259	*Samotherium boissieri*	Samos	NHML	462.7	56.4	119.1	60.8	98.6	39.0	61.9	30.0
M4260	*Samotherium boissieri*	Samos	NHML	447.1	62.0	114.8	62.7	95.4	40.1	56.3	30.0
M4262	*Samotherium boissieri*	Samos	NHML	462.8		105.0	58.6	91.7	37.7	54.8	35.3
M4261	*Samotherium boissieri*	Samos	NHML	449.0	49.6				37.7	62.5	30.0
M4264a	*Samotherium boissieri*	Samos	NHML		65.7	112.1					
M4264b	*Samotherium boissieri*	Samos	NHML				67.5	94.2	41.2	65.8	
M4263a(115)	*Samotherium boissieri*	Samos	NHML		63.5	112.0			51.6	58.5	29.2
M4263b(318)	*Samotherium boissieri*	Samos	NHML		65.6	113.8					
M4264d(323)	*Samotherium boissieri*	Samos	NHML				65.3	95.3			
M4264e*	*Samotherium boissieri*	Samos	NHML				58.1	94.0			
M4264f(336)	*Samotherium boissieri*	Samos	NHML				69.5	84.3			
M4264g(347)	*Samotherium boissieri*	Samos	NHML				62.4	87.8			
M4264h	*Samotherium boissieri*	Samos	NHML		65.5	96.2					
M4264i(319)	*Samotherium boissieri*	Samos	NHML		58.2	104.0			35.1	51.2	
M4265	*Samotherium boissieri*	Samos	NHML				68.0	85.2	38.2	51.5	

Appendix 4: Radius-Ulna

Specimen number	Species	Locality	Museum / author	L	DAPpr	DTpr	DAPd	DTd	DAPdia	DTdia	d
M4266	*Samotherium boissieri*	Samos	NHML				63.3	94.3			
M4314	*?Palaeotragus*	Samos	NHML		41.2	77.0			32.8	48.7	
M4313	*?Palaeotragus*	Samos	NHML	370.5	38.2	82.6	40.9	75.1	36.0	40.1	
M4265(107)		Samos	NHML				60.7	86.0	39.9	47.6	
KTD 17b	*Palaeotragus rouenii*	Kemiklitepe	Geraads, 1994			79.0				51.0	
KTD 46	*Palaeotragus rouenii*	Kemiklitepe	Geraads, 1994	453.0		79.5		70.0		48.0	
KTD 43	*Palaeotragus rouenii*	Kemiklitepe	Geraads, 1994					66.5		49.0	
	Samotherium major	Samos	Geraads, 1994	525.0		113.0				65.0	
	Samotherium major	Samos	Geraads, 1994	535.0		128.0				78.0	
Slq 687	*Samotherium major*	Salonique	Geraads, 1994	565.0		128.0		113.0		82.0	
PIK 1683	*Palaeotragus rouenii*	Pikermi	Geraads, 1994	495.0		69.0		63.0			
PIK 1685	*Palaeotragus rouenii*	Pikermi	Geraads, 1994	457.0		72.0		64.0			
	Palaeotragus rouenii	Pikermi	Geraads, 1994	480.0		74.0				48.0	
PNT 114	*?Decenatherium macedoniae*	Pentalophos	Geraads, 1989	555.0		111.0		90.0		79.0	
R.Pl. 105	*Bohlinia attica*	Ravin de la Pluie	Geraads, 1979	900.0				116.0			
DIT 1	*Bohlinia attica*	Ditiko 2	Geraads, 1979	850.0		120.0		115.0			
DIT 9	*Bohlinia attica*	Ditiko 3	Geraads, 1979	788.0		96.0					
NTK min	*Palaeotragus rouenii*	Nikiti 1	Kostopoulos et al.1996	452.5	45.2	81.1	45.0	71.7	30.6	49.5	
NTK max	*Palaeotragus rouenii*	Nikiti 1	Kostopoulos et al.1996	470.0	46.7	91.6	54.0	76.6	33.5	50.5	
NTK mean	*Palaeotragus rouenii*	Nikiti 1	Kostopoulos et al.1996	464.3	45.6	84.1	50.3	74.7	32.4	50.0	
NTK 201	*Helladotherium duvernoyi*	Nikiti 1	Kostopoulos et al.1996	580.0	73.0	116.0		83.0	50.0	80.0	
MAR 548	*Samotherium neumayri*	Maragha	Geraads, 1974	535.0	64.0	122.0	58.0	105.0		78.0	
MAR 549	*Samotherium neumayri*	Maragha	Geraads, 1974	528.0	58.0	116.0	48.0			70.0	
MAR 550	*Samotherium neumayri*	Maragha	Geraads, 1974		58.0	121.0				68.0	
MAR 551	*Samotherium neumayri*	Maragha	Geraads, 1974	545.0	65.0	120.0	53.0			78.0	
MAR 552	*Samotherium neumayri*	Maragha	Geraads, 1974	520.0						74.0	
Ex 5	*Samotherium sinense*	China	Bohlin 1926	550.0		128.0		128.0			
Ex 1	*Samotherium sinense*	116.00	Bohlin 1926	548.0		150.0					
Ex 2	*Samotherium sinense*	116.00	Bohlin 1926	571.0		162.0		127.0			
	Samotherium sinense	30.00	Bohlin 1926	554.0		168.0		132.0			
557.00	*Samotherium eminens*		Bohlin 1926	570.0		146.0		116.0			
MHNP1926-4	*Samotherium sinense*	China	Geraads, 1974	555.0	58.0	130.0		108.0			
Slq 689	*Helladotherium duvernoyi*	Salonique	Geraads, 1974	610.0		138.0		143.0		120.0	
	Helladotherium duvernoyi	Samos	Bohlin 1926	610.0		150.0		138.0		79.0	
K 1507- 1510, 15	*Helladotherium duvernoyi*	Pikermi	Geraads, 1974	565.0	62.0	129.0	59.0	108.0			

Appendix 4: Radius-Ulna

Specimen number	Species	Locality	Museum / author	L	DAPpr	DTpr	DAPd	DTd	DAPdia	DTdia	d
max	*Helladotherium duvernoyi*	Pikermi	Geraads, 1974	575.0	65.0	133.0	62.0	113.0			
MAR 700	*Palaeotragus coelophrys*	Maragha	Geraads, 1974	485.0	52.0	105.0		91.0			
MAR 701	*Palaeotragus coelophrys*	Maragha	Geraads, 1974	510.0				96.0			
MAR 702	*Palaeotragus coelophrys*	Maragha	Geraads, 1974		50.0	96.0					
PIK 1682	*Palaeotragus rouenii*	Pikermi	Geraads, 1974	455.0				62.0			
PIK 1683	*Palaeotragus rouenii*	Pikermi	Geraads, 1974	495.0	36.0	69.0		63.0			
PIK 1684	*Palaeotragus rouenii*	Pikermi	Geraads, 1974	500.0	37.0	71.0		69.0			
PIK 1685	*Palaeotragus rouenii*	Pikermi	Geraads, 1974	457.0	37.0	72.0		64.0			
116(1)	*Palaeotragus microdon*		Bohlin 1926	396.0		63.0		60.0			
PIK	*Bohlinia attica*	Pikermi	Geraads, 1974	800.0				97.0			
Slq 679	*Bohlinia attica*	Salonique	Geraads, 1974	690.0	47.0	92.0		83.0			
	Bohlinia attica	Pikermi	Gaudry, 1862	800.0				113.0			
	Helladotherium duvernoyi	Pikermi	Gaudry, 1862	570.0		138.0		128.0		73.0	
	Helladotherium duvernoyi	Pikermi	Bohlin 1926	585.0		149.0		127.0			
	Helladotherium duvernoyi	Veles	Schlosser, 1921	600.0		130.0		125.0		70.0	
	Samotherium major	Samos	Bohlin 1926	530.0		152.0		127.0		84.0	
194-x	*Decennatherium pachecoi*	Los Valles	Morales and Soria, 1981		52.0	94.3					

Notes

L = length of the radius

DAPpr = proximal anteroposterior diameter of the radius

DTpr = proximal transverse diameter of the radius

DAPd = distal anteroposterior diameter of the radius

DTd = distal transverse diameter of the radius

DAPdia = anteroposterior diameter of the radius in the middle of the diaphysis

DTdia = transverse diameter of the radius in the middle of the diaphysis

d = maximum width of the of the olecranon articular surface

specimens with a star (*) characterize juveniles

Appendix 5: Metacarpal III-IV

Specimen number	Species	Locality	Museum / author	L	DAPpr	DTpr	DAPd	DTd	DAPdia	DTdia	Robusticity index
Ke 99/40		Kerassia	AMPG		55.2						
Ke 99/41	*Helladotherium duvernoyi*	Kerassia	AMPG				64.3	110.5			
K1/Δ82	*Helladotherium duvernoyi*	Kerassia	AMPG	399.5	73.3	112.9	65.3	103.5	53.7	65.0	16.3
K1/Δ244	*Samotherium major*	Kerassia	AMPG	398.2	63.4		54.9	101.4	54.6		
K1/A9	*Samotherium major*	Kerassia	AMPG				52.4	96.6			
K3.335	*Palaeotragus rouenii*	Kerassia	AMPG		39.3	55.0					
K4/Δ86/1	*Helladotherium duvernoyi*	Kerassia	AMPG				67.8	113.2			
K4/Δ119/18	*Palaeotragus rouenii*	Kerassia	AMPG		45.8	62.4					
K4/Δ119/33	*Helladotherium duvernoyi*	Kerassia	AMPG	442.7	69.8	104.3	67.5	107.8	55.4	68.1	15.4
K4/Δ331/5	*Palaeotragus rouenii*	Kerassia	AMPG	445.0	50.0	64.1	43.7	67.3	39.0	38.4	8.6
K4/Δ340/1	*Helladotherium duvernoyi*	Kerassia	AMPG				66.3	110.0			
M11406a	*Palaeotragus rouenii*	Pikermi	NHML	405.3	38.2	60.5	32.7	52.6	33.6	35.0	8.6
M11406b	*Palaeotragus rouenii*	Pikermi	NHML		42.2	57.7			32.8	33.2	
*	*Palaeotragus rouenii*	Pikermi	Sedgwick				40.6	66.7	35.0	29.6	
M11403a*	*Bohlinia attica*	Pikermi	NHML		61.7	95.5			52.8	59.7	
M11401	*Bohlinia attica*	Pikermi	NHML		53.2	81.3			47.0	51.0	
M11404b	*Bohlinia attica*	Pikermi	NHML				48.6	73.3			
M11377	*Helladotherium duvernoyi*	Pikermi	NHML	425.8	62.7	105.5	59.2	103.4	53.2	66.2	15.6
M11382	*Helladotherium duvernoyi*	Pikermi	NHML	415.7	66.0	96.1	56.3	92.2	53.4	55.5	13.4
M4267a	*Samotherium boissieri*	Samos	NHML	338.3	47.1	70.3	39.7	62.2	35.5	38.1	11.3
M4267b(91)	*Samotherium boissieri*	Samos	NHML	352.7	53.2	76.2	47.3	76.2	33.7	40.7	11.5
M4267c(95)	*Samotherium boissieri*	Samos	NHML	358.7	46.6	80.7	45.7	90.0	38.6	46.3	12.9
M4266(109)	*Samotherium boissieri*	Samos	NHML		43.2	72.8					
M4267d(102)	*Samotherium boissieri*	Samos	NHML	338.3	47.5	78.7	43.2	78.2	36.9	40.7	12.0
M4267e(101)	*Samotherium boissieri*	Samos	NHML	331.8	47.6	76.2	42.9	76.1	38.7	41.3	12.5
M4267f(97)	*Samotherium boissieri*	Samos	NHML	339.9	44.5	69.2		70.7	37.2	38.9	11.4
M4267g(93)	*Samotherium boissieri*	Samos	NHML	337.0	46.2	73.2	41.0	66.0	34.7	36.4	10.8
without numbe	*Samotherium boissieri*	Samos	NHML		45.0	71.0					
M4267h(94)	*Samotherium boissieri*	Samos	NHML	356.4	52.1	77.9	44.2	82.5	38.5	42.2	11.8
M4267i(100)	*Samotherium boissieri*	Samos	NHML	344.3	50.5	74.6	41.3	80.8	37.3	37.0	10.8
M4267j(98)	*Samotherium boissieri*	Samos	NHML	336.9	53.9	72.4	40.4	76.9	41.0	41.5	12.3
M4268	*Samotherium boissieri*	Samos	NHML	337.6	46.1	65.4	40.7	71.2	36.8	42.1	12.5
M4267k(99)	*Samotherium boissieri*	Samos	NHML	327.8	47.0	77.8	40.2	77.8	33.6	42.1	12.8
M4317a	*Samotherium boissieri*	Samos	NHML		41.1	60.9					
M4269	*Samotherium boissieri*	Samos	NHML		53.9	63.2			34.0	35.7	
without numbe	*Samotherium boissieri*	Samos	NHML		44.5	76.3					
M4316*	*Samotherium boissieri*	Samos	NHML		42.0	72.2		72.6	29.2	33.6	
M4317b*	*Samotherium boissieri*	Samos	NHML		39.1	65.7			28.5	31.0	
M4317c	*Samotherium boissieri*	Samos	NHML		38.2	66.7			31.5	37.9	
M7411	*Samotherium boissieri*	Maragha	NHML	344.8	51.0	79.8	44.7	81.7	39.4	45.2	13.1
KTA 91	*Samotherium major*	Kemiklitepe	Geraads, 1994		62.0	94.0					
KTA 95	*Samotherium major*	Kemiklitepe	Geraads, 1994					107.0			
KTA 96	*Samotherium major*	Kemiklitepe	Geraads, 1994					109.0			
KTA133	*Samotherium major*	Kemiklitepe	Geraads, 1994	408.0	61.0	92.4	55.5	97.0	49.5	50.5	12.4
KTB 46	*Samotherium major*	Kemiklitepe	Geraads, 1994			88.0					
KTB61	*Samotherium major*	Kemiklitepe	Geraads, 1994	421.0	61.0	102.5	53.5	104.0	44.0	56.0	13.3

Appendix 5: Metacarpal III-IV

Specimen number	Species	Locality	Museum / author	L	DAPpr	DTpr	DAPd	DTd	DAPdia	DTdia	Robusticity index
KTD 24	*Samotherium ? sp.*	Kemiklitepe	Geraads, 1994	364.0		79.0		92.5		45.5	12.5
KTD 25	*Samotherium ? sp.*	Kemiklitepe	Geraads, 1994	372.0	53.0	82.0	48.7	88.6	40.6	44.0	11.8
KTD 45	*Samotherium ? sp.*	Kemiklitepe	Geraads, 1994			84.0				45.5	
KTA 7	*Palaeotragus rouenii*	Kemiklitepe	Geraads, 1994			56.0				32.5	
KTD 26	*Palaeotragus rouenii*	Kemiklitepe	Geraads, 1994	405.0		61.0		64.0		33.5	8.3
KTD 27	*Palaeotragus rouenii*	Kemiklitepe	Geraads, 1994			52.0				32.0	
P 1972/9	*Helladotherium duvernoyi*	Pikermi	Melentis, 1974	420.0	67.0	109.0	61.0	108.0	59.0	67.0	16.0
P 1972/11	*Helladotherium duvernoyi*	Pikermi	Melentis, 1974	413.0	63.0	108.0	60.0	104.0	46.0	65.0	15.7
PNT 7	*?Decenatherium macedoniae*	Pentalophos	Geraads, 1989			89.0					
PNT 324	*?Decenatherium macedoniae*	Pentalophos	Geraads, 1989	465.0	50.0	82.0					
VTK 79	*Bohlinia attica*	Vathylakos 2	Geraads, 1979	693.0		88.0			56.0	50.0	7.2
VTK80	*Bohlinia attica*	Vathylakos 3	Geraads, 1979	661.0		82.0			50.0	45.0	6.8
NKT137	*Palaeotragus rouenii*	Nikiti 1	Kostopoulos pers. com.	376.7	33.0	58.7	37.4	60.3	30.2	29.8	7.9
NKT141	*Palaeotragus rouenii*	Nikiti 1	Kostopoulos pers. com.	412.1	39.2	62.3	38.6	65.0	33.4	38.0	9.2
NKT26	*Palaeotragus rouenii*	Nikiti 1	Kostopoulos pers. com.		36.0	58.0					
NKT67	*Palaeotragus rouenii*	Nikiti 1	Kostopoulos pers. com.		41.0	69.5			33.1	43.2	
NKT131	*Palaeotragus rouenii*	Nikiti 1	Kostopoulos pers. com.		42.0	64.6			32.6	30.3	
NTK min	*Helladotherium duvernoyi*	Nikiti 1	Kostopoulos et al.1996				53.5	94.0			
NTK max	*Helladotherium duvernoyi*	Nikiti 1	Kostopoulos et al.1996				55.0	110.0			
NTK mean	*Helladotherium duvernoyi*	Nikiti 1	Kostopoulos et al.1996	444.5	51.0	111.5	54.3	102.0	45.0	75.7	17.0
NTK 171	*Bohlinia attica*	Nikiti 1	Kostopoulos et al.1996	680.0	60.0	85.0	47.0	78.0	45.8	51.8	7.6
S781	*Palaeotragus rouenii*	Andrianos, Samos	Kostopoulos pers. com.	410.0	45.0	63.2	39.2	61.2	39.4	37.4	9.1
S858	*Palaeotragus rouenii*	Andrianos, Samos	Kostopoulos pers. com.		42.8	56.0					
MAR 553	*Samotherium neumayri*	Maragha	Geraads, 1974	390.0	52.0	87.0	56.0	101.0	49.0	55.0	14.1
MAR 554	*Samotherium neumayri*	Maragha	Geraads, 1974	378.0	49.0	89.0	52.0	103.0	45.0	54.0	14.3
MAR 555	*Samotherium neumayri*	Maragha	Geraads, 1974	381.0		79.0	47.0	94.0	43.0	51.0	13.4
MAR 556	*Samotherium neumayri*	Maragha	Geraads, 1974	378.0	50.0		52.0	101.0	45.0	56.0	14.8
Lok 30	*Samotherium sinense*	China	Bohlin 1926	453.0	63.0	100.0		115.0			
4	*Samotherium sinense*	China	Bohlin 1926	452.0	57.0	90.0		102.0			
5	*Samotherium sinense*	China	Bohlin 1926	448.0	58.0	95.0		103.0			
a	*Samotherium sinense*	China	Bohlin 1926	466.0	63.0	93.0		103.0			
b	*Samotherium sinense*	China	Bohlin 1926	453.0	49.0	89.0		92.0			
c	*Samotherium sinense*	China	Bohlin 1926	425.0		90.0		99.0			
PIM	*Samotherium eminens*	China	Bohlin 1926	430.0	62.0	95.0		100.0			
	Samotherium boissieri		Bohlin 1926	410.0		90.0		100.0			
Slq 690	*Samotherium major*	Salonique	Geraads, 1974	419.0	50.0	83.0	51.0	92.0	43.0	51.0	12.2
Slq 691	*Samotherium major*	Salonique	Geraads, 1974	402.0	50.0	83.0	51.0	98.0	43.0	55.0	13.7
Slq 692	*Samotherium major*	Salonique	Geraads, 1974	403.0	49.0	84.0	50.0	96.0	43.0	51.0	12.7
VAT 3*	*Samotherium major*	Vathilakkos 3	Geraads, 1974	392.0	46.0	84.0	44.0	86.0	40.0	42.0	10.7
PIK 1525	*Helladotherium duvernoyi*	Pikermi	Geraads, 1974	427.0	56.0	87.0	58.0	97.0	47.0	62.0	14.5
PIK 1526	*Helladotherium duvernoyi*	Pikermi	Geraads, 1974	410.0	59.0	92.0	59.0	103.0	47.0	64.0	15.6
PIK 1527	*Helladotherium duvernoyi*	Pikermi	Geraads, 1974	407.0	55.0	97.0	57.0	102.0	48.0	71.0	17.4
MAR 764	*Palaeotragus coelophrys*	Maragha	Geraads, 1974	370.0					40.0	50.0	13.5
MAR 765	*Palaeotragus coelophrys*	Maragha	Geraads, 1974	370.0	44.0	68.0	44.0	78.0	42.0	38.0	10.3
MAR 766	*Palaeotragus coelophrys*	Maragha	Geraads, 1974	362.0	41.0	72.0	44.0	80.0	40.0	42.0	11.6
MAR 767	*Palaeotragus coelophrys*	Maragha	Geraads, 1974	352.0	43.0	72.0	45.0	83.0	42.0	47.0	13.4

Appendix 5: Metacarpal III-IV

Specimen number	Species	Locality	Museum / author	L	DAPpr	DTpr	DAPd	DTd	DAPdia	DTdia	Robusticity index
MAR 768	*Palaeotragus coelophrys*	Maragha	Geraads, 1974	395.0	44.0	75.0	49.0		41.0	45.0	11.4
PIK 1692	*Palaeotragus rouenii*	Pikermi	Geraads, 1974	435.0	34.0	51.0	37.0	58.0	36.0	27.0	6.2
	Palaeotragus microdon		Bohlin 1926	368.0	36.0	49.0		50.0			
PIK	*Bohlinia attica*	Pikermi	Geraads, 1974	710.0	54.0	83.0	56.0	80.0	52.0	47.0	6.6
PIK 1641	*Bohlinia attica (speciosa)*	Pikermi	Geraads, 1974				47.0	75.0			
DIT *	*Bohlinia attica*	Ditiko	Geraads, 1974	445.0	47.0	72.0			35.0	32.0	7.2
	Bohlinia attica	Pikermi	Gaudry, 1862	710.0		90.0		80.0			
	Helladotherium duvernoyi	Pikermi	Gaudry, 1862	420.0		109.0		100.0			
1973 XXI 57	*Samotherium boissieri (neumayri)*	Maragha	Erdbrink, 1978		56.0	91.0	56.0	96.0	42.0	53.0	
1974 XXI 50	*Samotherium boissieri*	Maragha	Erdbrink, 1978				43.0	79.0	41.0	47.0	
	Decennatherium pachecoi	Nombrevilla	Crusafont 1952		60.0	90.0			53.0	44.5	
18.00	*Birgerbohlinia schaubi*	Piera	Crusafont 1952	387.0	60.0	91.0		92.0	45.0	50.0	12.9
17.00	*Birgerbohlinia schaubi*	Piera	Crusafont 1952	375.0	53.0	81.0		82.0	38.0	50.0	13.3
21.00	*Birgerbohlinia schaubi*	Piera	Crusafont 1952	375.0	55.0	80.0		76.0	43.0	50.0	13.3
19.00	*Birgerbohlinia schaubi*	Piera	Crusafont 1952	400.0	60.0	102.0			42.0	60.0	15.0
20.00	*Birgerbohlinia schaubi*	Piera	Crusafont 1952	400.0	60.0	100.0				60.0	15.0
168.00	*Birgerbohlinia schaubi*	Piera	Crusafont 1952	350.0	55.0	82.0		83.0	42.0	47.0	13.4
174.00	*Birgerbohlinia schaubi*	Piera	Crusafont 1952	380.0	62.0	84.0			47.0	53.0	13.9
s.s.	*Decennatherium pachecoi*	Los Valles	Morales and Soria, 1981	388.0	45.0	72.4	45.6			36.4	9.4
969.00	*Decennatherium pachecoi*	Los Valles	Morales and Soria, 1981	408.0						45.3	11.1
	Birgerbohlinia schaubi	Crevillente 2	Montoya-Morales 1991	404.0	68.7	98.8	56.8	99.2		61.0	15.1
P.10 1963	*Samotherium boissieri*	Samos (SAM 5)	AMPG	386.0	49.8	83.0	46.9	88.2	40.5	53.3	13.8
ON	*Helladotherium duvernoyi*	Pikermi	Melentis, 1969	400.0	69.0	114.0	61.0	103.0	50.0	70.0	17.5
Nr 1969/91	*Helladotherium duvernoyi*	Halmyropotamos	Melentis, 1969		68.0	117.0					
S535 MGL	*Samotherium major*	Andianos	MGML, Kostopoulos pers. com.	423.0	57.0	90.7	53.3	100.0	45.7	50.3	11.9
S32 MGL	*Samotherium major*	Andianos	MGML, Kostopoulos pers. com.	415.0	54.0	86.0	49.3	104.3	43.8	47.6	11.5
Munster 327	*Samotherium major*	Samos	PIM, Kostopoulos pers. com.	435.0		96.0		98.0		55.0	12.6
Munster329	*Samotherium major*	Samos	PIM, Kostopoulos pers. com.	423.0		88.0		99.0		50.0	11.8

Notes

L = length

DAPpr = proximal anteroposterior diameter

DTpr = proximal transverse diameter

DAPd = distal anteroposterior diameter

DTd = distal transverse diameter

DAPdia = anteroposterior diameter in the middle of the diaphysis

DTdia = transverse diameter in the middle of the diaphysis

Robusticity Index = (Dtdia / L) * 100

specimens with a star (*) characterize juveniles

MGML: Musee Geologique et Mineralogique, Lausanne

PIM: Palaontologisches Institut, Munster

Appendix 6: Tibia

Specimen number	Species	Locality	Museum / author	L	DAPpr	DTpr	DAPd	DTd	DAPdia	DTdia
Ke 162	*Bohlinia attica*	Kerassia	AMPG	549.9	102.5	122.3	64.3	86.8	44.4	59.4
Ke 87	*Bohlinia attica*	Kerassia	AMPG	593.2	112.3	128.9		95.7	53.9	70.7
Ke 89	*Bohlinia attica*	Kerassia	AMPG				62.0	95.9		
K1/Δ341/1	*Samotherium major*	Kerassia	AMPG	517.5	142.1	152.9	80.0	103.6	58.6	75.6
K1/Δ138	*Palaeotragus rouenii*	Kerassia	AMPG				50.4	65.3		44.4
K4/Δ81	*Helladotherium duvernoyi*	Kerassia	AMPG				82.8	110.8	59.6	79.8
M48289	*Palaeotragus rouenii*	Pikermi	NHML		97.8	95.8			32.6	38.1
M11407	*Palaeotragus rouenii*	Pikermi	NHML	442.0			40.3	55.0	29.4	45.4
M11402	*Bohlinia attica*	Pikermi	NHML				70.7	101.8	49.0	78.5
M11379	*Helladotherium duvernoyi*	Pikermi	NHML	543.8	130.3	161.2	85.2	107.7	52.0	74.4
M11380a	*Helladotherium duvernoyi*	Pikermi	NHML				78.3	109.0	54.8	80.5
M11380b	*Helladotherium duvernoyi*	Pikermi	NHML				85.7	114.0	56.6	76.6
	Helladotherium duvernoyi	Pikermi	Sedgwick				83.5	110.4		
M4275a(143)	*Samotherium boissieri*	Samos	NHML	450.1	125.3		63.7	86.2	44.4	73.8
M4278	*Samotherium boissieri*	Samos	NHML	444.1	101.0	135.2	63.8	76.8	41.4	60.6
M4275b(145)	*Samotherium boissieri*	Samos	NHML	442.3	82.8	108.2	63.9	75.2	38.0	52.0
M4275c(76)	*Samotherium boissieri*	Samos	NHML	451.2	86.8	111.5	60.6	75.8	38.8	53.5
M4277	*Samotherium major*	Samos	NHML	497.8	102.8	136.9		95.6	49.3	71.3
M4275d(144)	*Samotherium boissieri*	Samos	NHML		120.7	134.3			50.3	65.0
M5432	*Samotherium major*	Samos	NHML	521.2		135.0	75.2	104.1	40.7	64.5
M4275e(290)	*Samotherium boissieri*	Samos	NHML	435.5	92.4	125.1	56.2	84.2	41.2	
M4275f(148)	*Samotherium boissieri*	Samos	NHML		69.9	121.9	57.0	80.1		61.8
M (147)	*Samotherium boissieri*	Samos	NHML		96.3	141.0	55.9	84.7	44.5	60.0
M4279a	*Samotherium boissieri*	Samos	NHML				64.5	90.5	44.3	
M4279b(375)	*Samotherium boissieri*	Samos	NHML				64.0	75.2		
M4279c(350)	*Samotherium boissieri*	Samos	NHML		106.2	129.1				
M4279d(339)	*Samotherium boissieri*	Samos	NHML		118.5	113.9				
M4279e(373)	*Samotherium boissieri*	Samos	NHML				69.0	81.7		
M4279f(370)	*Samotherium boissieri*	Samos	NHML				66.7	81.4		
M4280a(310)	*Samotherium boissieri*	Samos	NHML				60.5	89.5		
M4280b(139a)	*Samotherium boissieri*	Samos	NHML				65.0	68.1		
PQ-L.22186	*Sivatherium hendeyi*	Langebaanweg	SAM	573.0	115.0	164.0	95.0	132.0	58.0	79.0
L5420	*Sivatherium hendeyi*	Langebaanweg	Harris, 1976	530.0		169.0	81.0	122.0		
KTB 48	*Samotherium major*	Kemiklitepe	Geraads, 1994	510.0				90.0		73.0
KTB 50	*Samotherium major*	Kemiklitepe	Geraads, 1994	550.0				94.0		70.0
KTB 89	*Samotherium major*	Kemiklitepe	Geraads, 1994					85.0		
NHMW	*Samotherium major*	Samos	Geraads, 1994	550.0						78.0
NHMW	*Samotherium major*	Samos	Geraads, 1994	530.0						68.0
NHMW	*Samotherium major*	Samos	Geraads, 1994	520.0						60.0

Appendix 6: Tibia

Specimen number	Species	Locality	Museum / author	L	DAPpr	DTpr	DAPd	DTd	DAPdia	DTdia
DTK 183	*Bohlinia attica*	Ditiko 3	Geraads, 1979			140.0	70.0	95.0		
NTK min	*Palaeotragus rouenii*	Nikiti 1	Kostopoulos et al.1996	450.0			44.6	60.0	38.0	48.7
NTK max	*Palaeotragus rouenii*	Nikiti 1	Kostopoulos et al.1996	458.0			53.0	76.0	45.8	52.3
NTK mean	*Palaeotragus rouenii*	Nikiti 1	Kostopoulos et al.1996	454.0	89.0	88.0	48.9	66.1	40.7	50.8
NTK 200	*Helladotherium duvernoyi*	Nikiti 1	Kostopoulos et al.1996	580.0	160.0	144.0	101.0	127.0	68.0	90.0
NTK 170	*Bohlinia attica*	Nikiti 1	Kostopoulos et al.1996	>470	112.0	111.0			42.8	60.7
MAR 643	*Samotherium neumayri*	Maragha	Geraads, 1974				64.0	86.0		
MAR 644	*Samotherium neumayri*	Maragha	Geraads, 1974				59.0	83.0		
MAR 645	*Samotherium neumayri*	Maragha	Geraads, 1974	470.0			61.0	88.0		
3	*Samotherium sinense*	China	Bohlin 1926	508.0				108.0		
2*	*Samotherium sinense*	China	Bohlin 1926	477.0				91.0		
1	*Samotherium sinense*	China	Bohlin 1926	502.0	130.0	140.0		99.0		
4	*Samotherium sinense*	China	Bohlin 1926		138.0	134.0				
5	*Samotherium sinense*	China	Bohlin 1926			166.0				
	Samotherium eminens		Bohlin 1926	550.0		156.0		112.0		
	Samotherium boissieri		Bohlin 1926	530.0				95.0		
1	*P. microdon*		Bohlin 1926	398.0		80.0		55.0		
MAR 924	*Helladotherium duvernoyi*	Maragha	Geraads, 1974	555.0			72.0	93.0		
PIK 1582	*Bohlinia attica*	Pikermi	Geraads, 1974	625.0		134.0	61.0	86.0		
Slq 680	*Bohlinia attica*	Salonique	Geraads, 1974	575.0		115.0	52.0	69.0		
MAR	*Bohlinia attica?*	Maragha	Geraads, 1974	640.0			61.0	83.0		
MAR	*Palaeotragus coelophrys*	Maragha	Geraads, 1974	430.0			55-60	66-79		
PIK 1687	*Palaeotragus rouenii*	Pikermi	Geraads, 1974	435.0		94.0	41.0	55.0		
	Bohlinia attica	Pikermi	Gaudry, 1862	600.0						
	Helladotherium duvernoyi	Pikermi	Gaudry, 1862	490.0				106.0		
	Samotherium major	Samos	AMPG				82.4	110.6		
	Decennatherium pachecoi	Nombrevilla	Crusafont 1952			111.5	64.5	86.0		
170	*Birgerbohlinia schaubi*	Piera	Crusafont 1952	478.0	130.0	139.0	70.3	97.7		
31	*Birgerbohlinia schaubi*	Piera	Crusafont 1952	500.0			55.0	100.0		
s.s.	*Decennatherium pachecoi*	Los Valles	Morales and Soria, 1981	503.0	107.4	123.3	61.5	78.5	41.5	61.6
589x	*Decennatherium pachecoi*	Los Valles	Morales and Soria, 1981				61.0	80.0		
40875	*Decennatherium pachecoi*	Los Valles	Morales and Soria, 1981				58.0	74.6		
	Birgerbohlinia schaubi	Crevillente 2	Montoya-Morales 1991				73.0	85.5		
L1797	*Giraffa cf G. jumae*	Langebaanweg	Harris, 1976	655.0			89.0	114.0		
L13528	*Giraffa cf G. jumae*	Langebaanweg	Harris, 1976	590.0		156.0	76.0	113.0		

Notes

L = length

Appendix 6: Tibia

Notes continued
DAPpr = proximal anteroposterior diameter
DTpr = proximal transverse diameter
DAPd = distal anteroposterior diameter
DTd = distal transverse diameter
DAPdia = anteroposterior diameter in the middle of the diaphysis
DTdia = transverse diameter in the middle of the diaphysis
specimens with a star (*) characterize juveniles
NHMW: Naturhistorisches Museum, Wien

Appendix 7: Malleolus

Specimen number	Species	Locality	Museum / author	DAP	DT	H
K1/Δ343	*Samotherium major*	Kerassia	AMPG	55.1	26.6	45.4
K4/Δ314/7	*Helladotherium duvernoyi*	Kerassia	AMPG	59.0	27.3	
M4277	*Samotherium boissieri*	Samos	NHML	45.5	30.2	30.8
M4286a	*Samotherium boissieri*	Samos	NHML	50.9	25.4	36.0
M4286b	*Samotherium boissieri*	Samos	NHML	46.4	23.6	35.8
M4286c	*Samotherium boissieri*	Samos	NHML	45.6	19.7	36.1
M4286d	*Samotherium boissieri*	Samos	NHML	49.4	24.8	35.8
M4280a(139a)	*Samotherium boissieri*	Samos	NHML	50.7		
M4281(65)	*Samotherium boissieri*	Samos	NHML	49.8	26.7	35.9
M4280b(77)	*Samotherium boissieri*	Samos	NHML	49.8		35.5
M4280c(309)	*Samotherium boissieri*	Samos	NHML	51.3	25.0	35.5
M5432	*Samotherium major*	Samos	NHML	49.3		38.5
MAR 624	*Samotherium neumayri*	Maragha	Geraads, 1974	56.0	26.0	34.0
MAR 625	*Samotherium neumayri*	Maragha	Geraads, 1974	54.0	23.0	35.0
MAR 626	*Samotherium neumayri*	Maragha	Geraads, 1974	48.0	28.0	36.0
Lok. 30	*Samotherium sinense*	China	Bohlin 1926	68.0	32.0	35.0
Lok 116/1	*Samotherium sinense*	China	Bohlin 1926	58.0	30.0	32.0
Lok 116/2	*Samotherium sinense*	China	Bohlin 1926	53.0	26.0	29.0
Lok 116/3	*Samotherium sinense*	China	Bohlin 1926	64.0	30.0	32.0
Lok 116/4	*Samotherium sinense*	China	Bohlin 1926	68.0	31.0	37.0
	Samotherium eminens	China	Bohlin 1926	57.0	30.0	
PIK 1536-1540	*Helladotherium duvernoyi*	Pikermi	Geraads, 1974	53.0	26.0	33.0
	Helladotherium duvernoyi	Pikermi	Geraads, 1974	59.0	29.0	37.0
PIK 1582	*Bohlinia attica*	Pikermi	Geraads, 1974	47.0	24.0	30.0
VAT 2	*Bohlinia attica*	Vathylakkos 2	Geraads, 1974	50.0	28.0	33.0
MAR	*Bohlinia attica?*	Maragha	Geraads, 1974	51.0	26.0	31.0
	Decennatherium pachecoi	Nombrevilla	Crusafont 1952	45.5	21.0	29.0
152	*Birgerbohlinia schaubi*	Piera	Crusafont 1952	49.0	25.6	38.0
482	*Decennatherium pachecoi*	Los Valles	Morales and Soria, 1981	46.0	22.0	31.0
1095	*Decennatherium pachecoi*	Los Valles	Morales and Soria, 1981	45.0	23.5	30.5
2364	*Decennatherium pachecoi*	Los Valles	Morales and Soria, 1981	44.6	19.0	29.0
2588	*Decennatherium pachecoi*	Los Valles	Morales and Soria, 1981	41.0	17.0	26.6
930	*Decennatherium pachecoi*	Los Valles	Morales and Soria, 1981	43.5	21.0	29.7
2111	*Decennatherium pachecoi*	Los Valles	Morales and Soria, 1981	44.3	20.6	31.4
1226	*Decennatherium pachecoi*	Los Valles	Morales and Soria, 1981	44.5	22.0	30.0
15004	*Decennatherium pachecoi*	Los Valles	Morales and Soria, 1981	45.6	20.4	30.8
1971	*Decennatherium pachecoi*	Los Valles	Morales and Soria, 1981	46.2	21.7	34.5
262?	*Decennatherium pachecoi*	Los Valles	Morales and Soria, 1981	43.1	21.6	
min	*Birgerbohlinia schaubi*	Crevillente 2	Montoya-Morales 1991	47.0	22.7	33.6
av	*Birgerbohlinia schaubi*	Crevillente 2	Montoya-Morales 1991	48.8	24.7	35.1
max	*Birgerbohlinia schaubi*	Crevillente 2	Montoya-Morales 1991	50.5	25.9	37.8

Notes

DAP = anteroposterior diameter

DT = transverse diameter

H = height

Appendix 8: Calcaneous

Specimen number	Species	Locality	Museum / author	L	H	DT	α	β	γ	h	α/β
Ke 99/45	*Bohlinia attica*	Kerassia	AMPG	195.1	81.2	58.3	43.6	62.6	28.7	57.6	0.70
Ke 99/46	*Samotherium major*	Kerassia	AMPG	182.8	90.0	62.1	53.8	66.8	29.1	66.5	0.81
Ke 99/47	*Samotherium major*	Kerassia	AMPG	185.1	90.2	63.8	55.2	61.8	33.5	73.9	0.89
Ke 99/48	*Samotherium major*	Kerassia	AMPG		89.6	64.5			31.7	79.6	
K1/A2	*Samotherium major*	Kerassia	AMPG		88.7	61.5			27.3	66.3	
K1/Δ243	*Samotherium major*	Kerassia	AMPG	204.3	99.8	68.5	50.9	64.1	32.0	73.8	0.79
K4/Δ331/2	*Helladotherium duvernoyi*	Kerassia	AMPG	203.9	92.5	60.5	58.7	76.1	39.5	70.1	0.86
K4/Δ62	*Helladotherium duvernoyi*	Kerassia	AMPG	216.5	95.9	58.7	61.6	64.1	33.9	72.8	0.96
K4/Δ314/6	*Helladotherium duvernoyi*	Kerassia	AMPG		102.8	62.5			33.2	74.8	
M12922	*Palaeotragus rouenii*	Pikermi	NHML	123.5		39.5	31.3	36.0	19.3	42.4	0.87
M11386	*Helladotherium duvernoyi*	Pikermi	NHML	230.2	102.3	75.7	69.9	69.0	40.8	75.9	1.01
M11385a	*Helladotherium duvernoyi*	Pikermi	NHML	231.5	100.2	71.3	64.4	69.5	37.5	75.1	0.93
M11385b	*Helladotherium duvernoyi*	Pikermi	NHML	219.9	94.7	63.0	60.0	66.3	32.2	66.0	0.90
M49717	*Helladotherium duvernoyi*	Pikermi	NHML		92.7	68.2			30.8		
M48243	*Helladotherium duvernoyi*	Pikermi	NHML		87.0	55.4			31.8	57.4	
M48128	*Helladotherium duvernoyi*	Pikermi	NHML		89.7				26.1	61.6	
M4282a(87)	*Samotherium boissieri*	Samos	NHML	174.7	67.2	58.9	50.6	45.0	31.6	54.1	1.12
M4282b(89)	*Samotherium boissieri*	Samos	NHML	173.2	71.0	52.8		54.5	25.3	57.1	
M4282c(69)	*Samotherium boissieri*	Samos	NHML	169.5	73.1	51.2	45.1	52.5	24.7	55.5	0.86
M4282d(75)	*Samotherium boissieri*	Samos	NHML	162.8	67.5	44.5	40.3	48.8	23.8	47.0	0.83
M4282e	*Samotherium boissieri*	Samos	NHML	174.5	73.7	53.6	44.6	50.1	24.7	56.9	0.89
M4282f(311)	*?B. attica*	Samos	NHML	183.8	80.5	53.8	42.3	67.6	24.3	65.5	0.63
M4282g(307)	*Samotherium boissieri*	Samos	NHML		72.9					54.1	
M5432*	*Samotherium major*	Samos	NHML		87.2	64.5			29.4	56.0	
M4280a(297)	*Samotherium boissieri*	Samos	NHML	170.6		54.0	42.6	51.4	24.0	59.3	0.83
M4280b(309)	*Samotherium boissieri*	Samos	NHML	174.9	74.6	58.2	43.2	47.1	25.3	58.7	0.92
M4281(298)	*Samotherium boissieri*	Samos	NHML	172.7	73.2	53.3		47.2	26.2	58.3	
M4280c(310)	*Samotherium boissieri*	Samos	NHML	172.3	72.0	57.4	47.3	53.4	28.8	58.2	0.89
M4281(305)	*Samotherium boissieri*	Samos	NHML		59.4	45.1			19.5	45.0	
M4280d(77)	*Samotherium boissieri*	Samos	NHML	157.7	71.7	54.0			23.4	50.3	
M3888a	*Samotherium neumayri*	Maragha	NHML	194.5	91.5	64.0	57.6	63.5	32.4	68.6	0.91
M7413	*Samotherium neumayri*	Maragha	NHML	182.3	79.8	57.9	54.0		31.6	66.3	
M3888b	*Samotherium neumayri*	Maragha	NHML	190.0	82.3	56.4	53.3	62.9	30.2	63.9	0.85
M7413	*Samotherium neumayeri*	Maragha	NHML			60.0	51.8	57.0	27.1	62.5	0.91
M3888c	*Samotherium neumayeri*	Maragha	NHML	177.8	79.3	54.9	51.2	57.2	29.6	61.2	0.90
M3984	*?Palaeotragus coelophrys*	Maragha	NHML	167.3	71.5	53.0	43.9	52.0	29.3	51.5	0.84
L14336	*Giraffa jumae*	Langebaanweg	SAM	194.0	97.0	68.0	52.0	50.0	37.0	65.0	1.04
KTC 3	*Samotherium major*	Kemiklitepe	Geraads, 1994	200.0	89.0						

Appendix 8: Calcaneous

Specimen number	Species	Locality	Museum / author	L	H	DT	α	β	γ	h	α/β
KTB 45a	*Samotherium major*	Kemiklitepe	Geraads, 1994	215.0	100.0						
KTD 31	*Samotherium ? sp.*	Kemiklitepe	Geraads, 1994	170.0		59.0					
KTD 37	*Samotherium ? sp.*		Geraads, 1994	170.0		59.5					
DTK 183	*Bohlinia attica*	Ditiko 3	Geraads, 1979	188.0	80.0						
NKT 152	*Helladotherium duvernoyi*	Nikiti 1	Kostopoulos et al.1996	215.0	105.0	68.0					
	Samotherium neumayri	Maragha	Rodler & Weithofer,1890	193.0	88.0						
	Samotherium neumayri	Maragha	Rodler & Weithofer,1890	188.0	82.0						
	Samotherium neumayri	Maragha	Rodler & Weithofer,1890	197.0	89.0						
	Samotherium neumayri	Maragha	Rodler & Weithofer,1890	193.0	78.0						
	Palaeotragus coelophrys	Maragha	Rodler & Weithofer,1890	178.0	76.0						
	Palaeotragus coelophrys	Maragha	Rodler & Weithofer,1890	170.0	75.0						
min	*Samotherium neumayri*	Maragha	Geraads, 1974	190.0	75.0	54.0					
max	*Samotherium neumayri*	Maragha	Geraads, 1974	200.0	85.0	63.0					
average 10	*Samotherium neumayri*	Maragha	Geraads, 1974	194.0	82.0	57.0					
Slq 696	*Samotherium major*	Salonique	Geraads, 1974	195.0	82.0	56.0					
1	*Samotherium sinense*	30	Bohlin 1926		96.0	58.0					
2	*Samotherium sinense*	30	Bohlin 1926	206.0	93.0						
1	*Samotherium sinense*	116	Bohlin 1926	216.0	98.0	60.0					
2	*Samotherium sinense*	116	Bohlin 1926	219.0	96.0	60.0					
3	*Samotherium sinense*	116	Bohlin 1926	221.0	102.0	59.0					
4	*Samotherium sinense*	116	Bohlin 1926	225.0	100.0	61.0					
537	*Samotherium eminens*		Bohlin 1926	192.0							
Slq 685	*Helladotherium duvernoyi*	Salonique	Geraads, 1974	221.0	100.0	68.0					
MAR 908	*Helladotherium duvernoyi*	Maragha	Geraads, 1974	224.0	90.0	68.0					
PIK 1542	*Helladotherium duvernoyi*	Pikermi	Geraads, 1974	218.0	90.0	66.0					
PIK 1631	*Bohlinia attica (speciosa)*	Pikermi	Geraads, 1974	168.0	71.0	48.0					
PIK 1633	*Bohlinia attica*	Pikermi	Geraads, 1974	190.0	87.0	55.0					
	Bohlinia attica	Pikermi	Bohlin 1926	180.0	81.0	56.0					
Slq 697	*Bohlinia attica*	Salonique	Geraads, 1974	185.0	82.0	55.0					
	Bohlinia attica	Pikermi	Gaudry, 1862	184.0							
	Helladotherium duvernoyi	Pikermi	Gaudry, 1862	230.0							
1974 XXI 55	*Samotherium boissieri*	Maragha	Erdbrink, 1978		82.0	64.0					
	Palaetragus microdon	China	Bohlin 1926	130.0		33.0					
1	*Honanotherium sclosseri*	12	Bohlin, 1926	200.0	88.0						
	Bohlinia attica (Orasius)	Pikermi	Bohlin 1926	187.0	82.0	55.0					

Notes

L = length

Appendix 8: Calcaneous

Notes continued
H = maximum height
DT = maximum transverse diameter at the level of the sustentaculum tali
α = tuber calcanei width
β = tuber calcanei height
γ = transverse diameter at the base of the calcaneous body
h = height at the base of the calcaneous body
specimens with a star (*) characterize juveniles

Appendix 9: Astragalus

Specimen number	Species	Locality	Museum / author	L	l	DTpr	DTd	α	β
Ke 99/49	*Samotherium major*	Kerassia	AMPG		92.5		68.9	65.0	61.4
Ke 99/50	*Bohlinia attica*	Kerassia	AMPG		86.4	67.4	66.6	58.1	54.3
Ke 99/51	*Bohlinia attica*	Kerassia	AMPG	95.1	81.4	61.8	58.6	53.1	51.7
Ke 99/52	*Bohlinia attica*	Kerassia	AMPG			69.0		57.2	54.3
Ke 156	*Bohlinia attica*	Kerassia	AMPG	94.9	82.4	59.5		54.5	52.8
K1/Δ22	*Helladotherium duvernoyi*	Kerassia	AMPG	111.5	93.7	77.7	72.5	67.0	61.0
K1/Δ342	*Samotherium major*	Kerassia	AMPG	101.0	90.5	67.7	68.3	62.3	61.1
K4/Δ6/1	*Helladotherium duvernoyi*	Kerassia	AMPG	113.9	95.5	74.2	71.2	64.5	60.1
K4/Δ314/2-7	*Helladotherium duvernoyi*	Kerassia	AMPG	129.2	106.4	78.5	77.7	69.2	63.0
M11387a	*Helladotherium duvernoyi*	Pikermi	NHML	113.7		83.1	75.8	70.8	64.2
M11387b	*Helladotherium duvernoyi*	Pikermi	NHML	104.6		69.9	70.6	63.7	57.5
M11389	*Helladotherium duvernoyi*	Pikermi	NHML			70.6	70.4	58.2	59.8
M11388	*Bohlinia attica*	Pikermi	NHML	99.0		67.8	63.2	56.4	54.5
M11388b	*Bohlinia attica*	Pikermi	NHML	103.6		68.7	63.2	56.0	52.8
M4283(286)	*Samotherium boissieri*	Samos	NHML	85.5		59.3	56.7	49.0	48.7
M4283(285)	*Samotherium boissieri*	Samos	NHML	89.2		59.2	54.3	50.3	49.8
M4283(284)	*Samotherium boissieri*	Samos	NHML	88.9		56.6	57.5	43.0	44.8
M4283(283)	*Samotherium boissieri*	Samos	NHML	82.2		54.3	56.8	49.0	48.3
M4283(282)	*Samotherium boissieri*	Samos	NHML	90.0		55.5	54.8	45.2	51.2
M4283(278)	*Samotherium boissieri*	Samos	NHML	88.9		61.3	60.8	53.2	49.5
M4283(289)	*Samotherium boissieri*	Samos	NHML	87.4		56.6	55.7	48.7	47.0
M4283(288)	*Samotherium boissieri*	Samos	NHML	90.0		56.0	55.8	51.2	49.8
M4283(79)	*Samotherium boissieri*	Samos	NHML			50.0	51.1	40.0	37.2
M4278	*Samotherium boissieri*	Samos	NHML	77.7		62.5	58.4	47.9	48.0
M4281(280)	*Samotherium boissieri*	Samos	NHML	89.9		53.6	52.8	52.0	48.1
M4281(305)	*Samotherium boissieri*	Samos	NHML	78.2		59.5		30.8	
M4280(139)	*Samotherium boissieri*	Samos	NHML	87.6		53.5	49.8	52.5	
M4280(310)	*Samotherium boissieri*	Samos	NHML	86.8		57.2	51.2	47.3	
M4281(149)	*Samotherium boissieri*	Samos	NHML	85.1		65.7	53.2		47.8
M4281(65)	*Samotherium boissieri*	Samos	NHML			61.2	61.4	53.9	51.7
M4280(297)	*Samotherium boissieri*	Samos	NHML	82.0		55.1	53.0	55.8	
M4280(77)	*Samotherium boissieri*	Samos	NHML	76.9		59.2	58.4	47.7	
M4281	*Samotherium boissieri*	Samos	NHML	84.2		59.4	54.3	49.0	
M4281(298)	*Samotherium boissieri*	Samos	NHML	94.3		61.0	54.5		43.7
M4280(309)	*Samotherium boissieri*	Samos	NHML	90.8		58.3		52.7	
M4288(83)	*Samotherium boissieri*	Samos	NHML				54.0	49.3	
M4283(98)	*?Samotherium boissieri*	Samos	NHML	76.2		47.4	46.6	39.5	41.6
M5432*	*Samotherium major*	Samos	NHML	92.4		72.2	73.5	61.6	

Appendix 9: Astragalus

Specimen number	Species	Locality	Museum / author	L	l	DTpr	DTd	α	β
M3876a	*Helladotherium duvernoyi*	Maragha	NHML	103.0		75.9	68.8	69.9	64.1
M3876b(145)	*Samotherium neumayri*	Maragha	NHML	106.6		72.2	69.7	64.1	59.8
M3876c	*Samotherium neumayri*	Maragha	NHML	101.7		66.0	60.9	62.1	57.4
M3876d	*Samotherium neumayri*	Maragha	NHML	99.3		71.0	64.7	58.2	56.7
M3876e	*Samotherium neumayri*	Maragha	NHML	97.2		63.6	62.2	56.7	57.7
M3889a	*Samotherium boissieri*	Maragha	NHML	90.1		62.7	59.0	55.2	50.6
M3889b	*Samotherium boissieri*	Maragha	NHML	87.3		60.8	55.9	51.8	49.8
M3889c	*?Palaeotragus*	Maragha	NHML	78.0		50.6	50.2	45.8	41.8
ıithout number	*Samotherium boissieri*	Maragha	NHML	85.5		55.3	56.2	47.8	46.8
ıithout number	*Samotherium boissieri*	Maragha	NHML			56.1	53.7	48.8	45.8
PQ-L22186	*Sivatherium hendeyi*	Langebaanweg	SAM	124.0		95.0	83.0	73.0	70.0
KTA	*Samotherium major*	Kemiklitepe	Geraads, 1994		98.0		74.0		
KTA	*Samotherium major*	Kemiklitepe	Geraads, 1994		89.0		68.0		
KTB	*Samotherium major*	Kemiklitepe	Geraads, 1994		97.0		73.0		
KTB	*Samotherium major*	Kemiklitepe	Geraads, 1994		95.0		67.0		
KTB	*Samotherium major*	Kemiklitepe	Geraads, 1994		93.0		68.0		
P 1972/12	*Helladotherium duvernoyi*	Pikermi	Melentis, 1974	112.0		73.0		70.0	
P 1972/13	*Helladotherium duvernoyi*	Pikermi	Melentis, 1974	113.0		78.0		69.0	
DTK 183	*Bohlinia attica*	Ditiko 3	Geraads, 1979		81.0		59.0		
NIK 70	*Helladotherium duvernoyi*	Nikiti 2	Kostopoulos et al.1996	121.4		78.0	78.0	67.4	
	Samotherium neumayri	Maragha	Rodler and Weithofer,1890	100.0		69.0	68.0		
	Samotherium neumayri	Maragha	Rodler and Weithofer,1890	102.0			66.0		
	Samotherium neumayri	Maragha	Rodler and Weithofer,1890	98.0		60.0	60.0		
	Samotherium neumayri	Maragha	Rodler and Weithofer,1890	90.0		62.0	59.0		
	Palaeotragus coelophrys	Maragha	Rodler and Weithofer,1890	84.0		53.0	56.0		
	Palaeotragus coelophrys	Maragha	Rodler and Weithofer,1890	85.0		54.0	57.0		
	Palaeotragus coelophrys	Maragha	Rodler and Weithofer,1890	86.0		53.0	51.0		
	Palaeotragus coelophrys	Maragha	Rodler and Weithofer,1890	86.0		56.0	58.0		
	Palaeotragus coelophrys	Maragha	Rodler and Weithofer,1890	84.0		53.0	54.0		
	Palaeotragus coelophrys	Maragha	Rodler and Weithofer,1890	85.0		53.0	54.0		
min	*Samotherium neumayeri*	Maragha	Geraads, 1974		83.0		55.0	52.0	
max	*Samotherium neumayeri*	Maragha	Geraads, 1974		98.0		69.0	62.0	
average 26	*Samotherium neumayeri*	Maragha	Geraads, 1974		89.0		64.0	56.0	
1*	*Samotherium sinense*	China	Bohlin 1926		104.0		69.0	58.0	
2	*Samotherium sinense*	China	Bohlin 1926	120.0	105.0		77.0	58.0	
3	*Samotherium sinense*	China	Bohlin 1926	112.0	103.0		68.0	62.0	
4	*Samotherium sinense*	China	Bohlin 1926	117.0	103.0		75.0	67.0	
5	*Samotherium sinense*	China	Bohlin 1926	114.0	102.0		72.0	64.0	

Appendix 9: Astragalus

Specimen number	Species	Locality	Museum / author	L	l	DTpr	DTd	α	β
6	*Samotherium sinense*	China	Bohlin 1926	110.0	94.0		70.0	61.0	
7	*Samotherium sinense*	China	Bohlin 1926	103.0	93.0		66.0	58.0	
102/II	*Samotherium eminens*	China	Bohlin 1926	111.0			64.0	58.0	
116	*Palaeotragus microdon*	China	Bohlin 1926		56.0		38.0	34.0	
108	*Palaeotragus microdon*	China	Bohlin 1926	69.0			40.0		
Gr.r.	*Palaeotragus microdon*	China	Bohlin 1926	71.0	63.0		45.0	39.0	
Lok 78	*Palaeotragus coelophrys*	China	Bohlin 1926	75.0	67.0		47.0	44.0	
Slq 698A	*Helladotherium duvernoyi*	Salonique	Geraads, 1974		97.0		75.0	66.0	
min	*Helladotherium duvernoyi*	Pikermi,Maragha	Geraads, 1974		91.0		70.0	59.0	
max	*Helladotherium duvernoyi*	Pikermi,Maragha	Geraads, 1974		103.0		80.0	67.0	
average 9	*Helladotherium duvernoyi*	Pikermi,Maragha	Geraads, 1974		96.0		74.0	66.0	
PIK 1631	*Bohlinia attica (speciosa)*	Pikermi	Geraads, 1974		76.0		55.0	46.0	
PIK 1632	*Bohlinia attica*	Pikermi	Geraads, 1974		76.0		65.0	46.0	
PIK 1634	*Bohlinia attica*	Pikermi	Geraads, 1974		84.0		52.0	57.0	
PIK 1634B	*Bohlinia attica*	Pikermi	Geraads, 1974		81.0		59.0	50.0	
Slq 707	*Bohlinia attica*	Salonique	Geraads, 1974		72.0		51.0	57.0	
MAR	*Bohlinia attica*	Maragha	Geraads, 1974		81.0		61.0	46.0	
Kck	*Bohlinia attica*	Kucukcekmese	Malik & Nafiz 1933		72.0		45.0		
MAR min	*Palaeotragus coelophrys*	Maragha	Geraads, 1974		72.0		51.0	42.0	
MAR max	*Palaeotragus coelophrys*	Maragha	Geraads, 1974		83.0		59.0	57.0	
MAR av	*Palaeotragus coelophrys*	Maragha	Geraads, 1974		77.0		56.0	49.0	
PIK 1695	*Palaeotragus rouenii*	Pikermi	Geraads, 1974		62.0		43.0	38.0	
MAR	*Palaeotragus sp.*	Maragha	Geraads, 1974		70.0		47.0	40.0	
China	*Palaeotragus sp.*	China	Geraads, 1974		66.0			38.0	
	Bohlinia attica	Pikermi	Gaudry, 1862		86.0		70.0		
	Helladotherium duvernoyi	Pikermi	Gaudry, 1862		104.0		75.0		
1973 XXI 51	*?Samotherium sinense*	Maragha	Erdbrink, 1978	115.0	97.0	80.0	73.0	68.0	
1974 XXI 52	*Samotherium boissieri*	Maragha	Erdbrink, 1978	90.0		62.0		56.0	
	Samotherium cfr. neumayri		Bohlin, 1926	101.0	90.0		60.0	56.0	
	Samotherium major	Taskinpasa	Senyurek, 1952	106.0	96.0	74.0	72.0		62.0
	Samotherium major	Taskinpasa	Senyurek, 1952	107.0	97.0	75.0	72.5	66.0	58.0
	Samotherium major?	Samos	AMPG	96.2	82.2	62.3	61.6	55.1	56.0
12/88 PG 106	*Samotherium major*	Samos	AMPG	108.8	97.6	74.7	73.2	69.3	68.2
12/88 PG 102	*Samotherium major*	Samos	AMPG	109.0			72.7	68.7	66.6

Notes

L = lateral (maximum) length

l = medial length

Appendix 9: Astragalus

Notes continued
DTpr = proximal transverse diameter
DTd = distal transverse diameter
α = maximum medial anteroposterior diameter
β = maximum lateral anteroposterior diameter
specimens with a star (*) characterize juveniles

Appendix 10: Scaphocuboideum

Specimen number	Species	Locality	Museum / author	L	Ls	W	Ws	H
Ke 99/43	*Helladotherium duvernoyi*	Kerassia	AMPG	95.4	70.4	101.3	75.4	73.7
Ke 99/44	*Bohlinia attica*	Kerassia	AMPG	70.8	59.3	78.8	60.3	62.8
K1/Δ247/2	*Samotherium major*	Kerassia	AMPG	92.7	78.6	93.9	68.2	73.6
K1/Δ346	*Samotherium major*	Kerassia	AMPG	88.1	77.2	92.0	67.1	72.4
K4.8	*Helladotherium duvernoyi*	Kerassia	AMPG	97.7	84.1	105.6	82.9	80.5
K4/Δ314/1	*Helladotherium duvernoyi*	Kerassia	AMPG	100.0	76.0	98.5	75.4	79.7
M12923	*Palaeotragus rouenii*	Pikermi	NHML	57.4	43.3	54.8	43.2	37.5
M11390a	*Helladotherium duvernoyi*	Pikermi	NHML	105.0	76.6	100.2	75.5	71.0
M8365	*Helladotherium duvernoyi*	Pikermi	NHML	104.2	76.0	98.0	70.8	71.0
M11390b	*Helladotherium duvernoyi*	Pikermi	NHML	110.0	75.6	103.8	76.4	73.1
M11390c	*Bohlinia attica*	Pikermi	NHML	84.7	74.2	94.2	69.0	56.4
M4284(291)	*Samotherium boissieri*	Samos	NHML	70.7	61.5	65.8	51.6	66.7
M4287(80)	*Samotherium boissieri*	Samos	NHML	70.5	57.2	79.1	61.4	63.8
M4284(270)	*Samotherium boissieri*	Samos	NHML	71.7	60.6	74.1	58.8	
M4284(273)	*Samotherium boissieri*	Samos	NHML	74.9	59.8	75.2	54.0	52.0
M4284(277)	*Samotherium boissieri*	Samos	NHML	75.4	56.2	75.1	55.7	50.2
M4284(272)	*Samotherium boissieri*	Samos	NHML	72.4	58.2	71.8	58.2	57.3
M4278	*Samotherium boissieri*	Samos	NHML	63.6	61.0	81.9	57.3	
M4280(139	*Samotherium boissieri*	Samos	NHML	65.6	54.4	66.7	50.5	47.5
M4280(310)	*Samotherium boissieri*	Samos	NHML		52.7	70.3		
M4281(149)	*Samotherium boissieri*	Samos	NHML	73.7	61.4	72.0		48.2
M? (293)	*Samotherium boissieri*	Samos	NHML	80.0	65.5	73.2	54.9	66.5
M4281(65)	*Samotherium boissieri*	Samos	NHML	74.0	62.3	81.3	62.5	
M4280(297)	*Samotherium boissieri*	Samos	NHML	77.3	62.9	75.0	55.3	54.8
M4280(77)	*Samotherium boissieri*	Samos	NHML	65.8	56.0	70.4	63.6	54.8
M4287(271)	*Samotherium boissieri*	Samos	NHML	83.0	62.0	75.0	52.2	
M4280(309)	*Samotherium boissieri*	Samos	NHML	75.3	60.6	72.3	60.7	
M4289(61)	*Samotherium boissieri*	Samos	NHML	63.3	57.7	73.7	60.5	52.8
M4288(83)	*Samotherium boissieri*	Samos	NHML	67.5	60.1	62.9	51.8	
M5432	*Samotherium major*	Samos	NHML	83.3	59.5	93.5	74.3	79.1
M3877	*Samotherium neumayri*	Maragha	NHML	95.1	79.1	95.7	67.4	75.1
M3986		Maragha	NHML			79.5	57.7	62.5
KTA 132b	*Samotherium major*	Kemiklitepe	Geraads, 1994	92.0		95.0		
KTB 44	*Samotherium major*	Kemiklitepe	Geraads, 1994	90.0				
KTB 48a	*Samotherium major*	Kemiklitepe	Geraads, 1994	90.0		87.5		
KTB 87a	*Samotherium major*	Kemiklitepe	Geraads, 1994	91.0		83.0		
KTD 18a	*Samotherium ? sp.*	Kemiklitepe	Geraads, 1994	85.0		83.0		
KTD 33	*Samotherium ? sp.*	Kemiklitepe	Geraads, 1994	83.0		89.0		

Appendix 10: Scaphocuboideum

Specimen number	Species	Locality	Museum / author	L	Ls	W	Ws	H
KTD 41	*Samotherium ? sp.*	Kemiklitepe	Geraads, 1994	87.0				
min	*Samotherium neumayri*	Maragha	Geraads, 1974		57.0	80.0		
max	*Samotherium neumayri*	Maragha	Geraads, 1974		68.0	86.0		
average 8	*Samotherium neumayri*	Maragha	Geraads, 1974		62.0	83.0		
	Samotherium sinense	30	Bohlin 1926			90.0	67.0	45.0
1	*Samotherium sinense*	116	Bohlin 1926	104.0		92.0	68.0	46.0
2	*Samotherium sinense*	116	Bohlin 1926	101.0		101.0	74.0	45.0
3	*Samotherium sinense*	116	Bohlin 1926	96.0		96.0	66.0	49.0
4	*Samotherium sinense*	116	Bohlin 1926	104.0		99.0	70.0	49.0
	Samotherium eminens		Bohlin 1926	79.0		93.0	68.0	
Slq 693	*Samotherium major*	Salonique	Geraads, 1974					
min	*Helladotherium duvernoyi*	Pikermi	Geraads, 1974					
max	*Helladotherium duvernoyi*	Pikermi	Geraads, 1974					
average	*Helladotherium duvernoyi*	Pikermi	Geraads, 1974					
PIK 1553	*Bohlinia attica*	Pikermi	Geraads, 1974	66.0		82.0		35.0
PIK 1554	*Bohlinia attica*	Pikermi	Geraads, 1974	64.0		75.0		35.0
PIK 1636	*Bohlinia attica (speciosa)*	Pikermi	Geraads, 1974	53.0		70.0		29.0
VAT 2	*Bohlinia attica*	Vathylakkos 2	Geraads, 1974	63.0		70.0		29.0
MAR 763	*Bohlinia attica (speciosa)*	Maragha	Geraads, 1974	60.0		67.0		
MAR min	*Palaeotragus coelophrys*	Maragha	Geraads, 1974	55.0		66.0		27.0
MAR max	*Palaeotragus coelophrys*	Maragha	Geraads, 1974	61.0		78.0		35.0
MAR av	*Palaeotragus coelophrys*	Maragha	Geraads, 1974	58.0		74.0		31.0
PIK 1693	*Palaeotragus rouenii*	Pikermi	Geraads, 1974	37.0		51.0		22.0
	Bohlinia attica	Pikermi	Gaudry, 1862	84.0				
	Helladotherium duvernoyi	Pikermi	Gaudry, 1862	100.0				
	Samotherium cfr. neumayri		Bohlin, 1926	91.0		83.0		
	Samotherium major	Samos	AMPG	90.3	82.2	95.0	76.6	69.5
	Honanotherium sclosseri	27	Bohlin, 1926	89.0		82.0		
	Honanotherium sclosseri	35	Bohlin, 1926	95.0		91.0		

Notes

L = maximum (medial) length

Ls = lateral length

W = maximum width

Ws = width of the two proximal concavities (medial ridge of the medial concavity - lateral ridge of the lateral concavity)

H = maximum height

Appendix 11: Metatarsal$_{III-IV}$

Specimen number	Species	Locality	Museum / author	L	DAPpr	DTpr	DAPd	DTd	DAPdia	Dtdia	Robusticity Index
Ke 163	*Bohlinia attica*	Kerassia	AMPG		70.3	71.8				44.5	
K1/D15	*Palaeotragus rouenii*	Kerassia	AMPG			57.5			41.2	36.5	
K1/D83	*Helladotherium duvernoyi*	Kerassia	AMPG	429.8	86.6	87.9	58.3	92.4	56.2	58.7	13.7
K1/A1	*Palaeotragus rouenii*	Kerassia	AMPG				40.5	61.3			
K1/Δ153	*Helladotherium duvernoyi*	Kerassia	AMPG		79.8	84.4			56.5	47.7	
K1/Δ247/1	*Samotherium major*	Kerassia	AMPG	417.6	84.9	81.7	53.3	93.5	52.8	49.9	11.9
K1/Δ344	*Samotherium major*	Kerassia	AMPG	426.7	80.2	80.5	53.3	88.1	52.8	51.2	12.0
K4/Δ96/1	*Palaeotragus rouenii*	Kerassia	AMPG		49.9	56.6			40.8	32.3	
K4/D388/6	*Helladotherium duvernoyi*	Kerassia	AMPG		86.3	83.6					
K4/D331/1	*Helladotherium duvernoyi*	Kerassia	AMPG	460.3	87.7	82.2	60.7	97.2	53.7	61.9	13.4
M11408?	*Palaeotragus rouenii*	Pikermi	Bohlin 1926	401.0	54.0	48.0		50.0			
M11403c	*Bolhinia attica*	Pikermi	NHML						49.7	47.2	
M11403d	*Bolhinia attica*	Pikermi	NHML			57.1			54.0	48.0	
M11403e	*Bolhinia attica*	Pikermi	NHML				46.3	68.6			
M11403f	*Bolhinia attica*	Pikermi	NHML				50.7	79.0	51.3	49.2	
M11381	*Helladotherium duvernoyi*	Pikermi	NHML	438.4	88.2	88.9	57.5	91.6	61.5	61.6	14.1
M8364	*Helladotherium duvernoyi*	Pikermi	NHML	444.5	78.1	76.6	49.4	83.2	52.4	50.6	11.4
M11384	*Helladotherium duvernoyi*	Pikermi	NHML	456.8	91.1	85.7	57.8	94.2	60.5	51.2	11.2
M11382	*Helladotherium duvernoyi*	Pikermi	NHML	436.0	68.5	67.6	50.7	81.2	48.3	49.2	11.3
M11383	*Helladotherium duvernoyi*	Pikermi	NHML	462.7	80.3	79.4	50.1	83.8	53.0	48.3	10.4
M5432*	*Samotherium major*	Samos	NHML		70.8	78.2					
M4288(83)	*Samotherium boissieri*	Samos	NHML	381.1	64.8	54.1	44.0	63.7	43.7	33.7	8.8
M4980(310)	*Samotherium boissieri*	Samos	NHML		57.0	69.0					
M4289(121)	*Samotherium boissieri*	Samos	NHML	381.7	58.9	63.7	39.3	72.8	42.5	38.0	10.0
M4280(128)	*Samotherium boissieri*	Samos	NHML	376.8	62.3	70.2	46.1	71.3	43.6	44.4	11.8
M4289(70)	*Samotherium boissieri*	Samos	NHML	379.8	64.9	69.8	43.2	75.6	47.5	41.2	10.8
M4289(81)	*Samotherium boissieri*	Samos	NHML	397.2	67.2	71.5	41.3	81.4	36.8	50.4	12.7
M4289(62)	*Samotherium boissieri*	Samos	NHML	385.4	64.9	68.7	44.1	67.6	42.7	42.3	11.0
M4289(135)	*Samotherium boissieri*	Samos	NHML	389.0	65.2	64.3	41.7	69.6	40.2	40.3	10.4
M4289(99)	*Samotherium boissieri*	Samos	NHML	385.2	67.8	72.9	43.0		49.3		
M4289(123)	*Samotherium boissieri*	Samos	NHML	388.9	64.8	66.2	44.7	73.1	46.5	43.2	11.1
M4289(78)	*Samotherium boissieri*	Samos	NHML	404.2	65.8		41.7	75.5	38.0	37.1	9.2
M4289(138)	*Samotherium boissieri*	Samos	NHML	403.1	70.4	71.2	44.0		45.6	38.2	9.5
M4289(129)	*Samotherium boissieri*	Samos	NHML	374.6	62.3	60.5	41.0	72.4	39.6	38.5	10.3
M4289(131)	*Samotherium boissieri*	Samos	NHML	398.8		71.9	46.3	79.5			
M4289(137)	*Samotherium boissieri*	Samos	NHML	406.1	57.2	72.4	40.3	72.7	39.4	43.7	10.8
without number	*Samotherium boissieri*	Samos	NHML	385.8	58.0	64.3	35.0	59.8	39.6		
M4289	*Samotherium boissieri*	Samos	NHML				42.0	76.7			
without number(K2)	*Samotherium boissieri?*	Samos	NHML		53.3	46.8					
M4289	*Samotherium boissieri*	Samos	NHML	392.5	64.6	64.0	42.6		39.3	40.5	10.3
M4289(130)	*Samotherium boissieri*	Samos	NHML	382.6	66.0		41.8	77.9		42.3	11.1
M4289(126)	*Samotherium boissieri*	Samos	NHML	395.7	68.4	68.7		72.3		41.8	10.6
M4289	*Samotherium boissieri*	Samos	NHML	375.7				73.7	39.9	42.9	11.4
M4289(132)	*Samotherium boissieri*	Samos	NHML	376.4	68.7		41.2	65.6	45.4	36.0	9.6
M4289(61)	*Samotherium boissieri*	Samos	NHML	384.3	62.3	68.9	42.7	73.0	40.9	39.7	10.3
M4289(63)	*Samotherium boissieri*	Samos	NHML	392.3	65.5	64.0	43.0	69.4	43.7	36.8	9.4
M4289(136)	*Samotherium boissieri*	Samos	NHML	412.2	70.8	66.5	44.8	77.3	49.3		

Appendix 11: Metatarsal$_{III-IV}$

Specimen number	Species	Locality	Museum / author	L	DAPpr	DTpr	DAPd	DTd	DAPdia	Dtdia	Robusticity Index
M4289(122)	*Samotherium boissieri*	Samos	NHML	370.9		61.0	40.0		39.1	41.0	11.1
M4289	*Samotherium boissieri*	Samos	NHML		68.7	61.5			46.2	36.9	
M4289	*Samotherium boissieri*	Samos	NHML			65.7			39.7	48.3	
M4289(139)	*Samotherium boissieri*	Samos	NHML		64.0	57.1			43.7	34.6	
M4289	*Samotherium boissieri*	Samos	NHML		61.2	62.5					
M4289	*?Samotherium boissieri*	Samos	NHML	349.9	68.9	72.3	47.8	78.5	44.0	42.5	12.1
M4289	*Samotherium boissieri*	Samos	NHML		53.7	64.6					
without number(K3)	*Samotherium boissieri*	Samos	NHML		44.5	56.8			31.5		
without number(K4)	*Samotherium boissieri*	Samos	NHML				38.7	69.0			
M4290(80)	*Samotherium boissieri*	Samos	NHML				40.3	54.1			
M4289(134)*	*Samotherium boissieri*	Samos	NHML		58.0	68.2	41.1	67.0	37.7	37.8	
M7411	*Samotherium neumayri*	Maragha	NHML				45.0	82.0	47.1	42.0	
M3874	*Samotherium neumayri*	Maragha	NHML				52.5	93.3			
M3885	*Palaeotragus*	Maragha	NHML				37.7	60.6			
PQ-L22186	*Sivatherium hendeyi*	Langebaanweg	SAM	481.0	90.0	98.0	57.0	105.0	63.0	57.0	11.9
KTB 86	*Samotherium major*	Kemiklitepe	Geraads, 1994					98.0			
KTB 87	*Samotherium major*	Kemiklitepe	Geraads, 1994			70.0					
KTA 134	*Samotherium major*	Kemiklitepe	Geraads, 1994	462.0	84.0	87.0	54.0	95.0	53.3	53.8	11.6
KTD 18d	*Samotherium ? sp.*	Kemiklitepe	Geraads, 1994	412.0	70.0	76.0	50.4	86.2	46.7	48.4	11.7
KTD 21	*Samotherium ? sp.*	Kemiklitepe	Geraads, 1994	423.0		69.0		79.0		41.0	9.7
KTD 22	*Samotherium ? sp.*	Kemiklitepe	Geraads, 1994	382.0		64.0		77.0		38.5	10.1
KTD 28	*Samotherium ? sp.*	Kemiklitepe	Geraads, 1994					85.0			
KTD 28	*Palaeotragus rouenii*	Kemiklitepe	Geraads, 1994	377.0		48.5		56.0		30.0	8.0
P 1972/10	*Helladotherium duvernoyi*	Pikermi	Melentis, 1974	458.0	90.0	93.0	56.0	94.0	65.0	56.0	12.2
PNT 116	*?Decenatherium macedoniae*	Pentalophos	Geraads, 1989					79.0		48.0	
PNT 134	*?Decenatherium macedoniae*	Pentalophos	Geraads, 1989	480.0				68.0		44.0	9.2
DTK 183	*Bohlinia attica*	Ditiko 3	Geraads, 1979	658.0				76.0			
NTK min	*Palaeotragus rouenii*	Nikiti 1	Kostopoulos et al.1996	388.5	49.1	52.9	34.2	57.9	34.2	28.9	7.4
NTK max	*Palaeotragus rouenii*	Nikiti 1	Kostopoulos et al.1996	412.0	56.0	57.7	40.4	66.5	38.1	38.0	9.2
NTK mean	*Palaeotragus rouenii*	Nikiti 1	Kostopoulos et al.1996	403.8	53.5	54.7	37.3	61.4	36.7	34.3	8.5
NTK min	*Helladotherium duvernoyi*	Nikiti 1	Kostopoulos et al.1996	457.6		81.0	45.0	82.0	51.5	47.6	10.4
NTK max	*Helladotherium duvernoyi*	Nikiti 1	Kostopoulos et al.1996	460.0		83.0	57.2	91.8	52.5	52.5	11.4
NTK mean	*Helladotherium duvernoyi*	Nikiti 1	Kostopoulos et al.1996	458.8	79.0	82.0	50.4	86.6	52.0	50.0	10.9
NTK 24	*Bohlinia attica*	Nikiti 1	Kostopoulos et al.1996	670.0	70.0	75.0	50.5	73.6	48.7	55.5	8.3
NKT 47	*Bohlinia nikitiae*	Nikiti 2	Kostopoulos et al.1996		45.3	54.5					
	Samotherium neumayri	Maragha	Rodler & Weithofer,1890	430.0		76.0		85.0		48.0	11.2
	Samotherium neumayri	Maragha	Rodler & Weithofer,1890	410.0		79.0		87.0		48.0	11.7
	Samotherium neumayri	Maragha	Rodler & Weithofer,1890	420.0		75.0		89.0		48.0	11.4
	Samotherium neumayri	Maragha	Rodler & Weithofer,1890	415.0		80.0		83.0			
	Palaeotragus coelophrys	Maragha	Rodler & Weithofer,1890	370.0		66.0		71.0		38.0	10.3
min	*Samotherium neumayri*	Maragha	Geraads, 1974	402.0	63.0	63.0	46.0	80.0	45.0	43.0	10.7
max	*Samotherium neumayri*	Maragha	Geraads, 1974	444.0	77.0	80.0	52.0	90.0	52.0	61.0	13.7
average 13	*Samotherium neumayri*	Maragha	Geraads, 1974	424.0	70.0	72.0	48.0	86.0	48.0	48.0	11.3
	Samotherium sinense	30.00	Bohlin 1924	495.0	90.0	84.0		85.0			
1	*Samotherium sinense*	China	Bohlin 1925		94.0	87.0					
2	*Samotherium sinense*	China	Bohlin 1926	526.0	96.0	87.0					
3	*Samotherium sinense*	China	Bohlin 1926	503.0	88.0	71.0		83.0			

Appendix 11: Metatarsal$_{III-IV}$

Specimen number	Species	Locality	Museum / author	L	DAPpr	DTpr	DAPd	DTd	DAPdia	Dtdia	Robusticity Index
4	*Samotherium sinense*	China	Bohlin 1926	504.0	95.0	87.0		83.0			
6	*Samotherium sinense*	China	Bohlin 1926	449.0	84.0	80.0		98.0			
MHNP1926-4	*Samotherium sinense*	China	Geraads, 1974	540.0		80.0	50.0	92.0	52.0	51.0	9.4
	Samotherium eminens		Bohlin 1925	450.0	90.0	91.0		94.0			
	Samotherium major		Bohlin 1926	455.0	86.0	77.0		91.0			
Slq 694	*Samotherium major*	Salonique	Geraads, 1974	455.0	83.0	65.0	51.0	85.0			
PIK 1564	*Helladotherium duvernoyi*	Pikermi	Geraads, 1974	452.0		84.0	56.0	94.0	52.0	56.0	12.4
PIK 1565	*Helladotherium duvernoyi*	Pikermi	Geraads, 1974	433.0	67.0	70.0	47.0	83.0	49.0	51.0	11.8
PIK (type)	*Bohlinia attica*	Pikermi	Geraads, 1974	690.0	70.0	74.0		75.0			
?	*Bohlinia attica (speciosa)*	Pikermi	Geraads, 1974	>550	60.0	51.0	47.0	66.0	39.0	41.0	
Slq 681	*Bohlinia attica*	Salonique	Geraads, 1974		58.0				45.0	42.0	
Slq 682	*Bohlinia attica*	Salonique	Geraads, 1974	680.0			50.0	75.0	50.0	46.0	6.8
MAR	*Bohlinia attica*	Maragha	Geraads, 1974	675.0	70.0	77.0			56.0	52.0	7.7
MAR	*Bohlinia attica (speciosa)*	Maragha	Geraads, 1974	>500	60.0	57.0			43.0	36.0	
DIT *	*Bohlinia attica*	Ditiko	Geraads, 1974	410.0	60.0	62.0			37.0	30.0	7.3
	Helladotherium duvernoyi	Pikermi	Gaudry,1862	440.0		90.0		90.0			
MAR 769	*Palaeotragus coelophrys*	Maragha	Geraads, 1974	387.0	59.0	64.0	44.0	75.0	42.0	44.0	11.4
	Palaeotragus expectans(coelophrys)	Sebastopol	Borissiak, 1915	405.0	47.0	70.0	44.5	78.5	37.0	43.0	10.6
PIK 1691	*Palaeotragus rouenii*	Pikermi	Geraads, 1974	424.0	43.0	46.0	35.0	54.0	34.0	30.0	7.1
	Palaeotragus microdon	China	Bohlin 1926	401.0	54.0	48.0		50.0	38.0	30.0	7.5
	Palaeotragus sp.	Samos	Geraads, 1974	377.0	54.0	54.0	38.0	65.0	38.0	35.0	9.3
	Palaeotragus quadricornis(coelophrys)	Samos	Geraads, 1974	404.0	61.0	62.0	42.0	73.0	42.0	42.0	10.4
a	*Samotherium major*	Samos	AMPG		85.5	80.1			61.6	50.3	
b	*Samotherium boissieri*	Samos	AMPG				42.2	82.7	45.8	46.2	
P9 1963	*Helladotherium duvernoyi*	Samos (SAM 4)	AMPG	455.7	86.1	85.0	54.0	90.1	55.8	49.1	10.8
S95	*Samotherium major*	andrianos	MGML, Kostopoulos pers. com.	473.0	77.0	75.7	52.3	92.0	53.3	48.7	10.3
S94	*Samotherium major*	andrianos	MGML, Kostopoulos pers. com.	465.0	73.3	75.0	53.0	95.0	50.4	51.0	11.0
Munster348	*Samotherium major*	samos	PIM, Kostopoulos pers. com.	460.0		84.0		91.0		54.0	11.7
Munster344	*Samotherium major*	samos	PIM, Kostopoulos pers. com.	458.0				93.0		49.0	10.7
Munster346	*Samotherium major*	samos	PIM, Kostopoulos pers. com.	465.0		87.0		94.0		57.0	12.3
	Helladotherium duvernoyi		Bohlin 1926	465.0	86.0	85.0					

Notes

L = length

DAPpr = proximal anteroposterior diameter

DTpr = proximal transverse diameter

DAPd = distal anteroposterior diameter

DTd = distal transverse diameter

DAPdia = anteroposterior diameter in the middle of the diaphysis

DTdia = transverse diameter in the middle of the diaphysis

Robusticity Index = (Dtdia / L) * 100

specimens with a star (*) characterize juveniles

MGML: Musee Geologique et Mineralogique, Lausanne

PIM: Palaontologisches Institut, Munster

Appendix 12: Intermediolateral cuneiforme

Specimen number	Species	Locality	Museum / author	DAP	DT	H
K1/Δ45	*Samotherium major*	Kerassia	AMGP	55.2	37.2	17.2
K1/Δ247/3	*Samotherium major*	Kerassia	AMGP	52.9	37.1	18.0
K1/Δ341/2	*Samotherium major*	Kerassia	AMGP	56.9	36.4	17.5
M11391a	*Helladotherium duvernoyi*	Pikermi	NHML	56.0	37.6	19.1
M11391b	*Helladotherium duvernoyi*	Pikermi	NHML	48.8	33.6	14.7
M4285a	*Samotherium boissieri*	Samos	NHML	41.4	33.7	14.4
M4285b	*Samotherium boissieri*	Samos	NHML	43.2	28.8	14.2
M4285c	*Samotherium boissieri*	Samos	NHML	42.0	30.0	13.5
M4285d	*Samotherium boissieri*	Samos	NHML	43.0	30.5	14.0
M4285e	*Samotherium boissieri*	Samos	NHML	46.1	30.7	13.9
M4285f	*Samotherium boissieri*	Samos	NHML	48.7	31.5	
M4287(80)	*Samotherium boissieri*	Samos	NHML	50.5	38.7	17.5
M4284(291)	*Samotherium boissieri*	Samos	NHML	47.1	32.5	15.7
M4278	*Samotherium boissieri*	Samos	NHML	45.6	37.1	13.3
M4280(139)	*Samotherium boissieri*	Samos	NHML	42.0	33.7	11.5
M? (293)	*Samotherium boissieri*	Samos	NHML	45.9	33.2	14.4
M4280(77)	*Samotherium boissieri*	Samos	NHML	53.3	30.3	13.7
M4287(254)	*Samotherium boissieri*	Samos	NHML	51.1	33.9	14.9
M4289(99)	*Samotherium boissieri*	Samos	NHML	49.2	36.4	14.9
M4289(61)	*Samotherium boissieri*	Samos	NHML	41.5	33.5	11.8
M4288(83)	*Samotherium boissieri*	Samos	NHML	41.4	29.8	14.8
M5432*	*Samotherium major*	Samos	NHML	48.7	42.8	18.6
PQ-L22186	*Sivatherium hendeyi*	Langebaanweg	SAM	61.0	43.0	20.0
	Helladotherium duvernoyi	Pikermi	Gaudry, 1862	54.0		
	Samotherium sinense	30	Bohlin 1926	58.0	36.0	25.0
1	*Samotherium sinense*	116	Bohlin 1926	60.0	38.0	25.0
2	*Samotherium sinense*	116	Bohlin 1926	56.0	40.0	23.0
3	*Samotherium sinense*	116	Bohlin 1926	59.0	41.0	26.0
4	*Samotherium sinense*	116	Bohlin 1926	61.0	41.0	29.0
	Samotherium eminens		Bohlin 1926	61.0	39.0	21.0

Notes

DAP = anteroposterior diameter

DT = maximum transverse diameter

H = height in the middle of the bone

specimens with a star (*) characterize juveniles

Appendix 13: Phalanx I

Specimen number	Species	Locality	Museum / author	L	DAPpr	DTpr	DAPd	DTd
Ke 90	*Samotherium major*	Kerassia	AMPG	119.6	58.3	52.5	37.3	52.6
Ke 131	*Bohlinia attica*	Kerassia	AMPG	109.9	55.2	41.8	34.6	46.0
K3.4	*Helladotherium duvernoyi*	Kerassia	AMPG	131.3	65.4	54.7	38.6	50.5
K4/Δ354	*Heliadotherium duvernoyi*	Kerassia	AMPG	119.9	69.3	60.5	45.4	44.4
M12921	*Palaeotragus rouenii*	Pikermi	NHML	76.4	28.6	27.0	20.6	22.9
	Palaeotragus rouenii	Pikermi	Sedgwick		37.3	28.9		
	Palaeotragus rouenii	Pikermi	Sedgwick	86.9	39.0	29.8	25.4	25.5
M11404	*Bohlinia attica*	Pikermi	NHML	112.2	59.1	43.8	32.8	
M11393a	*Heliadotherium duvernoyi*	Pikermi	NHML	117.0	62.8	54.5	41.2	53.2
M11393b	*Helladotherium duvernoyi*	Pikermi	NHML	112.3	56.8	50.5	38.3	51.7
M11393c	*Helladotherium duvernoyi*	Pikermi	NHML	111.8	54.7	47.5	34.5	49.8
M11393d	*Helladotherium duvernoyi*	Pikermi	NHML	98.0	56.8	46.6	37.6	
M11393e	*Helladotherium duvernoyi*	Pikermi	NHML	100.6	57.9	49.7	36.5	47.8
M11393f	*Helladotherium duvernoyi*	Pikermi	NHML	110.9	57.0	53.4	40.0	53.3
M11393g	*Helladotherium duvernoyi*	Pikermi	NHML	106.5	56.9	49.0	36.0	41.5
M4290(80)	*Samotherium boissieri*	Samos	NHML	73.1	35.2	24.1	23.9	25.2
M4290	*Samotherium boissieri*	Samos	NHML	69.1	37.3	29.6	21.8	24.4
M4299(196)	*Samotherium boissieri*	Samos	NHML	77.1	37.3	28.8	22.3	26.3
M4299	*Samotherium boissieri*	Samos	NHML	83.2	36.9	29.0	23.6	
M4299	*Samotherium boissieri*	Samos	NHML	93.0	45.6	33.2	28.7	32.6
M4299	*Samotherium boissieri*	Samos	NHML	86.8	42.6	35.7	25.5	32.8
M4299	*Samotherium boissieri*	Samos	NHML	82.8	37.6		26.4	29.7
M4299(84)	*Samotherium boissieri*	Samos	NHML	90.2	44.5	28.7	27.4	27.3
M4303	*Samotherium boissieri*	Samos	NHML	84.6	40.5	35.3	26.7	34.0
M4299(356)	*Samotherium boissieri*	Samos	NHML	82.7	39.2	35.6	26.2	33.0
M4299(71)	*Samotherium boissieri*	Samos	NHML	86.8	42.9	33.5	24.1	30.6
M4299(72)	*Samotherium boissieri*	Samos	NHML	86.6	41.8		26.9	30.8
M4300(354)	*Samotherium boissieri*	Samos	NHML	90.0		41.2	28.3	38.5
M4300	*Samotherium boissieri*	Samos	NHML	89.3	39.6	37.2	27.9	33.5
M4300	*Samotherium boissieri*	Samos	NHML	87.2	43.7	40.5	29.7	37.4
M4300(352)	*Samotherium boissieri*	Samos	NHML	83.0	40.3	37.1	27.8	38.4
M4300(353)	*Samotherium boissieri*	Samos	NHML	80.3	40.6	33.6	25.7	32.5
M3897a	*Helladotherium duvernoyi*	Maragha	NHML	108.8	52.0	50.0	33.3	46.0
M3897b	*Samotherium neumayri*	Maragha	NHML	90.0	45.5	42.2	28.1	39.2
Ant min	*Samotherium neumayri*	Maragha	Geraads, 1974	93.0	38.0	40.0		
Ant max	*Samotherium neumayri*	Maragha	Geraads, 1974	99.0	40.0	46.0		
Post min	*Samotherium neumayri*	Maragha	Geraads, 1974	97.0	39.0	37.0		
Post max	*Samotherium neumayri*	Maragha	Geraads, 1974	106.0	41.0	40.0		
Ant	*Samotherium sinense*	China	Bohlin 1926	98.0	53.0	51.0		
Post	*Samotherium sinense*	China	Bohlin 1926	94.0	49.0	43.0		
Slq 699	*Samotherium major*	Salonique	Geraads, 1974	96.0	41.0	44.0		
Slq 700	*Samotherium major*	Salonique	Geraads, 1974	98.0		42.0		
Sans	*Samotherium major*	Salonique	Geraads, 1974	106.0	41.0	46.0		
PIK 1568	*Helladotherium duvernoyi*	Pikermi	Geraads, 1974	112.0	51.0	48.0		
PIK 1571	*Helladotherium duvernoyi*	Pikermi	Geraads, 1974	110.0	50.0	45.0		
VAT 2 A	*Bohlinia attica*	Vathylakkos 2	Geraads, 1974	108.0	39.0	43.0		
VAT 2 B	*Bohlinia attica*	Vathylakkos 2	Geraads, 1974		39.0	43.0		
Slq 701	*Bohlinia attica*	Salonique	Geraads, 1974	104.0	42.0	42.0		
1973 XXI 67	*Samotherium boissieri*	Maragha	Erdbrink, 1978	89.0	45.0	41.0	31.0	32.5
116	*P. microdon*		Bohlin 1926	83.0	36.0	29.0		
108	*P. microdon*		Bohlin 1926	76.0	34.0	28.0		

Notes
L = length
DAPpr = proximal anteroposterior diameter
DTpr = proximal transverse diameter
DAPd = distal anteroposterior diameter
DTd = distal transverse diameter

Conclusions

The issues elaborated in this thesis are multidisciplinary in nature. They involve the taphonomic investigation of the fossil mammal material, and the taxonomic study of the Giraffidae material from a new Late Miocene Greek locality, Kerassia. The taphonomic aspects highlighted in this study are the histological and biogeochemical alterations of fossil bones and teeth. This study provided not only taxonomic and taphonomic information but also information about the palaeoenvironment and the palaeoclimate of Kerassia.

To date, seven different fossiliferous sites have been found within the Kerassia region. Stratigraphic, sedimentological and geochemical data collected during this study suggest that at least two fossiliferous horizons occur. The sediments of the upper horizon are seen at sites K1 and K6, whilst the sediments of the lower horizon are seen at sites K2, K3, K4 and possibly K5. Data from site K7 are currently insufficient to determine which horizon it belongs to and thus, the existence of a third fossiliferous horizon cannot be ruled out. In addition, geochemical data, faunal data, the preservational state of the material and information by Doukas (pers. communication, 2001) indicate that the material from the 1982 excavation was collected from the upper horizon, and most probably from site K1.

The histological study of bone and tooth tissues from both horizons at Kerassia revealed the presence of extensive bacterial damage. The size of the microtunnels (150-600 nm) in the destructive foci of the damaged bone, dentine and cement tissues indicate that the invading microorganisms were soil bacteria. The rims of the foci appear more mineralised and are enriched in Ca and PO_4^{3-}, and the foci appear demineralised and depleted in Ca and PO_4^{3-}. Despite this, the Ca/P ratios for the three structural areas of the bioeroded tissues, the undamaged areas, the foci and the rims of the foci are practically the same. However, chemical differences do occur between the three structural areas. The concentrations of F are higher in the undamaged areas and lower in the foci and conversely, the concentrations of Cl, Mg and Na are relatively higher in the foci and lower in the undamaged areas. Early recrystallization of crystallites in the foci of damaged tissues that followed bacterial activity is most likely responsible for the differential incorporation of F. Probably, early recrystallization is also responsible for the differential leaching of Na, Cl and Mg from the three structural areas of the bioeroded tissues and may explain the distribution of these elements.

Such extensive bacterial damage indicates that favourable conditions for the development of bacteria prevailed during the Late Miocene of Kerassia; warm, relatively moist and near neutral soil conditions are considered as such favourable conditions (Paul and Clark, 1989). The presence of overlapping dark and bright foci in the studied material, and thus of two generations of foci, has been attributed to seasonality and more precisely to the two periods of growth of soil microorganisms in seasonal, Mediterranean type environments (Schaefer, 1973). The same or similar extensive bacterial damage has been also recognised in bone specimens from eight other Late Miocene Greek localities. Therefore, similar environmental conditions and a seasonal, Mediterranean type climate can be inferred for the Late Miocene of the Northeastern Mediterranean.

XRD analyses showed that fossil bone and dentine consist of carbonate fluorapatite with crystallinity indices significantly higher than those in modern fresh bone. The more compact and crystallized enamel consists of carbonate hydroxyapatite and presents much higher crystallinity indices than bone and dentine. The crystallinity and the overall chemistry of the different hard tissues is controlled by the physicochemical conditions of the localized burial environment and the chemistry of the local pore waters.

The study of the abundant and diverse giraffid material from Kerassia revealed the presence of five different species of giraffes. Four species, *Palaeotragus rouenii, Palaeotragus sp., Samotherium major* and *Helladotherium duvernoyi* were found in the lower horizon and four species were determined in the upper horizon, namely, *Palaeotragus rouenii, Samotherium major, Helladotherium duvernoyi* and *Bohlinia attica.* Although most of these species have a wide biostratigraphic range, the presence of *S. major* provides a more accurate means of dating. Kerassia can be correlated with the well dated Main Bone Beds at Samos locality (Greece) which contain *S. major* (Swisher, 1996; Bernor *et al.*, 1996; Koufos *et al.*, 1997). Therefore, the age of the sediments and fossils at Kerassia can be determined as early MN12 (Middle Turolian). According to recent work on masticatory morphology and tooth microwear (Solounias *et al.*, 1999; Solounias *et al.*, 2000; Solounias and Moelleken, 1988; Solounias and Dawson-Saunders, 1988), *H. duvernoyi* and *B. attica* were characterised as browsers, *S. major* as a grazer and *P. rouenii* as a mixed feeder. Moreover, if *P. sp.* is indeed related with *P. coelophrys*, it could be characterised as a grazer. The presence of four species in each horizon with different feeding adaptations and diets suggests that during the Middle Turolian in Kerassia there was enough tree coverage to support two browsing species, and grasslands to support the grazing species. The mixed feeding habits of *P. rouenii* possibly

indicate seasonal shifting from a browsing to a grazing diet depending on the available browsing or grazing each season. The above agrees with palaeobotanical data and the presence during the Late Miocene of sclerophylous hardwood floras and significant chaparral undergrowth which indicate a seasonal, Mediterranean type climate (Axelrod 1973, 1975; Guernet *et al.* 1976; Sauvage 1977; Orgetta 1979; Ioakim and Solounias 1985; Knobloch and Velitzelos 1987; Gregor and Velitzelos 1987; Solounias and Dawson-Saunders 1988; Bernor *et al.* 1988; Solounias and Moelleken 1992; Kloosterboer van Hoeve 2000; Ivanov *et al.* 2002).

The study of the giraffid material, the bacterially damaged bones and teeth from Kerassia and their chemistry shows that a seasonal Mediterranean type, relatively temperate to warm and moist climate can be inferred for the MN12 (Middle Turolian) of the Kerassia region. Further geochemical study of fossil bones and teeth and their host sediments would provide additional information on the burial environment and the overall climate of Kerassia. Initial results of my ongoing investigation of the chemistry of bones and teeth from Kerassia show that the conditions in the burial environment and the surrounding soils were slightly oxidising and moderately alkaline. The soils were well drained with significant carbonation, and the depth of the calcic horizons in the paleosol sequences indicates a mean annual precipitation between 700-1000 mm/yr. Seasonal fluctuations occurred in temperature and soil moisture, ranging between warm and dry conditions during the summer and cool and wet conditions during the winter.

In order to test and expand the findings of the present study, a detailed histological and geochemical study of fossil bones and teeth, including their surrounding sediments, should be expanded to other Late Miocene localities in the wider area of the North-Eastern Mediterranean and today's "Greco-Irano-Afganian" province. The Late Miocene was a critical period of tectonic and consequently climatic changes that affected the extinction of and the evolution of numerous species including humans. According to Solounias *et al.* (2000) a large number of recent Eurasian and African species originated from the so called "Pikermian" biome of the Late Miocene "Greco-Irano-Afganian" province. Such an investigation will provide further data to elucidate the palaeoenvironmental conditions that prevailed during the Late Miocene in this province.

The study of bones and teeth buried in soils from different climates and burial environments should be undertaken. This investigation will provide information on the effect that climatic

and burial conditions have on microbial focal destruction, and presents a challenging area of further research.

A revision of the Eurasian Late Miocene giraffidae is also considered as essential. During the last 100 years giraffid material has been collected from a significant number of localities in China and the former Soviet republics, and an unusually large number of new species has been determined (particularly those of *Samotherium*). In the past these collections were not easily accessible, thus they are not well studied. Thorough examination of these collections would elucidate the relationships of the Eurasian Late Miocene giraffids and would allow taxonomic revision, including the recognition of synonyms among the plethora of species names.

References

Apfelbaum, F., Mayer, I., and Featherstone, J.D.B., 1990, The role of HPO_4^{2-} and CO_3^{2-} ions in the transformation of synthetic apatites to β-$Ca_3(PO_4)_2$: Journal of Inorganic Biochemistry, v. 38, p. 1-8.

Abel, O., 1912, Grundzuge der Palaeobiologie der Wirbeltiere: Stuttgart, 708 p.

Abel, O., 1927, Lebensbilder aus der Tierwelt der Vorzeit: Jena, Verlag Gustav Fischer, 643 p.

Agusti, J., 1999, A critical re-evaluation of the Miocene mammal units in Western Europe: dispersal events and problems of correlation, in Agusti, J., Rook, L., and Andrews, P., eds., The evolution of Neogene terrestrial ecosystems in Europe, Volume 1: Hominoid evolution and climatic change in Europe: Cambridge, Cambridge University Press, p. 83-112.

Agusti, J., and Anton, M., 2002, Mammoths, sabertooths and hominids: New York, Columbia University Press, 313 p.

Agusti, J., Cabrera, L., Garces, M., Krijgsman, W., Oms, O., and Pares, J.M., 2001, A calibrated mammal scale for the Neogene of Western Europe. State of the art: Earth-Science Reviews, v. 52, p. 247-260.

Alexeiev, A., 1930, Die obersarmatische Fauna von Eldar. I. *Achtiaria borissiaki* nov. sp.: Trav. du Musee geol. Acad. Sc. URSS, v. 8, p. 167-204.

Arambourg, C., and Piveteau, J., 1929, Les Vertebres du Pontien de Salonique.: Annales de Paleontologie, v. 18, p. 59-138.

Ascenzi, A., and Silvestrini, G., 1984, Bone-boring micro-organisms: an experimental investigation: Jouranl of Human Evolution, v. 13, p. 531-536.

Axelrod, D.I., 1973, History of the Meditarranean ecosystem in California, in Castri, F.d., and Mooney, H.A., eds., Mediterranean type ecosystems: Origin and structure: London, Chapman and Hall Limited, p. 225-277.

Axelrod, D.I., 1975, Evolution and biogeography of Madrean-Tethyan sclerophyll vegetation: Annals Missouri Botanical Gardens, v. 62, p. 280-334.

Bakalov, P., 1953, The Hipparion fauna from Kalimanci and Kromidovo, Sandanski. IV. Artiodactyla-Selinodontia: Izvestiya Geologicheskiya Institut / Bulgarska Akademiya na Naukite, v. 2, p. 88-125.

Bartsiokas, A., and Middleton, A.P., 1992, Characterization and dating of recent and fossil bone by X-ray diffraction: Journal of Archaeological Science, v. 19, p. 63-72.

Baud, C.A., and Lacotte, D., 1984, Étude au microscope électronique a transmission de la colonisation bacterienne de l'os mort: C. R. Acad. Sc. Paris, v. 298, p. 507-510.

Behrensmeyer, A.K., 1978, Taphonomic and ecologic information from bone weathering: Paleobiology, v. 4, p. 150-162.

Behrensmeyer, A.K., 1988, Vertebrate preservation in fluvial channels: Palaeogeography, Palaeoclimatology, Palaeoecology, v. 63, p. 183-199.

Bell, L.S., 1990, Palaeopathology and diagenesis: An SEM evaluation of structural changes using backsctered electron imaging: Journal of Archaeological Science, v. 17, p. 85-102.

Bell, L.S., Boyde, A., and Jones, S.J., 1991, Diagenetic alteration to teeth in situ illustrated by backscattered electron imaging: Scanning, v. 13, p. 173-183.

Bell, L.S., Skinner, M.F., and Jones, S.J., 1996, The speed of mortem change to the human skeleton and its taphonomic significance: Forensic Science International, v. 82, p. 129-140.

Bernor, R.L., 1978, The mammalian systematics, biostratigraphy and biochronology of Maragheh and its importance for understanding Late Miocene hominoid zoogeography and evolution [PhD thesis]: Los Angeles, University of California.

Bernor, R.L., 1983, Geochronology and zoogeographic relationships of Miocene Hominoidea, in Ciochon, R.L., and Corruchini, R.S., eds., New interpretations of ape and human ancestry: New York, Plenum, p. 21-64.

Bernor, R.L., 1984, A zoogeographic theater and biochronologic play: the time/biofacies phenomena of Eurasian and African Miocene mammal provinces: Paleobiologie Continentale, v. 14, p. 121-142.

Bernor, R.L., Kovar-Eder, J., Lipscomb, D., Rögl, F., Sen, S., and Tobien, H., 1988, Systematic, stratigraphic, and paleoenvironmental contexts of first-appearing Hipparion in the Vienna Basin, Austria: Journal of Vertebrate Paleontology, v. 8, p. 427-452.

Bernor, R.L., Solounias, N., Swisher III, C.C., and Van Couvering, J.A., 1996, The correlation of three classical "Pikermian" mammal faunas - Maragheh, Samos and Pikermi - with the European MN unit system, in Bernor, R.L., Fahlbusch, V., and Mittmann, H.W., eds., The evolution of Western Eurasian Neogene mammal faunas: New York, Columbia University Press, p. 137-154.

Bernor, R.L., Tobien, H., and Van Couvering, J.A., 1979, The Mammalian biostratigraphy of Maragheh.: Annales Geologiques des Pays Helliniques. v. VII International Congress on Meditarranean Neogene, Athens, v. 1, p. 91-99.

Bohlin, B., 1926, Die Familie Giraffidae: Palaeontologica Sinica, Series C, v. 4, p. 178.

Bonel, G., and Montel, G., 1964, Sur une nouvelle apatite carbonatees synthetique: Comptes Rendus de l'Académie des Sciences, v. 258, p. 923-926.

Bonis, L. de, and Koufos, G., 1999, The Miocene large mammal succession in Greece, in Agusti, J., Rook, L., and Andrews, P., eds., The evolution of Neogene terrestrial ecosystems in Europe, Volume 1: Hominoid evolution and climatic change in Europe: Cambridge, Cambridge University Press, p. 205-237.

Bonis, L. de, Bouvrain, G., and Geraads, D., 1979, Artiodactyles du Miocene superieur de Macedoine.: Annales Geologiques des Pays Helleniques, v. VII International Congress on Meditarranean Neogene, Athens, 2, p. 167-175.

Bonis, L. de, Brunet, M., Heintz, E., and Sen, S., 1992, La province greco-irano-afgane et la repartition des faunes mammaliennes au Miocene superieur: Paleontologia I Evolucio, v. 24-25, p. 103-112.

Bono, A. de, 1998, Pelagonian margins in Central Evia Island (Greece): Stratigraphy and geodynamic evolution [PhD thesis]: Lausanne, Universite de Lausanne.

Borissiak, A., 1914, Mammiferes fossiles de Sebastopol. I: Memmoires du Comite Geologique, v. 87, p. 105-154.

Bosscha-Erdbrink, D.P., 1978, Fossil Giraffidae from the Maragheh area, NW Iran: Mitteilungen der Bayerischen Staatssammlung für Paläontologie und Historische Geologie, v. 18, p. 93-115.

Brown, R.W., 1934, *Celliforma spirifer*; the fossil larval chambers of mining bees: Journal of the Washington Academy of Sciences, v. 24, p. 532-539.

Bruijn, H. de, and Meulen, A.J. van der, 1979, A review of the Neogene Rodent succession in Greece.: Annales Geologiques des Pays Helliniques. Tome hors serie: VII International Congress on Meditarranean Neogene, Athens, v. 1, p. 207-217.

Carlson, S., 1990, Vertebrate dental structure, in Carter, J.G., ed., Skeletal biomineralization: Patterns, processes and evolutionary trends, Volume 1: New York, Van Nostrand Reinhold, p. 531-556.

Cerling, T.E., 2001, Evolution of modern grasslands and grazers, in Briggs, D.E.G., and Crowther, P.R., eds., Palaeobiology II: Oxford, Blackwell Science, p. 106-108.

Cerling, T.E., and Quade, J., 1990, Global ecologic and climatic change during the Neogene: stable isotopic evidence from soils: Chemical Geology, v. 84, p. 164-165.

Cerling, T.E., Harris, J.M., MacFadden, B.J., Leakey, M.G., Quade, J., Eisenmann, V., and Ehleringer, J.R., 1997, Global vegetation change through the Miocene/Pliocene boundary: Nature, v. 389, p. 153-158.

Cerling, T.E., Quade, J., Wang, Y., and Bowman, J.R., 1989, Carbon isotopes in soils and paleosols as ecological and paleoecologic indicators: Nature, v. 341, p. 138-139.

Child, A.M., Gillard, R.D., and Pollard, A.M., 1993, Microbially-induced promotion of amino acid racemication in bone: Isolation of the microorganisms and the detection of their enzymes: Journal of Archaeological Science, v. 20, p. 159-168.

Child, A.M., 1995, Microbial taphonomy of archaeological bone: Studies in conservation, v. 40, p. 19-30.

Churcher, C.S., 1970, Two new Upper Miocene Giraffids from Fort Ternan, Kenya, East Africa: Palaeotragus primaevus and Samotherium africanum: Fossil vertebrates of Africa, v. 2, p. 1-105.

Cordella, 1878, La Grece sous le rapport geologique et mineralogique: Paris, Edition Parent.

Cormack, D.H., 1987, Ham's histology: Philadelphia, J.B. Lippincott Company, 732 p.

Crusafont-Pairo, M., 1951, La cuestion del llamado Meotico espanol: Arrahona, v. 1-2, p. 25-36.

Crusafont Pairo, M., 1952, Los Jirafidos fosiles de Espana [Thesis]: Barcelona, Diputation provincial de Barcelona.

Crusafont-Pairo, M., and Villalta, J., 1954, Ensayo de sintesis sobre el Mioceno de la meseta castellana: Bolletin de la Real Sociedad Espanola de Historia Natural (Madrid), v. 1954, p. 215-227.

Daculsi, G., and Kerebel, B., 1978, High-resolution electron microscope study of human enamel crystallites: Size, shape and growth: Journal of Ultrastructure Research, v. 65, p. 163-172.

Dam, J.A. van, Alcala, L., Alonso-Zarza, A., Calvo, J.P., Garses, M., and Krijgsman, W., 2001, The Upper Miocene mammal record from the Teruel - Alfabra region (Spain). The MN system and the continental stage/age concepts discussed: Journal of Vertebrate Palaeontology, v. 21, p. 367-385.

Davis, P.G., 1997, The bioerosion of bird bones: International Journal of Osteoarchaeology, v. 7, p. 388-401.

Denys, C., Wlliams, C.T., Dauphin, Y., Andrews, P., and Fernandez-Jalvo, Y., 1996, Diagenetical changes in Pleistocene small mammals bones from Olduvai Bed I: Palaeogeography, Palaeoclimatology, Palaeoecology, v. 126, p. 121-134.

Deprat, J., 1904, Etude geologique et petrographique de l'ile d'Eubee: Besancon, Dodivers, 230 p.

Doetsch, R.N., and Cook, T.M., 1973, Introduction to bacteria and their ecobiology: Baltimore-London-Tokyo, University Park Press, 371 p.

Driessens, F.M.C., and Verbeek, R.M.H., 1990, Biominerals: Boca Raton, CPC Press.

Dumpert, K., 1981, The social biology of ants: London, Pitman Publishing Ltd, 278 p.

Ehrlich, H.L., 1990, Geomicrobiology: New York, Marcel Dekker, INC, 646 p.

Elliott, J.C., 2002, Calcium phosphate biominerals, in Kohn, M.J., Rakovan, J., and Hughes, J.M., eds., Phosphates: geochemical, geobiological, and materials importance, Volume 48: Reviews in Mineralogy and Geochemistry, Mineralogical Society of America - Geochemical Society, p. 427-453.

Elorza, J., Astibia, H., Murelaga, X., and Pereda-Suberbiola, X., 1999, Francolite as a diagenetic mineral in dinosaur and other Upper Cretaceous reptile bones (Lano, Iberian Peninsula): microstructural, petrological and geochemical features: Cretaceous Research, v. 20, p. 169-187.

Eppell, S.J., Tong, W., Katz, J.L., Kuhn, L., and Glimcher, M.J., 2001, Shape and size of isolated bone mineralites measured using atomic force microscopy: Journal of Orthopaedic Research, v. 19, p. 1027-1034.

Fabig, A., and Herrmann, B., 2002, Trace elements in buried human bones: intra-population variability of Sr/Ca and Ba/Ca ratios - diet or diagenesis?: Naturwissenschaften, v. 89, p. 115-119.

Fortelius, M., Werdelin, L., Andrews, P., Bernor, R.L., Gentry, A., Humphrey, L., Mittmann, H.W., and Viranta, S., 1996, Provinciality, diversity, turnover, and paleoecology in land mammal faunas of the Later Miocene of Western Europe, in Bernor, R.L., Fahlbusch, V., and Mittmann, H.W., eds., The evolution of Western Eurasian Neogene mammal faunas: New York, Columbia University Press, p. 414-448.

Gaudry, A., 1860, Resultats des fouilles executees en Grece sous les auspices de l' Academie: C.R. Acad. Sci., Paris, v. 51, p. 802-804.

Gaudry, A., 1861, Note sur la Girafe et l' *Helladotherium* trouvees a Pikermi (Grece): Bulletin Societe Geologique de France, Ser. 2, v. 18, p. 587-598.

Gaudry, A., 1862-67, Animaux fossiles et geologie de l' Attique.: Paris, 476 p.

Gaudry, A., and Lartet, E., 1856, Sur les resultats de recherches paleontologiques entreprises dans l'Attique sous les auspices de l' Academie: Comptes Rendus de l'Académie des Sciences, Paris, v. 43, p. 271-274.

Gentry, A., and Heizmann, E.P.J., 1996, Miocene ruminants of the Central and Eastern Tethys and Paratethys, in Bernor, R.L., Fahlbusch, V., and Mittmann, H.W., eds., The evolution of Western Eurasian Neogene mammal faunas: New York, Columbia University Press, p. 378-391.

Gentry, A.W., Rossner, G.E., and Heizmann, E.P.S., 1999, Suborder Ruminantia, in Rossner, G.E., and Heissig, K., eds., The Miocene land mammals of Europe: Munchen, Verlag Dr. Friedrich Pfeil, p. 225-258.

Geraads, D., 1974, Les giraffides du Miocene Superieur de la region de Thessalonique (Grece) [PhD thesis]: Paris, Universite de Paris VI.

Geraads, D., 1978, Les Palaeotraginae (Giraffidae, Mammalia) du Miocene superieur de la region de Thessalonique (Grece). Geologie Mediterranaenne, v. 5, p. 269-276.

Geraads, D., 1979, Le Giraffinae (Artiodactyla, Mammalia) du Miocene superieur de la region de Thessalonique (Grece). Bulletin Museum National d'Histoire Naturelle Paris, v. 4e ser., 1, section C, p. 377-389.

Geraads, D., 1986, Remarques sur la systematique et la phylogenie des Giraffidae (Artiodactyla, Mammalia). Geobios, v. 19, p. 465-477.

Geraads, D., 1989, Un nouveau Giraffide du Miocene superieur de Macedoine (Grece). Bulletin Museum National d'Histoire Naturelle Paris, v. 4e ser., 11, section C, p. 189-199.

Geraads, D., 1994, Les gisements de mammiferes du Miocene superieur de Kemiklitepe, Turquie: 8. Giraffidae: Bulletin Museum National d'Histoire Naturelle Paris, v. 4e ser., 16, section C, p. 159-173.

Gorceix, H., 1878, Notice sur le bassin miocenique d'eau douce de Koumi (Eubea): Ann. Ec. Norm. Sup., v. 2, p. 317-321.

Gray, J.E., 1821, On the natural arrangement of vertebrate animals: London Medical Repository, v. 15, p. 296-310.

Gregor, H.J., and Velitzelos, E., 1987, Evolution of Neogene Mediterranean vegetation and the question of a dry Upper Miocene period (salinity crisis): Annales of the Hungarian Geological Institute, v. 70, p. 489-496.

Gross, K.A., and Berndt, C.C., 2002, Biomedical application of apatites, in Kohn, M.J., Rakovan, J., and Hughes, J.M., eds., Phosphates: geochemical, geobiological, and materials importance, Volume 48: Reviews in Mineralogy and Geochemistry, Mineralogical Society of America -Geochemical Society, p. 631-672.

Grupe, G., 2001, Archaeological microbiology, in Brothwell, D.R., and Pollard, A.M., eds., Archaeological sciences: Chichester, John Willey and Sons, p. 351-358.

Grupe, G., and Piepenbrink, H., 1988, Trace element contaminations in excavated bones by microorganisms, in Grupe, G., and Hermann, B., eds., Trace elements in environmental history: Berlin, Springer-Verlag, p. 103-112.

Grupe, G., and Piepenbrink, H., 1989, Impact of microbial activity on trace element concentrations in excavated bones: Applied Geochemistry, v. 4, p. 293-298.

Guernet, C., 1971, Etudes Geologiques en Eubee, et dans les regions voisins (Grece): Paris.

Guernet, C., Keraudren, B., and Sauvage, J., 1976, La serie "Levantine" du cap Phocas (Ile de Kos, Dodecanese, Grece). Stratigraphie, palynologie et paleoecologie: Revue de Micropaleontologie, v. 19, p. 61-73.

Hackett, C.J., 1981, Microscopical focal destruction (tunnels) in exhumed Human bones: Medicine, Science and the Law, v. 21, p. 243-265.

Hamilton, W.R., 1978, Fossil giraffes from the Miocene of Africa and a revision of the phylogeny of the Giraffoidea: Philosophical Transactions of the Royal Society of London, B, v. 283, p. 165-229.

Handschin, R.G., and Stern, W.B., 1995, X-ray diffraction studies on the lattice perfection of human bone apatite (crista iliaca): Bone, v. 16, p. 355S-363S.

Hanson, D.B., and Buikstra, J., E., 1987, Histomorphological alteration in burried human bone from the lower Illinois valley: Implications for palaeodietary research: Journal of Archaeological Science, v. 14, p. 549-563.

Harper, E., 1980, Collagenases: Annual Review of Biochemistry, v. 49, p. 1063- 1078.

Harris, J.M., 1976, Pliocene Giraffoidea (Mammalia, Artiodactyla) from the Cape province: Annals of the South African Museum, v. 69, p. 325-353.

Hayek, L.A., Bernor, R.L., Solounias, N., and Steigerwald, P., 1992, Preliminary studies of hiparionine horse diet as measured by tooth microwear, in Forsten, A., Fortelius, M., and Werdelin, L., eds., Bjorn Kurten - A memorial volume, Volume Annales Zoologici Fennici volume 28: Helsinski, Finnish Zoological Publishing Board, p. 187-200.

Hedges, R.E.M., 2002, Bone diagenesis: An overview of processes: Archaeometry, v. 44, p. 319-328.

Hedges, R.E.M., and Millard, A.R., 1995, Bones and groundwater: Towards the modelling of diagenetic processes: Journal of Archaeological Science, v. 22, p. 155-164.

Hedges, R.E.M., Millard, A.R., and Pike, A.W.G., 1995, Measurements and relationships of diagenetic alteration of bone from three archaeological sites: Journal of Archaeological Science, v. 22, p. 201-209.

Heintz, E., 1970, Les Cervides Villafranchiens de France et Espagne. Vol. II: Memoires de Museum National d' Histoire Naturelle Paris, Nouvelle serie, v. 23.

Herrmann, B., 1977, Uber die reste des postcranialen Skeletten des Neanderthalens von Le Moustier: Zeitschrift fur Morphologie und Anthropologie, v. 68, p. 129-149.

Hilson, S., 1986, Teeth, in Brothwell, D., Cunliffe, B., Fleming, S., and Fowler, P., eds., Cambridge Manuals in Archaeology: Cambridge, Cambridge University Press, p. 376.

Hubert, J.F., Panish, P.T., Chure, D.J., and Prostak, K.S., 1996, Chemistry, microstructure, petrology, and diagenetic model of Jurassic dinosaur bones, Dinosaur National Monument, Utah.: Journal of Sedimentary Research, v. 66, p. 531-547.

Hughes, J.M., and Rakovan, J., 2002, The crystal Structure of apatite, $Ca_5(PO_4)_3(F,OH,Cl)$, in Kohn, M.J., Rakovan, J., and Hughes, J.M., eds., Phosphates: geochemical, geobiological, and materials importance, Volume 48: Reviews in Mineralogy and Geochemistry, Mineralogical Society of America - Geochemical Society, p. 1-12.

Iliopoulos, G., 2002, Bone invasion: Microbial focal destruction in Late Miocene mammal bone: Journal of Vertebrate Palaeontology, v. 22, p. 69A.

Iliopoulos, G., 2003, Invading the bone: Microbial focal destruction in Late Miocene mammal bone: Scanning, v. 25, p. 94-95.

Ioakim, C., and Solounias, N., 1985, A radiometrically dated dated pollen flora from the Upper Miocen of Samos Island, Greece: Revue de Micropaleontologie, v. 28, p. 197-204.

Ivanov, D., Ashraf, A.R., Mosbrugger, V., and Palamarev, E., 2002, Palynological evidence for Miocene climate change in the Forecarpathian Basin (Central Paratethys, NW Bulgaria): Palaeogeography, Palaeoclimatology, Palaeoecology, v. 178, p. 19-37.

Jackes, M., Sherburne, R., Lubell, D., Barker, C., and Wayman, M., 2001, Destruction of microstructure in archaeological bone: a case study from Portugal: International Journal of Osteoarchaeology, v. 11, p. 415-432.

Jacobi, B., 1982, Zur Stratigraphie und Sedimentpetrographie der Neogenen Susswasserablagerungen im bereich von Agia anna im Nordosten der insel Euboa (Agais) [Diplomarbeit thesis]: Rhein, Christian - Albrechts - Universitat Kiel.

Janis, C.M., 1982, Evolution of horns in ungulates: ecology and paleoecology: Biological Reviews, v. 57, p. 261-318.

Janis, C.M., 1989, A climatic explanation for patterns of evolutionary diversity in ungulate mammals: Palaeontology, v. 32, p. 463-481.

Jarvis, I., 1992, Sedimentology, geochemistry and origin of phosphate chalks: the Upper Cretaceous deposits of NW Europe: Sedimentology, v. 39, p. 55-97.

Johnsson, K., 1997, Chemical dating of bones based on diagenetic changes in bone apatite: Journal of Archaeological Science, v. 24, p. 431-437.

Katsikatsos, G., Bruijn, H. de, and Meulen, A.J. van der, 1981, The Neogene of the island of Euboea (Evia), a review: Geologie en Mijnbouw, v. 60, p. 509-526.

Katsikatsos, G., Migiros, G.P., Triantaphyllis, M., and Mettos, A., 1986, Geological structure of internal Hellinides (E. Thessaly - SW. Macedonia, Euboea - Attica - Northern Cyclades Islands and Lesvos), in I.G.M.E., ed., John Papastamatiou memorial issue: Special Issue, Geological and Geophysical Research: Athens, p. 191-212.

Kloosterboer - van Hoeve, M., 2000, Cyclic changes in the late Neogene vegetation of Northern Greece: A palynological study. LPP Contribution Series No 12 [PhD thesis]: Utrecht, University of Utrecht.

Knobloch, E., and Velitzelos, E., 1987, New leaf floras in the Neogene of Greece: Vestnik Ustredniho Ustavu Geologickeno, v. 62, p. 157-164.

Koenigswald, G.H.R. van, 1929, Bemerkungen zur Saugetierfauna des rheinhessischen Dinotheriensandes: Senckenbergiana, v. 11, p. 267-279.

Kohler, R.W., 1983, Zur stratigraphie, sedimentologie und petrographie Neogener ablagerungen im gebiet Kerasia - Papades - Ag. Anna: Im Nordosten der insel Euboa (Agais). [Diplomarbeit thesis]: Kiel, Christian - Albrechts - Universitat Kiel.

Kohn, M.J., Schoeninger, M.J., and Barker, W.W., 1999, Altered states: Effects of diagenesis on fossil tooth chemistry: Geochimica et Cosmochimica Acta, v. 63, p. 2737-2747.

Kojumdgieva, E., Nikolov, I., Nedjakov, P., and Busev, A., 1982, Stratigraphy of the Neogene in Sandanski Graben: Geologica Balcanica, v. 12, p. 69-81.

Koken, E., 1885, Ueber fossile Saugetiere aus China: Palaeontologische Abhand. Bd III, v. 2, p. 85.

Kostopoulos, D., Sen, S., and Koufos, G., 2003, Magnitostratigraphy and revised chronology of the Late Miocene mammal localities of Samos, Greece: International Journal of Earth Sciences, v. 92, p. 779-794.

Kostopoulos, D.S., Koliadimou, K., and Koufos, G.D., 1996, The Giraffids (Mammalia, Artiodactyla) from the Late Miocene Mammalian localities of Nikiti (Macedonia, Greece). Palaeontographica Abt. A., v. 239, p. 61-88.

Kostopoulos, D.S., Spassov, N., and Kovachev, D., 2001, Contribution to the study of Microstonyx: evidence from Bulgaria and the SE European populations: Geodiversitas, v. 23, p. 411-437.

Koufos, G.D., Syrides, G.E., Kostopoulos, D.S., Koliadimou, K.K., Sylvestrou, I.A., Seitanidis, G.C., and Vlachou, T.D., 1997, New excavations in the Neogene mammalian localities of Mytilinii, Samos island, Greece.: Geodiversitas, v. 19, p. 877-885.

Krijgsman, W., Garcés, M., Langereis, C.G., Daams, R., Dam, J. van, Meulen, A.J. van der, Agustí, J., and Cabrera, L., 1996, A new chronology for the middle to late Miocene continental record in Spain: Earth and Planetary Science Letters, v. 142, p. 367-380.

Kurten, B., 1952, The chinese Hipparion fauna.: Societas Scientiarium Fennica. Commentationes Biologicue, v. 8, p. 1-82.

Linnaeus, C., 1758, Systema Naturae, 824 p.

Lowenstam, H.A., and Weiner, S., 1989, On biomineralization: New York-Oxford, Oxford University Press, 324 p.

Lucas, J., and Prevot , L.E., 1991, Phosphates and fossil preservation., in Allison, P.A., and Briggs, D.E.G., eds., Taphonomy: Releasing the data locked in the fossil record, Volume 9: Topics in Geobiology: New York and London, Plenum Press, p. 389-409.

Lydekker, R., 1983, Siwalik Camelopardalidae: Palaeontologica Indica, Series X, v. 2, p. 44.

Made, J. van der, and Moya -Sola, S., 1989, European Suinae (Artiodactyla) from the Late Miocene onwards: Bolletino della Societa Paleontologica Italiana, v. 28, p. 329-339.

Magne, D., Pilet, P., Weiss, P., and Daculsi, G., 2001, Fourier transform infrared microspectroscopic investigation of the maturation of nonstoichiometric apatites in mineralized tissues: a horse dentin study: Bone, v. 29, p. 547-552.

Major, C.J.F., 1888, Sur un gisement d'ossements fossiles dans l'ile de Samos, contemporain de l'age de Pikermi: Comptes Rendus de l' Academie des Sciences, Paris, v. 107, p. 1178-1182.

Malik, A., and Nafiz, H., 1933, Vertebres fossiles de Kucukcekmece: Publ. Inst. Geol. Univ. Istanbul, v. 8, p. 119.

Marchiafava, V., Bonucci, E., and Ascenzi, A., 1974, Fungal osteoclasia: a model of dead bone resorption: Calcified Tissue Research, v. 14, p. 195-210.

Matthew, W.D., 1929, Critical observations upon Siwalik mammals: Bulletin of the American Museum of Natural History, v. 56, p. 437-560.

Mecquenem, R. de, 1924, Contribution a l' etude des fossiles de Maragha.: Annales de Paleontologie, v. 13, p. 135-160.

Mein, P., 1975, Resultats du Groupe de Travail des Vertebres, in Senes, J., ed., Report on activity of R.C.M.N.S. working groups, 6. Congress of the Regional Committee of Mediterranean Neogene Stratigraphy, Proceedings, v. 1, p. 78-81, Bratislava.

Melentis, J.K., 1967, Studien uber fossile vertebraten Griechenlands. 19. Die Pikermifauna von Halmyropotamos (Euboa-Griechenland), I Teil: Odontologie und craniologie: Annales Geologiques des Pays Helleniques, v. 19, p. 285-411.

Melentis, J.K., 1969, Studien uber fossile vertebraten Griechenlands. 19. Die Pikermifauna von Halmyropotamos (Euboa-Griechenland), II Teil: Osteologie.: Annales Geologiques des pays Helleniques, v. 21, p. 217-300.

Melentis, J.K. 1974, *Helladotherium duvernoyi* GAUDRY 1860 aus Pikermi (Griechenland): Scientific Annals of the Faculty of Physics and Mathematics, University of Thessaloniki, v. 14, p. 65-72.

Mettos, A., Rodogianni, T., Papadakos, G., Pashos, P., and Georgiou, H., 1991, New data in the geology of the Neogene sediments of Northern Euboea.: Bulletin of the Geological Society of Greece, v. 25, p. 71-83.

Michel, V., Ildefonse, P., and Morin, G., 1996, Assessment of archaeological bone and dentine preservation from Lazaret Cave (Middle Pleistocene) in France: Palaeogeography, Palaeoclimatology, Palaeoecology, v. 126, p. 109-119.

Michener, C.D., 1974, The social behaviour of bees:A comparative study: Cambridge, Masschusets, The Belhnap Press of Harvard University Press, 404 p.

Micozzi, M.S., 1991, Postmortem change in human and animal remains: A systematic approach: Springfield, Illinois, Charles C Thomas, 124 p.

Middleton, J., 1844, On fluorine in bones, its source, and its application to the determination of the geological age in fossil bones: Proceedings of the Geological Society of London, v. 4, p. 431-433.

Mitzopoulos, M.K., 1947, Die Verbreitung der Pikermistufe auf der Insel Euboea: Annales Geologiques des Pays Helleniques, v. 12, p. 209-216.

Montoya, P., and Morales, J., 1991, *Birgerbolinia schaubi* Crusafont, 1952 (Giraffidae, Mammalia) del Turoliense inferior de Crevillente-2 (Alicante, Espana). Filogenia e historia biogeographica de la subfamilia Sivatheriinae: Bull. Mus. natn. Hist. nat. Paris, 4e ser., v. 13, section C, p. 177-200.

Moodie, R.L., 1923a, Paleopathology, an introduction to the study of ancient evidences of disease: Urbana, University of Illinois press, 567 p.

Moodie, R.L., 1923b, The Antiquity of Disease: Chicago, The University of Chicago Press, 148 p.

Moodie, R.L., 1926, Pleistocene examples of traumatic osteomyelitis: Annals of medical history, v. 8, p. 413- 418.

Morales, J., and Soria, D., 1981, Los Artiodactylos de los Valles de Fuentiduena (Segovia). Estudios Geologicos, v. 37, p. 477-501.

Morgan, H., Wilson, R.M., Elliott, J.C., Dowker, S.E.P., and Anderson, P., 2000, Preparation and characterisation of monoclinic hydroxyapatite and its precipitated carbonate apatite intermediate: Biomaterials, v. 21, p. 617-627.

Morganthaler, P.W., and Baud, C.A., 1956, Sur une cause d'alteration des structures dans l'os humain fossile: Actes de la Société Helvétique des Sciences Naturelles, v. 136, p. 142-143.

Newesely, H., 1989, Fossil bone apatite: Applied Geochemistry, v. 4, p. 233-245.

Nielsen-Marsh, C.M., and Hedges, R.E.M., 1999, Bone porosity and the use of mercury intrusion porosimetry in bone diagenesis studies: Archaeometry, v. 41, p. 165-174.

Nielsen-Marsh, C.M., and Hedges, R.E.M., 2000, Patterns of diagenesis in bone I: The effects of site environments: Journal of Archaeological Science, v. 27, p. 1139-1150.

Nielsen-Marsh, C.M., Gernaey, A.M., Turner-Walker, G., Hedges, R.E.M., Pike, A., and Collins, M., 2000, The chemical degradation of bone, in Cox, M., and Mays, S., eds., Human osteology in archaeology and forensic science: London, Greenwich Medical Media Ltd, p. 439-454.

Opdyke, N., Mein, P., Lindsay, E., Perez-Gonzales, A., Moissenet, E., and Norton, V.L., 1997, Continental deposits, magnetostratigraphy and vertebrate paleontology, late Neogene of Eastern Spain: Palaeogeogrphy, Palaeoclimatology, Palaeoecology, v. 133, p. 129-148.

Orgetta, M., 1979, Erste Ergebnisse einer palynologischen Untersuchung der Lignite von Pikermi, Attica: Annales Geologiques de Pays Helleniques, v. VII International Congress on Meditarranean Neogene, Athens, 2, p. 909-921.

Osborn, H.F., 1910, The age of mammals: New York, MacMillan.

Owen, R., 1848, On the archetype and homologies of the vertebrate skeleton: London, J. Van Voorst, 203 p.

Ozansoy, F., 1965, Etude des gisements continentaux et des mammiferes du Cenozoique de Turquie: Memoire de la Societe Geologique de France, N.S., v. 44, p. 1-92.

Pate, D., and Brown, K.A., 1985, The stability of bone strontium in the geological environment: Journal of Human Evolution, v. 14, p. 483-491.

Pate, F.D., Hutton, J.T., and Norrish, K., 1989, Ionic exchange between soil solution and bone: towards a predictive model: Applied Geochemistry, v. 4, p. 303-316.

Paul, E.A., and Clark, F.E., 1989, Soil microbiology and biochemistry: San Diego, Academic Press, Inc, 273 p.

Person, A., Bocheren, H., Saliege, J.F., Paris, F., Zeitoun, V., and Gerard, M., 1995, Early diagenetic evolution of the bone phosphate: An X-ray diffractiometric analysis: Journal of Archaeological Science, v. 22, p. 211-221.

Pfretzschner, H.U., 2000, Microcracks and fossilization of Haversian bone: Neues Jahrbuch für Geologie und Paläontologie Abhandlungen, v. 216, p. 413-432.

Piepenbrick, H., 1986, Two examples of biogenous dead bone decomposition and their consequences for taphonomic interpretation: Journal of Archaeological Science, v. 13, p. 417-430.

Pilgrim, G.E., 1911, The fossil Giraffidae of India.: Palaeontologia Indica, New series, v. 4, p. 1-29.

Posner, A.S., 1987, Bone mineral and mineralization process, in Peck, W.A., ed., Bone and mineral research: Amsterdam, New York, Oxford, Elsevier, p. 65-116.

Price, T.D., 1989, Multielement studies of diagenesis in prehistoric bone, in Price, T.D., ed., The chemistry of prehistoric Human bone: School of American Research Advanced Seminar Series: Cambridge, Cambridge University Press, p. 126-154.

Quade, J., Solunias, N., and Cerling, T.E., 1994, Stable isotopic evidence from paleosol carbonates and fossil teeth in Greece for forest or woodlands over the past 11 Ma: Palaeogeography, Palaeoclimatology, Palaeoecology, v. 108, p. 41-53.

Quattropani, L., Charlet, L., Lumley, H.d., and Menu, M., 1999, Early Palaeolithic bone diagenesis in the Arago Cave at Tautavel, France: Mineralogical Magazine, v. 63, p. 801-812.

Retallack, G.J., 1990, Soils of the past: An introduction to paleopedology: London, Unwin Hyman, 520 p.

Retallack, G.J., 1997, A colour guide to paleosols: Chichester, Willey, 175 p.

Rodler, A., and Weithofer, K.A., 1890, Die Wiederkauer der Fauna von Maragha: Denkschriften der Mathematisch - Naturwissenschaftlichen Classe der Kaiserlichen Akademie Wissenschaften, v. 57, p. 753-771.

Roussiakis, S.J., and Theodorou, G.E., 2003, Carnivora from the Late Miocene of Kerassia (Northern Euboea, Greece): Deinsea, v. 10, p. 469-497.

Roux, W., 1887, Uber eine Knochen lebende Gruppe von Faderpilzen (*Mycelites ossifragus*): Zeitschrift fur Wissenschaftliche Zoologie, v. 45, p. 227-254.

Sauvage, J., 1977, Les etudes palynologiques du Neogene et du Quaternaire en Grece et leurs application a la neotectonique des Hellenides (Corinthie, Eubee, Beotie, Phocide et Attique): Bulletin Societe Geologique de France, v. 19, p. 695-700.

Schaffer, J.R., 1889, Uber den feinen Bau Fossilen Knochen: Akademi der Wissenschafen in Wien, Abteilung III, v. 98, p. 319-364.

Schaefer, R., 1973, Microbial activity under seasonal conditions of drought in Mediterranean climates, in Castri, F.d., and Mooney, H.A., eds., Mediterranean type ecosystems: Origin and structure: London, Chapman and Hall Limited, p. 191-198.

Schlosser, M., 1903, Die fossile Saugetiere Chinas: Abhandlungen der Bayerischen Akademie der Wissenschaften, Mathematisch-Physikalische Klasse, v. 12, p. 220.

Schlosser, M., 1921, Die Hipparionenfauna von Veles in Mazedonien.: Abhandlungen der Bayerischen Akademie der Wissenschaften. Mathematisch-physikalische klasse, v. 29, p. 1-54.

Sclater, P.L., 1901, On an apparently new species of zebra from Semliki Forest: Procceedings of the Zoological Society of London, v. 1.

Sen, S., 1996, Present state of magnetostratigraphic studies in the continental Neogene of Europe and Anatolia, in Bernor, R.L., Fahlbusch, V., and Mittmann, H.W., eds., The evolution of Western Eurasian Neogene mammal faunas: New York, Columbia University Press, p. 56-63.

Sen, S., 1997, Magnetostratigraphic calibration of the European Neogene mammal chronology: Palaeogeography, Palaeoclimatology, Palaeoecology, v. 133, p. 181-204.

Sen, S., 2001, Correlation of Turkish and Greek mammal localities and magnetostratigraphic data, in Latal, C., and Piller, W.E., eds., Environmental and ecosystem dynamics of the Eurasian Neogene (EEDEN): Stratigraphy and palaeogeography. Workshop Graz, 15-18.3.2001, Volume 4: Graz, Berichte des Institutes fur Geologie und Palaontologie der Karl-Franzens-Universitat Graz, p. 33-34.

Sen, S., and Valet, J.P., 1986, Magnetostratigraphy of late Miocene deposits in Samos, Greece: Earth and Planetary Science Letters, v. 80, p. 167-174.

Sen, S., Bonis, L. de, Dalfes, N., Geraads, D., and Koufos, G., 1994, Les gisements des mammiferes du Miocene superieur de Kemiklitepe, Turquie: 1. Stratigraphie et magnetstratigraphie.: Bulletin Museum National d'Histoire Naturelle Paris, v. 4e ser., 16, section C, p. 5-17.

Senyurek, M.S., 1954, A study of the remains of Samotherium found at Taskinpasa: Ankara Universitesi Dil ve Tarih-Cografya Fakiltesi Dergisi, v. 12, p. 1-32.

Shinomiya, T., Shinomiya, K., Orimoto, C., Minami, T., Tohno, Y., and Yamada, M., 1998, In- and out-flows of elements in bones embedded in reference soils: Forensic Science International, v. 98, p. 109-118.

Sigerist, H.E., 1951, A history of medicine: New York, Oxford University Press.

Sillen, A., 1986, Biogenic and diagenetic Sr/Ca in Pliocene - Pleistocene fossils of the Omo Shungura formation: Paleobiology, v. 12, p. 311-323.

Sillen, A., 1989, Diagenesis of the inorganic phase of cortical bone, in Price, T.D., ed., The chemistry of prehistoric Human bone: School of American Research Advanced Seminar Series: Cambridge, Cambridge University Press, p. 211-229.

Solounias, N., 1981, The Turolian fauna from the island of Samos, Greece. With special emphasis on the Hyaenids and the Bovids, New Haven, 232 p.

Solounias, N., and Dawson-Saunders, B., 1988, Dietary adaptations and paleoecology of the Late Miocene Ruminants from Pikermi and Samos in Greece: Palaeogeography, Palaeoclimatology, Palaeoecology, v. 65, p. 149-172.

Solounias, N., McGraw, W.S., Hayek, L.A., and Werdelin, L., 2000, The paleodiet of Giraffidae, in Vrba, E.S., and Schaller, G.B., eds., Antelopes, deer, and relatives: Fossil

record, behavioral ecology, systematics and conservation: New Haven and London, Yale University Press, p. 84-95.

Solounias, N., and Moelleken, S.M.C., 1992, Dietary adaptations of two goat ancestors and evolutionary considerations: Geobios, v. 25, p. 797-809.

Solounias, N., and Moellenken, S.M.C., 1993, Dietary adaptation of some extinct Ruminants determined by premaxillary shape: Journal of Mammalogy, v. 74, p. 1059-1071.

Solounias, N., Moelleken, S.M.C., and Plavcan, J.M., 1995, Predicting the diet of extinct bovids using masseteric morphology: Journal of Vertebrate Paleontology, v. 15, p. 795-805.

Solounias, N., Plavcan, J.M., Quade, J., and Witmer, L., 1999, The paleoecology of the Pikermian Biome and the savanna myth, in Agusti, J., Rook, L., and Andrews, P., eds., The evolution of Neogene terrestrial ecosystems in Europe, Volume 1: Hominoid evolution and climatic change in Europe: Cambridge, Cambridge University Press, p. 436-453.

Solounias, N., Teaford, M., and Walker, A., 1988, Interpreting the diet of extinct ruminants: the case of a non browsing giraffid: Paleobiology, v. 14, p. 287-300.

Spratt, T., 1847, On the geology of a part of Euboea and Boeotia: Quartenary Journal of the Geological Society of London, v. 3, p. 67-73.

Spratt, T., 1857, On the freshwater deposits of Euboea, the coast of Greece, and Salonica: Quartenary Journal of the Geological Society of London, v. 13, p. 177-184.

Steinbock, R.T., 1976, Paleopathological diagnosis and interpretation: Bone diseases in ancient human populations: Springfield, Illinois, Charles C. Thomas, 423 p.

Steininger, F.F., Berggren, W.A., Kent, D.V., Bernor, R.L., Sen, S., and Agusti, J., 1996, Circum-Mediterranean Neogene (Miocene and Pliocene) marine - continental chronologic correlations of European Mammal Units, in Bernor, R.L., Fahlbusch, V., and Mittmann, H.W., eds., The evolution of Western Eurasian Neogene mammal faunas: New York, Columbia University Press, p. 7-46.

Swisher III, C.C., 1996, New 40Ar/39Ar dates and their contribution towards a revised chronology for the Late Miocene nonmarine of Europe and West Asia, in Bernor, R.L., Fahlbusch, V., and Mittmann, H.W., eds., The evolution of Western Eurasian Neogene mammal faunas: New York, Columbia University Press, p. 64-77.

Symeonidis, N., and Marcopoulou-Diacantoni, A., 1977, La faune pikermienne et le Neogene: Bulletin Societas Geologiques du France, v. 1, p. 111-115.

Symeonidis, N., Bachmayer, F., and Zapfe, H., 1973, Ausgrabungen im pikermi bei Athens, Griechenland.: Annalen des Naturhistorischen Museums Wien, v. 77, p. 125-132.

Teaford, M.F., and Walker, A., 1984, Quantitative differences in dental microwear between primate species with different diets and a comment on the presumed diet of Sivapithecus: American Journal of Physical Anthropology, v. 64, p. 191-200.

Teller, F., 1880, Der geologische Bau der Insel Euboa: Denkschr. K. Akad. Wiss. Wien, v. 40, p. 129-181.

Theodorou, G., Athanassiou, A., Roussiakis, S., and Iliopoulos, G., 2003, Preliminary Remarks on the Late Miocene Herbivores of Kerassiá (Northern Euboea, Greece): Deinsea, v. 10, p. 519-530.

Thomasset, J.J., 1931, Sur un champignon fossile: *Mycellites ossifragus* (Roux): Bulletin de la Societa Géologique de France, 5 Series, v. 1, p. 597-603.

Tobien, H., 1967, Subdivision of Pontian mammal faunas. Committee Mediterranean Neogene Stratigraphy, Procceedings IV Session, Bologna 1967: Giornale di Geologia, v. 35, p. 1-5.

Trueman, C.N., 1998, Rare earth element taphonomy of vertebrate asemblages [PhD thesis]: Bristol, University of Bristol.

Trueman, C.N., and Martill, D.M., 2002, The long term survival of bone: The role of bioerosion: Archaeometry, v. 44, p. 371-382.

Trueman, C.N., and Tuross, N., 2002, Trace elements in recent and fossil bone apatite, in Kohn, M.J., Rakovan, J., and Hughes, J.M., eds., Phosphates: geochemical, geobiological, and materials importance, Volume 48: Reviews in Mineralogy and Geochemistry, Mineralogical Society of America - Geochemical Society, p. 489-521.

Turner-Walker, G., and Parry, T.V., 1995, The tensile strength of archaeological bone: Journal of Archaeological Science, v. 22, p. 185-191.

Turner-Walker, G., and Syversen, U., 2002, Quantifying histological changes in archaeological bones, using BSE-SEM image analysis: Archaeometry, v. 44, p. 461-468.

Turner-Walker, G., Nielsen-Marsh, C.M., Syversen, U., Kars, H., and Collins, M.J., 2002, Sub-micron spongiform porosity is the major ultra-structural alteration occuring in archaeological bone: International Journal of Osteoarchaeology, v. 12, p. 407-414.

Velitzelos, E., and Gregor, H.J., 1986, Geologische daten zu den fossilfuhrenden Fundstellen Lava, Prosilion, und Likoudi (Griechenland) nebst Bemerkungen zu deren Frucht und Samenfloren: Documenta Naturae, v. 29, p. 34-40.

Vrany, B., Hnatkova, Z., and Lettl, A., 1988, Occurence of collagen-degrading microorganisms in associations of mesophylic heterotrophic bacteria from varius soils: Folia Microbiologia, v. 33, p. 458-461.

Wagner, A., 1840, Fossile Uberreste von einem Affen und anderen Saugetieren aus Griechenland: Abhandlungen der II Classe der koniglichen Akademie der Wissenschaften, v. 3(1), p. 155-170.

Wagner, A., 1848, Urweltliche Saugthier-Ueberreste aus Griechenland. Abhandlungen der II Classe der koniglichen Akademie der Wissenschaften, v. 5(2), p. 335-378.

Webb, S.D., 1983, The rise and fall of the late Miocene ungulate fauna in North America, in Nitecki, M.H., ed., Coevolution: Chicago, University of Chicago Press, p. 267-306.

Wedl, C., 1864, Uber einen im Zahnbein und Knochen keimenden Pilz: Akademi der Wissenschafen in Wien. Fitzungberichte Naturwissenschaftliche Klasse ABI. Mineralogi biologi erdkunde, v. 50, p. 171-193.

Weidmann, M., Solounias, N., Drake, R.E., and Curtis, G.H., 1984, Neogene stratigraphy of the Eastern Basin Samos island,Greece: Geobios, v. 17, p. 477-490.

Weiner, S., and Price, P.A., 1986, Disaggregation of bone into crystals: Calcified Tissue International, v. 39, p. 365-375.

Welch, S.A., Taunton, A.E., and Banfield, J.F., 2002, Effect of microorganisms and microbial metabolites on apatite dissolution: Geomicrobiology Journal, v. 19, p. 343-367.

Werelds, R.J., 1962, Nouvelles observations sur les dégradations postmortem de la dentine et du cément des dents inhumées. (Etude de dents recueillés dans les ruines de l'ancienne Abbaye de Vivegnis, 1235-1790 AD, pres de Liege): Bulletin de la Groupment International Pour La Recherche Scientifique En Stomatologie Et Odontologie, v. 4, p. 554-591.

Wilson, B., Grigson, C., and Payne, S., 1982, Ageing and sexing animal bones from archaeological sites, in Hands, A.D., and Walker, D.R., eds., B.A.R. British Series, Volume 109: Oxford, The Individual Authors, p. 268.

Wilson, R.M., Elliott, J.C., and Dowker, S.E.P., 1999, Rietveld refinement of the crystallographic structure of human dental enamel apatites: American Mineralogist, v. 84, p. 1406-1414.

Woodward, A.S., 1901, On the bone beds of Pikermi, Attica and the similar deposits in Northern Euboea: Geological Magazine, v. 8, p. 481-486.

Yoshino, M., Kimijima, T., Miyasaka, S., Sato, H., and Seta, S., 1991, Microscopical study of estimation of time since death in skeletal remains: Forensic Science International, v. 49, p. 143-158.

Zittel, K.A. von, 1893, Handbuch der Palaeontologie, Abteilung I. Palaeozoology: Munchen, R. Oldenbourg, 799 p.